N-19117475 2052

COMET

DISTRIBUTION STATEMENT A
Approved for public release;
Distribution Unlimited

DTIC QUALITY INSPECTED 3

19970814 068

A Service of:

National Aeronautics and Space Administration

Scientific and Technical Information Program Office
Center for AeroSpace Information

26

N79-17501

DESIGN OUTLINE FOR A NEW MULTIMAN ATC SIMULATION FACILITY AT NASA-AMES RESEARCH CENTER

J. G. Kreifeldt O. Gallagher
Dept. of Engineering Design
Tufts University
Medford, Mass. 02155

ABSTRACT

A new and unique facility for studying human factors aspects in aeronautics is being planned for use in the Man-Vehicle Systems Research Division at the NASA-Ames Research Center. This facility will replace the existing three cockpit-single ground controller station and be expandable to include approximately seven cockpits and two ground controller stations.

Unlike the previous system, each cockpit will be mini-computer centered and linked to a main CPU to effect a distributed computation facility. Each simulator will compute its own flight dynamics and flight path predictor. Mechanical flight instruments in each cockpit will be locally supported and CRT cockpit displays of (e.g.) traffic and or RNAV information will be centrally computed and distributed as a means of extending the existing computational and graphical resources.

An outline of the total design will be presented which addresses the technical design options and research possibilities of this unique man-machine facility and which may also serve as a model for other real time distributed simulation facilities.

DTIC QUALITY INSPECTED 3

INTRODUCTION

Studying air traffic control systems requires a realistic simulation facility which faithfully captures pilot-pilot and pilot-controller interactions as well as those unique human characteristics vital to any evaluation of complex systems. A recent study(1) has shown the dangers of drawing conclusions from all computer studies or even from simulation studies not using actual piloted simulators.

The human factors problems in the present and proposed ATC systems are extensive. For example, to accommodate future increases in aircraft densities a very high emphasis will be placed on precision in both air and ground sides. Some of these human factors problems impacting precision are listed below.

The interactive air-ground and air-air control loops will affect precision through the time delays and lags between situation apprisement, commands and executions.

Errors, blunders, emergencies, failures, priorities, etc. as well as smaller perturbations from pilot or controller decisions will have a decided effect on maintaining any required precision. Recovery from local unplanned situations are crucial human factors aspects.

Basic ATC procedures for actual traffic management (e.g. multiple curved approaches) will affect precision. Different alternatives must be studied in the human contexts of information display requirements and realizations.

Both pilots and controllers will require displays specially designed for information, control and navigation purposes in order to achieve a high degree of precision without excessive workloads. High density could mean high display clutter for controllers.

Pilot and controller acceptances of the different or alternative regimes for traffic control must be determined to prevent enforcing a theoretically workable but practically unsatisfactory and hence error prone system.

The basic pilot and controller workloads could be excessive in strategic control particularly as related to closely spaced runways and other methods of handling high density traffic.

High speed decision making by controllers and pilots will be required to maintain high precision and safety. This basic ability is an issue by itself and can be expected to interact strongly with the displays used as well as possible computer aids to decision making.

General aviation must be accommodated in the future NAS as well as commercial aviation. Basic techniques, capabilities, workloads, displays, etc. must be determined for general aviation traffic control just as for commercial aviation. In fact, all of the comments made previously apply to general aviation as well.

These and other human factors issues must be studied on a fully interactive multiman simulation facility.

Considerable work has already been completed at NASA-ARC studying ATC alternative management regimes such as distributed management based on the availability of Traffic Situation Displays in the cockpit. A three pilot-two controller simulation facility was developed in 1972 for this purpose and has been used extensively since. However, the ever expanding problem size and types have nearly exhausted the resources of the present system. For instance, studies of simultaneous multiple curved approaches to two closely spaced runways cannot adequately be supported on the present 3 simulator-1 controller station facility primarily because of the low simulator density available for a required high density environment.

Therefore, to investigate either human factors problems impacting complex ATC systems and/or studying alternative ATC management regimes, a larger multiman interactive simulation facility is presently being planned for the Man-Vehicle Systems Research Division of NASA-ARC.

There is a third use of this facility as well. At present, human factors replication studies are performed sequentially. That is, single subjects are scheduled on successive days under the same experimental protocol. This naturally ties up the computer facility supporting the experiment for these experimental hours on the successive days. In addition, the set-up and take-down time is also incurred for each successive replication. Considering the number of other experiments and program developments always under way, this can be a very inefficient and nonproductive procedure.

The planned facility will lend itself to an ensemble manner of replications. Since the simulators will be identical and locally positioned, as many replications can be obtained simultaneously as the facility will support. For instance, instead of scheduling ten running days of two hours per day (1 hour-experiment, 1 hour-set up and take down) for a total of 20 hours (usually in prime time) to achieve 10 replications of a single pilot experiment, the same thing may be accomplished in (say) two days of two hours per day for a total of 4 hours with 5 simultaneous replications per day.

Planning of the facility is in the initial phases. A broad overview followed by some prototyping specifics will be given here.

DESIGN OVERVIEW

Figure 1 is a conceptual picture of the facility showing 10 identical fixed base simulator cabs, the two ATC controller stations (two man per station) and an experimenter station with a small local computer. A remotely located large computer and graphics system is also shown.

ORIGINAL PAGE IS
OF POOR QUALITY

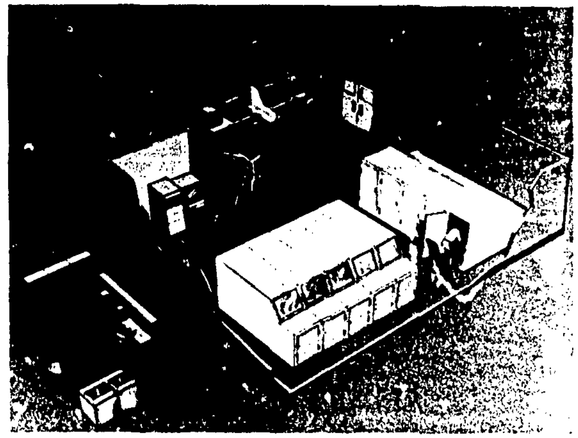

Figure 1 Conceptual Plan for the Multiman Interactive ATC Simulation Facility

In the planned facility, each simulator cab will contain a mini/micro computer enabling it to perform functions previously performed by the main large CPU. That is, instead of centralized computing, the planned facility will utilize distributed computing. A centralized computing system quickly becomes compute bound in real time simulation work. Distributed computing will support the increase in simulators needed as outlined previously.

The existing 3 simulator system is CRT based as well as centrally computer supported. The simulators use all electronic displays which also causes a graphic bottleneck when all 3 are simultaneously operating. Therefore, the CRT Vertical Situation Display will be replaced by traditional mechanical instruments and the CRT retained primarily for Horizontal Situation Information (HSI) and traffic display. Figure 2 is a conceptualization of a simulator showing the micro/mini, mechanical flight instruments and CRT HSI.

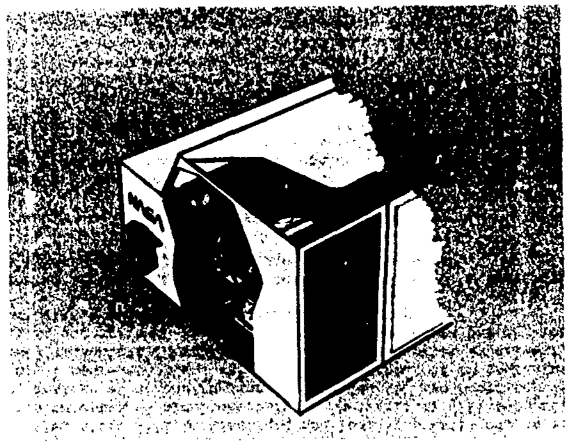

Figure 2 Conceptual Drawing of a Micro/Mini Computed Based Simulator

Figure 3 presents in more detail the major features of the facility.

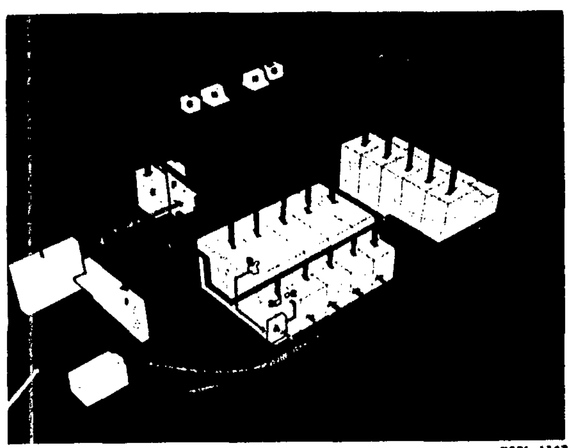

Figure 3 Major Information Linkages in the Multiman ATC Facility

The micro/mini computer simulators will be supported by a small host computer at the experimenter's station so that if the CRT is not needed the facility can stand alone from the main CPU which permits full utilization of all facilities.

PRELIMINARY DESIGN SPECIFICS

FLIGHT INSTRUMENTS

A PACER Mk II flight simulator(2) was chosen to supply the basic pilot inputs (aileron, elevator, throttle, rudder) and displays (altitude, navigation, status). Figure 4 shows the PACER unit (without rudder pedals).

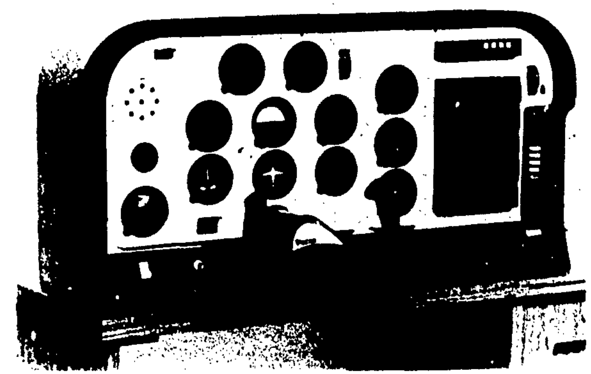

Figure 4 Basic Flight Instrument PACER Mk 2

This unit is capable of very realistic instrument flight and navigation from take off to landing. This unit will be modified to accept a small color CRT perhaps by relocating the navigation radios on the panel. The PACER is an all electronic system and thus is suitable for A/D and D/A interfacing. The unit as shown is a fully functional simulator-trainer.

COMPUTER

After considerable study and analysis, the LSI-11 computer from Digital Equipment Corporation was chosen as both the mini/micro for the PACER and as the host computer for the multiple identical simulators. The LSI-11 is a

16 bit system with an optional extended arithmetic unit. The smaller 8 bit machines do not presently provide the resolution and speed necessary for this real time application. For example, 8 bits provide a resolution of less than one degree which is not suitable for navigation purposes and double precision arithmetic is too slow for the anticipated computational load.

The LSI-11 also is well supported in hardware and software as well as a very wide range of physically compatible I/O circuitry. A/D and D/A, fast memory, multiple serial and parallel I/O are available from a multitude of sources.

DEVELOPMENT SYSTEM

Figure 5 shows the equipment purchased for development work.

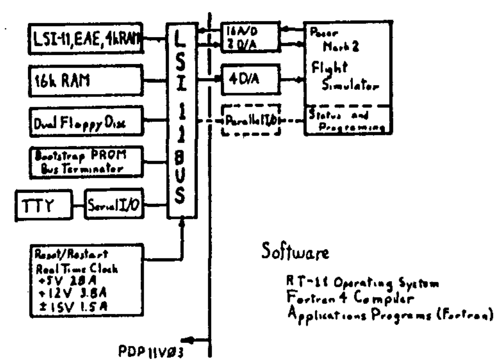

Figure 5 Development system Consisting of the PACER Mk II Simulator and PDP-11V03 Computer.

The equipment shown to the left of the bold line is essentially identical to DEC's minicomputer PDP-11V03. The unit as shown with 20k RAM and dual floppy discs will permit initial experimental development as to language, function allocation, etc. in order to make the basic PACER into a smart simulator. The optimal arrangement of task sharing between the analog dynamics of the simulator and digital dynamic calculations of the minicomputer will be implemented. There are three basic variations of task sharing.

1. Simulator as Display

In this mode, the simulator provides only input and output functions - yoke, throttle, rudder, etc., and the panel dials and status indicators. This arrangement does not make use of the existing analog dynamics and imposes a heavy computational load on its minicomputer. It is unlikely that this approach will be used in this strict form.

2. Simulator as Aircraft

This approach, which will be tried first, makes maximum use of the simulator dynamic functions. The minicomputer will perform some navigational tasks such as programming to follow curved approaches and input all necessary flight data (airspeed, etc.) for analysis purposes. The simulator basically sends aircraft attitude to its minicomputer which calculates map position and runs the navigation displays.

3. Simulator as Navigator.

This approach makes maximum use of all simulator functions with the simulator computer primarily a data gatherer and special purpose navigation computer. This approach may present problems in keeping reckoned aircraft positions in step throughout the system.

The minicomputer will in any case also have control over any additional status information such as flaps, warning lights, etc.

The basic philosophy is to push as much of the computing load as far toward each simulator as possible.

SMART SIMULATOR

Figure 6 shows a "smart simulator" as finally prototyped. This is identical to the development system with all unnecessary equipments stripped away.

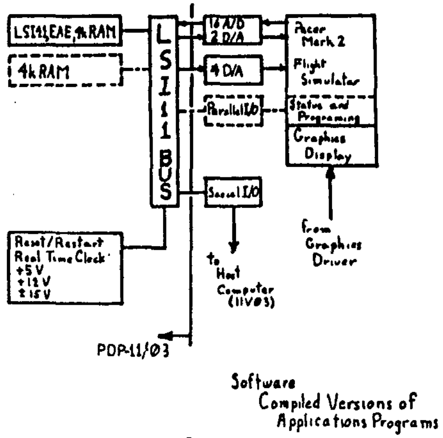

Figure 6 The Prototype Smart Simulator

This simulator can only execute programs down line loaded to it from the PDP-11V03 host computer. It is anticipated that 8k RAM will be sufficient for its local purposes. Note that a graphics display (CRT) is shown attached to the PACER unit. This display will be driven from the existing graphics system and main CPU.

All programs will be developed on the host computer except graphics and some data handling programs reserved for the remotely located CPU.

ATC FACILITY

Figure 7 shows the basic arrangement for the total multiman interactive ATC facility.

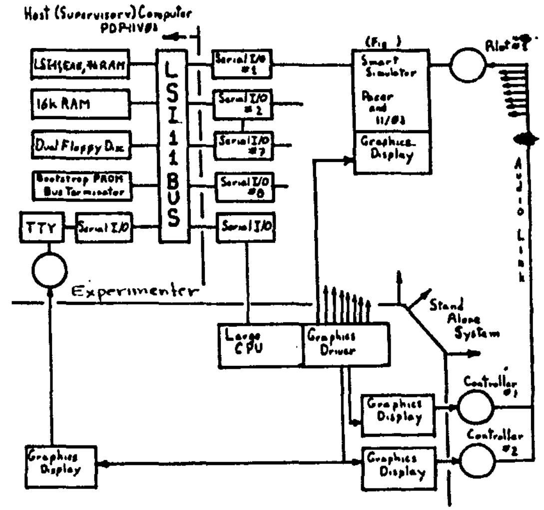

Figure 7 Minicomputer Based ATC Facility

The host computer (11V03) is essentially as shown in Figure 5 and the smart simulator as in Figure 6. Host and simulator are connected by two serial I/O units (one on each side). The host computer connects with the large CPU for two way exchange while the large CPU and graphics system supports the CRT in each simulator as well as graphics at each of the two controlled stations. As indicated, with the exception of the main CPU and graphics, the host + simulators will be a stand alone system for program development and some experimentation not requiring graphic displays.

All participants are connected by a programmable audio link which can simulate different verbal communication networks such as data link, etc.

SYSTEM OPTIONS

Next to digital computation of flight dynamics, path predictor computations produce a heavy computational load. Unloading flight dynamics to each simulator will free up considerable time in the system. Path predictors might possibly be computed locally or at the host computer or in the main CPU for each simulation.

Position information also could be done in the simulator, host of main CPU as could special navigation programming (e.g. curved approaches). Resolution of these and other options will occur during development.

STATUS

The development system is being assembled. For reference, a parts list and cost is given in Table 1. Pieces were obtained from different vendors for best price/delivery.

TABLE 1 Development System (PACER and 11V03) Parts List

Source	Item	Part #	Price
DEC	CPU with 4k RAM	KD11-F	$842
DEC	Extended Arithmetic	KEV-11	162
Monolithic systems	16k RAM with Refresh	---	1125
DEC	Bootstrap Prom/Bus Terminator	REV11-A	272
DEC	Serial I/O including Cables	DLV-11	251
ADAC	16 Channels Analog to Digital	600-LSI-11-16-PD-2[illegible]	795
ADAC	2 Channel D/A for above		400
ADAC	4 Channel Digital to Analog	600-LSI-11D-4-X	750
DEC	Dual Floppy Disc	RXV11-BA	3655
DEC	Cabinet	H909C	298
DEC	LSI-11 Bus Backplane 6x9	DDV-11B	340
Quadex	Power Supply Panel & Restart	---	150
Quadex	Cables & other Hardware	---	150
DEC	RT-11F/B Operating System	QJ003-AY	1173
DEC	Fortran 4	QJ925-AY	748
Power 1	Power Supplies	---	244
DEC	Decwriter 20ma loop	LA-36-DE	1475
Bud Radio	Rack Panel 30" Deep 21" High	---	381
Pacer Systems	Pacer Mark 2 Flight Simulator	(full capability)	3600
			$16811

The development system as acquired has capability for editing and compiling higher level languages (FORTRAN, PASCAL) in addition to executing machine language programs.

Parallel I/O may be required or it may be possible to substitute digital I/O for some of the analog I/O.

The simulator as aircraft is expected to be operational within 4-6 months. The aircraft will send attitude information to the computer with the computer calculating map position, predictor and running navigation displays.

The development system will then be stripped down to essentials for executing downline loaded optimized machine language programs. This smart simulator will be a prototype for replication.

The host computer will then be configured to support the 8 or 10 smart simulators as a single facility. Interfacing the host and main CPU will also be accomplished.

Estimated completion time for the total design is in the order of 1½-2 years. It is quite likely that by the time the prototype simulators are designed, more powerful and less expensive minicomputers will be available. These will be used in the final designs to the extent possible.

SUMMARY

The new mini/micro computer based ATC facility will greatly increase the complexity and realisms of ATC human factors problems for modeling and study. This will in turn permit a firmer and more translatable set of findings and designs. It is also necessary to develop in conjunction with the facility more sophisticated methods for treating multivariable, realistic simulation experiments.

REFERENCES

1. Kreifeldt, J.G., Parkin, L., Hart, S., "Air Traffic Control by Distributed Management in a MLS Environment." Proc. 13th Annual Conference on Manual Control. MIT 1977.

2. ———— Pacer Systems, Inc., 87 Second Ave., Northwest Industrial Park, Burlington, Mass., 01803.

ACKNOWLEDGMENT

This work is supported by funds from NASA Grant NSG-2156, Supplement No. 1.

Session V

MANIPULATORS AND PROSTHETICS

Chairman: J. W. Hill

PRECEDING PAGE BLANK NOT FILMED

N79-17502

DISPLAYS FOR SUPERVISORY CONTROL OF MANIPULATORS*

A. K. Bejczy
Member of Technical Staff

G. Paine
Member of Technical Staff

Jet Propulsion Laboratory

California Institute of Technology

Pasadena, California 91103

Abstract

The problem of displaying information generated by sensors attached to the terminal device of a remotely controlled manipulator is considered. The sensors under consideration are proximity, force-torque, tactile and slippage sensors. The paper describes and evaluates several examples that have been implemented in the JPL teleoperator project using audio and graphic displays of information generated by four proximity sensors attached to a manipulator end effector. Design schemes are also discussed related to the display of information generated by a six-dimensional force-torque sensor, a multipoint proportional tactile sensor, and a directional slippage sensor. The paper concludes with a discussion of future integrated displays of visual (TV) and handbased sensor information.

I. Introduction

Space missions planned for the shuttle era will involve an extensive use of various manipulators with associated tools to perform a variety of science and engineering tasks in space. Payload handling in the shuttle, satellite servicing or retrieval in earth orbit, assembly of large area structures in space such as antennas, solar power stations and space processing systems, unmanned in situ exploration of lunar and planetary terrains and materials or sample analysis in sealed space laboratories will require the extension and augmentation of man's manipulative capabilities by employing remotely operated manipulator systems with or without special purpose tools. Remote manipulation implies operating conditions which impose various information and control communication constraints.

A major challenge in the development of remotely controlled manipulator systems is the acquisition and use of sensor information which supplements the visual information for control. Non-visual information related to manipulator control can be obtained from proximity, tactile, slippage and force-torque sensors attached to the terminal device or arm mechanism. Proximity sensors provide information on short (few centimeters) distances in known direction between terminal device and objects. Tactile sensors provide information on the distribution and amount of contact area pressure between terminal device and objects. Slippage sensors provide information on the slip and possibly also on the direction of slip of an object on the inner surface of the mechanical "fingers". Force-torque sensors mounted between the terminal device and last wrist joint provide information on the amount of force and/or torque exerted by the terminal device on objects along three orthogonal directions referenced to the terminal device.

This paper considers the problem of displaying information generated by proximity, force-torque, tactile and slippage sensors attached to the terminal device of a remotely controlled manipulator. The sensor information displayed to the operator serves several purposes depending on the modes available to the operator for manipulator control. In a manual control mode, the sensor information displays are elements in the continum of a real-time control loop in the sense that they guide the operator's control inputs by providing continuous information feedback to the operator on the appropriate "external error state" of the manipulator. *In a computer control mode, the* sensor information displays are discrete elements outside the real-time control loop. They provide information to the operator prior to the selection and initialization of an appropriate control algorithm, and inform the operator about the performance of the control algorithm selected for the task at hand. Supervisory control by definition implies the availability and use of both computer and manual control modes for remote manipulator control.

The basic challenge in displaying sensor information to the operator is twofold: a) selection or design of a proper type of display, and, b) selection or design of a proper format for a given type of display so that the display presents all necessary information in a timely manner and in a form easily perceivable by the operator. Since the use of direct or indirect (TV) visual information is inevitable in remote manipulator control, a fundamental topic is the integration or integrated display of visual and non-visual sensor information.

Section II of the paper is devoted to some general considerations on various display concepts. Section III summarizes our work on audio and graphic displays of proximity sensor information, and compares the two types of displays in terms of actual control performance data. Graphic display of force-torque sensor data is discussed in Section IV. Graphic display of tactile and slippage sensor information is treated in Section V. *Implementation concepts for integrating visual and non-visual sensor information* are briefly discussed in Section VI.

---

*This work represents one phase of research carried out at the Jet Propulsion Laboratory, California Institute of Technology, under contract NAS7-100, sponsored by the National Aeronautics and Space Administration.

PRECEDING PAGE BLANK NOT FILMED

D27

II. Display Concepts

A wide variety of display types are available and can be used in teleoperator systems. Displays can employ a single bulb, the operators sense of touch, analog and digital meters, bar displays, audio tones, and black and white or color TV. The displays may either be presented separately or integrated into an overall workspace display. Each of these is appropriate to some sensor data types or teleoperator applications and inappropriate to others. They are considered here in the context of supervisory control of manipulators with data developed from hand mounted sensors.

The simplest display listed above is the single bulb or LED display. It can indicate task completion, initiation or completion of some event, or the simultaneous existence of some set of conditions, e.g., a hand is at the proper orientation and distance from a particular object. Unless the data to be presented is binary in form this type of display is limited. Blinking the display allows some relief from the basic binary nature of the display.

Individual bar displays where the bar length is an understood function of the sensor output provide improved resolution and ease of interpretation but are inflexible in an application where it is desirable to show the sensor data first in one orientation and then another. A display would be required for each orientation in this case. The display can, however, be interpreted quickly. Analog meters provide somewhat greater resolution but are less quickly interpreted. Digital meters, on the other hand, provide considerably increased resolution and accuracy but require even more time for interpretation.

The use of audio tones in remote manipulator control has been explored for proximity sensors to some extent and shown to be effective in improving performance as measured by time to task completion, efficient use of resources, or task accuracy (Ref. 1). The primary scheme employed is to display the outputs from various sensors as frequency or amplitude changes. Coded tone messages, e.g., Morse code or the code modulation schemes used in fire station could also be employed. While coded tones can transmit a much wider range of messages they also are slow. Tone displays also compete with background noise and thus the data can be lost. However, they do make use of a human perception channel that is always open, is omnidirectional, and does not depend on the operator's focus of attention. In common practice (Ref. 2) use of audio presentation of relevant information is recommended if: a) The message is simple. b) The message is short. c) The message will not be referred to later. d) The message deals with events in time. e) The message calls for immediate action. f) The visual system of the person is overburdened. These conditions define both the advantages and the limitations of displaying sensor information by audio means.

In an effort to overcome some of the limitations inherent to audio displays, graphic displays are being investigated. These displays offer adequate resolution for an operator to monitor or control a manipulator, are easy to change so that the sensor data can be seen in different perspectives, and are fast enough to keep up with the process and do not add more than a few hundredths of a second time delay. TV displays can be constructed using vector, line, or other scanning mechanisms. Line TV displays have been employed here for compatibility with other displays and because of the potential for integration of the sensor data into the operator's stereo or mono scene display. Color display of sensor data while also practical has not yet been investigated. It offers a means of providing scale change data to the operator.

III. Proximity Sensor Displays and Performance Evaluation

Proximity sensors which measure the distance between the hand and an object along a vector fixed to the hand, have been shown to be effective with tone displays as shown in Ref. 1. It was also shown that four tones were less effective than two due to the complexity of interpreting the data in that particular experiment.

For completeness, some performance data related to the combined use of visual and proximity sensor audio information are quoted in Table 1. In the performance experiment a parallel finger hand was equipped with four proximity sensors, with two sensors on each finger in a configuration as shown in Figure 1. The proximity sensors are described in Ref. 3.

In the control experiments, the signals of each proximity sensor are presented to the operator as a distinct audio tone. The tones are distinct in both pitch and source (loud speaker) location. The pitch of the tone generated through the voltage output of the proximity sensor indicates the distance between the sensor head and the objects. Each audio display of the four sensors covers a different pitch range. The maximum sensed distance is about 8-10 cm. The control is performed from a remote control station fully isolated from the task scene. The operator in the remote control station can utilize both mono and stereo TV displays, and listen to the audio tones of the four loudspeakers displaying the proximity sensor signals. The four loudspeakers are arranged in a two by two meters vertical quadrangle around the operator. In this way, the operator can easily identify the sensor source of the individual signal.

The vantage point of the stereo TV cameras is from the shoulder of the slave arm and about 0.5 m above it. The vantage point of the mono camera is from the side, varying between 50 to 90 degrees relative to the field of view of the stereo cameras. Neither the stereo nor the mono view can provide a complete visual feedback to the operator under the described setup. In particular, the visual feedback is highly degraded and obscured when the hand moves near solid objects.

The main point of the remote control experiments is to test whether the operator can integrate the information content of the proximity sensor signals presented by audio tones with an incomplete visual feedback and find control strategies to perform remote manipulator tasks which are very difficult or near impossible under the existing visual feedback arrangements. The information content of the proximity sensor signals can provide clues to the operator to solve two basic problems: overcome the lack of depth information apparent in the TV displays, and locate objects or parts of the work scene invisible in the TV displays.

Figure 2 shows two typical task arrangements for proximity control performance tests. The two tasks were:

> Task 1: Move from standby position to the rectangular block at "A", pick it up, and place it on top of another rectangular block located at "B", and align the two blocks. The two blocks are of equal size.
>
> Task 2: Move from standby position and pick up a partially obscured irregular object (a rock).

The performance data shown in Table 1 are related to Task 1 above. The data clearly show the validity of the following conclusions: 1) Proximity sensor information can replace or supplement part of the visual information required for control. 2) Control tasks which cannot be performed using visual information alone can be performed using a combination of proximity sensor audio tones and visual information. 3) Control performance is sensibly influenced by the location of the proximity sensors on the terminal device. 4) Number of independent proximity sensor signals significantly affects operator's control performance. This last conclusion is one of the main motivations for investigating graphic/TV techniques to display proximity and other sensor information to the operator.

As seen in Table 1, when the operator had to deal with signals from four proximity sensors the performance time increased by 30-40% as compared to the performance time related to the use of only two proximity sensors. It shows that signal detection and processing capabilities of man are very limited, and can be saturated very easily. Man is essentially a single-channel signal detector and processor at a given instant. It is interesting to note that the information content of four proximity sensor signals was considerably more complete for the control task than the information content of only two proximity sensors. Consequently, one could have expected a faster and more error free operator performance. It was not so, however, since the human operator had to derive the "completeness" of information by a mental integration process correlating different motions with different sensor signals.

The TV graphics offers an alternative means to display the proximity sensor data in an easily interpreted (geometric) form. It is the form in which the data is normally perceived. Given greater computational capabilities and dedicated special purpose displays the data could be even presented in stereo, rather than in mono as done here.

Two different graphic display representations have been tried. The first, see Figure 3, shows a line drawing of the hand in broad lines. The sensor data is represented by the four narrow lines. The two forward sensors are numbered 1 and 2; and the two down sensors are numbered 3 and 4. The letters "P" give the origin, and the length of the narrow line show the separation between the sensor and the object. For objects beyond the sensor's range the line length is bounded. In the case where the object is too close, the sensor output is on the inside of the bell shaped multivalued response curve and, since no discrimination is possible, a false value is shown. The location of the sensors is shown in the left part of Figure 3, and also in Figure 1. In Figure 3, none of the sensors "see" an object and all the proximity sensor outputs are shown as full length.

Figure 4 shows an actual task scene together with graphic display of proximity sensor signals as the operator uses the graphic display combined with stereo TV display in the remote control station. Since the mechanical hand partly obscures the blocks in front and below the hand, the operator has to rely on the graphic display of proximity sensor data to determine the hand's geometrical relation to the nearby blocks. As seen in the upper right part of Figure 4, this determination can be done easily and accurately from the graphic display.

The ability of this display concept to show geometric relationships can be seen from a comparison of Figure 5a with Figure 5b; Figure 5a with Figure 5c; and Figure 5b with Figure 5c. In each pair the first figure shows the scene being sensed, and the second shows the sensor/display response.

The second display representation tried is shown in Figure 6. There the preceding display has been put in a different perspective. It is this representation which was used in the performance tests summarized in Table 2.

The performance data shown in Table 2 are related to the following simple task: Move the terminal device from the standby position to a block on the table and stop it at a predefined distance in front of the block with a predefined elevation above the table. In the first set of experiments the audio tones used were generated by two (one out and one down) of the four proximity sensors in the form described previously. In this first set of experiments the predefined stop distance and elevation were set for 2.7 inches. In the second set of experiments the operator used graphic information display of proximity sensor signals in a form as shown in Figure 6. In the second set of experiments the stop distance

and elevation were set for 2.4 inches. In each set ten experiments were performed. The actual arm motion involved about 20 inches travel in each case. From time to time the block was slightly repositioned in order to prevent the operator's motion from the standby position to the desired stopping conditions from becoming a "habit". The TV visual field was arranged so that the stopping conditions could only partly be assessed visually, and even this partial visual assessment could only be a rough estimate. The overall experimental set-up was identical to that described previously.

Table 2 shows that graphic display improves task performance accuracy by a factor of nearly three as compared to task performance accuracy when audio displays are used. This accuracy improvement can be attributed to two factors: a) The eye can more easily compare absolute measurements from a multichannel signal than can the ear. b) The geometrical pattern context of the sensor signals is immediately apparent to the eye. In addition to accuracy improvements, task performance time with audio display was 14.7 sec. with 5.3 sec. standard deviation, but task performance time with graphic display has been reduced to 13.3 sec. with 4.0 sec. standard deviation. Further performance time improvements can be obtained with graphic display through an improved system integration in the control station. It is noted, however, that a selective and interpretive preprocessing of the sensor signals before the generation of the audio tones would reduce the mental load for the operator to interpret the complexity of the tones. This procedure would also lead to improved task performance.

For both display representation types (as shown in Figures 3 and 6, respectively) equivalent data processing was employed. The data from each sensor was converted into digital form by a 8 bit high speed (5 μs conversion) A/D converter. An IMSAI microprocessor, see Figure 3, which employs the Intel 8080 microprocessor chip, corrected the sensor data for nonlinearities, and computed the displayed scene. The display used has alpha-numeric and graphic capabilities. In the latter mode a standard TV frame can be subdivided into a 48 x 128 matrix of points. Each sensor's output was represented as a bar 0 to 12 or 0 to 31 points long. While this allows rapid interpretation of the data it provides only low accuracy. Although the scene is displayed at standard TV rates, the changes were updated only every 10-30 ms depending on the display representation and various timing parameters. The software for this processing requires only about 800 words of 8 bits each. The coding was performed in assembly language.

IV. Force Sensor Display

A force/torque sensor has been mounted at the wrist of the JPL CURV arm as shown in Figure 7. The sensor is described in detail in Ref. 4. Its mechanism has been developed by Vicarm Inc., while its electronics has been developed at JPL. The primary use of the sensor will be in supervisory control where the control computations are performed by an Interdata model 70 computer. To provide the operator with additional data by which to monitor the control process a force display is being developed. To relieve the Interdata from the display computations and to simplify the software development a distributed processing scheme will be employed. Here, since the sensor signals are already digitized for the Interdata, no separate A/D conversions will be made. Instead a special buffer has been developed which allows the IMSAI microprocessor to "listen" in on the CURV Interdata bus to acquire the sensor data. Preliminary force sensor display representations are shown in Figure 8. In the left part of Figure 8 the force sensor outputs in hand reference frame up (U), down (D), forward (F), backwards (B), right (R), and left (L) are shown nested in a hand schematic. In the right part of Figure 8 the proximity sensor data representation has been included also. In both cases the force sensor data is shown in each of its three orthogonal components. A similar representation is being considered for a torque display.

The dynamic range of the sensor is more than two orders of magnitude: from 2 oz. to 800 oz. force and from 8 in. oz. to 1840 in. oz. torque. It is expected that force-torque control tasks can be subdivided into three regions: low (2-40 oz.), medium (40-120 oz.) and upper (120-800 oz.) dynamic regions. In order to obtain adequate display resolution in all three regions, the use of appropriate scale changes is considered matching the range of each dynamic region. A further consideration is the display of the force and torque <u>vectors</u> in addition to their three orthogonal components. The vector displays would aid the <u>integrated</u> perception of the full dynamical changes acting at the terminal device.

The display of force or torque data is made more difficult by the fact that it is not fundamentally geometric perceived. With force or torque the point of application relative to the sensor and the grasping implement must be considered in addition to the force or torque sensed at the wrist base of the hand. Thus, the development of useful force-torque data displays is a demanding and non-trivial task. The problems of force-torque sensor information display have also been recognized elsewhere (Ref. 5).

V. Tactile and Slippage Sensor Displays

Figure 9 shows the breadboard of a multipoint proportional tactile sensor with a visual display based on an arrangement of light bulbs. Each bulb corresponds to a sensitive spot on the sensitive surface. The sensitive surface is built of two nets of electrodes separated by conductive rubber. The two nets of electrodes form a 4 x 8 matrix pattern. The sensitive surface will cover the inner and outer surfaces of the mechanical "fingers". The sensor will sense the amount of normal force (pressure) acting at a given point ("spot") on the finger.

The light bulbs used in the breadboard display provide only a very rough indication of the amount of pressure sensed at a given spot. The development of a graphic color display is under consideration where colors would be used to indicate the amount of pressure sensed at a given point on a finger. An alternative display concept would utilize only black and white frame. The frame would show the geometrical contours of each part of the finger equipped with the artificial skin. The sensitive spots would be indicated by a square net inside of the geometrical contours, each square corresponding to one sensitive spot. The amount of pressure sensed at a spot would be indicated by a number inside the square scaled to the measurable pressure range. Since the dynamical range of the sensing device under consideration is quite wide (more than two orders of magnitude), the combination of colors with numbers could also be explored to indicate pressure intensity at a given spot. For instance, a more refined extension of a color isoclinal display format could be that a given color indicates a certain pressure range and the number coded in that color indicates the level of pressure within that pressure range. In this case, the numbers could be restricted to a few, for instance from 1 to 9, since yellow 9 could be equivalent for instance to 9 oz. pressure, green 9 to 19 oz., red 9 to 29 oz., and so on. Figure 10 shows the sketch of a tactile sensor graphic display concept. In References 6 to 8 alternative schemes and techniques are described for tactile sensing displays.

Sensing the slip of an object on the surface of the finger due to insufficient grasp force (that is, sensing a tangential force acting on the surface of the mechanical finger) can be accomplished by direct and indirect means. An indirect sensing concept can be based on monitoring changes in the area distribution of pressure patterns sensed by a multipoint tactile sensor. An appropriate pattern recognition scheme could even indicate the mean direction of slip relative to the contact surface. The display of slip can easily be incorporated into the graphic display format of tactile sensing by using an arrow referenced to the contact surface. The orientation of arrow would indicate the direction of slip.

If the sensing of slip is accomplished by direct means (that is, by using a slippage sensor), the information display can be based on the rotating bar or rotating arrow concept shown in a graphic display screen. The length of the bar or arrow could indicate the rate of slip since direct sensing of slip can also provide information on the slip rate. Several slip sensor concepts are currently under implementation at JPL. Figure 11 shows an LED display of a directional slip sensor breadboard model under development at JPL. The display indicates sixteen directions in equal angular increments on a full circle.

VI. Integrated Displays

Integrated display of information generated by sensors attached to the terminal device of a remotely controlled manipulator can be considered in two stages. In the first stage the concern and task are the integration of proximity, force-torque, tactile and slippage sensor information within a given graphic display frame. In the second stage, the problem and goal are the integration of graphic display of the above quoted multisensor information with and/or within the picture of a TV display frame. Since not all sensor information may occur simultaneously in all cases, the integration scheme can be based on a "call" concept controlled by the operator.

The design of integrated display formats is under development at the JPL teleoperator program. Preliminary format concepts are shown in Fig. 12. Consideration is also given to the human factors relevant to the design and integration of audio and graphic displays for sensor information which is basically non-visual in nature. The development of various visual and non-visual displays is to be followed by a program of evaluating the utility of the displays in the performance of remote manipulation within the context of a supervisory control system, employing several test persons.

VII. Conclusion

The display of information generated by non-visual sensors attached to the terminal device of a remotely controlled manipulator is a relatively new area of research and development. In fact, even the development of the relevant sensors is a relatively new endeavor. Preliminary experiments at JPL have shown the utility and limitations of a few audio and visual display schemes employed for proximity sensors. In particular, it has been shown that appropriate graphic displays can substantially increase control performance in accuracy and time. However, considerable work is ahead before the development of visual and non-visual displays of non-visual sensor information for manipulator control will reach a high level of maturity.

References

1. Bejczy, A. K., "Effect of Hand-Based Sensors on Manipulator Control Performance", to appear in a special issue of Mechanism and Machine Theory, (1977).

2. H. P. Van Cott and R. Kinkade (editors), "Human Engineering Guide to Equipment Design", Handbook, U. S. Government Printing Office. 0-414-256 (1972).

3. Johnson, A. R., "Optical Proximity Sensors for Manipulators", JPL TM 33-678, (1974).

4. Bejczy, A. K., "Issues in Advanced Automation of Manipulator Control", Proceedings of the 1976 Joint Automatic Control Conference, Purdue University, W. Lafayette, Indiana, July 27-30, 1976.

5. Groome, R. C., Jr., "Force Feedback Steering of a Teleoperator System", MIT Draper Lab. Report T-575, August 1972.

6. Strickler, T. G. III, "Design of an Optical Touch Sensing System for a Remote Manipulator", MIT Dept. of Mechanical Engineering SM Thesis, 1966.

7. IEEE Transactions on Man-Machine Systems, Special Issue on the Tactile Display Conference, SRI, Menlo Park, California, April 1969, IEEE Report Volume MMS-11, No. 1, March 1970.

8. Hill, J. W., Bliss, J. C., "Tactile Perception Studies Related to Teleoperator Systems", Final Contract Report NAS2-5409, Stanford Research Institute, Menlo Park, California, June 1971.

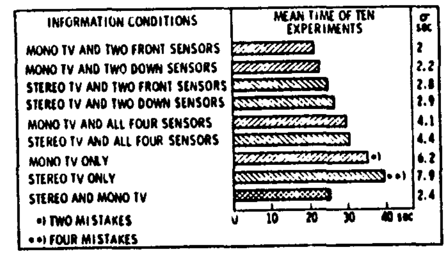

TABLE 1 Performance data for combined use of visual and proximity sensor audio information

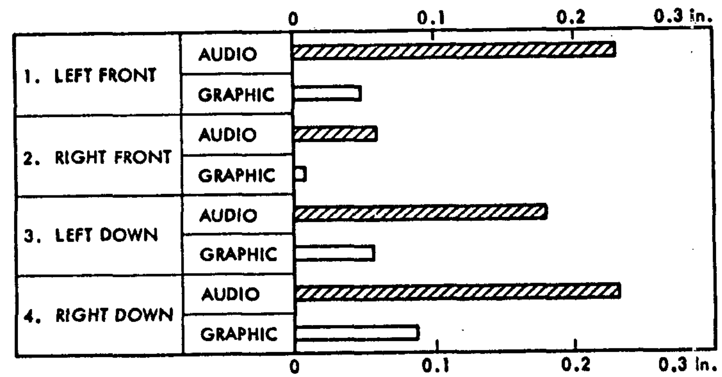

TABLE 2 Performance data for comparing utility of audio display versus graphic display of proximity sensor data. (Bars show difference between requested and actual positioning accuracy for ten experiments.)

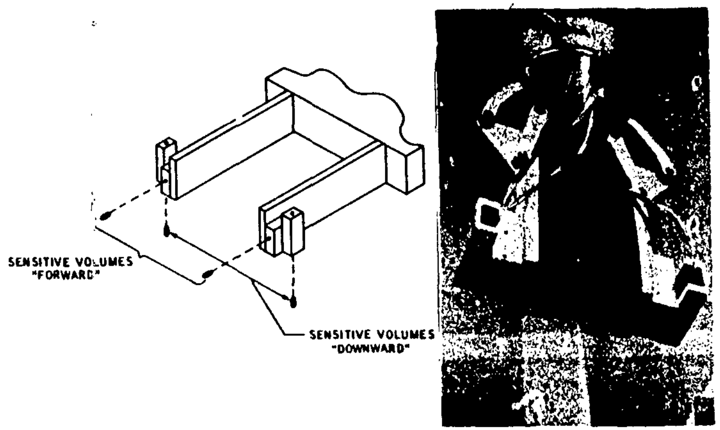

FIGURE 1 Four proximity sensors on parallel jaw terminal device.

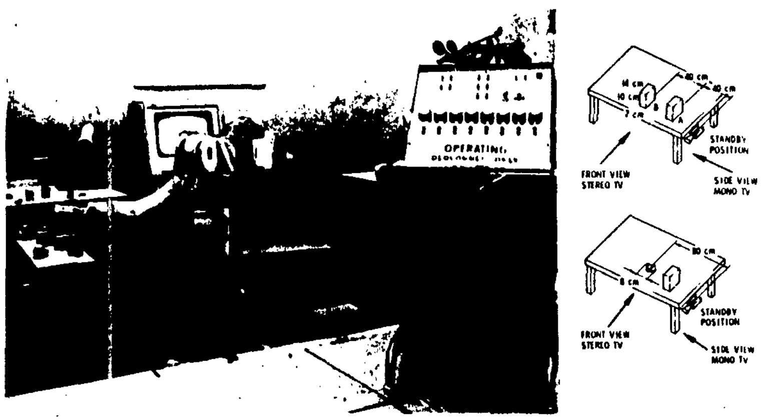

FIGURE 2 Task arrangements for proximity control performance tests.

ORIGINAL PAGE IS
OF POOR QUALITY

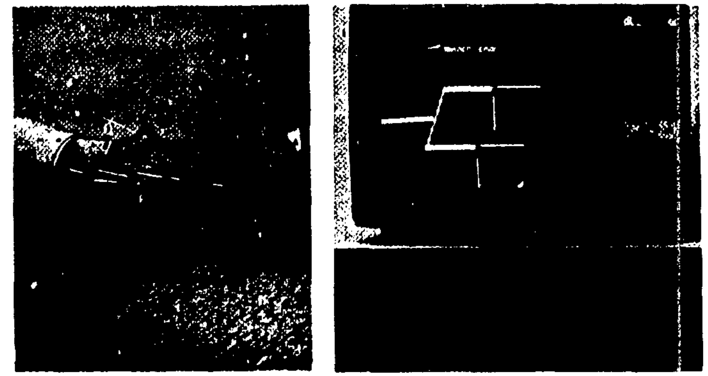

FIGURE 3 Graphic display of information from four proximity sensors

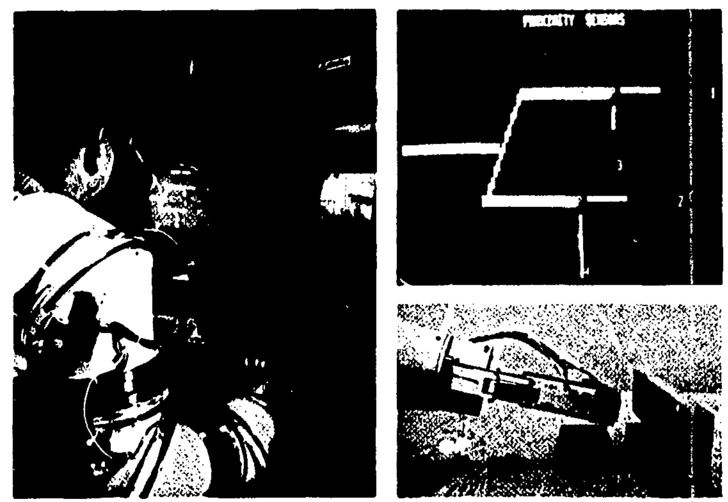

FIGURE 4 Operator working with graphic display of proximity sensor information.

a.

b.

c.

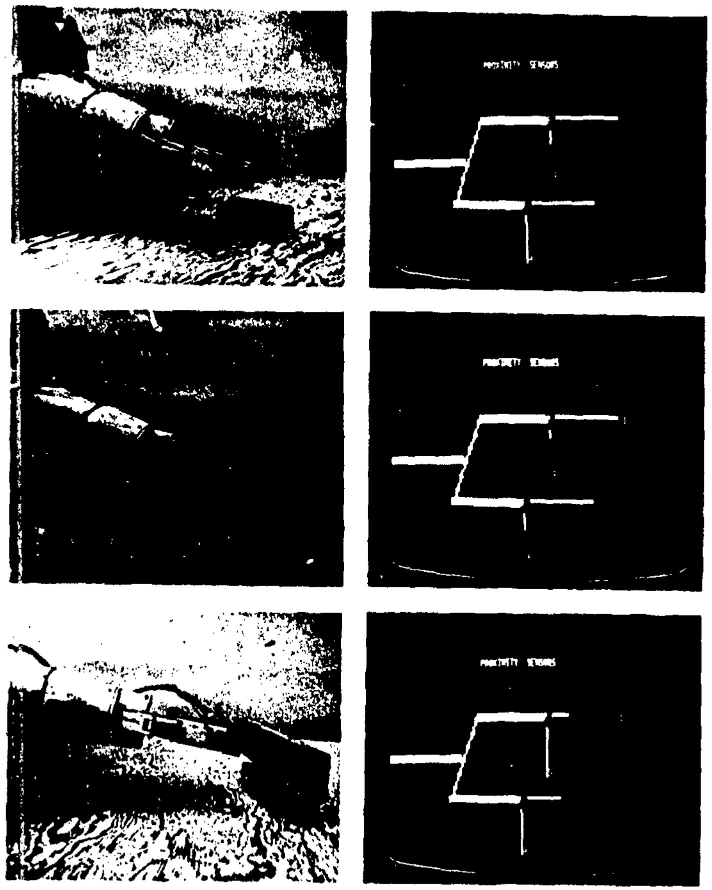

FIGURE 5 Different proximity scenes on graphic display.

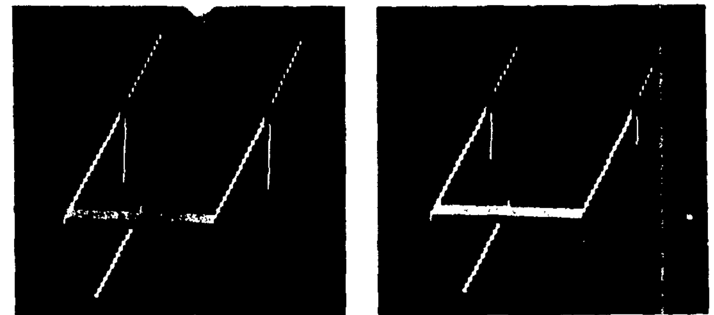

FIGURE 6 Graphic display of proximity sensors information in left-forward perspective.

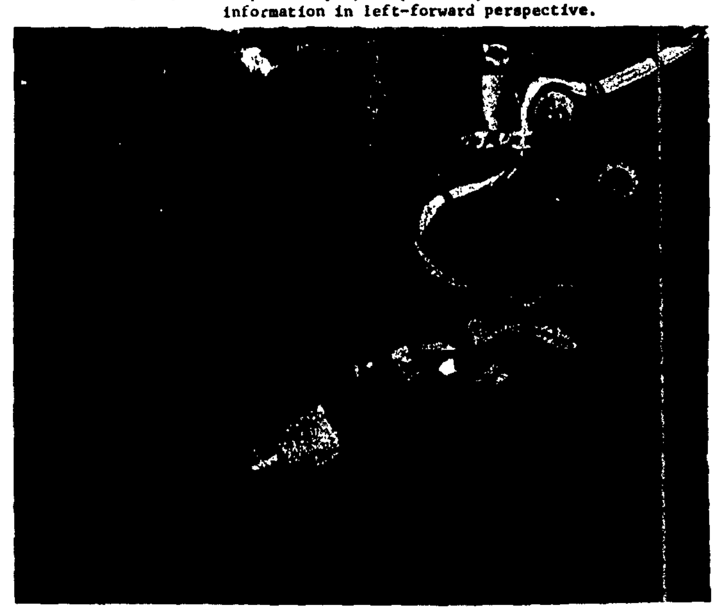

FIGURE 7 Force-torque sensor on JPL CURV arm.

ORIGINAL PAGE IS
OF POOR QUALITY

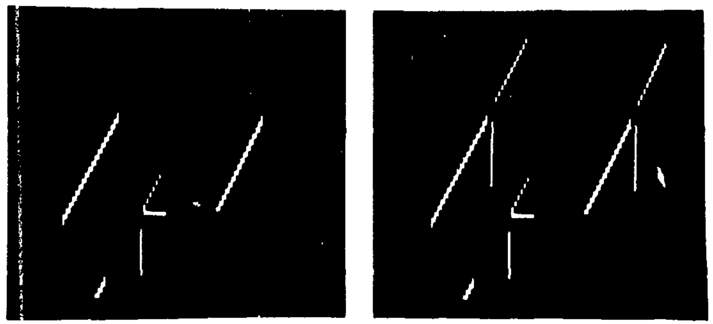

FIGURE 8 Preliminary formats for graphic display of force-torque sensor information alone and combined with proximity sensor information.

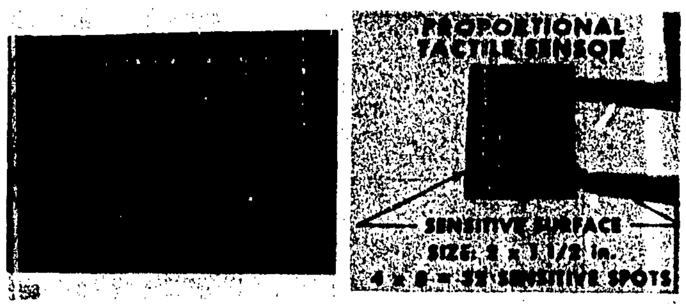

FIGURF 9 Tactile sensor breadboard with visual display.

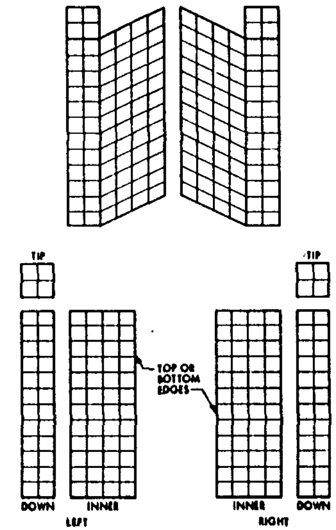

FIGURE 10 Tactile sensor graphic display concept.

FIGURE 11 Directional slip sensor breadboard display.

ORIGINAL PAGE IS
OF POOR QUALITY

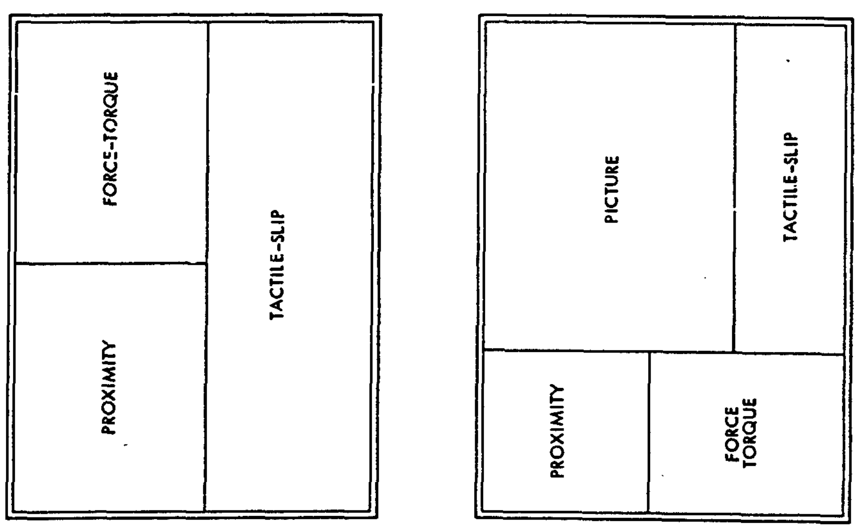

FIGURE 12 Integrated display concepts.

N79-17503

THIRTEENTH ANNUAL CONFERENCE ON MANUAL CONTROL

M.I.T., Cambridge Mass., June 1977

Informal Discussion

Multi-axis Hand Controller for the Shuttle Remote Manipulator System

Andrew L. Lippay, Staff Engineer, Manned Systems
CAE Electronics, Montreal, Canada

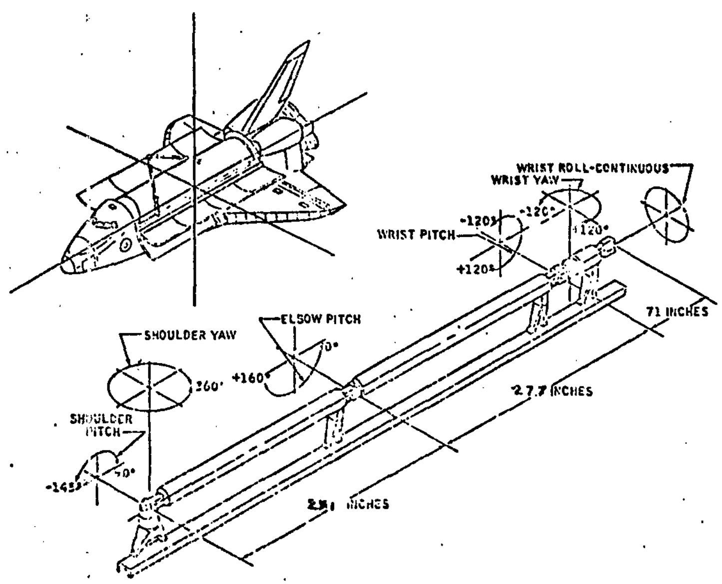

INTRODUCTION

The Shuttle Remote Manipulator System (SRMS), a Canadian contribution to the NASA Space Program, has an articulated arm of 50 ft. length with six motor-driven joints. The basic purpose is to establish physical contact with various space hardware items and maneuver these to the desired position and attitude with respect to the Orbiter, nulling out relative velocities and stabilizing the free-body system by managing residual energies.

The normal operating mode is resolved-motion end-point rate control by man-in-loop command. The translational freedoms are defined so that the End Effector (EEFTR) of the arm will move in planes parallel to the principal translational planes of the Orbiter, at a rate commanded by the displacement of the Translation Hand Controller (THC) in the corresponding freedom and direction. The rotational freedoms are rate-controlled by the Rotation Hand Controller (RHC) about pivot axes parallel to Orbiter roll, pitch and yaw, originating at the EEFTR reference point. Both sets of coordinates may be transposed to the EEFTR or to the mass/geometric center of the Payload, by appropriate software selections and adjustment, following which the freedoms will be defined by the EEFTR or Payload attitude with reepect to the Orbiter.

The THC and RHC form a bi-manual controller complex with six individual axes of freedoms, each of which may be displaced individually or in any combination to effect coordinated (vectorial) movement. The system depends on computer augmentation for end-point control and for semi-automatic and fully programmed sequences selectable by the Operator. Joint-by-joint control is available with computer support and by a hard-wired direct manual control system provided to permit the orderly termination of a mission under contingency conditions. The THC and RHC are not utilized in the joint-by-joint mode.

Weight and envelope constraints limit the manipulator arm strength to 10 lbf applied to the EEFTR at right angles. Fully extended, the arm will then deflect 1.0 in. The largest planned Payload has a mass of 65,000 lb in a 60 ft long 15 ft diameter envelope. Structural modes of the loaded arm will permit Payload movement at rates and accelerations similar to those caused by the arm responding to drive inputs. Clearances in the Cargo Bay are .. the order of 3.0 ins. Most of the larger Payloads will have complex contours and appendages easily damaged by even a light collision with the arm or the Orbiter. The Orbiter itself will be unable to land if one of its Cargo Bay door hinges is damaged and will burn up on re-entry if one of its ceramic tiles is cracked. All of this indicates that smooth, coordinated and transient-free operation of the SRMS is an essential requirement.

The development effort and manned test results carried out to date to produce a Translation Hand Controller suitable for this task will be the topic of this discussion.

28

CRITERIA & CONSTRAINTS

It is a well-known fact that each new manual control application has its own characteristic requirements and that the controller must typically be unique and compatible with the particular system and its task, in order to achieve proper functional matching at the man-machine interface. The problem is not so much that of providing the various components that will generate the necessary inputs for the machine, as it is one of packaging them into a device that can be operated as a comfortable hand tool in spatial harmony with the overall system task under all conditions, and that will generate proprioceptive feedback to instill confidence and to enable the human sensory system to be convincingly projected into the task area, with an acceptable workload. Rigorous system identification and elegant mathematics frequently overshadow the importance of the basic physical and handling qualities of the hardware in direct contact with the human neuromuscular channels, and only the great adaptive capability of the operator enables him to compensate for these imperfections and still predict system response.

Orbiter cockpit layout, size and weight constraints have defined many of the design parameters from the start. The THC envelope was not to exceed 6 x 4 x 4.5 inches. This and limitations in weight and available computational capacity ruled out an active force feel feedback system. (Development of a single-input-point command device was denied as a high schedule and design risk item.) The THC-RHC complex must be operable by 5th percentile female to 95th percentile male Crewmembers. All will be elevated to the same design eye point approximately in line with the center of the aft window. Configuration "G" of a NASA-JSC study of controller locations places the THC near shoulder height and some 11 inches left of the body centerline. This is currently used as a baseline.

Conceptual design specifications required a ± 2.0 ins or arc-ins travel on each axis for adequate manual resolution. From previous experience, a deflection-type action was preferred to a force-stick. Input rate limiting (damping) was to be generated by the THC rather than by electronics further downstream, in order to preserve tactile feedback. Springloaded return to zero was required, so it was decided to initially set the maximum rate-dependant resistance equal to the maximum deflection-dependent forces, the sum never to exceed 10 lbf in view of the weightless operator. The spring system was to be preloaded to provide a breakout step force and identify the null point on each axis. A detent cartridge has been designed but not tested so far. All of the above was based on best estimates of system characteristics and on maximum permissible energy transfer through the arm, since no valid model existed at the time. In order to enhance display dynamics and facilitate predictive control, a quickened command/actual display was proposed, but this became impracticable when the rate meters were deleted from the SRMS panel design.

Rate-dependent damping was seen as the most appropriate passive means of generating input rate feedback, force feel, static and motional stability. Viscous dampers offered acceptable unit size for the force levels, convenient adjustment and freedom from the very objectionable stick-slip characteristics of other friction devices. Viscous damping in manual controllers is by no means new, but some unexpected observations will be related here.

TEST OBJECTIVES & APPROACH

A THC Demonstration Model has been built by CAE Electronics in Montreal to verify that adequate mechanical design and handling qualities can be contained in the envelope specified, and to set the initial force feel variables. Design recommendations would then be made based on manned testing.

The Model was equipped with a T-bar handgrip, vertical at first and rotated to horizontal for the final tests. The Hand Pressure Point (HPP) was defined as the intersection of the stem with the T-bar and all travels and forces were referred to this point. Angular displacements of ± 12 deg or ± 1.0 arc-ins constituted the vertical (Z-axis) and the lateral (Y-axis) freedoms. The X-axis was mechanized as a ± 0.55 in linear displacement, the maximum permitted by the enclosure.

Control laws of the SRMS and a task presentation software were inserted in a real-time digital facility associated with the SRMS modelling and software development effort at CAE. A kinematic model of the arm was lagged by arbitrary time constants of 3.0 sec in all axes to approximate dynamic behaviour of the loaded EEFTR. The task software was designed to drive or position a target, to accept command inputs and move a cursor symbol, EEFTR and to calculate vectorial and partial error (X, Y, Z) and partial rates on line. The resulting tracking task was presented to the Test Operators on a 23 in CRT as two triangular symbols of different color. The target moved vertically, laterally, rotated to represent Orbiter-referenced roll, and varied in size according to its computed distance to the observer, all within the geometry of the Orbiter Cargo Bay.

Positioning, rate-tracking and trajectory-control task modules were developed, totaling more than sixty, designed to elicit single-, two-, or three-axis inputs from the Operator, i.e., exercise the hand controller in any axis or combination desired, from full-scale maximum-rate displacement to minimum amplitude precision adjustments. Quick-stop maneuvers were included to simulate an error in the original estimate of the target position or trajectory. The roll axis was also available but seldom used since the available Apollo ACA and a breadboard RHC model were not representative of the SRMS requirements. Wherever possible, the task simulated events and controller activity expected to be seen in SRMS missions.

Performance data were collected on disc and recorder hard copy, showing the command activity in each axis, the vectorial error and its time integral. No statistical analysis was performed since the basic objectives could be achieved by inspection and debriefing, but full performance analysis will be executed probably following SRMS system integration.

The Operator, the THC Model and the Task Display were enclosed in a darkened cubicle with reasonable isolation from external noise and disturbances. A simple set of blocks was used to elevate their eyes to the center of the CRT serving as the aft window. The THC handgrip and the (inactive) RHC were installed in representative positions according to NASA Configuration G, the latter used as a hand positioner.

RESULTS & CONCLUSIONS

Two Test Operator groups consisted of one 5th percentile female, a medium and a tall male subject each. The females had little or no man-machine experience, the males were familiar with the SRMS and its tasks. Two had had previous practice during the shakedown trials, the other two had extensive control experience in aircraft and flight simulators.

Sixteen tests were conducted with the initial force settings. Eleven tests, essentially repetitions of the above were performed with the dampers disconnected. Five further tests had the T-bar handgrip oriented horizontally and the damping set at 50% of the initial value. Each data run was repeated three times. Operators were immediately debriefed by discussing the command traces and having them explain their strategies, difficulties and general assessment of the task and controller. This method produced meaningful information in quantity and identified patterns of agreement.

Operators reported the visual presentation to be reasonably convincing, and produced consistent and repeatable results, despite the very simplistic symbolic imagery. The dynamics seemed to be more important, as was to be expected. Some visual problems did exist, e.g. poor depth perception at 50-55 ft range, due to the increase/decrease of image size being a step function of the CRT raster line dimensions, but similar difficulties will exist in real life due to optical effects.

Spatial correspondence was good, very few starting errors were noted. The two angular freedoms were used simultaneously by instinct, and were reported to have sufficient travel, good positional feedback and little tendency to unwanted inputs. Rotating the handgrip to horizontal relieved the tensions at the wrist without affecting this assessment, but removal of the damping degraded the perception of the null position. The latter was an observation not encountered before.

The fore-aft (X-axis) travel was found marginally insufficient and the spring forces (2.4 lbf for full scale) created a tendency to drift, especially with the damping removed. Operators tried to establish a finger reference point by touching the casing or the gimbal sleeve with their middle- and index fingers. A two-ring finger fixture will be added as a design improvement. The experienced operators would have preferred a detent-type null identification with damping.

Command traces show typical patterns for male, female, expert and novice Operators almost to the point where individuals could be identified by their command signatures and error performance patterns. The experienced Operator applied coordinated inputs in all required axes and proceeded to reduce the vectorial error in a straight-line fashion even when the target was unexpectedly moved. The female subjects tended towards a bang-bang method with high peaks, especially when making small adjustments with low amplitudes. Cross coupling was more evident than with the males, but the traces identified this as a result of their shoulders being as much as eight inches out of line with the controller, making orthogonal movements difficult. All operators were required to keep their right hand on the RHC as a hand positioner. The undamped controller induced more cross-coupling and bang-bang inputs in all operators.

A consistent coasting approach was developed with the lagged positioning tasks, as a learning effect. The cursor was accelerated vectorially towards the target, then the commands were nulled so as to arrive at a point corresponding to eight feet from the "Payload Grapple Point". Small additional inputs were then used to cover the target, the experienced males using coordinated displacements, the females tending to small spikes. When asked to use a minimum of time, Operators maintained the rates longer, then applied counter-commands to assist in the deceleration. This has not been validated as an acceptable command strategy but harmonious and instinctive use of the THC was again indicated.

Some inter-controller coupling has been noted, mainly due to the wide separation of the THC and RHC, as shown by the case of the small percentile female Operators. This will be further explored as soon as an engineering quality RHC becomes available, but controller force patterns are expected to provide an adequate solution, in the light of the following discussion.

Operators agreed that the handing qualities, and particularly the rate-dependent damping was a key factor in their assessment and use of the controller. The command traces show more coordinated (vectorial) inputs, less cross-coupling and overshoots, and generally less command activity with the damped controller. On-line voice-taped comments and debriefings proved this to be more than the physical restraining effects of the viscous friction; operators commented on the static and motional stability, reported a more

confident approach to the estimated inputs required, and consequently produced less hunting and overshoots. They even claimed to derive positional information from the damping resistance, not attainable from spring forces alone, which is surprising in view of the low levels used, but which explains the reduction in drift and improvement in long-term maintained inputs. From the systems point of view, a marked reduction of transients, and better coordination in at least two axes were the most significant results ascribed to the controller handling qualities.

RELEVANT OBSERVATIONS

When assessing controller forces, Operators are not aware of the difference between spring rates and damping as such, but their remarks and command behaviour indicate the effects related to each. Generally, low forces are preferred, especially by the female subjects, but all agree that some damping is necessary for stability and force feel. With the short travels typical of the sidearm controller family, spring rates do not yield adequate information on deflection, and tend to cause drift as the haptic receptors accommodate to the stick pressures. The SRMS requirements, except for the hands-off return to zero, could probably be satisfied with hand controllers having optimized rate-dependent forces and adequate null identification (detent or electronic notch.). Adjustment of such a system is far more convenient than replacing the special springs normally found in hand controllers. Individual operator preferences and wide variations in the task dynamics, Payload mass etc. could be accommodated this way even by a passive system.

The command behaviour of the small-frame lightweight subjects in unity gravity, i.e. a tendency to spiky inputs and bang-bang modes, may well be indicative of future problems with lightly restrained Orbiter Crewmembers in zero gravity. Photo exhibits at NASA-JSC show a Skylab Astronaut holding onto a countertop with one hand, wrapping three fingers of the other around the base of a lollypop-type controller while deflecting it with thumb and index finger against spring tension. The SRMS Operator will be restrained at the feet and probably at the waist, but will need to use both hands, often simultaneously, on a number of controls in a coordinated manner. Force patterns will again yield essential feedback.

When the T-bar handgrip of the THC was rotated from the vertical to the horizontal, the lateral axis suddenly became "too sensitive", although no parameters related to stick gain have been altered. In retrospect, the horizontal grip required arm movement as against wrist deflections, and produced less position feedback than the vertical grip. Operators applied excessive inputs and saw excessive responses. A similar effect in reverse can be observed in flight simulators where the (purposeful) degradation of the motion cues brings complaints about the control forces being too heavy, when in fact the response has been made inadequate. During this period the dampers of the THC have been disconnected and the spring forces could not generate the expected resistance. In the other two axes the Operators used fingertip touch and wrist deflections, and were able to compensate for the lack of damping, but complained of "white knuckles" effort to stabilize the handgrip.

The comments of the Operators reacting to the task presentation and to questioning by the Test Conductor strongly support the concept of an "inner model" whereby an active picture is developed of the task and the system, probably at a high cranial level. This fast-running model responds to all sensory inputs and generates outputs in an outer-loop fashion, involving complex pattern recognition and predictive processes. The system outputs or controlled variables must then display corresponding behaviour as expected, to match the model. The same phenomenon is very much evident in observations involving pilot assessment of flight simulators, various man-machine combinations and the control and acceptance of powered artificial limbs. In the latter case, the concept of "body image" is widely recognized in physical medicine.

It appears that dynamic effects, especially in the short term, are particularly significant in satisfying the expectations of the inner model; pictorial details and accuracy are of secondary importance. (However, motion-visual relationships and phasing are critical, such as in the case of whole-body and vestibular motion cues.) The haptic proprioceptive sensors can derive direct and significant information from the dynamic handling qualities of the hand controller and enhance the integration of man and machine.

N79-17504

THE DEVELOPMENT OF A SIX DEGREE-OF-CONSTRAINT ROBOT PERFORMANCE EVALUATION TEST

by

David A. Thompson
Department of Industrial Engineering
Stanford University
Stanford, California

ABSTRACT

A remote manipulator performance evaluation test was developed jointly by Stanford Research Institute and NASA Ames Research Center to test certain tool mating configurations not possible with the standard peg-in-hole type of test. The test attempted to evaluate robot manipulator (the Ames Arm) performance over a full range of six degrees of freedom of motion between a tool and its intended receptacle. The test consists primarily of four different tool geometries and three different receptacle geometries which provide for a progressive reduction in the degrees of freedom of motion, and a progressive increase in the degrees of constraint (DOC) over motion, between the tool and the receptacle. The manipulation times of actual tools (wrenches, screwdrivers) and couplings would be predicted by the times for the test tool most like it geometrically (with appropriate time allowance for the actual mating clearance). In addition, the influence of four different transmission delays was tested. The results indicate that tool manipulation time can vary by a factor of about four depending on the degrees of constraint over final tool positioning. The effect of transmission time delay is independent of the degrees of constraint and increased manipulation times for all DOC's by as much as an order of magnitude for a 3-second delay.

Thirteenth Annual Conference on Manual Control
Cambridge, Massachusetts, June 15-17, 1977

THE DEVELOPMENT OF A SIX DEGREE-OF-CONSTRAINT
ROBOT PERFORMANCE EVALUATION TEST

David A. Thompson
Department of Industrial Engineering
Stanford University
Stanford, California

A remote manipulator performance evaluation test was developed jointly by Stanford Research Institute (Hill, 1976) and NASA Ames Research Center to test certain tool mating configurations not possible with the standard peg-in-hole type of test.

The test attempted to evaluate robot manipulator performance over a full range of six degrees of freedom of motion between a tool and its intended receptacle. The test consists primarily of four different tool geometries and three different receptacle geometries which, in the combinations illustrated in Figure 1, provide for a progressive reduction in the degrees of freedom of motion, and a progressive increase in the degrees of constraint (DOC) over motion, between the tool and the receptacle. The manipulation times of actual tools (wrenches, screwdrivers) and couplings would be predicted by the times for the test tool most like it geometrically (with appropriate time allowance for the actual mating clearance).

The test was then run using the "Ames Arm" -- a standardized teleoperator manipulator which utilizes remote viewing through a stereo TV link. The tools were moved approximately eight inches from a "START"

D29

electrical contact to be positioned and inserted into one of the three shaped openings as appropriate. Separate times were recorded for the time from START to the first contact with the opening (TRANSPORT) and from first contact to a one inch insertion (POSITION and INSERT) into the opening. Four subjects performed five trials of each of the six degree-of-constraint tests, for each of the four transmission delays arranged in a latin square design. The resulting data are the mean performance times averaged over all trials of all subjects for each degree of constraint for each transmission delay.

The mean times for the complete motion (TRANSPORT + POSITION + INSERT) are shown in Figures 2 and 3. Figure 2 shows the effect of signal transmission delay on manipulation time for each of the six degrees of constraint, and Figure 3 shows the effect of various degrees of constraint on manipulation time for each of the four levels of transmission delays.

The results indicate that tool manipulation time can vary by a factor of about four depending on the degrees of constraint over final tool positioning. Therefore, this is an important characteristic to consider in evaluating remote manipulation performance.

Interestingly enough, the effect of transmission time delay is independent of the degrees of constraint. A 1/3-second delay results in manipulation times roughly twice as long as no delay, a 1-second delay produces manipulation times about four times as long as no delay, and a 3-second delay causes an order of magnitude change in manipulation times compared with no delay. Studies are continuing to develop a predictive display to offset the pervasive effect of the time delay on manipulation times and accuracies.

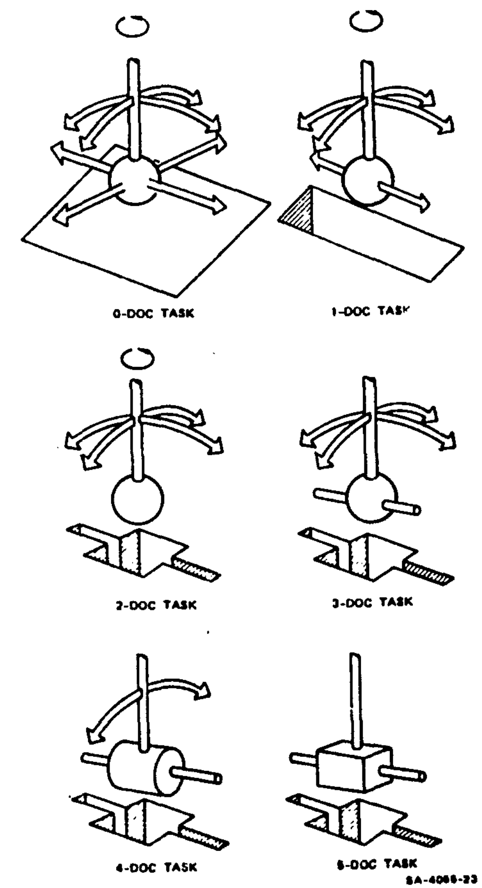

FIGURE 1: SIX TASKS FITTING TOOLS INTO RECEPTACLES

REFERENCE

Hill, J. W., "Study to Design and Develop Remote Manipulator Systems" Annual Report 1, Contract NAS2-8652, SRI, Menlo Park, CA, July, 1976.

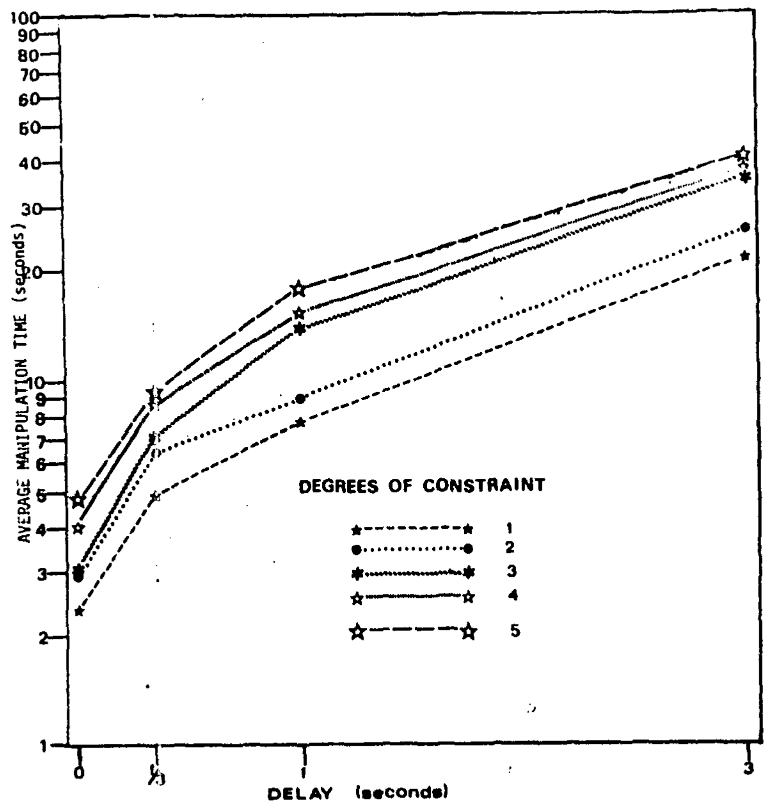

FIGURE 2: Remote Teleoperator Manipulation Time.
The average manipulation time for all 5 subjects as a function of the transmission delay is shown for each of the degrees of constraint over positioning the tool in the workplace receptacle. Manipulation time includes transport to the workplace, positioning, and inserting the tool in the receptacle.

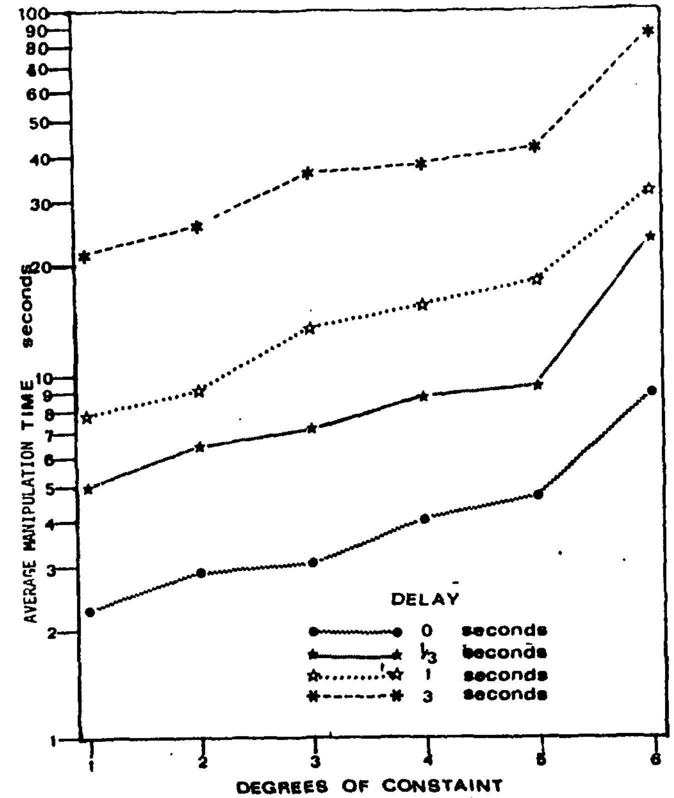

FIGURE 3: Remote Teleoperator Manipulation Time.
The average manipulation time for all 5 subjects as a function of the degrees of constraint over the final tool positioning is shown for each of the transmission delays. Manipulation time includes transport to the workplace, positioning, and inserting the tool in the receptacle.

N79-17505

Prosthetic EMG Control Enhancement Through the Application of Man - Machine Principles

W.A. Simcox
Tufts University
Medford, Mass.

J.G. Kreifeldt
Tufts University
Medford, Mass.

An area in medicine that appears suitable to man-machine principles is rehabilitation research, particularly when the motor aspects of the body are involved. If one considers the limb, whether functional or not, as the machine, the brain as the controller and the neuromuscular system as the man-machine interface, the human body is reduced to a man-machine system that can benefit from the principles behind such systems.

The area of rehabilitation that this paper deals with is that of an arm amputee and his prosthetic device. Reducing this area to its man-machine basics, the problem becomes one of attaining natural multiaxis prosthetic control using Electromyographic activity (EMG) as the means of communication between man and prothesis.

In order to use EMG as the communication channel it must be amplified and processed to yield a high information signal suitable for control. The most common processing scheme employed is termed Mean Value Processing. This technique for extracting the useful EMG signal consists of a differential to single ended conversion to the surface activity followed by a rectification and smoothing as shown conceptually in Fig. 1.

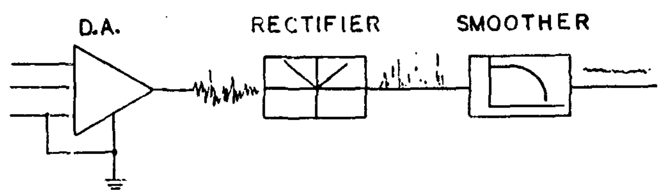

Figure 1 - Mean Value Processing

Raw EMG is a complex bidirectional wave form, that if averaged over time yields a zero mean value. If constant muscle tension is to be maintained under a constant force isometric contraction the information content of the EMG describing the contraction should ideally be a constant DC voltage. If the bidirectional waveform results with a DC component produced. As the contraction level increases and decreases so will the mean value producing both a DC and low frequency component (1). The low pass filter is used to extract the mean value and low frequency components while attenuating the high frequencies present in the unidirectional waveform.

The output of the smoothing filter bears a monotonic relation to contraction effort in steady state. However, the output has a noise superimposed on it, similar to unrectified EMG, that increases with increasing contraction. A theoretical model shows that this increasing noise must be the case for linear low pass filtering of rectified EMG (2).

The nature of this superimposed noise is shown in Fig. 2. The figure illustrates that rectification not only introduces the DC value but also a low frequency component and harmonics of that component. The use of the low pass filter to extract the DC value is clearly evident in the figure.

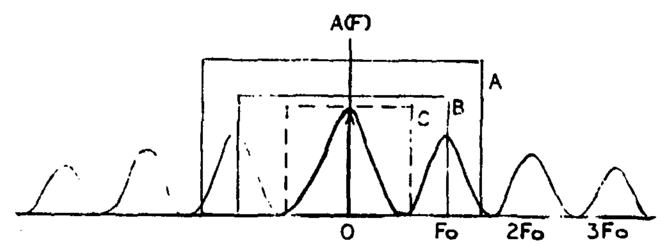

Figure 2 - Effects of Rectification on Myoelectric Activity

One way to reduce this noise is by decreasing the bandwidth of the filter which increases the amount of smoothing. But by doing this the system's step response deteriorates introducing a more pronounced exponential time lag leading to a sluggish system response. Control of sluggish systems is characteristically difficult for humans because of the time lag in the feedback of information between the user's control action and the system response.

D30

Studies in controlling inherently sluggish system (3,4) suggest that a technique based on feedback of predicted as well as instantaneous device behavior allows these highly uncontrollable systems to be controlled quite easily. Studies indicate that control using this technique is highly natural in that very little training, attention and concentration is required to achieve the quality of control which would otherwise be very difficult or impossible. Therefore, the detrimental characteristic of sluggish response is prosthetic control caused by the large amount of smoothing needed to yield a high information EMG control signal can be greatly reduced if predictor feedback technology is introduced. It should be noted that predictor technology works best on sluggish systems that are used in a self-paced manner - a characteristic of EMG controlled devices with a high degree of smoothing of the EMG activity. Thus the otherwise apparently detrimental characteristic to produce a "clean" EMG control signal becomes a key element for imperfection of predictor techniques in feedback control.

A research investigation was undertaken to determine the suitability of visual predictive feedback technology in controlling a simulated two axis assistance device. Specifically, two major hypothesis were addressed.

1) The work will provide basic information on a new approach to information feedback for EMG control of assistance devices. If this approach is successful as anticipated, the goal of simultaneous coordinated EMG control of a multi-degree-of-freedom device from several EMG activity sites will be much closer.

2) The application of predictor technology to EMG control may also cut through the apparent impass of the smoothing - sluggishness relationship which governs simple EMG signal processing by utilizing this relationship as a beneficial rather than detrimental subsystem characteristic.

In addition to these two major hypotheses a subjective assesment of predictor technology for this specific type of control was addressed.

The dynamincs of the artificial device used to developthe simulated predictor equations were obtained from the EMG controlled "Boston Arm", a prototype of which is located at the Liberty Mutual Research Center, Hopkinton, Massachusetts. The "Arm" is a single degree of freedom prosthesis that can be controlled by above elbow amptuees using electromyographic signals from the biceps and triceps. A block diagram of the "Arm" electronics is shown in Figure 3. The procedure for obtaining the dynamics was as follows:

Neglecting the preamplifiers, since a specific preprocessing technique was used, two input voltage steps of 1.5 and 2.5 volts were applied to the summer input. The response was obtained from the techometer output yielding the system's impulse response. Figures 4 and 5 show the ouput velocity for the input steps introduced. The dynamics derived from the 1.5 volt step are used for the X direction with the derived dynamics from the 2.5 volt step used as the Y direction with the derived yielding a two-axis device dynamics. The figures suggest a simple arm model consisting of an integrate with an experimental time lag. The equation describing this simple model is:

$$\ddot{V}o + b\,\dot{V}o = a\,Vin \qquad (1)$$

where:

$$a = \begin{cases} .987 & \text{for 1.5 V input step} \\ .5.6 & \text{for 2.5 V input step} \end{cases}$$

$$b = \begin{cases} 1.48 & \text{for 1.5 V input step} \\ 5.6 & \text{for 2.5 V input step} \end{cases}$$

Equation (1) is the expression used to generate the predictor equations.

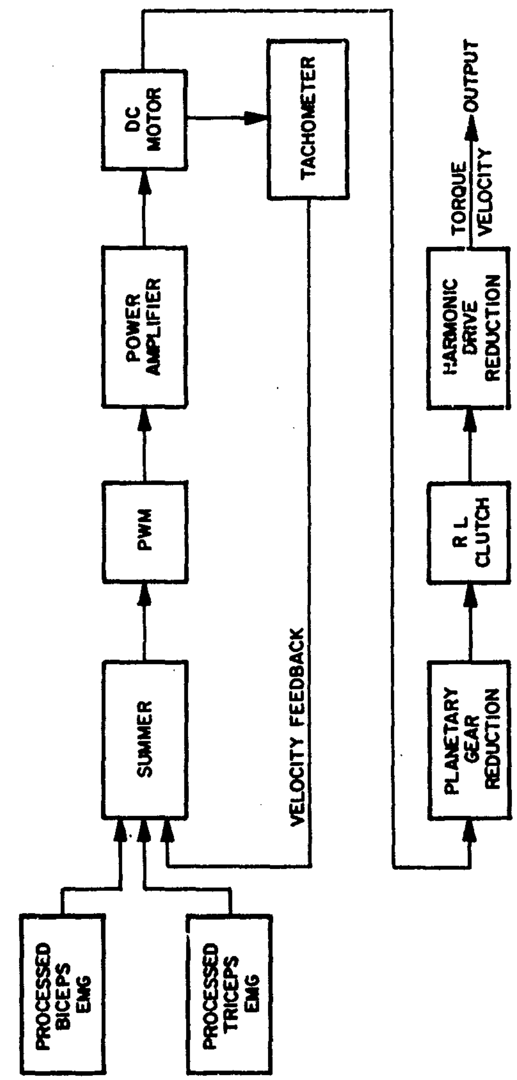

Figure 3 - Arm Block Diagram

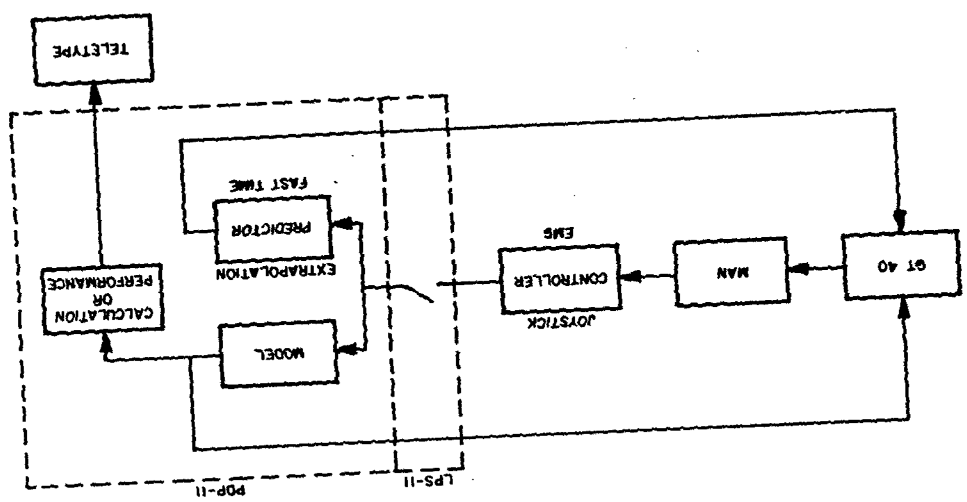

Figure 6 - Experimental Setup

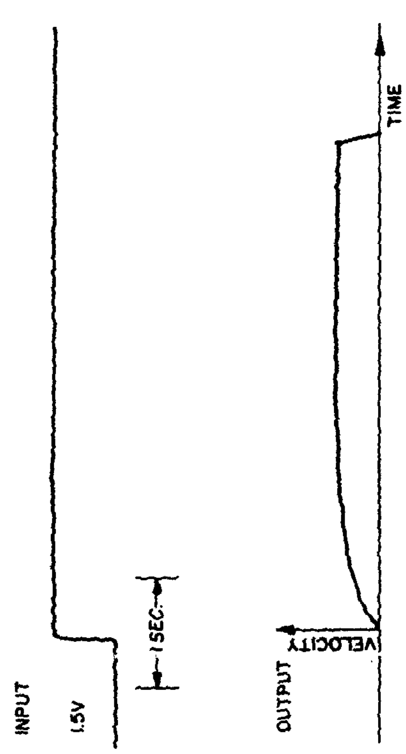

FIG.4 OUTPUT FOR 1.5 V INPUT

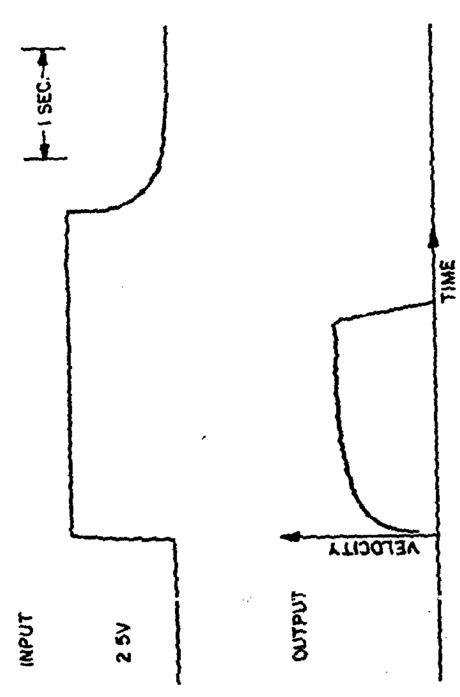

FIG.5 OUTPUT FOR 2.5 V INPUT

The instrumentation used in the investigation consisted of an X-Y potentiometer joystick (Measurement Systems model 521), four EMG processors, a PDP-11 computer with an LPS-11 peripheral interface and GT-40 graphics display (Digital Equipment Corporation).

The digital computer samples the EMG processor outputs, calculates the arm dynamic responses, the predictor information, calculates all the display elements and records the performance. A "BASIC" computer language program implements the software needed to perform these functions. Figure 6 shows a functional diagram of the experimental setup.

The task to perform was to move a cross representing the position of the "TRM" in two dimensions, with or without its predicted path, through one of three sets of randomly presented mazes to a final circle as typified by figure 7.

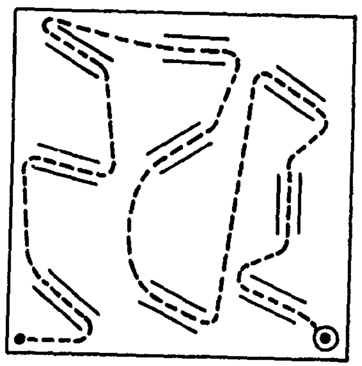

Figure 7 - Task Representatives

Each element of the maze was of equal length and width (1.59 x 1.09cm) and 6.3 cm apart from center to center. Only the randomly chosen orientation angles differed.

Subjects were instructed to move the cross as quickly and as accurately as possible going up the first column and down the second and third. If upon entering a channel the cross steps out of the boundary an error is recorded. At the end of each run the task completion time and task errors were recorded.

The combination of three prediction spans (P) of 0,1 and 2 seconds and two time constants (T) of 1 and 2 seconds made a total of 6 experimental conditions per subject. Two other experimental conditions, one using the joystick, a second prediction and 2 second time constant, the other using the joystick, 1 second prediction span and 1 second time constant were also included to provide baseline values. Therefore each subject had a total of 8 conditions per day.

Six subjects (normal males between the ages of 22 and 28) took part in the final testing phase using the following procedure. Electrodes were placed on the biceps and triceps of both arms. The right bicep controlled the +x direction while the right tricep controlled the -x direction. The left bicep controlled the +Y direction and the left tricep controlled the -Y direction. The subjects were presented with a randomly chosen control combination of prediction span, time constant and EMG or joystick and given five runs of each. The task completion time and errors were then recorded for the final two runs of each of the eight control combinations. In addition a special purpose circuit was constructed to measure the degree of simultaneous control. Upon completion of the experiment a short questionnaire was filled out by each subject.

Table I presents the data for the variables in this experiment, and Table II provides an analysis of variances found.

TABLE I

SOURCE	Task Completion Time (sec.)		Task Errors	
	MEAN m	STD. DEV.	MEAN m	STD. DEV.
1 SEC. SMOOTHING (Γ_1)	157.72	112.98	6.83	4.88
2 SEC. SMOOTHING (Γ_2)	205.64	125.38	7.22	6.17
PREDICTOR OFF (P_0)	282.17	116.03	12.08	6.55
1 SEC. PRED. (P_1)	114.23	61.05	4.33	2.02
2 SEC. PRED. (P_2)	128.19	65.84	4.66	2.76
SUBJECT 1	216.00	182.36	11.17	8.03
SUBJECT 2	194.75	64.31	8.17	3.09
SUBJECT 3	140.58	67.05	5.58	4.26
SUBJECT 4	203.92	85.23	6.92	4.92
SUBJECT 5	144.83	60.51	3.75	2.31
SUBJECT 6	189.50	74.99	6.58	5.69

TASK COMPLETION TIME

SOURCE	DOF	SS	MS	F	%MS	
PREDICTION SPAN (P)	2	367259	183629	17.3	39.4%	***
SMOOTHING (T)	1	41712	41712	8.8	5.3%	**
SUBJECT (S)	5	59247	11849	8.8	9.2%	***
PXT	2	39079	19539	2.5	5.7%	
PXS	10	106250	10625	7.9	12.4%	***
TXS	5	23614	4723	3.5	3.5%	**
PXTXS	10	76852	7685	5.7	17%	***
WITHIN ERROR	35	47249	1350		7.5%	
TOTAL	70	761265				

Table II

1) Task Completion Time: From Table I the task completion time increased with the smoothing time constant (p .05) but inspection of figure 8 indicates that when using the predictor, completion time is independant of the amount of smoothing. Without the predictor however, there is a 42% increase in task completion time for the more sluggish time constant which is to be expected. It has been shown that a two second time constant increases the signal to noise ratio approximately 90% over the one second time constant but the systems settling time increases causing a sluggish system response The use of the predictor completely offsets this problem.

Inspection of figure 8 indicates another very important result. In all cases using EMG control with the predictor, task completion times are lower than joystick or hand control using no predictor. It must be noted that the control combinations using the joystick were approximate estimates of best and worst conditions. Given this result a set of posteriori tests on means were performed using Duncan's multiple range statistic.

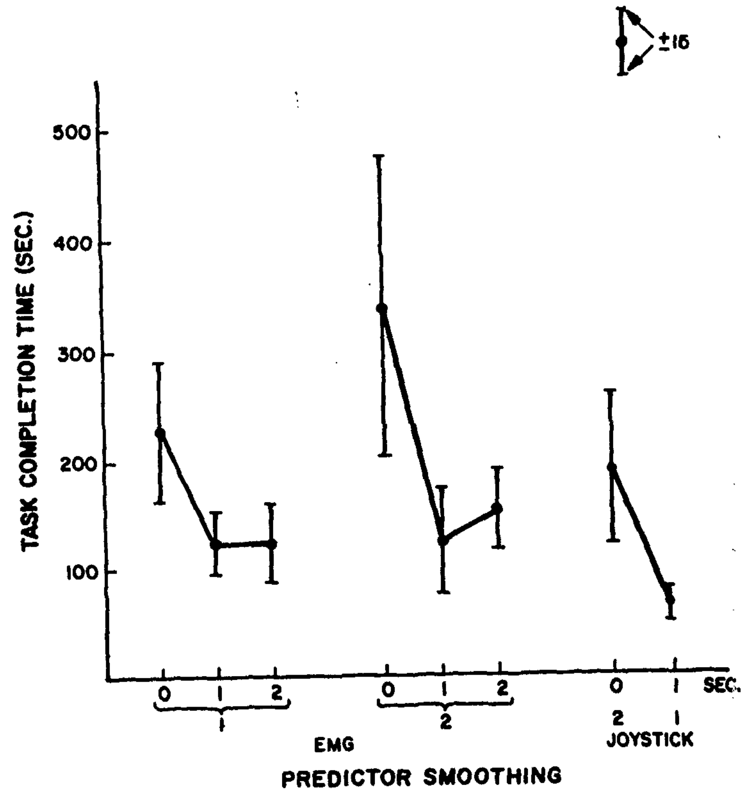

Figure 8 - Completion Time vs Experimental Variables

The results of these tests indicate which means are significantly different from the rest of the group. The analysis of means of figure 8 is plotted in figure 9. The results of these comparisons are indicated by the solid and dashed lines in the figure. Each member of a group of means that lies under the solid or dashed lines cannot be considered as significantly different from every other member of that group at the 5 and 1 percent levels respectively. Figure 9 shows that there is no significant difference in EMG control combinations using the predictor but these control combinations are significantly different from the no predictor case and joystick control.

Figure 10 shows task completion times versus subjects with the different combinations of predictors. There is a significant interaction between subjects and predictors but one result is apparent. All subjects task completion times were lower when using the predictor over no predictor.

2) Task Errors: Task errors and task completion times are fairly dependent measures of one another (r=0.81), therefore results of one predicts the results of the other.

After completing the experiment, the subjects were asked to answer 7 questions. The results of the most important of these questions are briefly discussed below.

The subjects were first asked to what degree was the predictor used. All subjects used it more than half the time while three responded they used it all the time.

In the second question the subjects expressed what they liked about the predictor. All subjects indicated that the predictor helped them maintain the right direction and orientation. One subject indicated that the predictor gave him a feeling of velocity. Another subject stated that the predictor allowed him to line up the cross as he approached a channel of the maze instead of "tweaking" one muscle at a time. The subject response indicates a more coordinated simultaneous control using the predictor.

Subjects expressed their dislikes about the predictor in the third question. Most subjects felt the larger prediction spans were more distracting than the shorter although objectively there was no significant difference in the spans. Subjects also expressed a dislike to the system lag time when using no predictor.

The fourth question was designed to enquire as to the strategy exhibited in using the predictor. All subjects responded that they coordinated their muscle activity to line up the predictor and "shoot" it through each channel of the maze.

The fifth question was designed to find out if the subjects felt they used less muscle contraction in completing the task with the predictor. All responded that the task was accomplished with less contractions although graphs of integrated EMG taken concurrently with the task indicate that this is not the case. The perceived response of less contraction may have been stated with respect to overall task time which took larger with no predictor.

In addition the task time, task error and questionnaire data, some method of recording simultaneous EMG control was needed. The circuit of figure 11 was used. Raw EMG signals from both sets of control sites are added and multiplied together. This multiplied output, which represents the EMG combination from both arms, is used to trigger the comparator whose output is monitored by a chart recorder. (MFE Model CP-2).

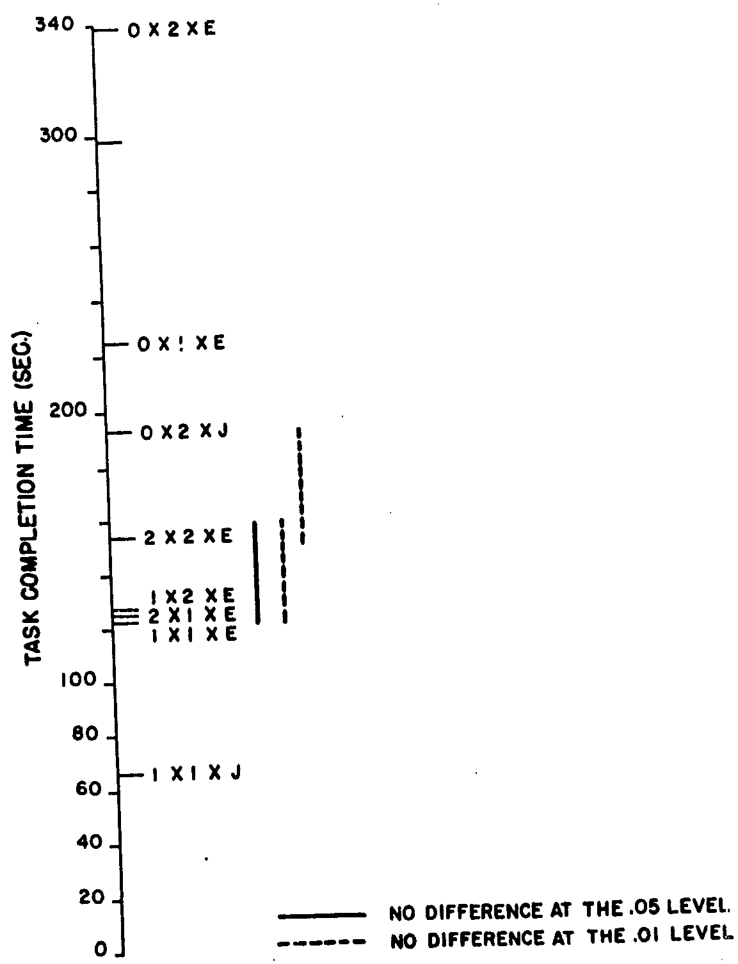

Figure 9 - Analysis of Means of Task Completion Time vs Experimental Variables

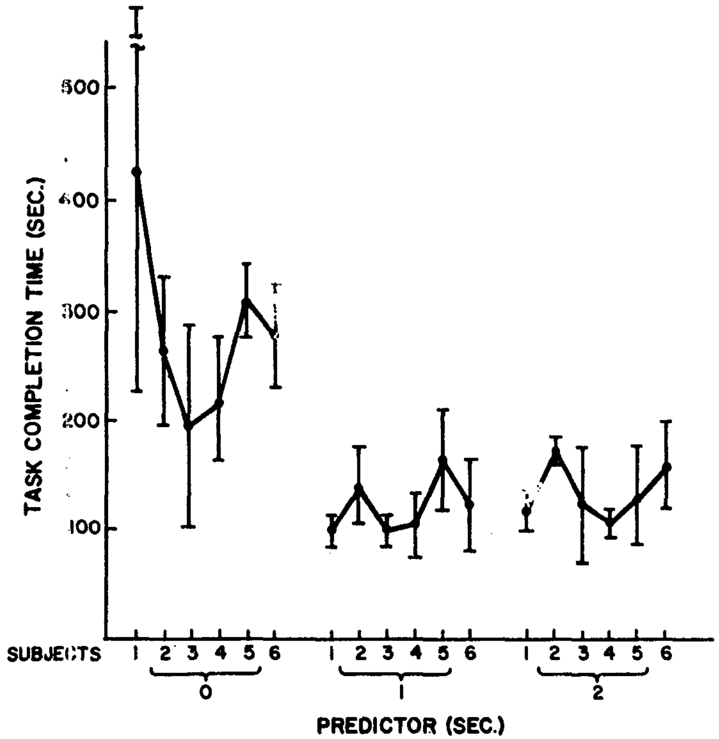

Figure 10 - Completion Times vs Subject Predictor Interaction

Therefore if a discrete type of control approach is used (movement in one direction first followed by movement in the other) the comparator output is zero. If a combinational approach is used (moving in both directions together) the comparator output becomes one. Therefore, the degree of simultaneous control is measured by the *number of ones* at the comparator output. Figure 12 shows the degree of simultaneous control versus the three predictor conditions. Simultaneous control occurred 46% of the time using no predictor. With the 1 second prediction span, simultaneous control was achieved 73% of the time, an increase of 60%. Using the 2 second predictor resulted in a 53% increase in control.

There is sufficient information from the analysis of the data to state the following conclusions.

1) *EMG Control with the predictor feedback* resulted in substantially reduced task completion time (on the order of 100% (p .05).

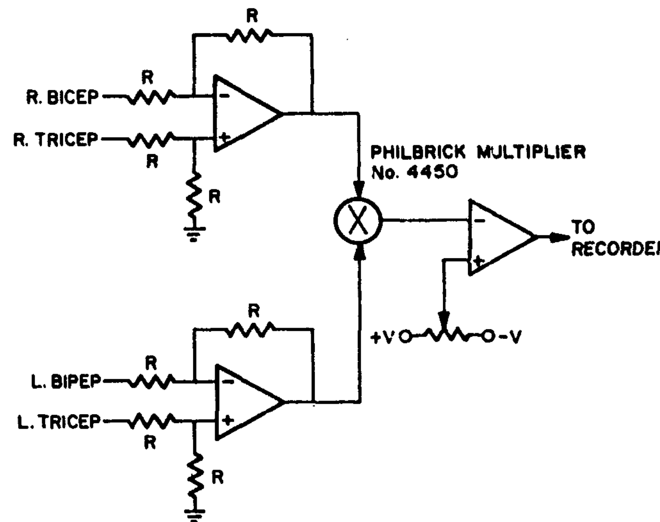

Figure 11 - Circuit used to Measure Degree of Simultaneous Control

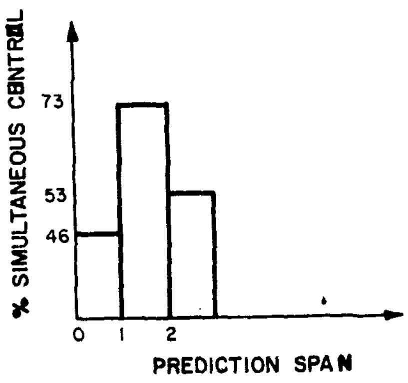

Figure 12 - % Simultaneous Control vs Prediction Span

2) Task completion time and task errors are independent of the amount of filter smoothing where using predictor feedback. When no predictor information feedback is used, task completion time increased by 40% when the task time was doubled. It appears that increased SNR can be attained at control levels not approached in the past.

3) Manual control with a joystick and no predictor feedback was inferior to EMG control with predictor feedback.

4) Using predictor feedback substantially reduces the variance in performance permitting pre-evaluations.

5) Predictor information feedback allows for more simultaneous coordinated EMG control leading to a smooth multiaxis system response.

6) The strong subject, predictor interaction indicates that prediction spans could be "tailored" for each subject as needed.

The results of this investigation indicate that in treating the human as a man machine system it is possible to benefit from principles behind such systems. It also provides a basis for the beginning of these principles in other areas of Rehabilitation Research.

1. Kreifeldt, J: "Signal Versus Noise Characteristics pf Filtered EMG Used as a Control Source." IEEE Transactions on Biomedical Engineering, Vol. 18 No. 1

2. Kreifeldt, J: "EMG as Amplitude Modulated Noise", Cybernetic Systems Group, Engineering Design Center Case Western Reserve University, Cleveland, Ohio, Memo 1968.

3. Kelly, C. : "Predictor Displays-Better Control for Complex Manual Systems" Control Engineering, Aug. 1967

4. Warner, J.: "A Fundamental Study of Predictive Display Systems." NASA Contract Report NASA CR-1274, Feb. 1969.

N79-17506

STANFORD RESEARCH INSTITUTE
Menlo Park, California 94025 · U S A

TWO MEASURES OF PERFORMANCE IN A PEG-IN-HOLE MANIPULATION TASK WITH FORCE FEEDBACK*

John W. Hill
SRI International
Menlo Park, CA

ABSTRACT

This paper describes the results from two manipulators on a peg-in-hole task, which is part of a continued effort to develop models for human performance with remote manipulators. Task difficulty is varied by changing the diameter of the peg to be inserted in a 50 mm diameter hole. An automatic measuring system records the distance between the tool being held by the manipulator and the receptacle into which it is to be inserted. The data from repeated insertions are processed by computer to determine task times, accumulated distances, and trajectories. Experiments with both the MA-11 cable-connected master-slave manipulator common to hot cell work and the MA-23 servo-controlled manipulator (with and without force feedback) are described. Comparison of these results with previous results of the Ames Manipulator shows that force feedback provides a consistent advantage.

INTRODUCTION

The task investigated in this paper is the peg-in-hole experiment previously examined by McGovern[1] and Hill.[2] The experiment board has been rebuilt to be more precise and to be incorporated into the measuring system. The experiment has been expanded to use three different moving distances (100, 200, and 400 mm) to provide a broader data base for the models.

Two manipulators were chosen for these experiments. The first was the French MA-11, a lightweight cable-connected manipulator designed for hot cell work. Similar to the Model 8 developed at Argonne Labs, it is representative of a large class of manipulators in use throughout the world in radioactive environments. With about 30,000 cable-connected manipulators in use in the world, they provide a standard for comparison with other types of manipulators. They offer the operator a low mass (5 kg) manipulation link to tasks with only six degrees of freedom. This link essentially removes the enormous dexterity and tactile sensibility of the human hand and limits the operator to motion and sensing with the six degrees of freedom provided.

The second manipulator chosen was the MA-23 force reflecting servo manipulator developed by the French Atomic Energy Commission (CEA). This manipulator system may be run with force feedback either turned on or off. It is one of about 20 manipulators in the world with this feature. An attempt was made to run the experiments with a similar American manipulator, the E-4 manipulator at Fermi National Accelerator Laboratory, Batavia, Illinois, but it was not operational at the time scheduled for the experiment. Manipulators with force feedback capability were sought to characterize the changes in performance attributable to force feedback.

The performance measuring system is based on a tensioned string that measures the distance between the tip of a tool and a receptacle into which the tool is to be inserted. The string also permits the progress into the hole to be monitored as the tool is inserted. From records of string length as a function of time, tool trajectories as well as velocities and task times can be determined. The system makes a permanent record of the string length 25 times a second as the tool is moved to and into the receptacle.

PORTABLE DATATAKER

A portable data collection system was designed and constructed to obtain and compare performance of different teleoperators. The system measures the distance from a tool to a receptacle in which the tool is to be inserted. The datataker records the distance between the end of the tool and the bottom of the receptacle as a function of time. This distance is measured by a dacron string of low extensibility to the

*This work was supported by the National Aeronautics and Space Administration under Contract NAS2-8652 with Stanford Research Institute.

D31

nearest 2 mm and is punched on paper tape at the rate of 25 measurements/sec. The range is calibrated from 0 to 510 mm in 256 steps (8 bits).

The entire experimental arrangement is shown in Figure 1. The experimenter operates the tape perforator, while the subject manipulates

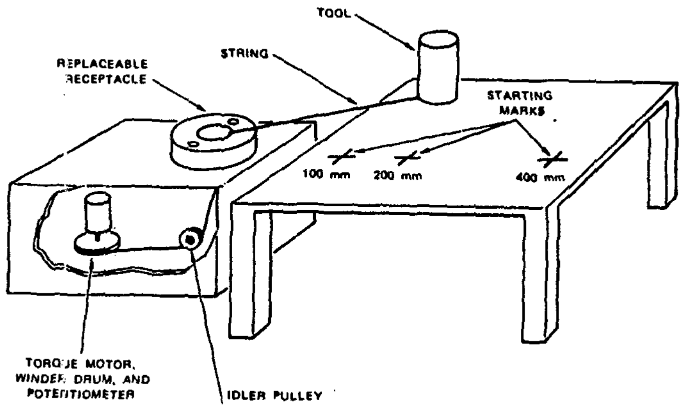

FIGURE 1 TASK CONFIGURATION WITH MEASURING UNIT AND ACCESSORY TABLE

the tool. The measuring string connects the tool and the string puller. This system is similar to that previously described[2] for measuring the X, Y, and Z coordinates of the manipulated tool, except that a single string is used. This simplification in measuring was suggested by the results of two previous studies using a more sophisticated datataker.[1,3] In these studies the distance between hole and tool as a function of time was the most important parameter in explaining the experimental results. This measurement could be used to divide the task into different therbligs and to proportion a fixed amount of time for each one. Detailed descriptions of the equipment including dimensions of the task boards and operation of the datataker are given in a technical report.[4]

A data reduction program reads the paper tapes and makes a set of measurements on the trajectories. The measurements, a sample of which is shown in Figure 2, are briefly described below:

Reaction Time--Reaction time is the time after the experimenter turns on the punch, which is the audible signal for the subject to begin, until the subject pulls the string 4 mm from its initial length (time zero).

Zero Length--Zero length is the string length when the tool is at the entrance to the receptacle. This length is determined from the calibration recordings.

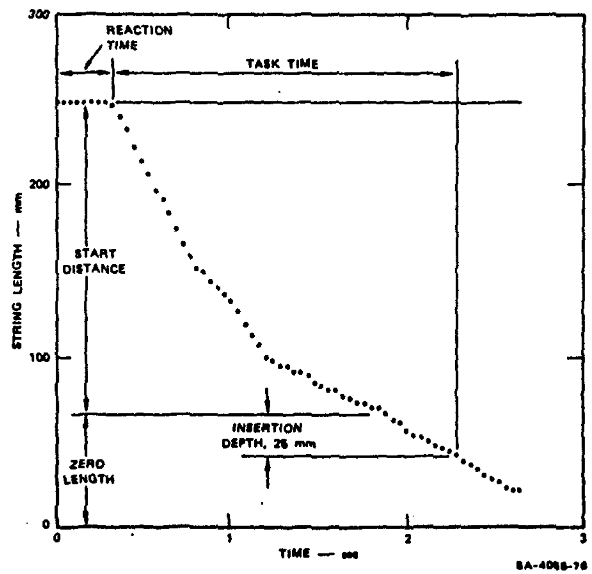

FIGURE 2 SAMPLE TRAJECTORY MEASURED BY DATATAKER

Start Distance--Start distance is the difference between the string distance at time zero and zero length as defined above.

Task Time--Task time is the time from when the tool is first moved until it has been inserted 25 mm into the receptacle.

In addition to these parameters, the first times to a set of given distances from the hole entrance are determined in order to plot the average trajectory. The set of distances are: 350, 300, 250, 200, 150, 100, 90, 80, 70, 60, 50, 40, 30, 20, 10, and 0 mm from the hole and 10, 20, 25, and 30 mm into the hole.

PEG-IN-HOLE EXPERIMENT

The object of the task was to insert a set of pegs into a round receptable. The difficulty of the experiment was varied by using pegs of different diameter. The experimental apparatus is basically the same as that used by McGovern.[1] The same pegs were used but a more precise receptacle was installed on the taskboard. Tool trajectories were recorded as a function of time, using the data acquisition system.

Manipulators

Two different manipulators were chosen for use in the experiment: a lightweight master-slave manipulator (MA-11) of the family used for hot cells and a heavy duty servo manipulator (MA-23) that has more general purpose use. These manipulators are shown in Figures 3 and 4. Technical descriptions including dimensions, load capability, speed, and backlash for the MA-11 and MA-23, respectively, are given in a technical report.[4] Both manipulators were developed by the French Atomic Energy Commission at Saclay, France, for radioactive handling by Dr. Jean Vertut's Environmental Protection group.[5,6]

Experimental Design

The basic experiment consists of the 7 × 3 × 8 factorial design shown in Figure 5. For each distance and peg combination, eight insertions of the peg into the receptacle were made. Seven pegs were used (Pegs 2, 4,

ORIGINAL PAGE IS
OF POOR QUALITY

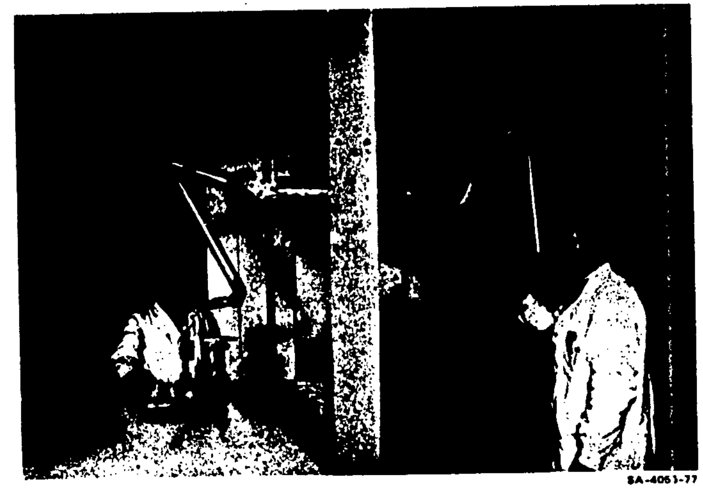

SA-4061-77

FIGURE 3 MA-11 CABLE-CONNECTED MASTER-SLAVE MANIPULATOR

(a) MA-23 FORCE-REFLECTING MASTER (6 kg)

(b) MA-23/200 HEAVY DUTY SLAVE (25 kg)

SA-4065-78

FIGURE 4 MA-23 SERVOMANIPULATOR

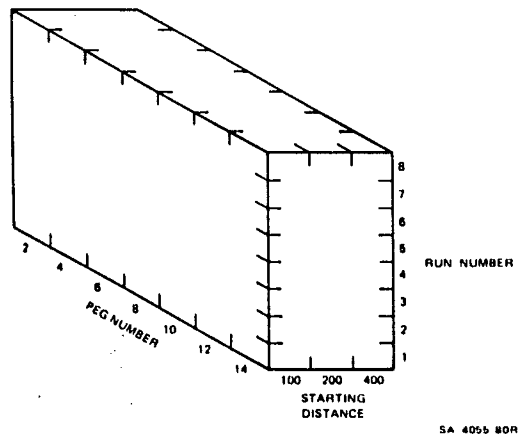

FIGURE 5 PEG-IN-HOLE EXPERIMENTAL DESIGN

6, 8, 10, 12, and 14, which are respectively 25.40, 38.10, 44.45, 47.62, 49.23, 50.39, and 50.70 mm in diameter). The diameter of the hole is 50.4C mm (2.000 inch). This design is similar to that previously used,[9] except that three distances, 100, 200, and 400 mm are used. These distances increase by multiples of two for convenience of using and testing Fitts law.[6]

Procedure

The experimental protocol was as follows: For each sequential condition, a new peg, if called for, was rigidly fixed inside the manipulator jaws by means of a small C-clamp. The subject was permitted to make a few practice movements, and, if a new tool or manipulator were being introduced for the first time, the subject was encouraged to practice a few times. For each of the eight repeated insertions, the subject positioned the tip of the tool over the appropriate starting mark (100, 200, or 40C mm). The experimenter punched the run number, waited a second or two, and switched on the punch, which had a distinct noise. When the subject heard the noise, he proceeded to move the tool into the receptacle. When the tool tip disappeared inside the receptacle (about 50 mm) the experimenter turned off the punch and the subject returned the tool to the starting mark to prepare for the next insertion.

MA-11 RESULTS

The peg-in-hole experiment was run with two subjects in the manner previously described and the resulting trajectories analyzed by computer program to obtain task times and details on the trajectories. Task completion time is defined as the time from the beginning of the move until the tip of the tool is inserted 25 mm into the receptacle. At this point the tool is first inside the 25 mm thick receptacle, and the angular and translational degrees of freedom are constrained as determined by the geometry of the tool and receptacle.

Basic task times for the peg-in-hole task are shown in Figure 6. These times increase as the difficulty of the task (peg number) increases. Differences between the three trajectory lengths appear to be constant, all three increasing with peg number. This suggests that the times are accounted for by the sum of two functions; one a function of trajectory length, the other a function of peg number (difficulty).

Since the precision of fit of each peg is double that of the preceding one, the abscissa on Figure 6 is also a measure of task difficulty as defined by Fitts.[7] An interesting feature of the results is their upward curvature: task time is an accelerating function of difficulty, whereas Fitts law predicts a linear function of difficulty. Analyses of variance were performed on the total task times to obtain the statistics for testing hypotheses about these functions.

Task time is a strong function of the peg number [$F(1,294) = 56.49$, $p < 0.001$] and is nonlinear [$F(4,294) = 12.4$, $p < 0.001$]. Task time is also a strong function of the trajectory length [$F(2,294) = 43.80$, $p < 0.001$] but there is insufficient evidence to show that it is nonlinear [$F(1,294) = 0.05$, $p > 0.05$]. The interaction between peg and trajectory

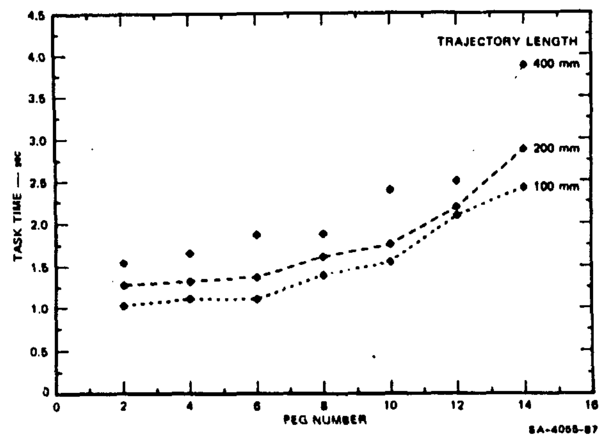

FIGURE 6 MA-11 TASK COMPLETION TIMES

length [$F(12,294) = 1.69$, $p > 0.05$] is not statistically significant, suggesting independence between these two parameters. With this information we can assume the following model for this task:

$$\text{Task time} = f_1(\text{peg}) + K_1(\text{trajectory length}) \quad (1)$$

where f_1 is an accelerating function of the peg number and K_1 is a linear function of trajectory length.

Trajectories for Pegs 2, 8, and 14 are shown in Figure 7. The trajectories show a transition between the smooth insertions with Peg 2 to the two-stage insertion with Peg 14, where the insertion is practically stopped at the entrance to the hole. Similar transitions between smooth and two-stage insertions were observed in previous experiments[1,2] as the task difficulty was increased. Note that the initial trajectories for the three pegs shown in Figure 7 have the same slope even though the scale change makes it appear that Peg 14 is inserted faster.

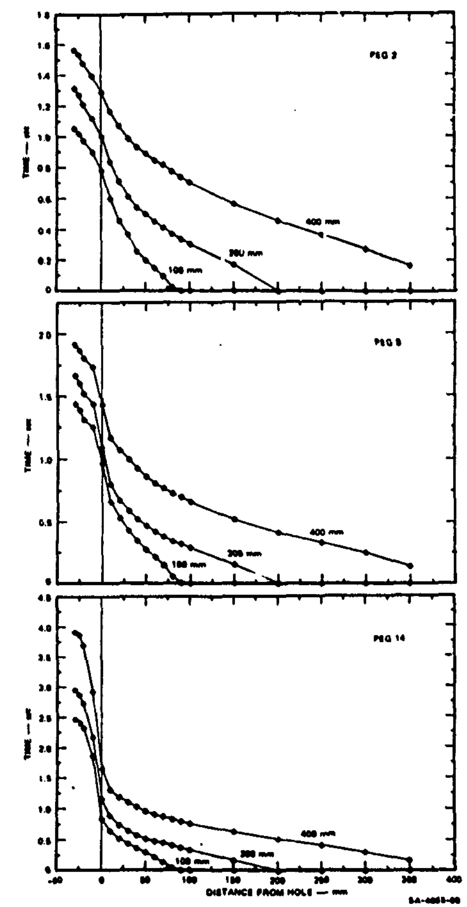

FIGURE 7 MA-11 TRAJECTORIES WITH INCREASINGLY DIFFICULT PEGS

MA-23 RESULTS

In part of a program to determine the advantages of force feedback in different manipulation tasks, the Peg-in-hole task was run on an MA-23 manipulator with and without force feedback. The comparison was made with two subjects who served in both the force and no-force conditions. The experiment was balanced for practice effects by starting one subject on the force and the other on the no-force condition and running the two through the design in reverse directions.

The task times shown in Figure 8 are of the *same shape* as those of the MA-11. Generally, the MA-23 is 30 to 40% slower without force feedback than with it. There are no distinctive changes as the peg number increases except for the most difficult peg (Peg 14). Here the insertion time is doubled when force feedback is removed.

An analysis of variance of the MA-23 task times shows that times with force feedback are significantly shorter than without it [$F(1,588) = 129$, $p < 0.001$]. Task completion times are *also* strong functions of the peg and the trajectory length, both being statistically significant at the 0.001 level. Task completion times are nonlinear functions of the peg number, as with the MA-11, because the nonlinear term is statistically significant at the 0.001 level [$F(5,588) = 19.16$, $p < 0.001$]. The nonlinear term in the trajectory length [$F(1,588) = 0.19$, $p > 0.05$] is not significant, indicating that, again, the time is a linear function of trajectory length. Of the three interactions, force feedback and peg number interact significantly ($p < 0.001$), whereas force feedback and trajectory length do not ($p > 0.05$), and peg number and trajectory length do not ($p > 0.05$). These results indicate that there are two models for MA-23 performance in this task. With force feedback we have

$$\text{Task time} = f_f(\text{peg}) + K_2(\text{trajectory length}) \qquad (2)$$

and without force feedback we have

$$\text{Task time} = f_{\bar{f}}(\text{peg}) + K_2(\text{trajectory length}) \qquad (3)$$

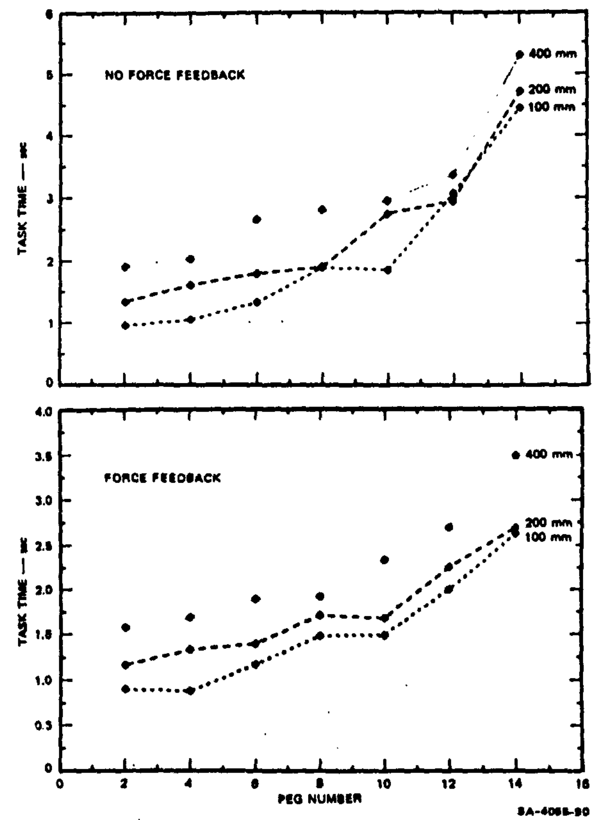

FIGURE 8 COMPARISON OF TASK COMPLETION TIMES WITH AND WITHOUT FORCE FEEDBACK

where the two curving functions, f_f and $f_{\bar{f}}$ of peg size are different, and the linear functions of K_2 of trajectory length are identical.

The trajectories shown in Figure 9 also indicate the general reduction in task time with force feedback. There is a slowing down near the receptacle entrance (between 0 and 10 mm from receptacle) when force feedback is absent, and the insertions take about twice as long without force feedback as with it. The general increase in time without force feedback is apparent throughout the results; gross trajectories as well as fitting movements require more time. With the shortest trajectory (100 mm from the receptacle) gross motion and fitting are intertwined, and it may be impossible to separate these motions (or therbligs) from the data without a model.

SUMMARY

The formulation for the peg-in-hole task with the two manipulators (Equations 1, 2, and 3) shows that task time is a sum of two independent functions--a nonlinear function of peg number and a linear function of trajectory length.

Task times as a function of peg are illustrated in Figure 10 for several situations. Shown are data from the 400-mm trajectories performed with the MA-11 and MA-23 taken from this experiment and data from McGovern[1] (406 mm trajectories) using the Ames Arm and the unaided human hand. The same set of pegs was used in each experiment. Nearly identical functions were obtained under the two force feedback and the two no force feedback conditions, although different manipulators and test subjects were used. Two functions explain the results of all the manipulators: one for force feedback (f_1, from Equation 1, and f_f from Equation 2), the other for no force feedback ($f_{\bar{f}}$ from Equation 3). It thus appears that the task time can be predicted from the geometry of the task (peg number) and the presence or absence of force feedback.

Task times as a function of trajectory length are shown in Figure 11. The linearity of the results as well as the similarity of the two force feedback conditions are obvious for the MA-11 and MA-23 (no force

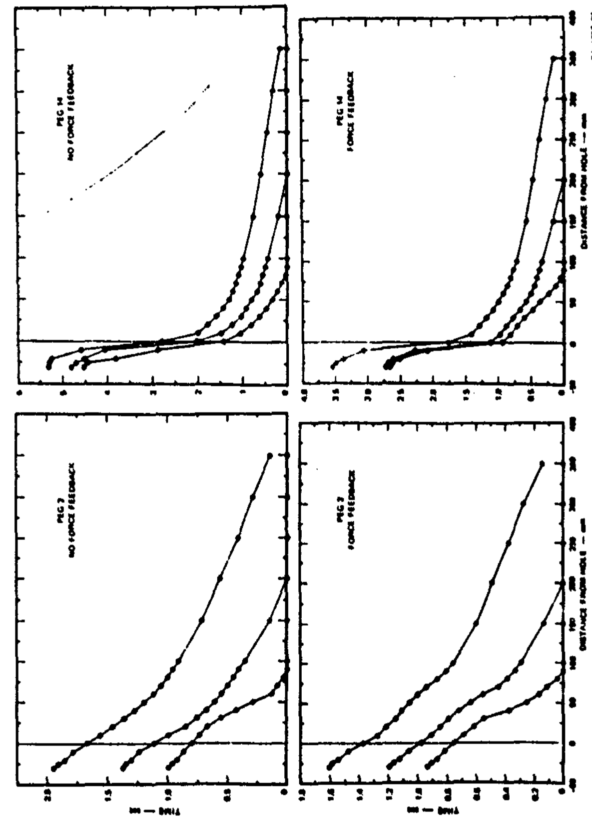

FIGURE 9 COMPARISON OF MA-23 TRAJECTORIES WITH AND WITHOUT FORCE FEEDBACK

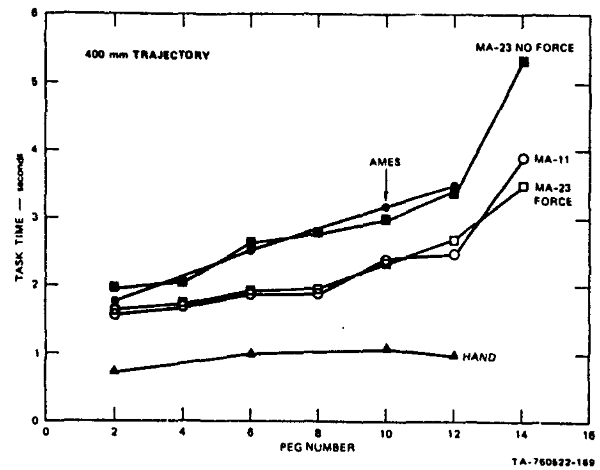

FIGURE 10 TASK TIMES FOR FIVE DIFFERENT PEG-IN-HOLE EXPERIMENTS

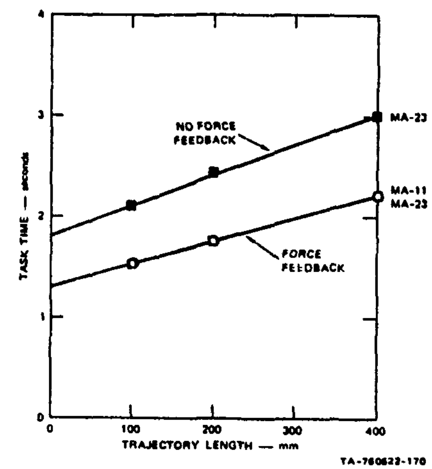

FIGURE 11 AVERAGE TASK TIME VERSUS TRAJECTORY LENGTH

feedback) experiments. A statistical analysis of the results indicates that there is insufficient evidence to show that the slopes of the two lines are different [$F(1,488) = 1.76$, $p > .05$]. This suggests that a common linear function describes the trajectory times of the task for both manipulators (K_1 from Equation 1 equals K_2 from Equations 2 and 3).

In conclusion, the functions for peg number and trajectory length offer a mathematical basis that there are two independent parts of the task, a trajectory part and a fitting part, which substantiate the results of Hill and Matthews[n] with a degree-of-constraint task, and the industrial time-and-motion studies with additive transport and positioning times. These results do not agree with Fitts' Law,[4] which assumes an inverse relation between trajectory length and precision. Thus, the distance moved and the type of force feedback appear to be basic measures of manipulator performance, independent of manipulator.

REFERENCES

1. D. E. McGovern, "Factors Affecting Control Allocation for Augmented Remote Manipulation," Ph.D. Thesis, Stanford University, Stanford, California (1974).

2. J. W. Hill, "Study to Design and Develop Remote Manipulator Systems," Annual Report 1, Contract NAS2-8652, Stanford Research Institute, Menlo Park, California (July 1976)..

3. J. W. Hill and S. J. Matthews, "Modeling a Manipulation Task of Variable Difficulty," Proceedings of the Twelfth Annual Conference on Manual Control, NASA Technical Memorandum, NASA TM X-73170, pp. 639-660 (May 1976).

4. J. W. Hill, "Study to Design and Develop Remote Manipulator Systems," Quarterly Reports 5 and 6 combined, Contract NAS2-8652, Stanford Research Institute, Menlo Park, California (January 1977).

5. Société La Calhène, "Use of the Electronic Master-Slave Manipulator MA-23 in Reprocessing and Vitrification Facilities," Manual No. 43, Bezons, France (May 1976).

6. J. Vertut, J. Charles, P. Coiffet, and M. Petit, "Advance of the New MA-23 Force Reflecting Manipulator System," Paper presented at the RoManSy-76 Symposium, Warsaw, Poland, 14-17 September 1976 (Proceedings will be published through CISM in 1977).

7. P. M. Fitts, "The *Information Capacity* of the Human Motor System in Controlling Amplitude of Movement," Journal of Experimental Psychology, Vol. 47, pp. 381-391 (1954).

Session VI

AEROSPACE VEHICLE CONTROL

Chairman: R. E. Curry

PRECEDING PAGE BLANK NOT FILMED

D32

N79-17507

PREDICTION OF PILOT-AIRCRAFT STABILITY BOUNDARIES AND PERFORMANCE CONTOURS*

Robert F. Stengel and John R. Broussard
The Analytic Sciences Corporation
Six Jacob Way
Reading, Massachusetts 01867

ABSTRACT

Control-theoretic pilot models can provide important new insights regarding the stability and performance characteristics of the pilot-aircraft system. Optimal-control pilot models can be formed for a wide range of flight conditions, suggesting that the human pilot can maintain stability if he adapts his control strategy to the aircraft's changing dynamics. Of particular concern is the effect of sub-optimal pilot adaptation as an aircraft transitions from low to high angle-of-attack during rapid maneuvering, as the changes in aircraft stability and control response can be extreme. This paper examines the effects of optimal and sub-optimal effort during a typical "high-g" maneuver, and it introduces the concept of minimum-control effort (MCE) adaptation. Limited experimental results tend to support the MCE adaptation concept.

INTRODUCTION

Since Tustin first likened the command and response patterns of anti-aircraft gunners to rudimentary control systems (Ref. 1), the intriguing notion that control-theoretic mathematical models can characterize the human operator has been carried to a high state of development. Frequency-domain models have proven capable of capturing fundamental aspects of the human operator's behavior in a straightforward and logical fashion (as in Refs. 2 and 3), while time-domain models have demonstrated that a well-motivated subject can, in fact, behave like an optimal control system in various single- and multi-axis tracking tasks (Refs. 4 to 6). Nevertheless, a number of perplexing problems remain in the study of what might be called the pilot's "discretionary control behavior," i.e., given that the subject is physically and emotionally capable of performing a task in an optimal manner, why might that subject choose to do otherwise?

The matter is of particular concern when the subject is a skilled pilot and the task is controlling a maneuvering aircraft, for the success of the mission and the pilot's own safety are strong motivating factors. During rapid maneuvering, the aircraft's dynamic characteristics can change markedly in a matter of seconds, and the pilot may be called upon to make changes in his control strategy just to maintain stability, much less carry out his mission. More often than not, the pilot who performs such maneuvers has mastered the necessary procedural adaptation and executes it with precision. On rare occasions, even the skilled pilot may get into trouble, adapting his control strategy to suit poorly chosen criteria, or perhaps not adapting at all. In high-performance aircraft, this apparent lapse can cause a pilot-induced "departure," i.e., a loss-of-control incident which, if not corrected immediately, can lead to a spin and possible loss of the aircraft. The problems for study are not only how to model the pilot's discretionary behavior in departure-prone maneuvering tasks, but how to relate such a model to the more frequent, near-optimal behavior of the skilled pilot.

The approach taken in this paper is to define a sequence of optimal-control pilot models which correspond to the aircraft's changing dynamics as it performs a nominal maneuver and to examine the effects of pilot-aircraft model mismatch on closed-loop stability and statistical tracking error. The maneuver -- a "wind-up turn" -- begins at low angle of attack (α_0) and proceeds to a high α_0. As the maneuver progresses, there is a dramatic variation in the optimal piloting strategy, including, in some cases, a change in sign of the pilot's stabilizing commands to the aircraft. From the outset, it is clear that sufficient mismatch could lead to closed-loop instability, but the rationale for large mismatch remains to be determined.

A hypothesis for mismatch is found in the minimum-control-effort model of pilot adaptation, which, simply stated, suggests that the pilot selects not the optimal strategy but the one which minimizes the variance of stick and pedal motions (in the mismatched case). With the minimum-control-effort (MCE) pilot model, closed-loop stability can be maintained, but the margin for error is reduced, by comparison to the optimal strategy. Where the pilot has a choice of control outputs, (e.g., stick alone, pedal alone, or combination of the two), the MCE pilot model also predicts the point during the maneuver at which the pilot may choose to transition from one command mode to another to maintain stability with minimum effort.

The MCE pilot model has yet to be validated by exhaustive experimentation, but there is remarkable agreement between

*Presented at the 13th Annual Conference on Manual Control, Cambridge, Massachusetts, June 15-17, 1977.

PRECEDING PAGE BLANK NOT FILMED

the model's predictions and piloted, ground-based simulation results, one of which is shown below.

PILOT AND AIRCRAFT MODELS

A block diagram of the pilot and aircraft models is shown in Fig. 1, and it is seen to be similar in structure to the systems of earlier studies (Refs. 5 and 6). The aircraft is modeled as a linear, time-invariant system with state vector, $\Delta\underline{x}$, control vector, $\Delta\underline{u}$, and output vector, $\Delta\underline{y}$. The pilot observes the output, adding noise, $\Delta\underline{v}_y$, in the process and introducing a perceptual delay, τ. The pilot model estimates the aircraft's states (as well as the added states due to the observation delay and neuromuscular lag), from the delayed outputs, $\Delta\underline{y}_p$, and forms a feedback control strategy based upon $\Delta\hat{\underline{x}}$. Neuromotor noise, $\Delta\underline{v}_u$, is added to the pilot's internal command, $\Delta\underline{u}_c$, and these are subjected to a neuromuscular lag prior to commanding the aircraft model via $\Delta\underline{u}$. The primary parameters of the pilot model are τ, the Kalman filter gain matrix, K, the linear-optimal regulator matrix, C, and the neuromuscular lag matrix, R_L. Further details of the model structure can be found in Refs. 7 to 9, which illustrate the distinguishing features of the model used here (including use of the Padé approximation, uncoupled multiple pilot commands with differing neuromuscular time constants, and use of a "contraction mapping" sequence in finding the gains of the pilot model).

Attention is directed to the effects that the pilot model has on a high-performance aircraft which is in a "wind-up turn" maneuver, described by the first four columns of Table 1. The pilot model is formulated to control only the lateral-directional modes of the aircraft using observations of Euler angles and angular rates. The pilot model can control the aircraft with lateral stick motions (which control differential stabilators and spoilers), foot pedal motions (which command rudders), or both. Beginning in straight-and-level flight, the aircraft is rolled into a turn that eventually achieves a steady-state body-axis pitch rate of 7.5 deg/sec. As velocity decreases, the angle of attack, α, must increase to maintain the earth-relative turn rate (hence, the name, "wind-up turn"), and the dynamic characteristics of the aircraft change markedly during a short period of time. In particular, the aircraft's lateral control surfaces (used primarily for roll control at low α) develop an adverse yaw characteristic for α beyond 12 deg, their control "power" is reduced, and there is a region of Dutch roll instability for α beyond 18 deg.

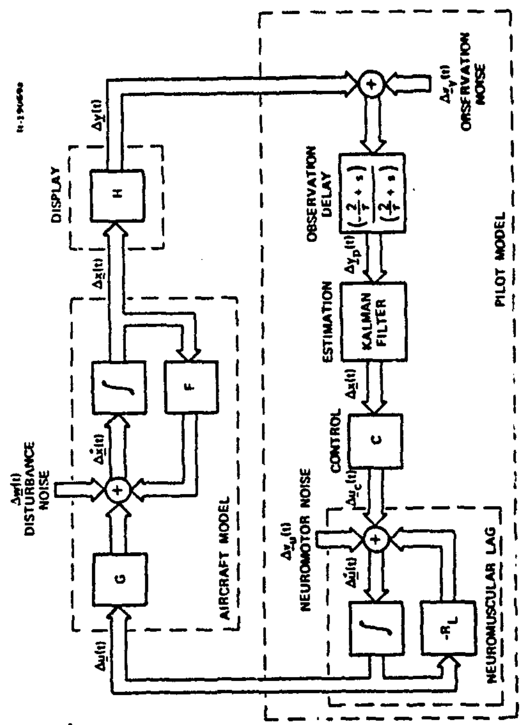

Figure 1: Block Diagram of the Pilot-Aircraft Model

Table 1

Eigenvalues of the Wind-Up Turn with Pilot Using Lateral Stick Alone for Control

MANUEVER CONDITION				PILOT LATERAL STICK/SPIRAL		DUTCH ROLL		ROLL	YAW
V_o, m/s	α_o, deg	n_o, "g"	q_o, deg/sec	ω_n, rad/sec	ζ, -	ω_n, rad/sec	ζ, -	τ, sec	τ, sec
244	1.02	1.0	0.0	7.38	0.740	2.40	0.468	0.892	6.9
244	8.72	4.3	7.5	7.00	0.679	1.62	0.614	0.781	1.72
213	11.1	3.8	7.5	6.69	0.655	1.11	0.683	0.642	1.84
183	15.4	3.3	7.5	6.48	0.635	0.296	0.775	0.535	1.19
152	19.8	2.9	7.5	6.11	0.642	0.486	0.861	0.521	2.39
137	24.6	2.5	7.5	6.09	0.614	0.266	0.722	0.532	0.855

Using lateral stick motions alone, the optimal pilot model develops adapted control strategies which stabilize the entire maneuver very well, as shown by the remaining six columns of Table 1. The real roots associated with the pilot's lateral arm motions and the aircraft's spiral mode coalesce to form a damped, oscillatory mode; the aircraft's Dutch roll mode remains well-damped, although its natural frequency decreases sharply in the region of adverse yaw; the roll mode time constant decreases by 40 percent during the manuever; and the mode which results from feeding back yaw angle observations quickens with increasing α.

A close look at the adapted control gains (Table 2) reveals that substantial variations in strategy are required to maintain optimal control during the maneuver. Not only must the gains increase in magnitude to account for decreasing control power, but several gains change sign -- in fact, the yaw rate gain ($\partial\delta/\delta r$) changes sign three times. The first change occurs as a result of the increased pitch rate, which changes the nature of the Dutch roll mode. The second change occurs at the onset of adverse yaw, while the third can be attributed to the unstable open-loop Dutch roll mode. Although it is well within an actual pilot's psychomotor ability to behave as an optimal controller at each flight condition, the demands for smooth adaptation during the course of the maneuver are excessive. It is likely, therefore, that the pilot may choose to adapt in sub-optimal fashion when using the stick alone for control.

Table 2

Control Gains of the Adapted Pilot Using Lateral Stick Alone

AIRCRAFT ANGLE OF ATTACK, deg	SIDE VELOCITY $\partial\delta/\partial v$, deg/fps	YAW RATE, $\partial\delta/\partial r$ deg/deg/sec	ROLL RATE, $\partial\delta/\partial p$ deg/deg/sec	ROLL ANGLE, $\partial\delta/\partial\phi$ deg/deg	YAW ANGLE, $\partial\delta/\partial\psi$ deg/deg
1.02	+0.522	-0.123	-4.93	-0.345	-1.68
8.72	-0.509	-0.619	+1.74	-0.582	-1.23
11.1	-0.544	-1.02	+1.43	-0.827	-1.62
15.4	-0.433	-3.52	-2.98	-3.40	-3.72
19.8	-0.417	-3.26	+18.8	+2.89	+3.74
24.6	-1.50	-3.66	+18.07	+1.80	+4.12

As shown in Table 3, if the pilot chooses to use foot pedals as well as lateral stick motions for control, the need to make large changes in strategy to maintain optimal control is greatly reduced. The only sign change in lateral stick gains occurs near the onset of adverse yaw for side velocity feedback, while roll and yaw angle feedback to foot pedals change sign when positive pitch rate is established. The range of adapted gain magnitudes still is large, but the procedural changes required of the pilot are less than in the previous case.

Should the pilot choose to stabilize the maneuver using foot pedals alone, his strategy is not significantly different from the foot pedal strategy required for dual controls. A comparison of Tables 3 and 4 shows that the foot pedal gains have the same signs at all but the first flight condition, and the gain magnitudes are very close as well. Thus, it is clear that the degree of adaptation required for foot pedal control is relatively low, although there is substantial change in gain magnitudes to account for changing control power.

STABILITY BOUNDARIES

While the adapted pilot model maintains a high level of stability throughout the wind-up turn, it is apparant that adap-

Table 3
Control Gains of the Adapted Pilot Model Using
Lateral Stick and Foot Pedals

CONTFOL	AIRCRAFT ANGLE OF ATTACK, deg	SIDE VELOCITY ∂δ/∂v, deg/fps	YAW RATE ∂δ/∂r, deg/deg/sec	ROLL RATE ∂δ/∂p, deg/deg/sec	ROLL ANGLE ∂δ/∂ψ, deg/deg	YAW ANGLE ∂δ/∂ψ, deg/deg
Lateral Stick	1.02	-0.645	-0.367	-0.386	-0.764	-2.08
	8.72	-0.0299	-0.026	-0.559	-0.853	-2.19
	11.1	+0.0302	-0.42	-0.947	-1.22	-3.29
	15.4	+0.548	-2.84	-2.84	-2.98	-8.78
	19.8	+0.884	-4.34	-3.31	-3.00	-9.16
	24.6	+0.160	-3.88	-4.44	-3.48	-10.56
Pedals	1.02	+0.0342	-0.995	+0.0572	+0.109	+0.101
	8.72	+0.0137	-1.074	+0.0387	-0.0901	-0.397
	11.1	+0.0474	-1.48	+0.0451	-0.169	-0.721
	15.4	+0.154	-2.39	+0.073	-0.369	-1.57
	19.8	+0.339	-3.90	+0.259	-0.625	-2.82
	24.6	+0.454	-5.42	+0.119	-1.04	-4.66

Table 4

Control Gains of the Adapted Pilot Model Using
Foot Pedals Alone

AIRCRAFT ANGLE OF ATTACK, deg	SIDE VELOCITY ∂δ/∂v, deg/fps	YAW RATE, ∂δ/∂r, deg/deg/sec	ROLL RATE, ∂δ/∂p, deg/deg/sec	ROLL ANGLE, ∂δ/∂φ deg/deg	YAW ANGLE, ∂δ/∂ψ, deg/deg
1.02	+0.0276	-1.049	-0.0281	-0.1618	-0.339
8.72	+0.0574	-1.097	+0.0327	-0.181	-0.324
11.1	+0.127	-1.449	+0.0526	-0.218	-0.440
15.4	+0.276	-2.01	+0.126	-0.269	-0.625
19.8	+0.503	-2.96	+0.294	-0.403	-0.987
24.6	+0.772	-4.33	+0.373	-0.729	-1.74

tation is itself a difficult task. The pilot may choose to adopt response patterns which are more consistent and, therefore, sub-optimal with respect to the criteria used to generate the pilot model. Furthermore, even if the pilot chooses to adapt optimally in a dynamic maneuver, there is likely to be a lag between the aircraft's actual flight condition and the pilot's adaptation point. Consequently, it is instructive to examine cases in which the aircraft's dynamics and the control strategy adopted by the pilot are mismatched. In the examples which follow, it is assumed that the pilot formulates an optimal control strategy for an assumed angle of attack, α_P, which may or may not be the same as the aircraft's angle of attack, α_A, during the maneuver.

Figure 2 illustrates the boundaries between pilot-aircraft stability and instability for independent variations of α_A and α_P (during the wind-up turn). When the pilot model output is lateral stick command alone (Fig. 2a), mismatch introduces regions of Dutch roll and spiral mode instability which are approximately symmetric about the line of perfect adaptation. There is a "stability neck" in the vicinity of α_A=18 deg, where α_P must be very close to α_A to maintain stability. Not only is adaptation in this region potentially difficult (as indicated by Table 2), it is crucial that it be nearly optimal to prevent loss of control. If the pilot model uses foot pedals as well as lateral stick (Fig. 2b), stability margins are substantially increased, and there are no unstable regions for α_P greater than α_A. If the pilot model uses foot pedals alone for control, the entire region is stable; in other words, a mismatch of as much as 30 deg between α_A and α_P causes no instability if the pilot model does not use lateral stick motions for control.

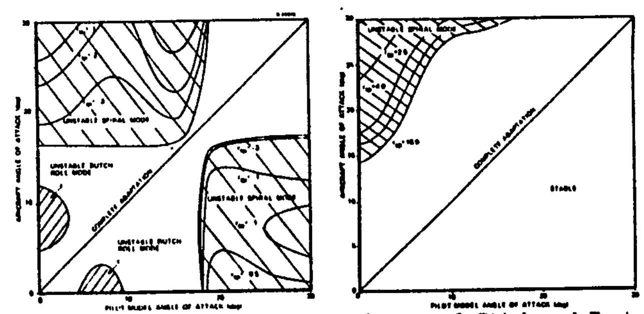

a) Lateral Stick Alone b) Lateral Stick and Foot Pedals

Figure 2: Effects of Pilot Model Adaptation on Maneuvering Flight Stability

The "separation theorem" of stochastic, linear-optimal control (Ref. 10) is only partially applicable to the optimal-control pilot model. The stability results presented here depend on the pilot's control strategy, but not on his estimation law; therefore, control results are separated from estimation results, but the converse is not true. The pilot model estimator gains (K) and eigenvalues depend on the control strategy as a consequence of signal-dependent neuromotor and observation noise, but the pilot model control gains (C) and "closed-loop" aircraft eigenvalues do not depend on K. Thus, the stability boundaries of Fig. 2 apply as long as the pilot model is able to make a stable estimate of the aircraft's state. "Vertigo" is an example of a circumstance in which the pilot estimator does not converge. In the present case, the pilot model experiences estimator divergence with dual control at high α_A (Fig. 2b) because the signal-dependent neuromotor noise is free to grow without bound in the estimator solution (Ref. 9); however, if the neuromotor noise level is bounded (standard deviation of 1 in for stick motion and 0.7 in for pedal motion), a stable estimator solution is obtained for all α_p.

PERFORMANCE CONTOURS

In addition to predicting stability boundaries for varying flight conditions, the pilot-aircraft model (Fig. 1) can be used to predict the statistics of tracking errors and control usage within the stable regions. (Outside the stable regions, these statistics grow without bound). The method applied here is covariance analysis (Ref. 11), in which the aircraft is assumed to be driven by a gaussian disturbance (turbulence with an rms level of 1.52 m/sec (5 fps) and a correlation time of 0.3 sec), and the pilot-aircraft model is used to compute the rms values of state and control perturbations which result.* Since the covariances of system variables are used to define the pilot model estimator gains, the same equations can be used to evaluate the statistical performance of the pilot. In order to use these equations, the pilot model estimator is assumed to be adapted at each flight condition (defined by α_A); hence, when $\alpha_p \neq \alpha_A$, only the pilot model control gains are mismatched. The results which follow demonstrate the effects of sub-optimal control strategy on piloting performance; the effects of sub-optimal estimation remain to be determined.

Figure 3 presents contours of equal rms values under the assumption that the pilot uses lateral stick motions alone for control. These contours would scale up or down as the turbulence level changed, so absolute values are less important than relative values in evaluating the figure.

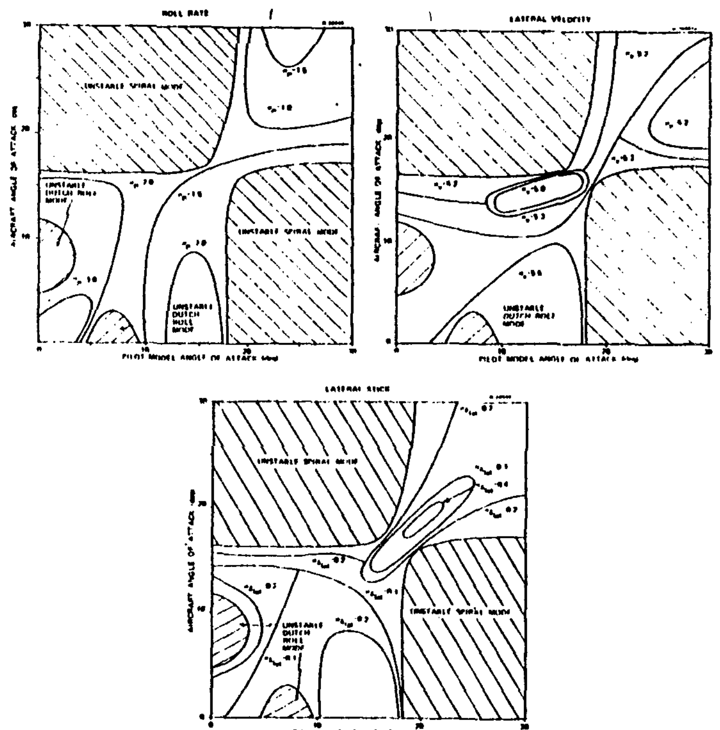

Figure 3: Performance Contours for Control with Lateral Stick Alone

*The state covariance matrix, X, is defined as the expected value of the products of the states, i.e., $X=E(\Delta\underline{x}\Delta\underline{x}^T)$, and the rms values of the states are the square roots of the diagonal elements of X. The control covariance matrix, U, and the associated rms values are similarly defined. The covariance propagation equations are detailed in Ref. 9.

The contours for roll rate rms (σ_p), side velocity rms (σ_v; equivalent to sideslip angle times forward velocity), and stick motion rms ($\sigma_{\delta_{lat}}$) define surfaces of rms values in much the same way as a topographical map displays hills and valleys. It is apparent that the valleys in Fig. 3 do not lie along the line of perfect adaptation, nor do they overlay each other with complete regularity. There are two reasons for this. Although the control gains are meant to minimize a weighted sum of state and control covariances, this is no guarantee that the covariances of individual components will be minimized at the same time. There is a tradeoff between tracking error and control usage, so it is likely that decreases in one component will be accompanied by increases in another. The second reason is that the partial breakdown in the separation theorem leads to the possibility that alternate control strategies could yield lower values of control cost than the separately optimal control law.

Controlling to minimize $\sigma_{\delta_{lat}}$ does have the effect of approximately minimizing σ_p, although increased control activity is required in the region of the stability neck (Fig. 3). Maintaining perfect adaptation for α_A = 17 to 20 deg requires four times the rms control motion that is used at low α_A. In addition to substantial gain variation with flight condition (Table 2), perfect adaptation also leads to increased control effort, again suggesting that the pilot may choose to change his control mode or to adapt in sub-optimal fashion.

Performance contours for a pilot model using both stick and pedals demonstrate that the addition of pedal control has little effect on σ_p (except at low α), but it does reduce σ_v (as might be expected) and increase stability margins (Fig. 4). The pilot model can retain low σ_p and σ_v to high angles of attack with low control effort by fixing α_P in the vicinity of 10 deg (Fig. 5), a decidely sub-optimal policy by the criteria used for pilot model computation. Sub-optimal or not, this adaptation approach could have definite appeal to the human pilot, for it provides perceptably low tracking error and control effort with minimal adaptation; however, if the pilot wishes to fly to α_A=30 deg and beyond, he must adopt a marked change in control strategy to avoid spiral mode instability and estimator divergence. Reference 9 presents additional results for pedal-alone control which demonstrate that stability and low control effort can be maintained with the stick centered for all α_A considered.

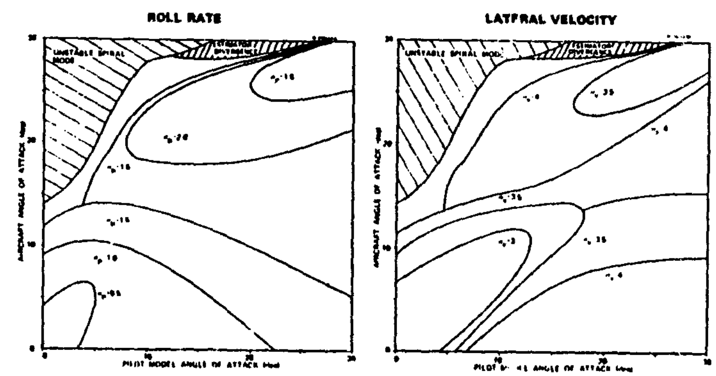

Figure 4 Performance Contours for Control with Lateral Stick and Foot Pedals

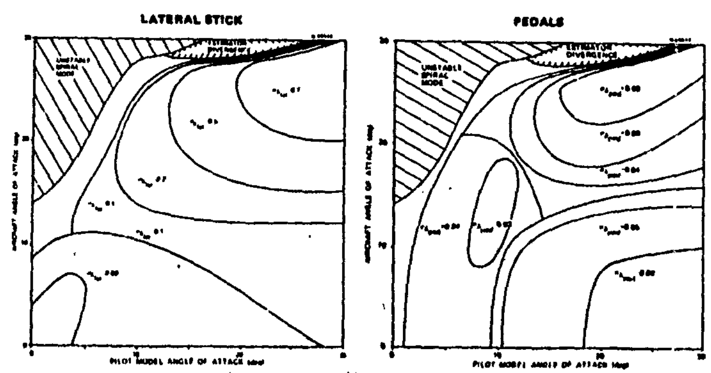

Figure 5 Control Usage Contours for Control with Lateral Stick and Foot Pedals

MINIMUM-CONTROL-EFFORT PILOT MODEL

The combination of reduced control effort and reduced variation in control strategy suggests a hypothesis for minimum-control-effort (MCE) pilot adaptation, which also can predict at what point the pilot is likely to switch his control mode. Figure 6 illustrates two MCE adaptation patterns for the wind-up turn, with the heavy line tracing the corresponding α_A-α_p relationship. For α_A below 12 deg, there is no significant lateral control reduction associated with using the pedals as well as the stick, and the MCE model is "content" to use stick alone. The MCE model is slightly overadapted at low α_A and slightly underadapted at α_A=12 deg; hence, the net amount of adaptation is lower than that implied by fully optimal control.

As α_A increases, the MCE strategy is headed for a stability boundary; the pilot can avoid the boundary by adopting a more nearly optimal strategy, but this requires substantially increased control effort. As alternatives, he can either blend in foot pedal command (coordinated adaptation) or use the pedals alone (stick-centered adaptation) for lateral-directional control. The advantage of the first approach is that relatively good maneuvering precision can be maintained with both controls without requiring counter-intuitive control style; however, the coordinated use of both controls is a difficult task. Judging from Table 4, the use of pedals alone may be a more easily learned task which results in modest increases in σ_p and σ_v.

Experimental results indicate that the MCE pilot model hypothesis does, in fact, describe a realistic pattern of pilot adaptation. Figure 7 is a partial time history of a wind-up turn maneuver in which a trained pilot is flying a ground-based simulation of the subject aircraft. The aerodynamic model of the aircraft is the same as that used in the linear analysis, although the nonlinear, time-varying equations of motion drive the simulator. Below 18-deg angle of attack, the pilot controls with stick alone. As α_A increases beyond 10 deg, stick motions and sideslip excursions build up. At α_A = 18 deg, the pilot begins to use the rudder pedals actively, while his use of the stick is substantially diminished. This result tends to confirm the MCE pilot model, although further validation is warranted.

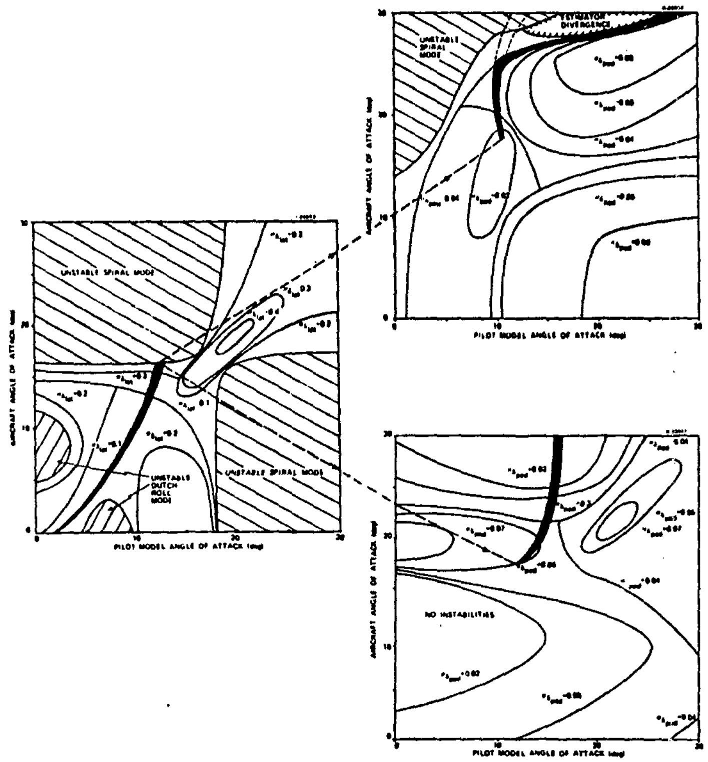

Figure 6 Prediction of Pilot Behavior with Minimum-Control-Effort (MCE) Adaptation Model

ORIGINAL PAGE IS OF POOR QUALITY

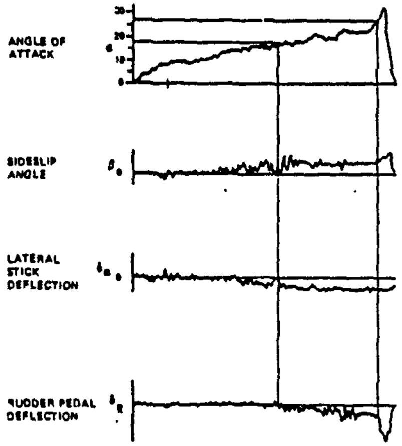

Figure 7 Results of Manned Simulation

CONCLUSION

Whether or not a pilot experiences difficulties in maneuvering flight depends upon how he adapts his control strategy to changing flight conditions. Stability boundaries plotted as functions of the aircraft's actual α and the α assumed by the pilot model in forming a control strategy illustrate that the pilot's adaptation must be very nearly *optimal to maintain* stability in certain flight conditions. Consideration of statistical tracking error and control usage within stable boundaries leads to the concept of minimum-control-effort (MCE) adaptation in the pilot model. The MCE model provides a rationale for non-optimal adaptation which accounts for fundamental changes in the control modes selected by the pilot, such as the decision to use stick and pedals in a coordinated fashion rather than stick alone.

ACKNOWLEDGMENT

This work was conducted under Contract No. N00014-75-C-0432 for the Office of Naval Research.

REFERENCES

1. Tustin, A., "The Nature of the Operator's Response in Manual Control and Its Implications for Controller Design," Journal of IEE, Vol. 94, 1947, pp. 190-202.

2. McRuer, D.T., and Jex, H.R., "A Review of Quasi-Linear Pilot Models," IEEE Transactions on Human Factors in Electronics, Vol. HFE-8, No. 3, Sept. 1967, pp. 231-249.

3. McRuer, D.T., "Development of Pilot-in-the-Loop Analysis," Journal of Aircraft, Vol. 10, No. 9, Sept. 1973, pp. 515-524.

4. Obermayer, R.W., and Muckler, F.A., "Modern Control System Theory and Human Control Functions," NASA CR-256, July 1965.

5. Kleinman, D.L., Baron, S., and Levison, W.H., "An Optimal Control Model of Human Response," Automatica, Vol. 6, No. 3, May 1970, pp. 357-383.

6. Kleinman, D.L., and Baron, S., "A Control Theoretic Model for Piloted Approach to Landing," Automatica, Vol. 9, No. 3, May 1973, pp. 339-347.

7. Stengel, R.F., Taylor, J.H. Broussard, J.R., and Berry, P.W., "High Angle of Attack Stability and Control," ONR-CR215-237-1, April, 1976.

8. Broussard, J.R., and Stengel, R.F., "Stability of the Pilot-Aircraft System in Maneuvering Flight," Proceedings of the 12th Annual Conference on Manual Control, May 1976, pp. 778-794.

9. Stengel, R.F., Broussard, J.R., Berry, P.W., and Taylor, J.H., "Modern Methods of Aircraft Stability and Control Analysis," ONR-CR215-237-2, May 1977.

10. Tse, E., "On the Optimal Control of *Stochastic Linear Systems*," IEEE Transactions on Automatic Control, Vol. AC-16, No. 6, Dec. 1971, pp. 776-785.

11. Gelb, A., ed., Applied Optimal Estimation, M.I.T. Press, Cambridge, 1974.

N79-17508

DISCRETE TIME MODELING OF HEAVY TRANSPORT PLANE PILOT BEHAVIOR

by Daniel CAVALLI

Office National d'Etudes et de Recherches Aérospatiales (ONERA)
92320 Chatillon (France)

1 - Introduction

The desire to improve flight safety leads to a classification of various flight troubles in three groups :

- troubles from sensitivity to flight disturbances,
- maneuverability troubles (whenever a correction maneuver induces an unexpected deviation on another parameter),
- pilot troubles (pilot overload when required attention is excessive or underload entailing a loss of vigilance).

Sensitivity to disturbances and maneuverability of a given aircraft may be evaluated from the early design stage. Evaluation of the pilot behavior, however, may be realized only in actual flight or with a flight simulator, that is quite late in the development period. For this reason, it is desirable to have available, at the design stage, a model of the pilot behavior to command the differential system describing the envisionned aircraft.

This aim implies two major requirements. First, the program must be compatible with a wide range of possible aircraft designs; ideally, the program should be self-learning. Second, mental load and overall pilot performance must be modeled.

Following J.C. Wanner [1] , a flight may be decomposed into a sequence of "phases", each having a long-term objective. Typical phases are ILS approach and landing. Each phase may be eventually divided in sub-phases with short-term objectives. For instance, the ILS approach phase may be broken into localizer beam engagement, glide beam engagement, push over and final descent.

The pilot's task (fig.1) may be defined by data describing.

- a flight sub-phase,
- the aircraft state,
- atmosphere conditions,
- the required control law to follow a nominal flight path during the sub-phase,
- secondary activities (e.g., radio communications, ...).

The objective of the pilot's task is the same as that of the corresponding sub-phase, namely to ensure a short-term safety, thus enabling to execute the next sub-phase with a reasonable chance of success. At the end of this sub-phase, the flight parameters must be within a given window of admissible deviations about the nominal values. Respect of immediate safety consists for the pilot on maintaining the actual flight path close to the nominal values.

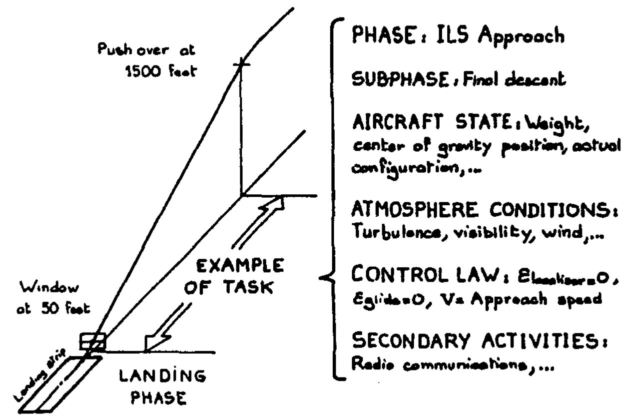

Figure 1 - Pilot's task

A second aspect of flight safety is relative to the pilot workload. This workload may be decreased by a better presentation of the necessary data. Therefore, it would be useful to determine which data are the most appropriate to supply to the pilot in order to reduce his workload and thus increase flights safety and regularity. For instance, data may be supplied by means of a head-up display [2] , but in the present study it is assumed that informations are provided only by a classical instrument panel and without external vision.

2 - Model of aircraft considered

We consider the model of a twin-engine heavy transport plane of Airbus A300B type. During the flight sub-phase considered in this study (final descent of ILS approach), the aircraft keeps a constant configuration (fully deflected flaps and landing gear down). The flight equations have been simplified and only the most relevant variables, including couplings, have been retained to describe the transport plane in its normal domain of flight. The only controls that the pilot (actually, the model) may use to achieve the required control law are :

δl = lateral control } on the stick
δm = longitudinal control }
δn = rudder control
δz = throttle lever .

to which elevator trim may be added.

3 - Assumptions

The conventional assumption of the pilot acting in a continuous manner and represented by transfer functions has not been retained here. Instead, another approach has been used in considering the pilot's behavior as a sequential process.

D33

3.1 - Assumptions on the pilot's behavior

We have made the same assumptions that in the previous study [3] and these assumptions have been confirmed by experimentation. The pilot's behavior has been investigated for the case of the "final descent" sub-phase, on a static simulator cockpit. An electro-oculometer equipment (EOM) has been used, thus allowing continuous determination of the pilot's line of sight.

Due to these experimental conditions, the pilot's control activity is being considered here only as a monitoring and control activity of the data as displayed on the instrument panel. "Secondary activities", such as communication with air traffic control and other crew members, have not been taken into account. Moreover , any "involuntary" information perceived by the pilot has been neglected, for instance peripheral sight of the instrument panel and of outside environment, acceleration effects on the inner ear, noise, etc. It may be noted that, in IFR conditions, an important part of the pilot's training consists on neglecting the involuntaryly perceived information (especially accelerations).

We shall then consider :

1) that, at a given time, the pilot can either make a decision or take one of the three following elementary actions :

- act on one control
- read an information on the instrument panel,
- monitor a given parameter reading on a dial;

2) that the strategy used by the pilot, that is the whole of the heuristic rules he is using, is a function of the flight situation defined [1] by the aircraft type and state, the type of flight sub-phase and the atmosphere environmental conditions (turbulence, visibility, wind, etc);

3) that, it is a priori important to take into account the sequential character of the pilot's decision making, as opposed to the conventional view taken in automatic control on this same problem.

3.2 - Mechanism of the pilot's actions (Fig.2)

It is assumed that the pilot's memory contains :

1) a catalog of "actions". The pilot selects one action out of the catalog as a function of the differences between the image of the actual situation he has in memory and the image of the typical situation in which the implementation of each of these actions is proposed.

2) an operating insight, that is an internal model of the aircraft allowing him to foresee the aircraft reactions, therefore to evaluate the situation while taking into account the previous actions taken; this evaluation is, of course, re-actualized after each reading.

The model of pilot including this evaluation of the actual situation, called "memorized situation", can calculate, while using his operating insight, foreseen situations and select the action to be taken as a function of these foreseen situations and of their subjectively-appreciated seriousness.

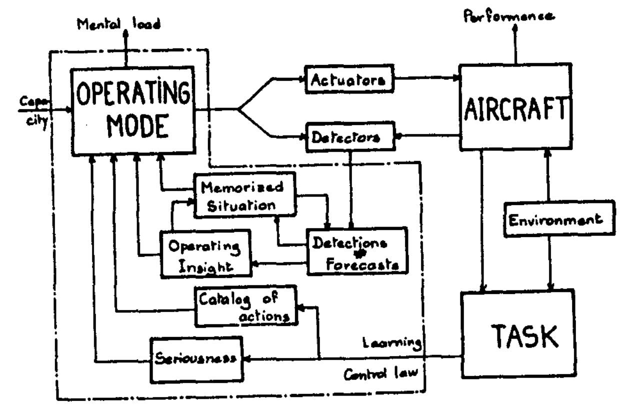

Figure 2 - Mechanism of the pilot's actions

4 - Experimentation

The dynamical flight equations of the heavy transport plane previously described (§2) were wired on a hybrid computer connected to a static simulator cockpit.

4.1 - Experimental conditions

The requirement of knowing which information is read at a given time by the pilot leads to a particular type of instrument panel. Several informations usually gathered within a single given instrument have been separated in order to associate a single information to a given line of sight (for instance, the ILS whose two informations were separated). For the final descent sub-phase, the following nine instruments were used :

- two instruments resulting from the ILS split, i.e. localizer deviation indicator ε_{loc}, glide path deviation indicator ε_{glide}.
- roll indicator ϕ , pitch indicator θ , yaw indicator ψ .
- vertical speed indicator $\dot{z}$, an altimeter z.
- thrust indicator F, airspeed indicator V.

The cockpit includes also the five controls described in §2 : lateral control δl, longitudinal control δm, rudder control δn, throttle lever δz and an elevator trim.

Eye motion can be determined through an EOM equipment (Fig.3). Potential differences depending on the relative position of the eyes with respect to the skull were measured by electrodes applicated on the pilot's face. Assuming that the pilot's head remains fixed, the dial observed by the pilot at any given time can be determined from the amplified and filtered EOM signals.

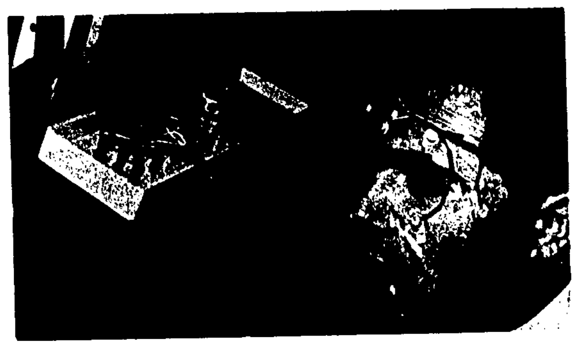

Figure 3 - Electro-oculameter (EOM) equipment

4.2 - Remarks and results

In a first experimental phase, the simulated aircraft was "flown" by five professional pilots. When pilots are asked about the simulated aircraft and its dynamics, they express their operating insight in terms of relations between the parameters and between the parameters and controls. This insight conforms with the linearized equations of the aircraft flight dynamics with respect to the lateral control, but seems much more complex with respect to the longitudinal mode (Eglide-airspeed coupling) (Fig.4).

The pilot model incorporates this operating insight as illustrated by a state vector representing the memorized situation of the aircraft and a set of equations describing the flight dynamics used mentally by the pilot to take his forecasts.

In a second phase, the results of all flight phases simulated by human pilots have been analyzed while distinguishing three levels of activity in the pilot's operating mode [3] (Fig.5). This classification is only a working assumption which seems close to the observed reality.

Short term safety is the objective of the strategy. Immediate safety is a constraint that can be satisfied only with a correction procedure that keeps the actual flight path close to the nominal path.

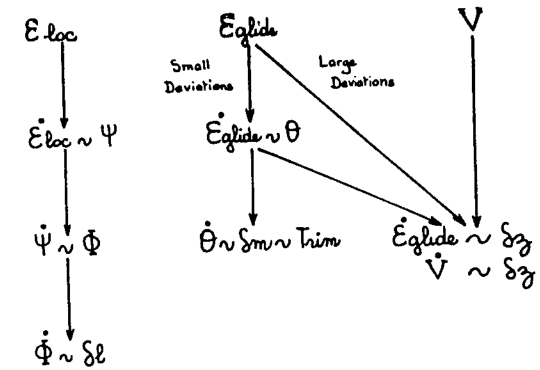

Figure 4 - Operating insight

LEVEL	DEFINITION	OBJECTIVE	COST
STRATEGY	Choice of Correction Procedures	Short-term Safety	Mental Load (Decision)
CORRECTION PROCEDURE	Algorithmic sequence of elementary actions	Immediate Safety	Mental Load (Memorisation)
ELEMENTARY ACTION	• Read indicator • Act on one control • Monitor one dial		Physical Load

Figure 5 - Levels in operating mode

The recorded phases are further divided in correction procedures or in monitoring of the instrument dials. Various quantities are determined such as mean reading time, monitoring frequency for each parameter, action laws on controls, sequence of monitored dials, etc. On example of correction procedure for localizer deviation is given on figure 6.

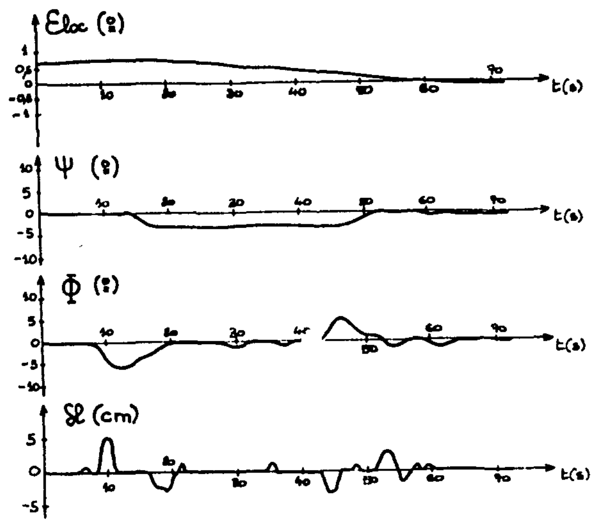

Figure 6 - Localizer correction procedure effectued by a human pilot.

5 - Digital model

5.1 - Program description

The flow chart is given on figure 7.

After initializations, the pilot's model selects the correction procedure to be used as a function of the strategy followed. This correction procedure is then further divided in a sequence of elementary actions (instrument reading, monitoring of a parameter, action on a control) which are successively taken.

As a matter of fact, while a parameter is being monitored, the model can select and undertake the execution of another correction procedure which acquires a higher priority. The abandoned correction procedure is then resumed.

During an elementary action, the time increment dT controls on the one hand, the integration of the flight path according to the equations of motion and, on the other hand, the integration of the situation as memorized by the model.

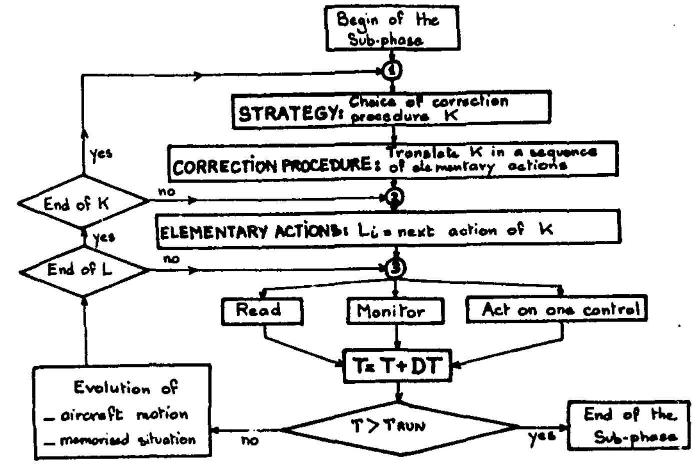

Figure 7 - Program description

5.2 - Model of strategy used

Strategy is the most elaborate level of the pilot's behavior. In the digital program, the strategy allows the pilot's model, at a given time, to select which correction procedure or dial monitoring he will take. This choice is made while complying with short-term safety.

The strategy model described here is a synthesis of two previously used model [3]. Care has been exercised to make a clear distinction between the choice of dials monitoring (a strategy with Markov readings of random nature is used) and the manner to select the parameter corrections (a heuristic strategy using short-term evaluation). Differenciation between these two strategies is based on the concept of seriousness of the instantaneous situation as perceived by the pilot's model defined by

$$G = \max_{\text{on the main parameters}} \left| \frac{\text{estimated deviation}}{\text{permissible deviation}} \right|$$

This is the maximum ratio, over the sub-phase main parameters, between the estimated deviation (memorized or foreseen) and the permissible deviation on a parameter.

The permissible deviations were determined experimentally.

5.2.1 - Strategy for dials monitoring

For this strategy, reading of instruments depends upon two random processes as far as digital simulation is concerned. The sequence of looked up dials is regarded as a Markov chain and the sequence of reading times as a Poisson process.

The sequence of looked dials is governed by a matrix of conditional probability to read one instrument after another. This matrix is called here switching matrix. After every instrument reading, the value of a random variable determines, taking into account the switching matrix, which dial will be read next.

Reading of the dials is made at a variable rhythm and the mean time between switchings is denoted by MT33. This time interval is the time necessary for the simulated pilot to acquire one datum.

The random character of the sequence of observed dials . eliminated if one or more parameters exceed or have exceed at the time t a certain level preset for each parameter. Then, the process becomes deterministic.

If only one parameter exceeds its threshold. It is the instrument corresponding to this parameter which is read. If at the reading time, several parameters have exceeded the preset threshold, it is the instrument with the greatest probability according to the switching matrix which will be read.

The phenomenon can be seen experimentally : if an instrument diverges, the pilot's line of sight is generally directed at the corresponding instrument because his peripheral sight allows him to detect any significant deviation on one of the dials. If several parameters diverge, the pilot is busy with the parameter which has higher priority in his opinion and temporily neglects other parameters which keep diverging.

A switching matrix determined experimentally by using the simulator cockpit and the electro-oculometer equipment in the case of the final descent is given on figure 8.

5.2.2 - Strategy for correction procedures

This strategy is based on the fact that the pilot makes decisions depending on the short-term predicted evolution of the situation, while taking into account intended actions.

The model has not access to the equations governing the aircraft dynamics. Its operating insight conforms with that determined at the beginning of the experimental phase. Its task consists in correcting the detected deviation in order to maintain the difference between the road-out values and the nominal values of the main parameters of the sub-phase within a certain tolerance on each of them.

Switching matrix

	ε_{glide}	ε_{loc}	ϕ	φ	θ	Ψ	F	γ	V
ε_{gl}	0,03	0,10	0,11	0,04	0,15	0,03	0,06	0,21	0,20
ε_{lo}	0,28	0,15	0,05	0,21	0,06	0,23	0,05	0,05	0,08
ϕ	0	0,03	0,06	0,07	0,10	0,06	0,06	0,11	0
φ	0,10	0,33	0,12	0,25	0,18	0,28	0,17	0,03	0,10
θ	0,40	0,14	0,20	0,16	0,25	0,13	0,15	0,21	0,18
Ψ	0,08	0,12	0,16	0,13	0,13	0,10	0	0,16	0,09
F	0	0,01	0,10	0,01	0	0,05	0,11	0	0,03
γ	0,03	0,04	0,13	0,07	0,07	0,11	0,12	0,12	0,08
V	0,08	0,02	0,07	0,02	0,02	0,02	0,24	0,05	0,20
Σ	=1	=1	=1	=1	=1	=1	=1	=1	=1

Matrix obtained with EOM equipment

- All parameters $x_i < L_i$ ⇒ Instrument readings are governed by the switching matrix
- One parameter $x_i \gg L_i$ ⇒ Reading of x_i
- Several parameters $x_i > L_i$ ⇒ Reading of x_i which has the greatest probability in the switching matrix

L_i : Level given in advance for each parameter x_i

Figure 8 - Strategy for dials monitoring

Let S_0 be the memorized situation at time t_0, the model may use its operating insight to compute the predicted situation S_1 at $t_1 = t_0 + \Delta t_1$ if it does not intervene. It may also imagine that, during the time Δt_1, it will implement the K_1 correction procedure on the P_1 parameter. The predicted situation S_1' will then be similar to S_1 to the difference that F_1 will be corrected and that the dials whose reading are necessary to carry out K_1 will have been read out.

This prediction capacity is applied by the model to select whenever necessary, the "best correction procedure" to carry out to comply with the short term safety. This choice is made by unfolding a logical tree (Fig.9) for which

- the root is the memorized situation,
- branches are correction procedures whose implementation is considered,
- nodes other than the root are situations predicted from the root by means of the operating insight while taking into account the intended correction procedures.

The instantaneous seriousness $G(K)$ is computed at each node K. Considering that it remains constant during the time Δt_1 elapsed from the previous node to the node I, the model computes a short term mean seriousness $\mathcal{G}(I)$ on each path leading to a terminal node. To that end, the instantaneous seriousness is weighted by the time elapsed on each branch and the result is divided by the total time elapsed on the path. The short-term mean seriousness of a path (I,J) is then denoted by :

$$\mathcal{G}([I,J]) = \frac{1}{t_J - t_I} \sum_{K = I \to J} G(K).\ \Delta t_K$$

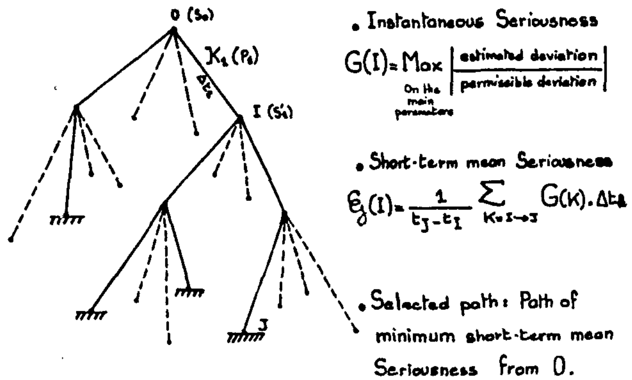

Figure 9 - Strategy for correction procedures

The mean seriousness of the best path $\mathcal{G}_J([I,J])$ chosen in I is noted $\mathcal{G}_J(I)$. This choice is made simply by taking, among all possible paths from I, the one which has the minimum mean seriousness.

The path from the root with the minimum mean seriousness is then selected and the implementation of the correction procedure corresponding to its first branch may begin.

5.2.3 - Overall strategy used

It is assumed that a correction procedure has just been completed. It may be the first part of a correction procedure (and there is then a dial monitoring phase usable in the framework of the strategy), or the second part of this correction (a fully completed correction procedure).

The model returns to the strategy (Fig.10) and begins with the evaluation of the instantaneous seriousness $G(0)$ at the root of the tree. This evaluation is restricted to the main parameters present in the memory and those read too far in the past are omitted (the omission phenomenon changes the seriousness of the situation as perceived by the pilot and makes his behavior more realistic).

After the evaluation of $G(0)$, the model asks itself the following question . is the situation serious ? (is $G(0)$ over a certain level of minimum seriousness ?).

- If the answer is "no", the model monitor dials while using the strategy with Markov readings and begins again the evaluation of the instantaneous seriousness $G(0)$.
- If the answer is "yes" the model asks itself whether the situation is well recognized.

If the situation is not recognized, the model makes all necessary readings in a deterministic manner, thus allowing full knowledge of this situation.

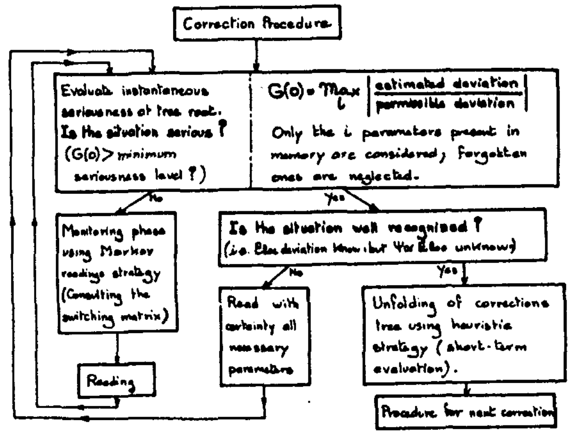

Figure 10 - Overall strategy

If the situation is serious and well recognized, the model unfolds the tree of the all possible corrections and makes a choice between them while evaluating the short-term situation.

6 - Results

Final descent sub-phases have been made by the model with conventional instrument without external vision (IFR conditions). These sub-phases have been displayed on the scope of a Cathode Ray Tube display with superposition of the head-up information (Fig.11) only for illustration of the results.

It has been shown in the introduction that a better display of information could decrease the pilot's workload and therefore improve flight safety. Information display by a head-up display is one of the solution that could be considered.

If a program with self-learning features is used, such a display mode of information will sensibly change the strategy and the correction procedures with beneficial effects on the overall system performance and the pilot's workload.

The various returns to the strategy during a final descent sub-phase are indicated on Fig. 12 for the case of initial airspeed (+8 kts), glide (+0,2°) and localizer (+0,5°) deviations. One can see on the same figure the unfolding of the first tree (with a single branch) and the various seriousness associated with each branch; the latter led to the choice of the correction on the parameter with the branch of minimum seriousness.

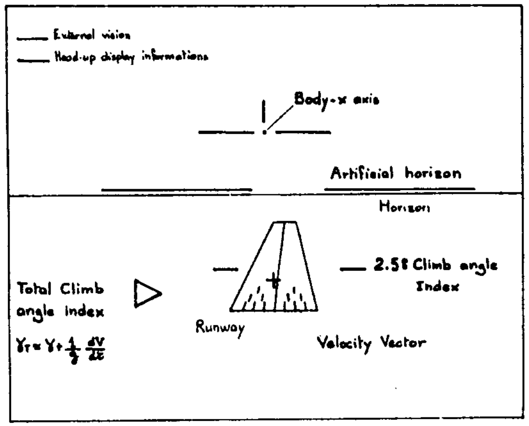

Figure 11 - Head-up display information

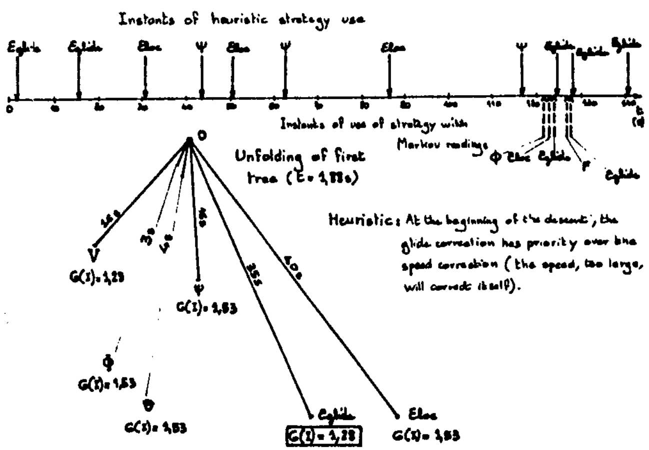

Figure 12 - Example of strategy use

The digital model responses have been compared, in the case of the final descent considered above, with the responses of a human pilot on our static simulation cockpit. The correction procedure coefficients (parameter of the magnitude laws) of the digital model have been adjusted in order to obtain approximate coincidence between the two types of responses (Fig.13). A good coincidence is achieved during the first correction procedure; responses, then, become oscillatory with small amplitude about nominal values.

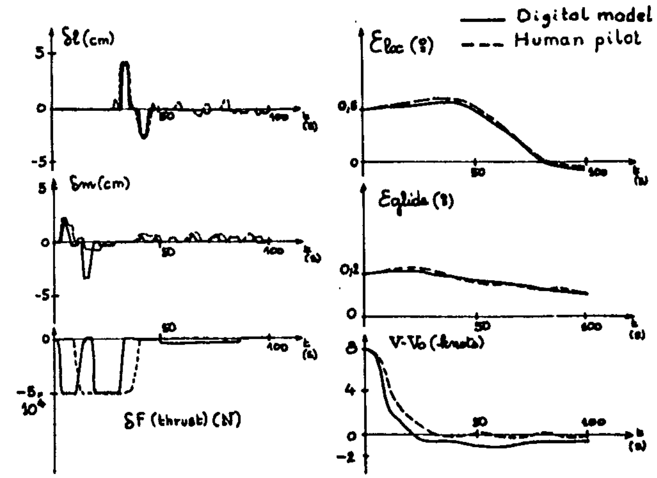

Figure 13 - Responses comparison

7 - Conclusion

A digital program simulating the behavior of the pilot of a transport plane (of Airbus A300B type) is now operating for one flight sub-phase (final descent of the ILS approach).

Future investigations will be concerned with the introduction of the self-learning capability, that is the auto-adaptation of the pilot's model to any type of new aircraft and also the analysis of the influence of information display on the pilot's behavior and workload. These investigations will be implemented using a moving flight simulator at the Istres Flight Test Center.

REFERENCES

[1] - Wanner JC.- General guideline for the design of manned aerospace vehicles, dans "Automation on Manned Aerospace System" - AGARD Conf. Proc. n°114 (1973).

[2] - Wanner JC.- Présentation des informations nécessaires pour le décollage et l'atterrissage, dans "Take-off and Landing" - AGARD Conf. Proc. n°160 (1975) - Mémoire n°10.

[3] - Cavalli D., Soulatges D. - Discrete time modelization of human pilot behavior - Proceedings of the 11th Annual Conference on Manual Control - NASA-Ames Research Center, Ca., May 1975. NASA TM X-62, 464.

MULTIPLE CURVED DESCENDING APPROACHES AND THE AIR TRAFFIC CONTROL PROBLEM

Sandra G. Hart   Duncan McPherson   John Kreifeldt
San Jose State University Foundation   Tufts University
San Jose, California   Medford, Mass.

ABSTRACT

Several modifications of the current terminal area air traffic control system were investigated in the multi-cockpit ATC facility located in the Man-Vehicle Systems Research Division at NASA-Ames Research Center. The purpose was to evolve a system in which the projected increase in air traffic could be accomodated safely and expeditiously. The concepts which were investigated included: (1) One minute separation at the Missed Approach Point, (2) the use of traffic situation displays in the cockpit coupled with a distributed air traffic management system, (3) multiple curved descending final approaches that merge on a common final within one mile of the field, and (4) parallel runways certified for independent and simulataneous operation under IFR conditions.

Three groups each consisting of three commercial airline pilots and two air traffic controllers flew a combined total of 450 approaches. Piloted simulators were supplied with computer generated traffic situation displays and flight instruments. The controllers were supplied with a terminal area map display and digital status information.

On the average, aircraft arrived at the Missed Approach Point at 64 sec intervals, which was approximately the separation set as the goal of the task. Performance was typically better under the distributed than under the ground centralized traffic management system and both pilots and controllers felt that the distributed management system enhanced flight safety, expeditiousness, and orderliness. Pilots reported that they would prefer the alternative of multiple curved descending finals, with wider spacing between aircraft, to having closer spacing on single straight-in finals. Controllers, on the other hand, reported that closer spacing on single straight-in finals was a preferable way to deal with increased aircraft density than multiple curved finals converging on a short straight-in final. Both pilots and controllers felt that parallel runways certified for independent and simultaneous operation under IFR conditions, such as simulated in the present study, would be an acceptable, ever desirable, solution.

omit

omit

MODELING AAA TRACKING DATA USING THE OPTIMAL CONTROL MODEL

by

David L. Kleinman
University of Connecticut

and

Betty Glass
Systems Research Laboratory

ABSTRACT

We demonstrate the process of applying the optimal control model of human response to study tracking performance in a AAA system. A priori values for the model parameters are chosen easily; these can be fine-tuned to match the tracking characteristics of a given gunner. The resulting model and parameter set are shown to give excellent predictions of tracking error ensemble statistics, for arbitrary aircraft flybys, in both lateral and longitudinal axes.

omiT

PILOT/VEHICLE MODELING FOR DETERMINING AIRCRAFT SIMULATION REQUIREMENTS

Sheldon Baron and Ramal Muralidharan
Bolt Beranek and Newman Inc.
Cambridge, Massachusetts

ABSTRACT

The development of engineering requirements for man-in-the-loop digital simulation is a complex task involving numerous trade-offs between simulation fidelity and costs, accuracy and speed, etc. The principal issues confronting the developer of a simulation involve the design of the cue (motion and visual) environment so as to meet simulation objectives and the design of the digital simulation model to fulfill the real-time requirements with adequate accuracy.

This paper discusses the second problem, design of the simulation model. This problem has become increasingly important and difficult as digital computers play a more central role in the simulations. Although there has been considerable analysis of digital simulation of continuous control systems, this analysis has virtually ignored the problems associated with having a human controller in the loop. But the human pilot is a unique controller in many ways, having special limitations and adaptive capabilities. To understand the significance of various sub-system errors and their interaction when a human operator is the controller, a closed-loop analytic model is needed. In this paper, we discuss such a model based on the optimal control model of the human operator and present preliminary analytical results showing the effects of simulation limitations on performance and workloads.

MONTE-CARLO SIMULATION OF HUMAN OPERATOR RESPONSE

by

David L. Kleinman
University of Connecticut

Jeffrey Berliner
Bolt Beranek and Newman, Inc.

Walt Summers
Aerospace Medical Res. Lab

ABSTRACT

The optimal control model of human response is used to generate simulated time histories of pertinent variables in a closed-loop man-machine control task. The methods by which Monte-Carlo sample paths are generated, including model formulation, equation discretization, and on-line estimation of noise covariances, are discussed. The results apply to both stationary and non-stationary tasks. Using a AAA tracking problem as an example, sample paths are compared with real data. The ensemble statistics of these model-generated paths are compared with averaged data and analytic covariance propagation results.

Session VII

MOTION AND VISUAL CUES

Chairman: L. R. Young

N79-17509

USING MODEL ORDER TESTS TO DETERMINE SENSORY INPUTS IN A MOTION STUDY*

D. W. Kepperger A. M. Junker

Aerospace Medical Research Laboratory
Wright-Patterson Air Force Base, Ohio 45433

ABSTRACT

In the study of motion effects on tracking performance, a problem of interest is the determination of what sensory inputs a human uses in controlling his tracking task. In the approach presented here a simple canonical model (PID or a proportional, integral, derivative structure) is used to model the human's input-output time series. Using a test discussed by Astrom [1], a study of significant changes in reduction of the output error loss functional is conducted as different permutations of parameters are considered. Since this canonical model includes parameters which are related to inputs to the human (such as the error signal, its derivatives and integration), the study of model order is equivalent to the study of which sensory inputs are being used by the tracker. The parameters are obtained which have the greatest effect on reducing the loss function significantly. In this manner the identification procedure converts the problem of testing for model order into the problem of determining sensory inputs.

*The research reported in this paper was sponsored by the Aerospace Medical Research Laboratory, Aerospace Medical Division, Air Force Systems Command, Wright-Patterson Air Force Base, Ohio 45433. This paper has been identified by the Aerospace Medical Research Laboratory as AMRL-TR-77- . Further reproduction is authorized to satisfy needs of the U. S. Government.

I. Introduction

The study of the effects of motion on human tracking performance is an area which has achieved increased emphasis and importance in the Air Force. One example of this need is in a quantitative assessment of how a pilot's control behavior is modified by the presence of motion cues which has immediate application in the area of motion base simulator design.

At the Aerospace Medical Research Laboratory (AMRL), Wright-Patterson Air Force Base, Ohio, an extensive motion program is currently being conducted to study many of the different aspects of motion effects on the human involved in a tracking task. The roll axis tracking task at AMRL was investigated for a variety of plant dynamics and has been documented in [2] and [3]. An extension of the Roll Axis Tracking Study was the peripheral display experiment which has been discussed in [4], [5], and [6], with an application of modeling in [7].

Recently at AMRL the study of motion effects has been extended to investigate the effects of washout in an improved version of the Roll Axis Tracking Simulator. A study of washout effects will answer the question as to the credibility of a ground base simulator as compared to the actual flight mission. A second simulator called the Multi Axis Tracking Simulator (MATS) has been recently added to AMRL and this simulator has the capability of providing motion in the roll, pitch, and yaw axes. By using the MATS and applying the Bolt Beranek and Newman (BBN) optimal control model to determine those experimental design conditions which would give rise to performance changes, a study was run [8,9] in which the model predicted experimental results prior to executing the experiment.

The model predictions were within one standard deviation of the means of the experimental results for approximately 80% of the experimental

PRECEDING PAGE BLANK NOT FILMED

34

variables considered. These results were averaged across six subjects involved in four tracking tasks. The data base was taken from the MATS experiment for this paper to investigate a modeling approach based on a simple canonical model termed the PID or Proportional Integral Derivative modeling approach.

II. Motivation for Using a Simple Canonical Model

In the study of manual control problems in which data has already been collected there exists several advantages in studying data when model parameters can be expressed in a PID formulation. The primary motivation for such a representation of a human is in the quantification of the ability of the human to differentiate (lead generation).

Figure (1a) illustrates the man-in-the-loop problem considered here. For the purposes of analysis, the time series variables that are available for modeling are illustrated in Figure (1b). The displayed error signal e(t) which is the input to the man is also the input time series to the computer model. The output time series of the man is denoted as ST(t). The computer model has an output $\hat{ST}(t)$ which is the best (*in the sense of least squares*) estimate of ST(t) based on the structure of the model assumed and the available data e(t) and ST(t). This type of modeling is termed output error because the difference between two time series outputs are considered. The modeling error is denoted as $e_M(t)$ and it satisfies

$$e_M(t) = ST(t) - \hat{ST}(t) \tag{1}$$

The objective of this identification procedure is to choose a transfer function H(s) to minimize the output error loss functional J denoted as:

$$J = \frac{1}{N} \sum_{i=1}^{N} [e_M(t_i)]^2 \tag{2}$$

where N is the number of samples of data.

The choice of the canonical model H(s) is the primary motivation for the approach presented in this paper. If H(s) can be chosen in a manner such that the human can be characterized by parameters which quantify the amount of differentiation or lead generation in a tracking task, then this model has application in the study of manual control problems. In addition, it will be shown in the sequel, that for each possible displayed variable (such as e(t), $\dot{e}(t)$, and $\ddot{e}(t)$), a noise source associated with these displayed variables can be determined. First the canonical model will be specified as follows:

$$H(s) = \frac{a_0 + a_1 s^1 + a_2 s^2 + \frac{a_3}{s}}{(1 + s/\alpha)^3} \tag{3}$$

where s is the Laplace transform variable. Equation (3) is an ideal representation of the man-in-the-loop for several reasons. The coefficients a_0, a_1, and a_2 represent differentiation (or lead generation) in the tracking task. Therefore, instead of giving heuristic arguments as to whether the describing function of the man has more lead in one experimental condition as compared to another, the coefficients a_0, a_1, and a_2 will quantitatively indicate this fact. Also, the coefficient a_3 allows the consideration of precognitive effects in a quantitative manner. The coefficient α in equation (3) is used to generate a third order pole for some value of α greater than 10 radians. This allows the transfer function H(s) to have a denominator with a higher order polynomial of s than the numerator and hence can be realized using state variables. The form of equation (3) allows the transfer function H(s) to have any amount of lead (including up to double differentiation) *for frequencies from 0 to α radians.* The amount of lead generation will depend on the numerical values of the coefficients a_0, a_1, and a_2.

Another interpretation of the transfer function H(s) in equation (3) can be seen in Figure (2). In Figure (2) the man is replaced by a parallel processing channel which describes the input signal e(t) and the output signal ST(t). The coefficients a_0, a_1, a_2 and a_3 indicate with what importance this

particular time signal is converted or processed into the stick signal ST(t). If $a_2 >> a_o$ and $a_2 >> a_1$ then one would expect the signal ST(t) to be dominated by double differentiation of e(t). On a Bode plot of $\frac{ST(s)}{E(s)}$, one would expect to see second order lead characteristics. Also, in Figure (2) the vector white noise sources $\xi_1(t)$, $\xi_2(t)$, $\xi_3(t)$, and $\xi_4(t)$ have special significance. These noise sources can be determined by identifying the coefficients a_o, a_1, a_2, and a_3 and injecting the modeling error into these noise sources. This approach is similar to the vector white noise Remnant Model proposed by Levison, Baron, and Kleinman [10] which has been validated experimentally. In the approach presented here the modeling error is generally a fixed percent of the magnitude (usually 5-10%) of the unknown coefficients (a_o, a_1, a_2 or a_3). Let β denote the percent of modeling error for a specific parameter (for example, a_o in Figure (2) which corresponds to an input e(t)), then:

$$\xi_1(t) = \beta\, a_o\, e(t) \tag{4}$$

For a time history an integral multiple of the periods of the sine waves, the following mean and variance of $\xi_1(t)$ results:

$$\xi_1 \text{ mean} = 0 \tag{5a}$$

$$\text{Var}\,[\xi_1(t)] = \beta^2 a_o^2\, \text{Var}\,[e(t)] \tag{5b}$$

Therefore, the variance of the noise sources $\xi_1(t)$ scales in proportion to the input channel error variance. This type of scaling of the noise variances in proportion to the variance of that component of the displayed error signal is what is desired. This Weber's law scaling effect has been discussed by Jex et al. [11] for an equivalent scalar injected noise source at the observation point of the human operator in the loop. Therefore, this approach allows uncorrelated human response to scale in proportion to the perceived variable. The implementation of this identification procedure is now presented to describe in detail the manner of computing the unknown parameters.

III. Implementation of This Identification Procedure

In reference [7], an identification approach was applied to roll axis tracking data for a specified choice of state variables. In [7] it was difficult to validate the model because of the complex manner of the implementation procedure. This paper will illustrate a much simplier manner of implementing a PID type model and, in addition, provide several ways to validate such a model. Figure (3) illustrates the implementation procedure used in this paper which is equivalent to the diagram in Figure (2). The first step in the implementation procedure is to determine the prefiltered variables $\hat{e}(t)$, $\dot{\hat{e}}(t)$, $\ddot{\hat{e}}(t)$, and $\int_o^t e(\tau)d\tau$ by the following realizable transfer functions (capital letters indicate Laplace Transform Variables):

$$\hat{E}(s) = E(s) \tag{6a}$$

$$\frac{\hat{\dot{E}}(s)}{E(s)} = \frac{s}{(1 + s/a)^2} \tag{6b}$$

$$\frac{\hat{\ddot{E}}(s)}{E(s)} = \frac{s^2}{(1 + s/a)^2} \tag{6c}$$

$$\frac{\int_o^t \hat{E}(\tau)d\tau}{E(s)} = 1/s \tag{6d}$$

Equations (6a-d) are easily implemented by using digital filter techniques. The identification stage of this implementation procedure requires the choosing of state variables so that a_o, a_1, a_2, and a_3 can be obtained. In the identification procedure, the following relationship holds:

$$ST(t) = ST_1(t) + ST_2(t) + ST_3(t) + ST_4(t) + \xi_1 + \xi_2 + \xi_3 + \xi_4$$

To implement these equations choose state variables:

$$X_1 \triangleq ST_1(t) \tag{7a}$$

$$X_2 \triangleq ST_2(t) \tag{7b}$$

$$X_3 \triangleq ST_3(t) \tag{7c}$$

$$X_4 \triangleq ST_4(t) \tag{7d}$$

Then

$$\frac{X_1(s)}{E(s)} = \frac{a_0}{1 + s/\alpha} \quad (8a)$$

$$\frac{X_2(s)}{\dot{E}(s)} = \frac{a_1}{1 + s/\alpha} \quad (8b)$$

$$\frac{X_3(s)}{\ddot{E}(s)} = \frac{a_2}{1 + s/\alpha} \quad (8c)$$

$$\frac{X_4(s)}{\int_0^t E(\tau)d\tau} = \frac{a_3}{1 + s/\alpha} \quad (8d)$$

The implementation of equations (8a-d) proceeds as follows:

$$\begin{bmatrix} \dot{X}_1 \\ \dot{X}_2 \\ \dot{X}_3 \\ \dot{X}_4 \end{bmatrix} = [-\alpha] \begin{bmatrix} X_1 \\ X_2 \\ X_3 \\ X_4 \end{bmatrix} + [\alpha a_0,\ \alpha a_1,\ \alpha a_2,\ \alpha a_3] \begin{bmatrix} e(t) \\ \dot{e}(t) \\ \ddot{e}(t) \\ \int_0^t e(\tau)d\tau \end{bmatrix} \quad (9a)$$

$$ST(t) = [1,\ 1,\ 1,\ 1] \begin{bmatrix} X_1 \\ X_2 \\ X_3 \\ X_4 \end{bmatrix} + \sum_{i=1}^{4} \zeta_i(t) \quad (9b)$$

Therefore, the variable α is just the prefiltering variable, the unknowns are αa_0, αa_1, αa_2, and αa_3 which are determined from a least squares identification algorithm. The PID identification algorithm is determined by identifying α, a_0, a_1, a_2, and a_3.

In this implementation, the time series $e(t)$ was delayed by 0.20 seconds, $\dot{e}(t)$ was delayed by 0.12 seconds, and $\ddot{e}(t)$ was delayed by 0.04 seconds. The manner of achieving these delays was accomplished by shifting the real time series by an integral multiple of the sampling rate (.04 seconds). The assumption of different delays on the perceptual variables is perhaps a better assumption than a single, constant delay on all four channels. In the case of tracking with a motion disturbance it is reasonable to assume that information from rates and accelerations may be processed more rapidly than position information. Since the desire of this paper is to produce a lumped representation of a human, these lags were chosen over four experimental conditions of the motion experiment. Once this model is sufficiently validated, future work can be done to investigate the lags of each individual channel and for the different experimental conditions considered here.

A description of the MATS experiment and data base used for this study is next presented.

IV. The Multi Axis Tracking Simulator (MATS)

Figure (4) illustrates a physical diagram of the MATS. A brief description of this simulator will be presented here. A more complete description can be found in [8,9].

The MATS simulator was used only in the roll axis for this study with two independent inputs: ϕ TARGET and ϕ DISTURBANCE as indicated in Figure (4). Four modes of tracking were conducted:

(1) STATIC DISTURBANCE
ϕ Target = 0 with ϕ Disturbance $\neq$ 0 with no motion

(2) MOTION DISTURBANCE
ϕ Target = 0 with ϕ Disturbance $\neq$ 0 with roll motion

(3) TARGET STATIC
ϕ Target $\neq$ 0 with ϕ Disturbance = 0 with no motion

(4) TARGET MOTION
ϕ Target $\neq$ 0 with ϕ Disturbance = 0 with roll motion

The two input spectrums ϕ Target and ϕ Disturbance were designed based upon apriori guesses of inputs that gave rise to performance changes as indicated by the BLN optimal control pilot vehicle model. Figure (5) is a plot of the two input spectrums. The effective plant dynamics controlled by the subjects was specified by:

$$G(s) = \frac{10.0}{s(1 + s/5)\ (1 + s/20)} \tag{10}$$

The subjects involved in the experiment were six college students (male and female) 18-25 years of age. The subjects tracked each of the four experimental conditions for 165 seconds each day with the runs presented in a random sequence. The subjects were told to minimize the following score:

$$C = \text{Score} = \sigma^2_{\phi\ \text{error}} + 0.1\ \sigma^2_{\ddot{\phi}\ \text{plant}} \tag{11}$$

At the end of each run the subjects were told the score, $\sigma^2_{\phi\ \text{error}}$, and $0.1\ \sigma^2_{\phi\ \text{plant}}$. They were instructed to minimize the total score. When the scores reached asymptotic levels, subject training was assumed to be accomplished. The experiment was then run for an additional eight days and data was collected. The performance results are summarized in Table I for the eight days of collected data.

TABLE I

		TARGET MOTION	TARGET STATIC	DISTURBANCE MOTION	DISTURBANCE STATIC
C (Score)	Mean	66.1	72.8	78.0	197.0
	S.D.	7.5	8.9	15.5	29.0
e^2_{RMS}	Mean	46.245	56.4558	16.248	66.6688
	S.D.	13.2547	11.45549	8.910	16.71518

One can see from Table I that in the disturbance mode of operation the effects of motion on performance were quite profound. In the target mode of operation the effects of motion were not that pronounced.

Another measure of performance is the variances of the error, error rate, and error acceleration. For the disturbance input case these variables became the plant position, rate and acceleration with just a -180° sign change in this signal. These variables were calculated and averaged across subjects. The results of these time series answers are displayed in Table II.

TABLE II

		TARGET MOTION	TARGET STATIC	DISTURBANCE MOTION	DISTURBANCE STATIC
σ_e	Mean	6.90	7.06	4.2	8.83
	S.D.	0.78	0.74	1.5	1.80
$\sigma_{\dot{e}}$	Mean	11.8	11.9	6.81	11.9
	S.D.	0.79	0.7	1.41	1.3
$\sigma_{\ddot{e}}$	Mean	40.02	39.522	24.0	33.6
	S.D.	15.161	8.33	1.9	5.0

The numerical values in Table II are also measures of performance which are an important aspect of this experiment.

V. Parametric Results From the Identification Algorithm:

Using various values of $a = 5$ to $a = 50$ radians, the identification scheme was applied to the time series data e(t) and ST(t) over the four conditions of motion inputs. Table III illustrates the resulting parametric values for $a = 20$.

In order to show that such a model has credibility it was validated two different ways. *The purpose of a validation is to demonstrate that this* lumped, simplified model can adequately represent the human in the tracking task. Model order tests were used to determine which parameters (or inputs) to the human had the greatest effect in reducing the output error loss functional of equation (2). In the following sections we present the validation results and parameter sensitivity tests.

TABLE III - α = 20

		TARGET MOTION	TARGET STATIC	DISTURBANCE MOTION	DISTURBANCE STATIC
a_o	Mean	.0526004	.090332	-.4435146	-.161328667
	S.D.	.008456306	.00710845	.058885703	.02343810
a_1	Mean	.00397449	.00590767	-.1141918	-.01287437
	S.D.	.0028907	.00352572	.015809079	.0058299
a_2	Mean	.0002010	-.000792808	-.00121983	.0136601
	S.D.	.0003102	.000462707	.00130466	.001958
a_4	Mean	-.003723948	-.0002520066	.001952651	.0004614711
	S.D.	.0086512954	.0007673611145	.0030386457	.001072189

VI. Two Methods of Model Validation

The lumped model developed here was validated in the frequency domain and also in the time domain. The first method of model validation was a comparison of averaged values of spectra plots (Fast Fourier Transforms) to averaged values of the PID parameters. In this manner a spectra identification procedure is compared to a parametric identification algorithm. Using a Fast Fourier Transform program developed at AMRL, ensemble averages of the spectra of the time series e(t) and ST(t) were obtained for the four tracking tasks considered here. In addition, the parametric plots of Table III were obtained for the mean values of the parameters and two additional plots of the mean values of the parameters ± 1 standard deviation of these parameter values. Since the describing functions obtained from the FFT's were also plotted as mean values ± 1 standard deviation of each spectra estimate, the two ensemble plots can be overlaid and compared.

Figures (6), (7), (8), and (9) illustrate the plots of the two identification schemes overlaid. The results of Figures (6-9) indicate that the two schemes match best for the case of static disturbance and motion disturbance conditions. For the static target and motion target case, the two identification schemes match with less consistency.

In all four cases the uncertainty envelope obtained from one standard deviation of the parametric plots about their mean when overlaid with the corresponding envelope obtained from the spectra plots, results in overlap of these envelopes. One interpretation of this result is that the uncertainty in the parametric estimation scheme is no worse than the uncertainty in the spectra estimates.

The second method of model validation is to consider how well the time series $\hat{ST}(t)$ generated from the computer model matches the experimental time history data ST(t). The ratio R given in equation (12) is a measure of this match. The ratio considered is

$$R = \left[1 - \frac{\sum_{i=1}^{N} [ST(t_i) - \hat{ST}(t_i)]^2}{\sum_{i=1}^{N} [ST(t_i)]^2} \right] (100\%) \qquad (12)$$

This variable is calculated and the results are displayed in Table IV.

TABLE IV

	TARGET MOTION	TARGET STATIC	DISTURBANCE MOTION	DISTURBANCE STATIC
R_{mean}	89.98%	94.76%	95.36%	95.94%
$R_{S.D.}$	1.6084	.86197	1.5274	1.1502

From the results of Table IV we can see that there is a high correlation between the model output time series and the output series from the empirical data.

It is now of interest to complete a sensitivity study on which parameters (a_o, a_1, a_2, or a_3) will reduce the output error loss functional of eq. 2. For the PID model developed here, the parameter which is most sensitive will indicate which of the possible inputs ($e(t)$, $\dot{e}(t)$, $\delta(t)$, or $\int_0^t e(\tau)d\tau$) is most important in describing the input-output characteristics of the human as a parallel processor of information. In this manner some incite can be obtained as to which input

sensory variable may be used by the human when he is represented in Figure (2).

VII. Using Model Order Tests to Validate the Model and to Determine Sensory Inputs To The Human

In an effort to investigate which sensory inputs are used by the human in the tracking task, two tests on the correct model order were considered. The two tests considered were Astrom's F-Ratio test [1] and a parameter consistency test [12] used in the mathematical biosciences literature. Before any tests are conducted, it is necessary to calculate values of the output error loss functional for different combinations of input parameters. In order to obtain a table of output error loss functional values, the following sequence of steps was performed on one experiment from each of the four motion modes of operation:

(1) Assume the human can be represented by one parameter.

(2) Calculate the loss functional J_1 of equation (2) for one parameter.

(3) Now assume the human can be represented by two parameters.

(4) Calculate J_2 for the two parameter case.

(5) Assume the human is represented by 3 parameters.

(6) Calculate J_3.

(7) Assume all four parameters characterize the human.

(8) Calculate J_4.

Using Astrom's test [1], a measure of which parameter significantly reduces the loss functional was conducted. Table V lists the values of the loss functional obtained here.

Since Table V contains many entries due to the numerous combinations of parameters considered here, it is desirable to study which patterns of parameters are important to investigate. The index of parameter consistency developed in [12] provides a method of simplifying the results in Table V. The following

TABLE V - VALUES OF LOSS FUNCTION

		TARGET MOTION	TARGET STATIC	DISTURBANCE MOTION	DISTURBANCE STATIC
J_1 = One Parameter Loss Function	a_0	.2976	.6274	.7576	.6249
	a_1	.5549	1.075	1.516	1.514
	a_2	.4633	.7532	1.564	1.241
	a_3	.5690	1.064	1.367	1.430
J_2 = Two Parameter Loss Function	a_0, a_1	.2815	.3309	.7208	.6136
	a_0, a_2	.2727	.5226	.6792	.6043
	a_0, a_3	.2934	.6040	.7099	.4130
	a_1, a_2	.4389	.7501	1.468	1.192
	a_1, a_3	.5549	1.064	1.439	1.149
	a_2, a_3	.4557	1.536	1.536	1.123
J_3 = Three Para-Meter L.F.	a_0, a_1, a_2	.2657	.2890	.5561	.5991
	a_0, a_1, a_3	.2622	.3205	.6922	.4123
	a_1, a_2, a_3	.4379	.7483	1.401	1.004
	a_0, a_2, a_3	.2647	.5094	.6091	.3833
J_4	a_0, a_1, a_2, a_3	.2394	.2697	.5030	.3784

index of parameter consistency was used [12]:

$$\text{index} = \frac{1}{M} \sum_{i=1}^{M} \frac{\sigma_i}{\mu_i} \qquad (13)$$

where M = the number of parameters considered, σ_i is the standard deviation of the parameter, and μ_i is the mean value of the absolute value of this parameter. According to the test in [12], this index of consistency is smallest when the correct system order is determined. Table VI lists the calculations of this index of consistency for the parameters displayed in Table III.

From Table VI it can be seen that when the parameter a_3 is included with any other group of parameters, the index of consistency increases substantially. This can be seen, for example in the motion target case where

$$\text{index}\ (a_0, a_1) = .312$$
$$\text{index}\ (a_0, a_1, a_3) = ..413$$

TABLE VI - THE INDEX OF PARAMETER CONSISTENCY

PARAMETERS CONSIDERED	TARGET MOTION	TARGET STATIC	DISTURBANCE MOTION	DISTURBANCE STATIC
a_o	.107	.169	.102	.107
a_1	.538	.749	.158	.231
a_2	.305	.179	.149	.058
a_3	2.411	.842	1.415	2.367
a_o, a_1	.312	.165	.102	.432
a_o, a_2	.224	.175	.103	.100
a_o, a_3	1.067	.652	1.075	1.014
a_1, a_2	.383	.684	.148	.139
a_1, a_3	.832	6.172	.844	.664
a_2, a_3	5.304	.961	.960	2.767
a_o, a_1, a_2	.283	.177	.732	.475
a_o, a_1, a_3	1.413	.352	1.993	1.726
a_1, a_2, a_3	.246	3.368	.420	.662
a_o, a_2, a_3	1.565	.588	.688	.147
a_o, a_1, a_2, a_3	1.789	.554	.809	.824

This result is to be expected because the integration parameter a_3 (corresponding to an input $\int_o^t e(\tau)d\tau$) was by far the most inconsistent parameter. Since this tracking task was compensatory in nature with an input that was randomly appearing to the subjects, one would not expect a memory term such as a_3 to be representative of a human's input-output characteristics. Table VI also has some other interesting results. For the motion target case, the combination of parameters which produced the lowest index was a result of only a_o (or only the input $e(t)$). Referring to the describing function of the human (Figure (9)), this describing function is essentially flat (no lead). From Figure (9) we would conclude that the human is predominately acting as a gain; the model order test in Table VI confirms this fact in the time domain using this modeling approach.

For the static target case, Table VI indicates that the pair (a_o, a_1) (or the time series $e(t)$ and $\dot{e}(t)$) are probably the time series that are being processed by the human. With reference to Figure (7) it is observed that a small amount of lead is indicated at the upper frequencies. In this case the frequency results show concurrence with the model order tests.

In the disturbance motion case the results of the index test were not that clear because the values of index (a_o), index (a_o, a_1), and index (a_o, a_2) were very close together. From Figure (6) there is a small amount of lead compensation and one would expect this effect to show up in the parameters. This result can be observed by using the parameters in Table III and calculating the ratios $\frac{a_i}{a_o}$ i=1,2. Using the mean values of the a_i coefficients, i=1,2 the ratios are illustrated in Table VII.

TABLE VII

	TARGET MOTION	TARGET STATIC	DISTURBANCE MOTION	DISTURBANCE STATIC
$\frac{a_1}{a_o}$	.0755600718	.065399526	.257470216	.0798021222
$\frac{a_2}{a_o}$	.0038212637	.008776602	.002750372	.08467249

The ratio $\frac{a_1}{a_o}$ is the greatest for the motion disturbance case with the ratio $\frac{a_2}{a_o}$ the smallest. From Table VII the conclusion is that the term a_1 has the most dominant effect in the motion disturbance case. Astrom's test which is considered to be more sensitive [13] was used to investigate the aspect further.

In the disturbance static case, the lowest value of the index occurred for the high lead case (a_o, a_2) which corresponds to using the time series $e(t)$ and $\ddot{e}(t)$. Since motion inputs are not available in this task, one would not, in general, expect the human to obtain this type of information from displayed variables. One possible explanation of this effect is the need to reduce the

score C in equation (11) which has a penalty weighting on $\ddot{e}(t)$. From Table VII the ratio $\frac{a_2}{a_o}$ is greatest for the static disturbance case as compared to the other three conditions. This agrees with the model order test.

Astrom's model order test was applied to Table V and plots of the loss function were obtained. In order to examine Astrom's test, the following values of the cost function were compared.

$$J(a_o) \text{ to } J(a_o, a_1) \text{ to } J(a_o, a_1, a_2)$$

$$J(a_o) \text{ to } J(a_o, a_2) \text{ to } J(a_o, a_1, a_2)$$

In this manner we could determine if either a_1 or a_2 was the dominant factor in reducing the output error loss functional. Figures (10a-d) illustrates plots of this test for the four modes of operation.

In figure (10a) for the target motion case the parameter a_o appears to be the only significant parameter. This concurs with the index of consistency test used previously.

For the target static case the significant parameter appears to be a_1 in lieu of a_2. This agrees with the index of consistency test and the Bode diagrams. It should be noted that when the human acts as a first order differentiator in the static mode of operation, he is obtaining this information from the visual display of the error signal.

For the disturbance motion case it appears that all three parameters are necessary. The results of Astrom's test are not that definite and it is difficult to draw conclusions. In the disturbance static case the term a_2 has a slightly better effect in reducing the loss functional then a_1. This is the same result as from the parameter consistency index, however, the conclusion is not that strong. One would expect that in the static disturbance case information of the form $\ddot{e}(t)$ is not available from any motion sensory loop or from the visual display. The slope of Figure (8) is slightly greater than 20 db/decade which indicates differentiation is the greatest for this mode of the experiment.

In the disturbance mode of operation the primary factor was the d.c. gain a_o. From Table VII, the ratio $\frac{a_{o\,DM}}{a_{o\,SM}}$ was 2.749. The same ratio in the target condition was $\frac{a_{o\,MT}}{a_{o\,ST}} = .5823$. These results can be summarized as follows:

DISTURBANCE INPUT

(1) The d.c. gain a_o is 2.7 times as high in the motion case as compared to the static case.

(2) The lead terms a_1 and a_2 are much smaller in the motion case. In the static case, more lead generation is required to compensate for a low d.c. gain. This lead generation must be obtained from the visual display.

TARGET INPUT

(1) The d.c. gains differed slightly (static is larger than motion).

(2) There is more lead in the static case then in the motion case. Again, this lead generation must be due to visually displayed signals.

To complete this paper, Astrom's test was used to draw some conclusions from a statistical analysis. The test in [1] is based on the ratio Δ, defined by:

$$\Delta = \frac{J_1 - J_2}{J_2} \cdot \frac{N - n_2}{n_2 - n_1}$$

where J_1 and J_2 are values of the loss functional for n_1 and n_2 parameters, respectively and N is the number of input-output pairs of data points. The variable Δ is F distributed with $n_2 - n_1$, $N - n_2$ degrees of freedom. For N = 300 pairs of data points, if $\Delta > 3.09$ implies the loss functional has dropped significantly (with 95% probability). If $\Delta \leq 3.09$, no conclusions can be drawn. The following tests were conducted to study Figures (10a-d).

PAGE IS

CASE I - (Target Motion):

Tests

(1) Compare $J(a_o)$ to $J(a_o, a_1)$

(2) $J(a_o)$ to $J(a_o, a_2)$

(3) $J(a_o, a_1)$ to $J(a_o, a_1, a_2)$

CASE II - (Target Static):

Tests

(1) Compare $J(a_o)$ to $J(a_o, a_1)$

(2) $J(a_o)$ to $J(a_o, a_2)$

(3) $J(a_o, a_2)$ to $J(a_o, a_1, a_2)$

CASE III - (Disturbance Motion):

Tests

(1) Compare $J(a_o)$ to $J(a_o, a_1)$

(2) $J(a_o)$ to $J(a_o, a_2)$

(3) $J(a_o, a_1)$ to $J(a_o, a_1, a_2)$

CASE IV - (Disturbance Static):

Tests

(1) Compare $J(a_o)$ to $J(a_o, a_1)$

(2) $J(a_o)$ to $J(a_o, a_2)$

(3) $J(a_o, a_1)$ to $J(a_o, a_1, a_2)$

The results of the test appear in Table VIII.

Astrom's test is very sensitive to N the number of input-output pairs and a value of $\Delta < 3.09$ is required to reject the hypothesis that the drop in cost functional is significant (with 95% probability). The larger the value of Δ, implies the cost functional has dropped with greater significance (more sensitivity). The results of Astrom's test indicate the following:

DISTURBANCE CONDITION

(1) For the disturbance static condition, the cost functional does not drop substantially for any parameter. This result agrees with Figure (10d). Of the four parameters, a_2 appears to have the most sensitive effect on the reduction of the output error loss functional.

(2) In the disturbance motion case, the variable a_2 had the most sensitive effect (of the four parameters) on the cost functional in tests (2) and (3).

It is noted that in the disturbance conditions the statistical test is somewhat biased because the d.c. gain a_o changed by almost a factor of 3. Table VII with the normalized ratios provides the best method of comparison of the motion and static disturbance inputs.

TARGET CONDITION

(1) For the motion target case the terms a_1 and a_2 were not the sensitive parameters. This agrees with the previous tests in which a_o was determined to be the most significant parameter.

(2) For the static target case the term a_1 is the most sensitive parameter as indicated by tests (2) and (3). This result is in concurrence with the previous tests and the describing function plots.

The results of these model order tests can be summarized as follows:

(1) For the motion target case the dominant perceptual variable was $e(t)$.

(2) For the static target case the dominant perceptual variable was $\dot{e}(t)$.

(3) For the static disturbance case, the $e(t)$ variable was less dominant in the static case but substantially more lead was required. This lead is assumed to come from the visual display.

(4) In the motion disturbance case, less lead appeared in the human's transfer function. This is an indication that the trackers may be using their motion information to increase their d.c. gain and reduce the requirement of differentiating the displayed error signal.

TABLE VIII - ASTROM'S TEST

	TARGET MOTION	TARGET STATIC	DISTURBANCE MOTION	DISTURBANCE STATIC
TESTS (1) Δ =	17.044	267.020	15.214	5.488
TESTS (2) Δ =	27.210	59.759	34.398	10.214
TESTS (3) Δ =	17.661	240.066	87.962	7.188

It is noted that the coefficients a_0, a_1, and a_2 obtained in the disturbance condition and the spectra plots obtained here concur with many of the results in the data base obtained by Shirley and Young [14]. This can be seen by the fact that in the disturbance condition, there is a higher d.c. gain in the motion condition as compared to the static condition. In the static disturbance condition, the lower d.c. gain results in more slope in the describing function of the human. These results concur with the earlier spectra results [14] and support the conclusion that roll-motion cues permit the pilot to increase his gain without a loss of system closed-loop stability for the disturbance condition.

Using the optimal control model to model the earlier data [14], Curry, et al. [15] treated the vestibular signal strictly as an additional measurement used in the control feedback loop. The same conclusions (i.e. the pilots tendency to increase his gain without a loss of system closed-loop stability) appear as a result of the modeling effort [15].

VIII A. Third Method of Validation - Analog Simulation

Since the model developed in this paper shows credibility in both the time domain and in the frequency domain, one would expect that an analog simulation could replace the human in the loop. In an effort to observe how an auto-pilot could replace the man in the loop, a simulation was constructed for the parameters from the target motion condition (table III) and inserted in the loop. Using an analog simulation of the MATS, the autopilot was required to track the MATS for the target input condition. Figure (11a) illustrates the resulting spectrums of the mean error signal from the data (composed of correlated and uncorrelated parts). Also plotted in figure (11a) is the spectrum of the error signal for the condition of the autopilot in the loop.

From figure (11a) it is easily seen that the correlated spectrum of the error signal from the data and the autopilot appear to match. The uncorrelated portion of the error signal does not match because the autopilot is strictly a deterministic model. Since the input forcing function is deterministic (sum of sines) and the plant was linear, the error signal should have no uncorrelated response. From figure (11a), the -50 db level of $e_{Uncor.}$ for the autopilot is due to noise from the analog simulation and the process of computing the spectra.

In an effort to match the two error spectrums, white-gaussian noise passed through a low pass filter was injected at the stick in the autopilot simulation. Figure (11b) shows the resulting spectra for the autopilot with the noise inserted in the loop. The power in the noise that was inserted into the loop was determined by the power in the $e_{Uncor.}$ spectrum in figure (11a) with the fact that the uncorrelated part of e can only be due to the white noise as it is passed through the transfer function of the plant. From figure (11b) we see that the autopilot can reproduce similar performance results if it replaces the man in the loop.

The important point in the autopilot simulation considered here is that in order to describe the humans characteristics, it was necessary to both insert a deterministic model, and in addition, to insert a white noise source to account for the human's randomness.

IX. Summary and Conclusions

A study of model order was conducted using statistical analysis and a canonical PID model. The results of the model order test give incite as to which displayed quantity was being used by the human in the tracking task. The data base used in this study was part of a motion study involving humans in a multi axis tracking simulator.

REFERENCES

[1] Astrom, K. J. and Eykhoff, P., "System Identification-A Survey", Automatica, Vol. 7, pp. 123-162, 1971.

[2] Junker, A. M., and C. Replogle, "Motion Effects on the Human Operator in a Roll Axis Tracking Task", Aviation, Space and Environmental Medicine, Vol. 46, pp. 819-822, June, 1975.

[3] Levison, W. H., Baron, S., and Junker, A. M., "Modeling the Effects of Environmental Factors on Human Control and Information Processing", AMRL-TR-76-74, August, 1976.

[4] Junker, A. M. and Price, D. R., "Comparison Between a Peripheral Display and Motion Information on Human Tracking About the Roll Axis", AIAA Visual and Motion Simulation Conference, Dayton, Ohio, April, 1976.

[5] Moriarty, T. E., Junker, A. M., and Price, D. R., "Roll Axis Tracking Improvement Resulting from Peripheral Vision Motion Cues", The Twelfth Annual Conference on Manual Control, University of Illinois at Urbana-Champaign, May 25-27, 1976.

[6] Price, D. R., "A Study of the Effect of Peripheral Vision Motion Cues on Roll Axis Tracking", Master of Science Thesis, Air Force Institute of Technology, December, 1975.

[7] Repperger, D. W., and Junker, A. M., "PID (Proportional Integral Derivative) Modeling Techniques Applied to Studies of Motion and Peripheral Display Effects on Human Operator Performance", The Twelfth Annual Conference on Manual Control, NASA TMX-73, 170, pp. 703-718, 1976.

[8] Junker, A. M. and Levison, W. H., "Recent Advances in Modeling the Effects of Roll Motion on the Human Operator", submitted for publication, Aviation, Space, and Environmental Medicine.

[9] Junker, A. M. and Levison, W. H., "Use of the Optimal Control Model in the Design of Motion Cue Experiments", The Thirteenth Annual Conference on Manual Control, MIT, 1977.

[10] Levison, W. H., Baron, S., and Kleinman, D. L., "A Model for Human Controller Remnant", IEEE Transactions on Man-Machine Systems, Vol. MMS-10, No. 4, December, 1969, pp. 101-108.

[11] Jex, H. R., Allen, R. W., and Magdaleno, R. E., "Display Format Effects on Precision Tracking Performance, Describing Functions, and Remnant", AMRL-TR-71-63, August, 1971.

[12] Desai, V. K. and F. W. Fairman, "On Determining the Order of a Linear System", Mathematical Biosciences, Vol. 12, pp. 217-224, 1971.

[13] Chan, C. W., Harris, C. J., and Wellstead, P. E., "An Order-Testing Criterion for Mixed Autoregressive Moving Average Processes", International Journal of Control, Vol. 20, No. 5, pp. 817-834, 1974.

[14] Shirley, R.S. and Young, L.R., "Motion Cues in Man-Vehicle Control", IEEE Transactions on Man-Machine Systems, Vol. MMS-9, No. 4, December, 1968, pp. 121-128.

[15] Curry, R.E., Hoffman, W.C., Young, L.R.,"Pilot Modeling For Manned Simulation" AFFDL-TR-76-124, Volumn 1, December, 1976.

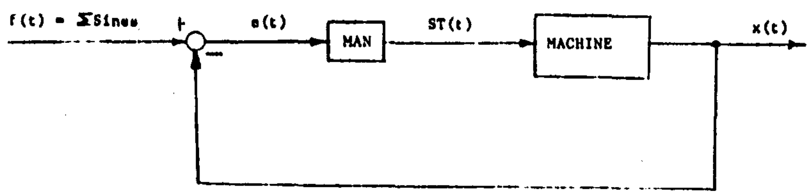

Figure (1a) - The Closed Loop Tracking Task

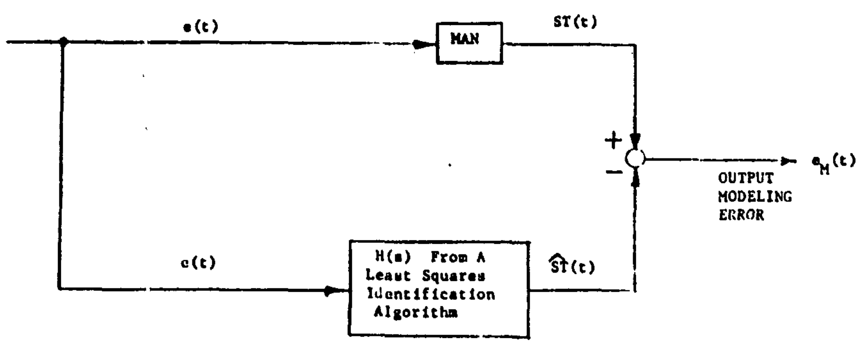

Figure (1b) - The Internal Loop Approach

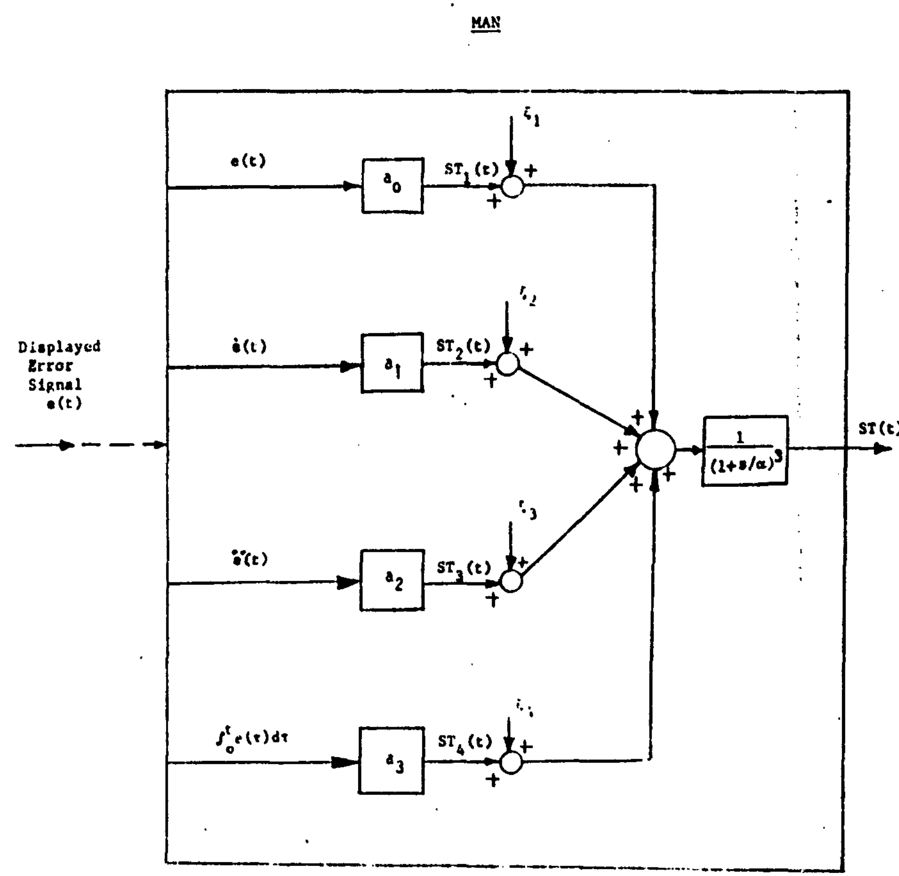

Figure (2) - Man As A Parallel Information Processor

Figure (4) - The Mixed Axis Tracking Simulator (MATS)

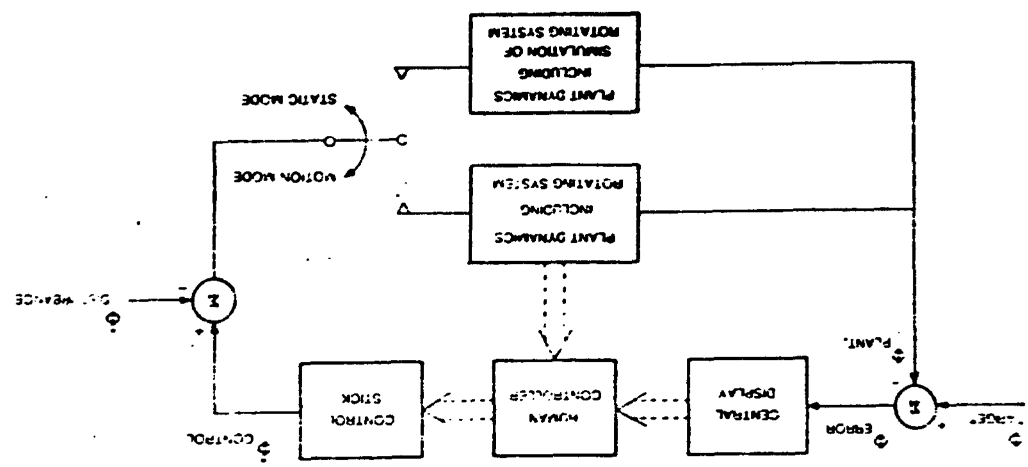

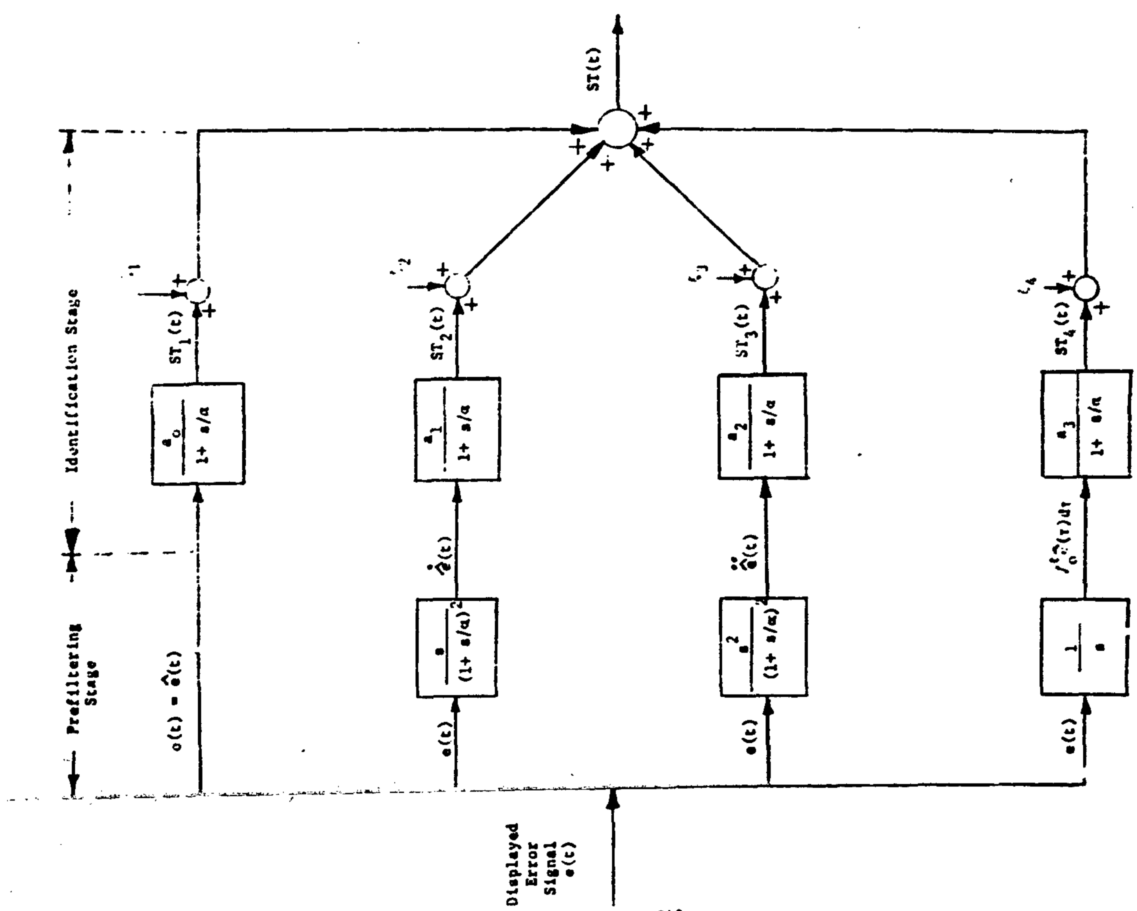

Figure (3)- Implementation of This Identification Approach

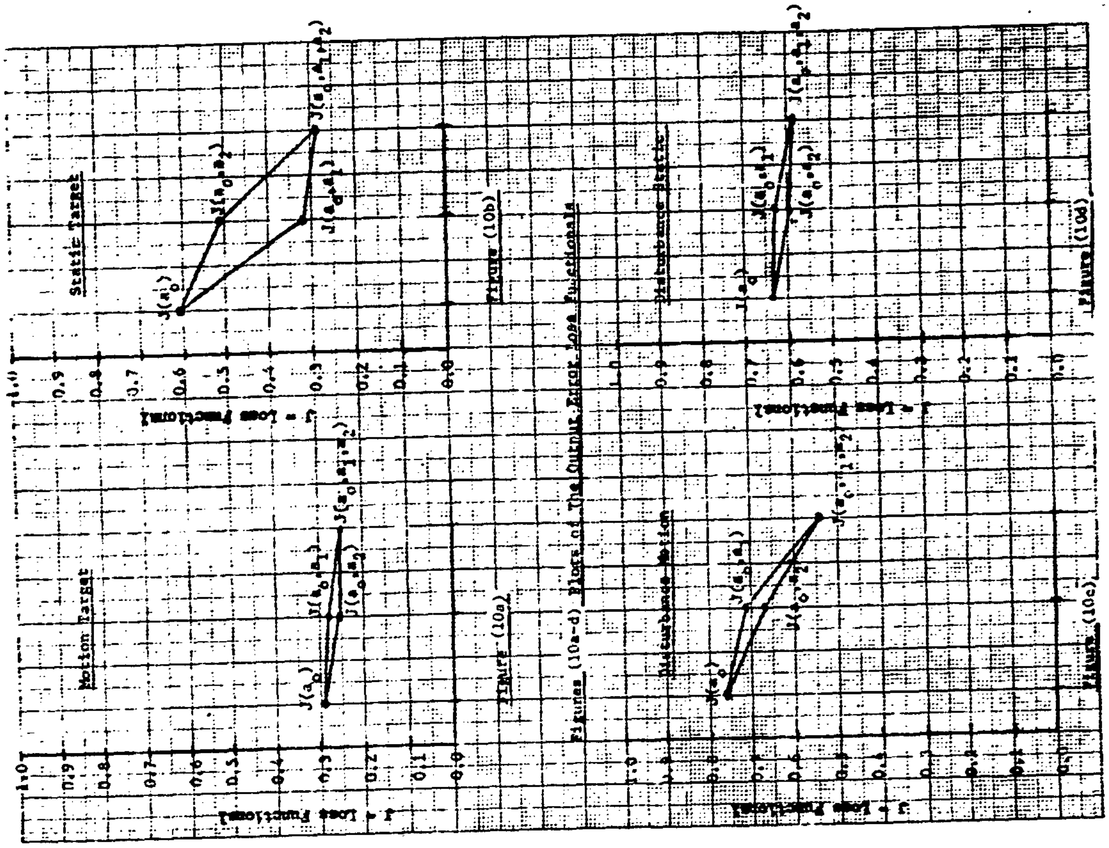

Figures (10a-d) Plots of The Output Error Loss Functionals

ORIGINAL PAGE IS
OF POOR QUALITY

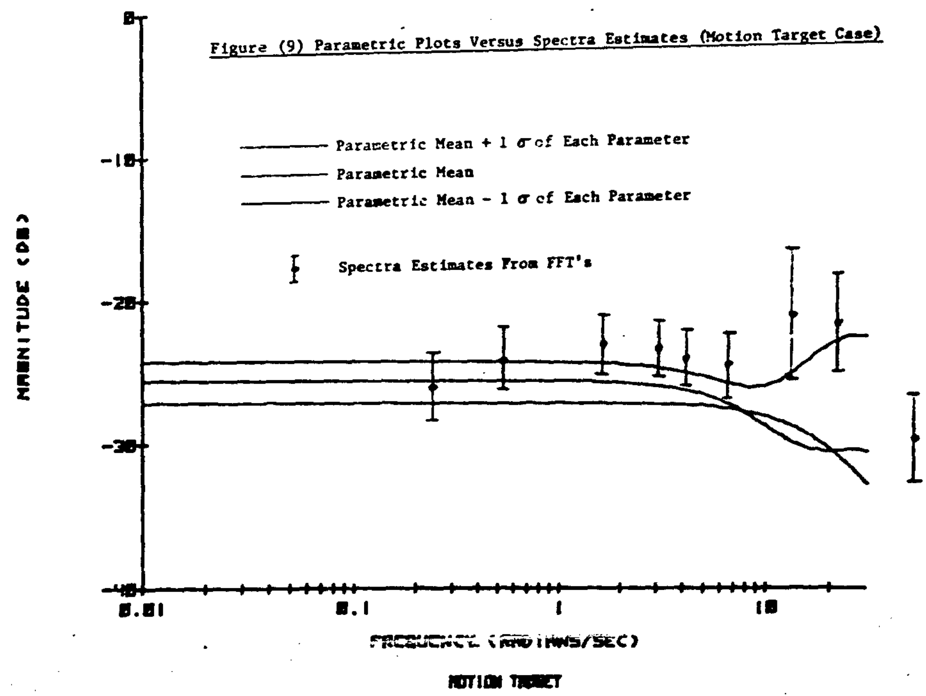

Figure (9) Parametric Plots Versus Spectra Estimates (Motion Target Case)

Figure (6) Parametric Plots Versus Spectra Estimates (Static Disturbance Case)

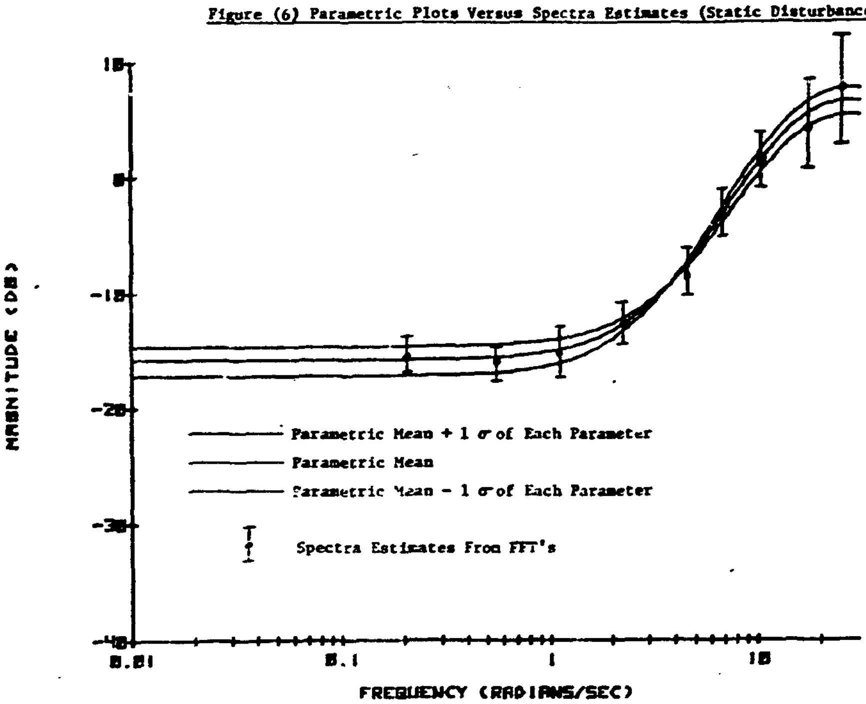

STATIC DISTURBANCE

Figure (7) Parametric Plots Versus Spectra Estimates (Static Target Case)

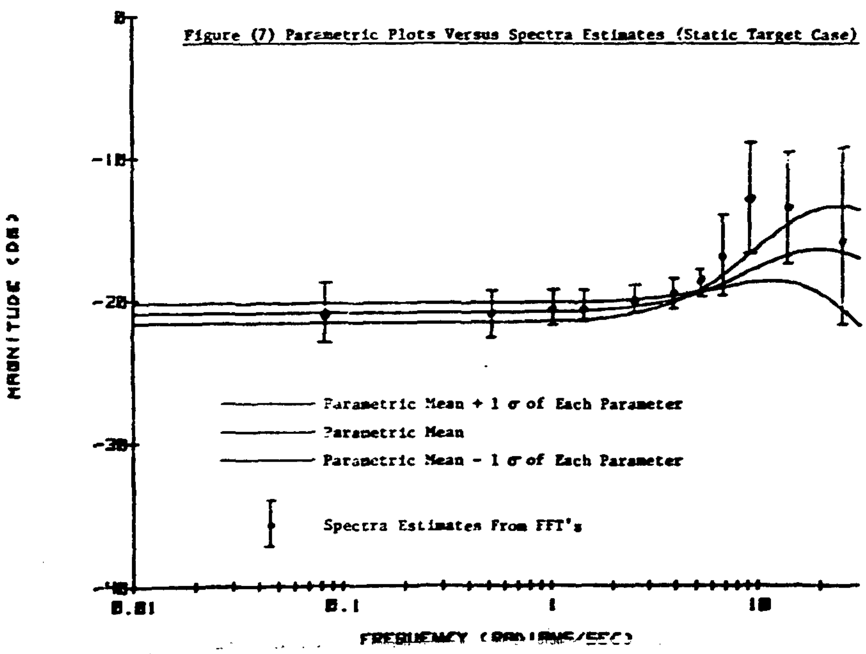

STATIC TARGET

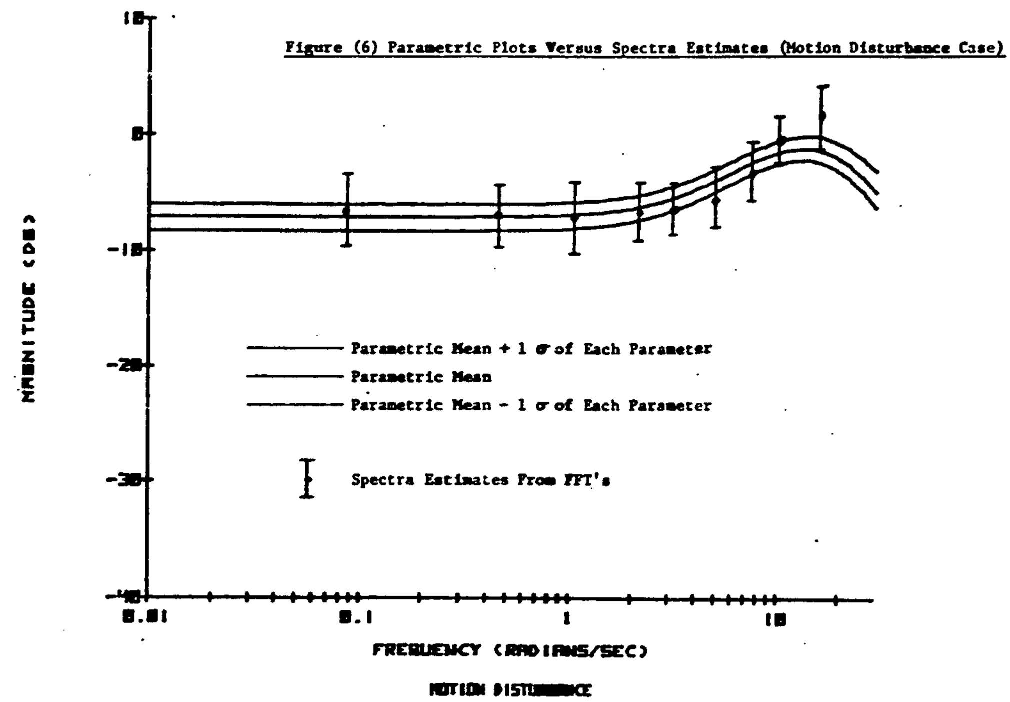

ORIGINAL PAGE IS OF POOR QUALITY

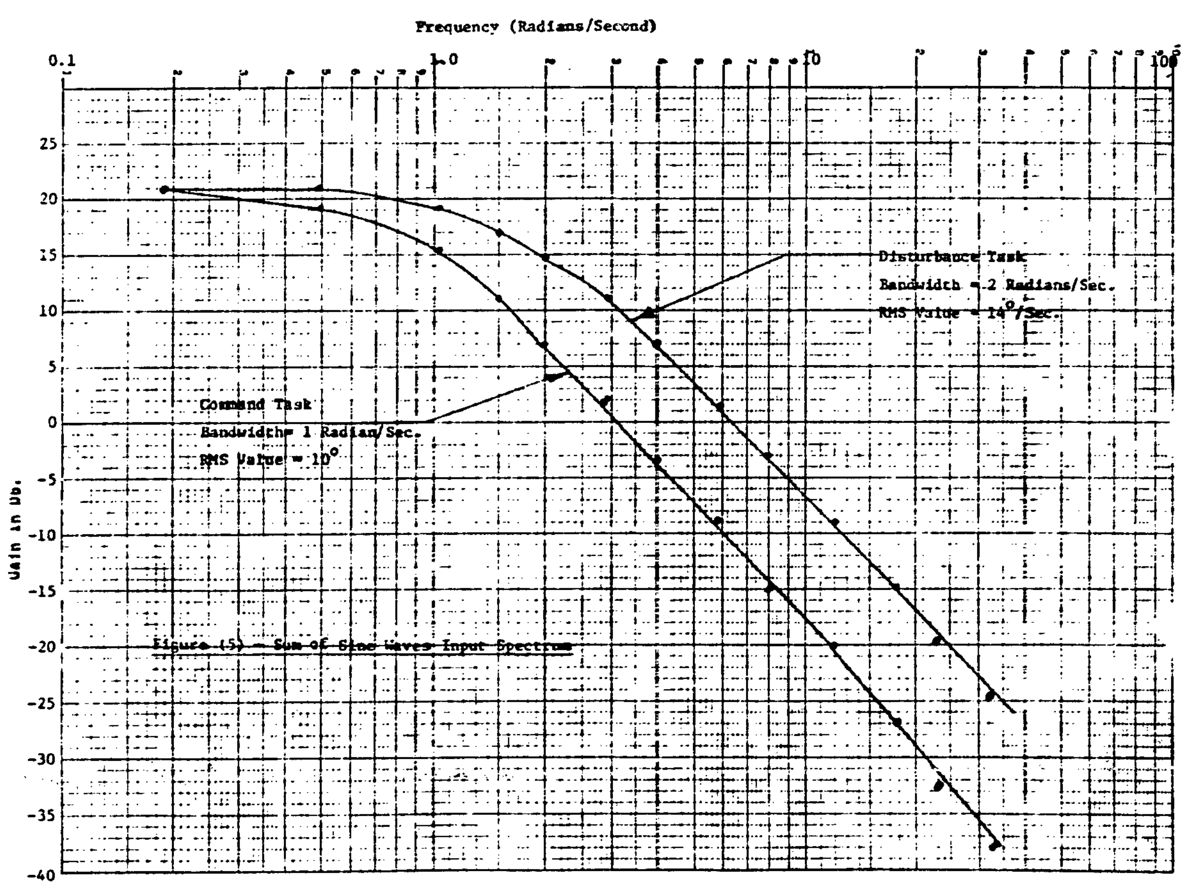

Figure (5) — Sum of Sine Waves Input Spectrum

ORIGINAL PAGE IS
OF POOR QUALITY

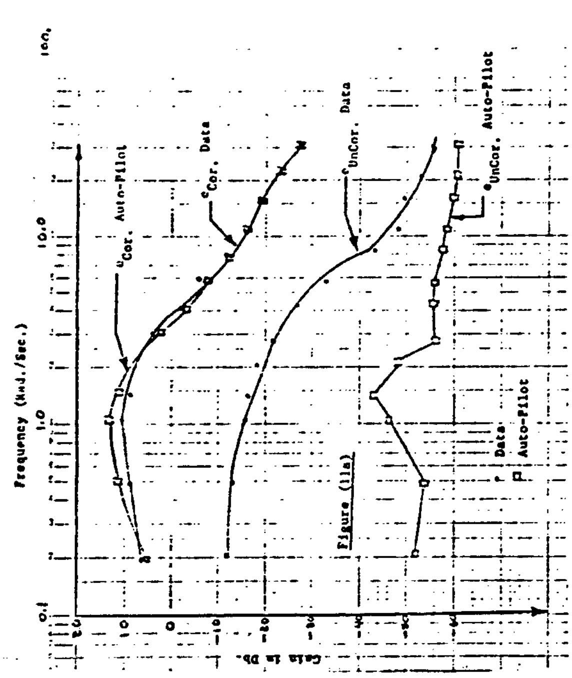

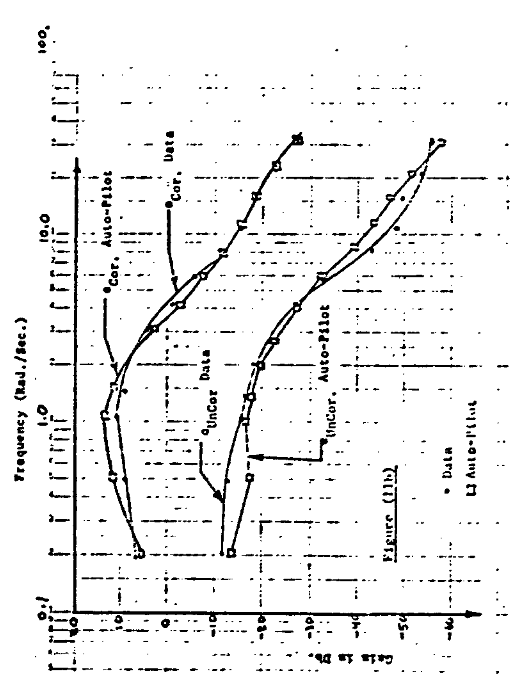

N79-17510

USE OF THE OPTIMAL CONTROL MODEL IN THE DESIGN OF MOTION CUE EXPERIMENTS*

By Andrew M. Junker and William H. Levison

Aerospace Medical Research Laboratory
Wright-Patterson Air Force Base, Ohio 45433
and
Bolt Beranek and Newman
50 Moulton Street
Cambridge, Massachusetts 02138

ABSTRACT

An experiment is presented in which the effects of roll motions on human operator performance were investigated. The motion cues considered were the result of commanded vehicle motion and vehicle disturbances. An optimal control pilot-vehicle model was used in the design of the experiment and to predict system performance prior to executing the experiment. The model predictions and experimental results are compared. Seventy-eight per cent of the model predictions are within one standard deviation of the means of the experimental results. The high correlation between model predictions and system performance indicate the usefulness of the predictive model for experimental design and for prediction of pilot performance influenced by motion cues.

INTRODUCTION

A requirement exists in the Air Force for a predictive human operator pilot model which is sensitive to complex motion environments. Such a model would have a number of important applications. For example, one might use the model to (1) determine whether or not motion cues are used by the pilot in a particular control situation; (2) extrapolate the results of fixed-base simulation to a motion environment; (3) facilitate the design of ground-based simulators; (4) identify situations where misinterpretation of motion cues is likely to cause a pilot response that seriously degrades system performance. At the Environmental Medicine Division of the Aerospace Medical Research Laboratory (AMRL), a research program is being pursued to satisfy this requirement. It is directed towards developing a generalized description of the manner in which a pilot uses motion cues, with the ultimate goal of providing a model that can predict the effects of motion cues on system performance in a variety of control situations.

Although a number of experimental studies have been conducted to determine the effect of motion cues on pilot response behavior (1-5), a generalized model has not been developed and tested. Rather, the conclusions reached in these studies have been restricted to the context of the experiments yielding the data. In addition, other than the pitch axis motion experiment performed by vanGool and Mooij (5), the work done in this area has principally been for compensatory systems with the motion cues resulting from vehicle disturbance inputs. At AMRL, we are also interested in the effects of motion cues on performance resulting from commanded inputs as encountered in air-to-air combat situations. Therefore, a series of experiments were performed at AMRL to investigate the effects of motion cues resulting from commanded inputs on tracking performance (6,7,8).

One of the products from this research effort was a modification of the Bolt Beranek and Newman optimal control pilot-vehicle model to account for changes in performance caused by the presence of motion cues due to commanded inputs. Since the pilot model has predictive capabilities, the next step was to ascertain how well it could predict pilot performance under different experimental conditions. The ability of the model to predict human performance and aid in experimental design is the topic of this paper.

A moving base simulator, different from the one used in the earlier series of experiments, was employed. Different vehicle dynamics were used and motion cues resulting from both commanded vehicle motion and vehicle disturbances were explored. In addition, the pilot model was used to aid in preliminary experimental design to insure that vehicle motions resulting from pilot inputs would remain within the linear operating range of the simulator. After experimental conditions had been selected, the optimal control pilot-vehicle model was exercised for the various conditions and performance scores were computed. Human tracking was then performed and performance data was collected. The control vehicle, experimental design and results from model prediction and human tracking are presented and discussed in this paper.

EQUIPMENT

A Multi-Axis Tracking Simulator (MATS) was used as the controlled vehicle for this experiment. Only the roll axis motion capabilities of the MATS were used. The simulator consisted of a single seat cockpit with a television monitor display and side mounted force stick for vehicle control. The cockpit was configured such that the pilot sat one inch above the roll axis of the simulator. The vehicle cockpit was light-tight to eliminate external visual cues. The roll axis system dynamics were identified and simulated on a hybrid computer. The system characteristics are presented in Table I. To test the capabilities of the optimal control pilot-vehicle model, it was decided to investigate the effects of two types of motion cues in this experiment. One was defined as the Command condition because vehicle motion was commanded as a result of following a target and the other the Disturbance condition because disturbance inputs drove the vehicle directly. Both conditions were investigated with and without the drive system on, making a total of four experimental conditions. The block diagram for the experiment, presented in Figure 1, shows all conditions. For the command condition, the

*The research reported in this article was conducted by personnel of the Aerospace Medical Research Laboratory, Aerospace Medical Division, Air Force Systems Command, Wright-Patterson Air Force Base, Ohio. The voluntary informed consent of the subjects used in this research was obtained as required by Air Force Regulation 80-33. Further reproduction is authorized to satisfy the needs of the U.S. Government. Reprints of this article are identified by the Aerospace Medical Research Laboratory as AMRL-TR-77- .

D35

disturbance input ($\phi_{DISTURBANCE}$) was set to zero and for the disturbance condition the target input (ϕ_{TARGET}) was set to zero. A low pass filter with breakpoint at 5 radians per second was added to the vehicle making the equivalent plant dynamics for all experimental conditions as given in equation 1.

$$\text{Plant Dynamics} = \frac{\phi_{PLANT}\ (\text{Deg})}{u_{CONTROL}\ (\text{Lbs})} = \frac{K}{s\left(\frac{s}{5}+1\right)\left(\frac{s}{20}+1\right)} \qquad (1)$$

In addition, a time delay of 95 milliseconds due to digital computation, visual display delay and an in-line signal filter existed in the visual pathway. In the command condition, the task was to follow a target aircraft in the roll axis. The difference between the target roll angle and the controlled vehicle position was provided to the human operator on a 9 inch diagonal television monitor. The inside-out display consisted of a 1.25 inch long rotating line whose center was superimposed upon a stationary horizontal line as indicated in Figure 2. A 0.083 inch perpendicular line at the center of the rotating line provided upright orientation. The angle between the rotating and stationary line depicted the difference between the controlled plant roll angle and the target roll angle. The display was centered in azimuth a distance of 20.5 inches from the controller's eyes. Subjects' sitting heights were such that the display was within 10 degrees of eye level of each subject. For the disturbance conditions, since $\phi_{TARGET} = 0$, the displayed error equalled the bank angle of the controlled vehicle and the task was to null out the bank angle by keeping the controlled vehicle upright.

EXPERIMENTAL DESIGN

With the vehicle to be controlled identified and the four tracking conditions chosen, the next step was to select task parameters for the experiment. The following constraints and design goals motivated the selection of parameter values:

1. To achieve face validity, we desired to simulate roll axis dynamics representative of high performance aircraft in air combat. The dynamics of equation (1) were chosen on this basis.

2. In order to assure that roll motion would be well above the subject's threshold of perception, and to allow comparison with a recent study (8), an RMS bank angle of 10 degrees was desired.

3. Physical limitations on the roll rate and roll acceleration of the rotating simulator had to be considered. Specifically, our goal was to achieve experimental RMS roll rates and accelerations that were no greater than 1/3 the corresponding limits so that these limits would be reached less than 1% of the time.

4. A wide bandwidth of pilot response was desired to maximize our ability to analyze the effects of motion cues on pilot response behavior; at the same time, we wanted to avoid a tracking task that was unreasonably difficult.

5. In order to test our model for motion cue utilization, we desired tasks in which motion would have a significant effect on pilot response behavior.

Experimental parameters that we could adjust to meet these goals consisted of (1) RMS amplitude and spectral shape of the tracking input, (2) control gain, and (3) performance criterion.

The input amplitude was adjusted to induce vehicle response of the desired magnitude, and the control gain was adjusted to allow such response to be achieved with comfortable control forces. A second order noise process was considered for the tracking input and the critical frequency of the input spectrum was chosen to achieve the desired balance between measurement bandwidth and tracking difficulty.

To keep RMS response rate and acceleration well below the physical limitations of the rotating simulator, as well as to encourage the test subjects (who were not trained pilots) to respond in a smooth manner, a performance criterion was defined as the weighted sum of mean-squared tracking error and mean-squared vehicle acceleration. That is,

$$C = \sigma^2_{\phi_{ERROR}} + W\,\sigma^2_{\ddot{\phi}_{PLANT}} \qquad (2)$$

where C is the total "cost", $\sigma^2_{\phi_{ERROR}}$ the variance of the tracking error, and $\sigma^2_{\ddot{\phi}_{PLANT}}$ the variance of the acceleration of the vehicle or simulated vehicle, in the absence of motion cues.

The immediate effect of introducing a penalty for vehicle acceleration was to limit the gain of the subject's response; the larger the weighting W, the lower the pilot gain. Pilot gain directly influenced overall man/machine system bandwidth, which in turn influenced roll rate and roll accelerations achieved during tracking.

Task parameters were selected in the following way. An initial set of parameters was chosen based on knowledge gained from previous experimental studies, and predictions of pilot-vehicle performance were obtained with the pilot-vehicle model. Task parameters were readjusted in an attempt to better meet the experimental constraints, and the system was reanalyzed. We iterated on this procedure until satisfied with the expected outcome of the experiment.

The optimal control pilot-vehicle model used in this procedure has been described in the literature (9-12) and is reviewed briefly in a companion paper (13). Independent pilot-related model parameters were held fixed throughout this procedure at values obtained from previous analysis. Specifically, time delay was set at 0.17 second, the "motor time constant" (a first-order lag associated with pilot response) was 0.1 seconds, and the "noise/signal ratio" (to account for pilot response randomness) was set at -20 dB. Visual-only tracking was represented by considering only tracking error and tracking error rate in the set of informational quantities available to the pilot. Roll angle, roll rate, and roll acceleration of the simulated vehicle were added to this informational set to account for the presence of motion cues.

As a result of this iterative design process, the following task parameters were selected. The force stick gain was adjusted to produce 10 degrees/second vehicle roll rate for one pound of force measured at thumb height on the control grip and the cost weighting W (equation 2) was set to 0.1. In addition, both the target and disturbance inputs were constructed from 13 sinusoids whose amplitudes were selected to simulate random noise processes having power spectral densities of the form

$$\Phi_{ii}(\omega) = \left| \frac{K}{(j\omega + \omega_i)^2} \right|^2$$

where ω_i was 1.0 rad/sec for the target input and 2.0 rad/sec for the disturbance input. Input amplitude was adjusted to provide an RMS target input of 10 degrees and an RMS disturbance input of 14 deg/sec. In order to prevent subjects from learning the input waveforms during the experiment, a random number generator was used to vary the phase relationships of the input sinusoids from one experimental trial to the next.

EXPERIMENTAL PROCEDURE

Six healthy college students between 18 and 25 years of age were used for the experiment. Subjects tracked each condition each day. Tracking under each condition was considered one run. Each run lasted 165 seconds and the four conditions or runs were presented in a random order each day. At the end of each run, subjects were presented their three performance scores for that run; total cost C, error variance σ^2_{ERROR} and weighted acceleration $0.1\,\sigma^2_{\ddot{\Phi}PLANT}$. They were instructed to minimize the total cost C. In addition, they were told that it was the sum of the other two, that the error score was related to how much error they allowed and that the acceleration score was related to how smoothly they tracked. They were not told predicted scores, nor were they told how to divide their total score between error and acceleration. To maintain subject motivation, subjects were also made aware of each other's performance scores. Each subject wore a flight helmet with intercom capability while performing the tracking task. The subject was permitted to perform the task briefly prior to each scored run in order to adjust mentally and physically to the tracking task.

Performance scores were plotted daily in order to evaluate subject and group performance. Once the error scores indicated that the subjects had "learned" the tracking tasks for all experimental conditions, tracking was continued for another eight days and time history data was collected for subsequent analysis. From these last eight days of runs, performance scores were computed for each subject for each condition, making a total of 48 measurements per condition. For purposes of comparing the experimental results to predicted values for each condition, the results of the six subjects were averaged together.

RESULTS AND DISCUSSION

Once subject training had been accomplished, data was collected for eight days for all subjects. Training was considered completed when subject performance, as measured by total cost C for all conditions, had reached asymptotic levels.

From the collected data, various system parameter values were computed and averaged together across days and subjects. The experimental results along with the predicted model values are given in Table II for the command condition and Table III for the disturbance condition. The experimental values include the mean and standard deviation resulting from averaging together the six subjects' results. From Tables II and III we can see that the model predictions are quite accurate, 28 of the 36 predictions are within one standard deviation of the means of the experimental values and the remainder are within two standard deviations of the mean.

To better compare predicted and experimental results across conditions, these values are also presented graphically for total cost (PERFORMANCE SCORE) and pilot input (RMS CONTROL FORCE) in Figure 3, for plant position (RMS Φ PLANT) and system error (RMS Φ ERROR) in Figure 4, and plant velocity (RMS $\dot{\Phi}$ PLANT) and acceleration (RMS $\ddot{\Phi}$ PLANT) in Figure 5. Experimental conditions are indicated on the abscissa of each graph; C/M indicates the command with motion condition, C/S command-static, D/M disturbance-motion and D/S the disturbance-static condition. From Figure 3 we see that with the model we were able to predict total performance score and the control force the pilot used for the four conditions. The same trends can be observed in Figures 4 and 5 for the vehicle motions and the error the pilot allowed.

The experimental results also indicate that our design goals were achieved. One of the requirements was that the control tasks not be unreasonably difficult. The control forces used by the subjects (Figure 3) indicate that the tasks were not excessively difficult to control and that the forces were within the design region of 0.5 to 1.5 pounds. To insure that the roll motion would be well above pilot thresholds, we desired an RMS bank angle of approximately 10 degrees. From Figure 4 we see that this requirement was also met. For the disturbance motion case, the subjects were able to reduce the bank angle error below what the model predicted. Also for the static-disturbance case, the model predictions were less than the experimental results. As mentioned earlier, there existed a 95 ms time delay in the visual loop that was not present in the motion cue loop. Model predictions did not include the presence of the visual time

delay. These circumstances may account for the differences between the model predictions and experimental results. The physical limitations of the simulator, namely a velocity limit of 60 deg/sec and an acceleration limit of 100 deg/sec^2, had to be considered during motion tracking. Our design goals were to achieve experimental RMS roll rates and accelerations that were no greater than 1/3 the corresponding limits. The experimental results (Figure 5) indicate that these goals were satisfied.

As stated earlier, the motion sensitive aspects of the model were developed for experimental conditions different from those investigated in this study and a different simulator with narrower bandwidth vehicle dynamics (8). These facts further emphasize the usefulness of the predictive capabilities of the model. The next step in the study was to determine what model parameter adjustments were needed to improve the match to the data. This is the subject of a companion paper in these Proceedings. By readjusting the model parameters, we hope to gain additional insight into how the pilot utilizes motion information.

CONCLUSIONS

The major objectives of our experimental program have been (1) to investigate the usefulness of the model as an experimental design tool, (2) to demonstrate the ability of the model to predict the influence of motion cues on pilot-vehicle performance for different tracking tasks and (3) to provide a data base from which we could improve our understanding of how the pilot utilizes and is effected by motion cues. In conclusion, we feel the results of this experiment demonstrate the usefulness of the predictive optimal control pilot-vehicle model. With the model, we were able to predict pilot-vehicle response for the various motion cue conditions. In addition, by making use of the model, the experimental design process was not only simplified, we were assured that useful data could be collected.

ACKNOWLEDGEMENTS

The authors would like to take this opportunity to thank the following individuals: James S. Ater, Warren G. Miller, Harry S. Boal and Marvin Roark for their excellent technical assistance, and, of course, the subjects, Becky, Dana, Eric, KC, Jennifer and Tom.

REFERENCES

1. Ringland, R.F., R. L. Stapleford, and R. E. Magdaleno, "Motion Effects on an IFR Hovering Task--Analytical Predictions and Experimental Results", NASA CR-1933, November 1971.

2. Stapleford, R.L., R.A. Peters, and F. Alex, "Experiments and a Model for Pilot Dynamics with Visual and Motion Inputs", NASA CR-1325, May 1969.

3. Shirley, R.S., "Motion Cues in Man-Vehicle Control", M.I.T., Cambridge, Massachusetts, ScD Thesis, January 1968.

4. Ringland, R.F. and R.L. Stapleford, "Experimental Measurements of Motion Cue Effects on STOL Approach Tasks", NASA CR-114458, April 1972.

5. vanGool, M.F.C. and H.A. Mooij, "A Comparison of Inflight and Ground-Based P[illegible]ch Attitude Tracking Experiments", Twelfth Annual Conference on Manual Control, NASA TM X-73, 170.

6. Junker, A.M. and C.R. Replogle, "Motion Effects on the Human Operator in a Roll Axis Tracking Task", Aviation, Space and Environmental Medicine, Vol. 46, pp. 819-822, June 1975.

7. Junker, A.M. and D. Price, "Comparison Between a Peripheral Display and Motion Information on Human Tracking About the Roll Axis", Proceedings AIAA Visual and Motion Simulation Conference, 26-28 April 1976.

8. Levison, W.H., S. Baron, and A.M. Junker, "Modeling the Effects of Environmental Factors on Human Control and Information Processing", AMRL-TR-76-74, Aerospace Medical Research Laboratory, Wright-Patterson Air Force Base, Ohio.

9. Kleinman, D.L., S. Baron, and W.H. Levison, "An Optimal Control Model of Human Response, Part I: Theory and Validation", Automatica, Vol. 6, pp. 357-369, 1970.

10. Kleinman, D.L. and S. Baron, "Manned Vehicle Systems Analysis by Means of Modern Control Theory", NASA CR-1753, June 1971.

11. Kleinman, D.L., S. Baron, and W.H. Levison, "A Control Theoretic Approach to Manned-Vehicle Systems Analysis", IEEE Trans. on Auto. Control, Vol. AC-16, No. 6, December 1971.

12. Baron, S. and D.L. Kleinman, et al, "An Optimal Control Model of Human Response - Part II: Prediction of Human Performance in a Complex Task", Automatica, Vol. 6, pp. 371-383, Pergamon Press, London, England, May 1970.

13. Levison, W.H., "A Model for Human Controller Performance in Vibration Environments", Proceedings of the 15-17 February 1977 Symposium on Biodynamic Models and Their Applications, supplemental issue of Aviation, Space and Environmental Medicine.

C-5

TABLE I

MULTI-AXIS TRACKING SIMULATOR

ROLL AXIS CHARACTERISTIC

TRANSFER FUNCTION: $\dfrac{\phi_{PLANT}\ (\mathrm{deg})}{u_{CONTROL}\ (\mathrm{pounds})} = \dfrac{K}{s\left(\frac{s}{20}+1\right)}$

POSITION LIMIT: $\phi_p = \pm 90$ deg

VELOCITY LIMIT: $\dot{\phi}_p = \pm 60$ deg/sec

ACCELERATION LIMIT: $\ddot{\phi}_p = \pm 100$ deg/sec^2

TABLE II

PREDICTED VERSUS EXPERIMENTAL RESULTS FOR THE

[illegible] CONDITION

VARIABLE	UNITS	STATIC PREDICTED	STATIC EXPERIMENTAL MEAN	STATIC EXPERIMENTAL 1σ	MOTION PREDICTED	MOTION EXPERIMENTAL MEAN	MOTION EXPERIMENTAL 1σ
Total Cost	--------	67.0	72.6	8.9	53.1	66.1	7.5
Cost on ϕ_E	--------	52.4	50.7	11.9	45.5	48.2	11.1
Cost on $\ddot{\phi}_p$	--------	14.5	12.2	9.7	7.57	17.90	8.64
σ_u	pounds	0.730	[illegible]	0.120	0.516	[illegible]	0.156
σ_{ϕ_p}	deg	10.1	9.2	0.9	6.37	7.63	1.25
$\sigma_{\dot{\phi}_p}$	deg/sec	6.86	7.10	[illegible]	4.84	6.74	1.69
$\sigma_{\ddot{\phi}_p}$	deg/sec^2	12.1	14.6	3.1	8.70	12.9	3.51
σ_{ϕ_E}	deg	7.24	7.06	[illegible]	6.75	6.90	0.79
$\sigma_{\dot{\phi}_E}$	deg/sec	11.7	11.9	0.7	10.7	11.8	0.79

PAGE IS

TABLE III

PREDICTED VERSUS EXPERIMENTAL RESULTS FOR THE

DISTURBANCE INPUT CONDITION

VARIABLE	UNITS	STATIC			MOTION		
		PREDICTED	EXPERIMENTAL		PREDICTED	EXPERIMENTAL	
			MEAN	1σ		MEAN	1σ
Total Cost	--------	178	[illegible]	29	91.6	[illegible]	[illegible]
Cost on ϕ_E	--------	86.2	[illegible]	[illegible]	37.2	[illegible]	[illegible]
Cost on ϕ_P	--------	91.5	[illegible]	36.7	54.4	[illegible]	9.2
σ_δ	pounds	1.56	1.55	0.14	1.49	[illegible]	[illegible]
σ_{ϕ_P}	deg	9.29	[illegible]	1.80	6.1	4.2	1.5
$\sigma_{\dot{\phi}_P}$	deg/sec	12.1	11.9	1.3	7.76	6.81	1.41
$\sigma_{\ddot{\phi}_P}$	deg/sec^2	[illegible]	[illegible]	5.0	23.3	24.0	1.9

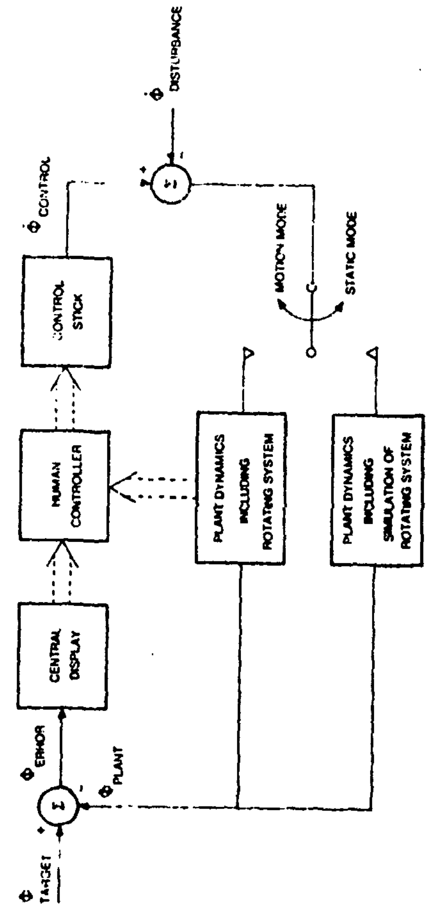

FIGURE 1. System flow diagram.

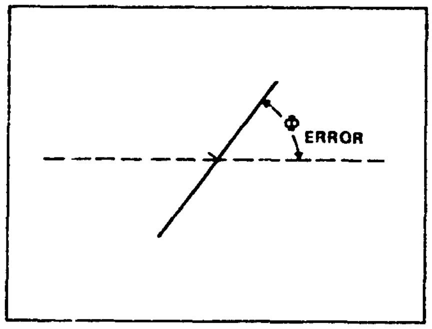

FIGURE 2. Visual display.

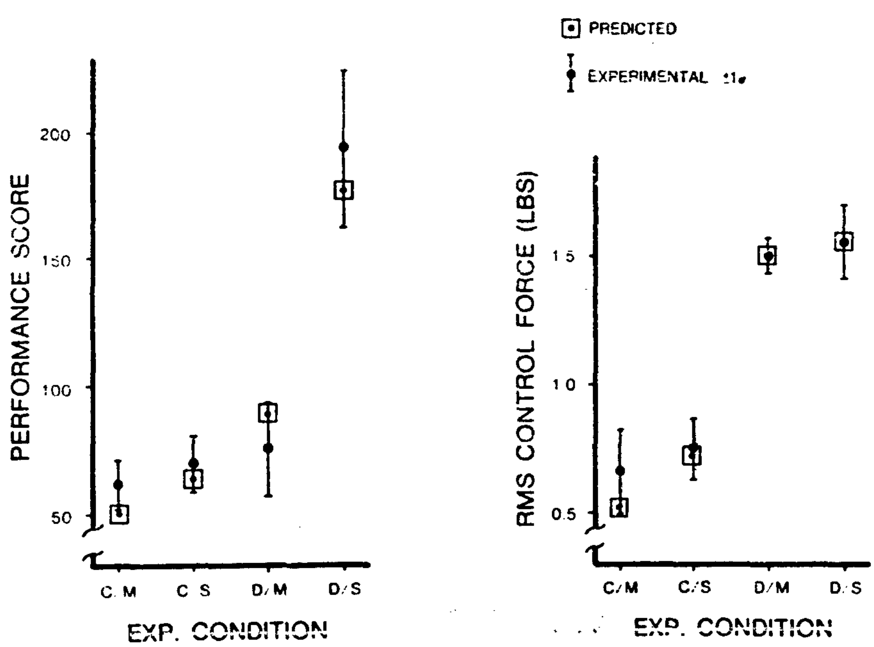

FIGURE 3. Comparison between model and experimental results for performance and control force.

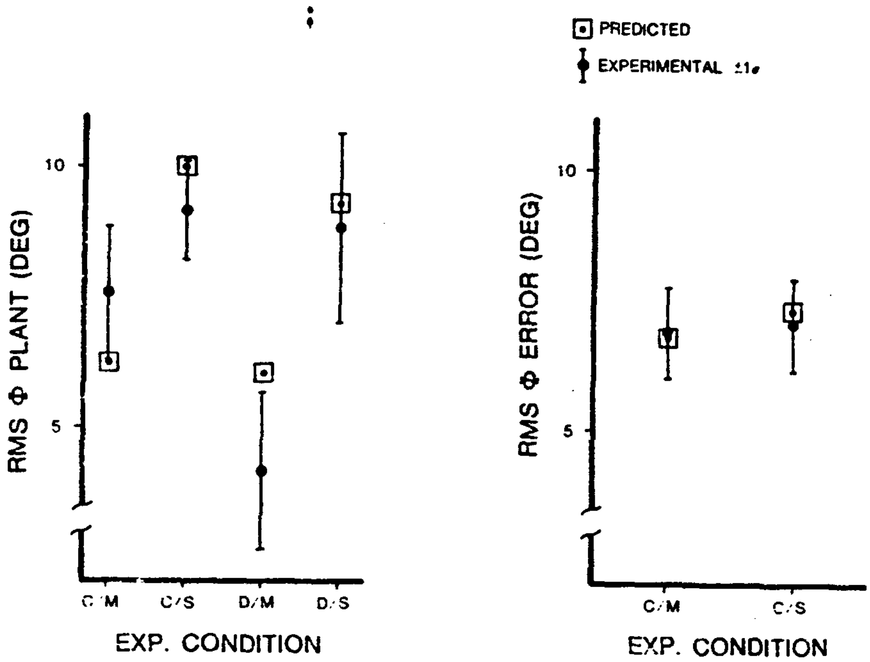

FIGURE 4. Model and experimental results compared for vehicle position and system error.

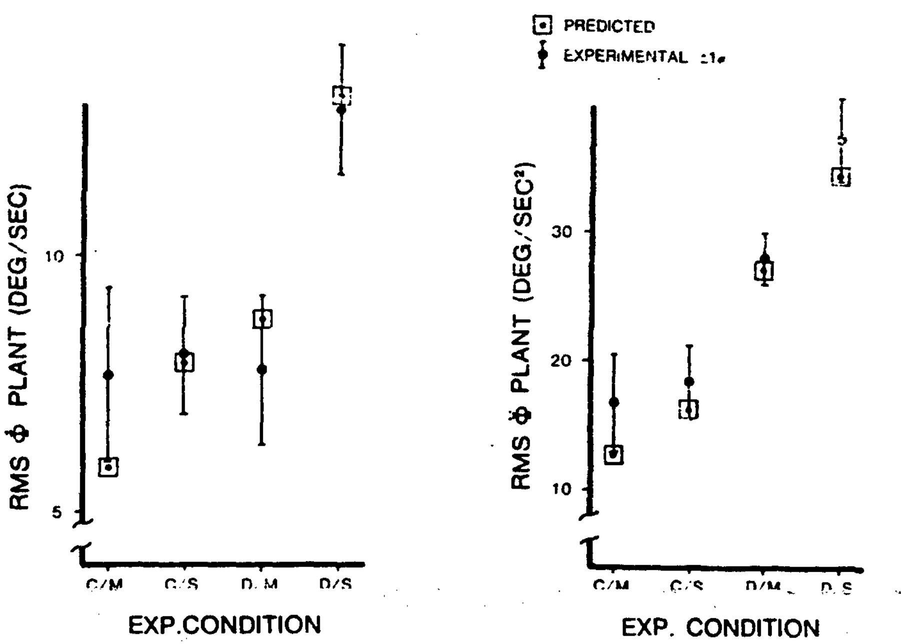

FIGURE 5. Comparison between model and experimental results for vehicle velocity and acceleration.

N79-17511

THE EFFECT OF A VISUAL/MOTION DISPLAY MISMATCH IN A SINGLE AXIS COMPENSATORY TRACKING TASK

By
Douglas K. Shirachi
and
Richard S. Shirley

May 1977

Prepared under Contract
No. NAS2-7806 by
COMPUTER SCIENCES CORPORATION
Mountain View, California

for

NATIONAL AERONAUTICS AND
SPACE ADMINISTRATION

Ames Research Center
Moffett Field, California 94035

Introduction

It is possible for a pilot to "fly" a simulated aircraft which duplicates the sensations of flight without leaving the ground. The keys to such a realistic simulation are the simulator cab and computers. The simulator cab, as sketched in Figure 1, provides the pilot with the physical sensations of aircraft flight. Included are cab motions, operational instruments normally found in the aircraft being simulated, controls with the same force-feel as the simulated aircraft, TV and/or computer graphics displays of the outside visual scene, and simulation of the engine and landing gear sounds. The computers control the simulation hardware which provides these sensations to the pilot, monitor pilot responses and control commands, and use a mathematical model of the aircraft to calculate its response to the pilot commands.

The simulation of visual and motion cues for the pilot is basic to most simulations at NASA-Ames Research Center. The most commonly used visual display is a TV picture of a terrain model. A six-degree-of-freedom servo-system, under digital computer control, drives the TV camera to simulate the pilot's view out the cockpit window as if he were flying the actual aircraft. Similarly, a six-degree-of-freedom servo-system is used to move the entire simulator cab in order to give the pilot motion cues. Motion cues help the pilot control the simulated aircraft, and enhance the realism of the simulation.

The motion simulator cab has significantly greater mass than the TV camera, and consequently requires considerably more power to accelerate than the TV camera. Consequently, one often finds a difference in performance between the servo-system driving the cab motion and that driving the visual display. The frequency response of visual systems is typically unity from 0 to 20 rad/sec, while that of motion systems typically falls off in the vicinity of 6 rad/sec. The question arises as to what effect, if any, such a difference in servomechanism performance has on the simulation. Is pilot performance reduced by the conflict between displays? Would a more realistic simulation occur if the visual servomechanisms were degraded to match the motion servomechanisms? Does the pilot need and use the higher frequency information

D36

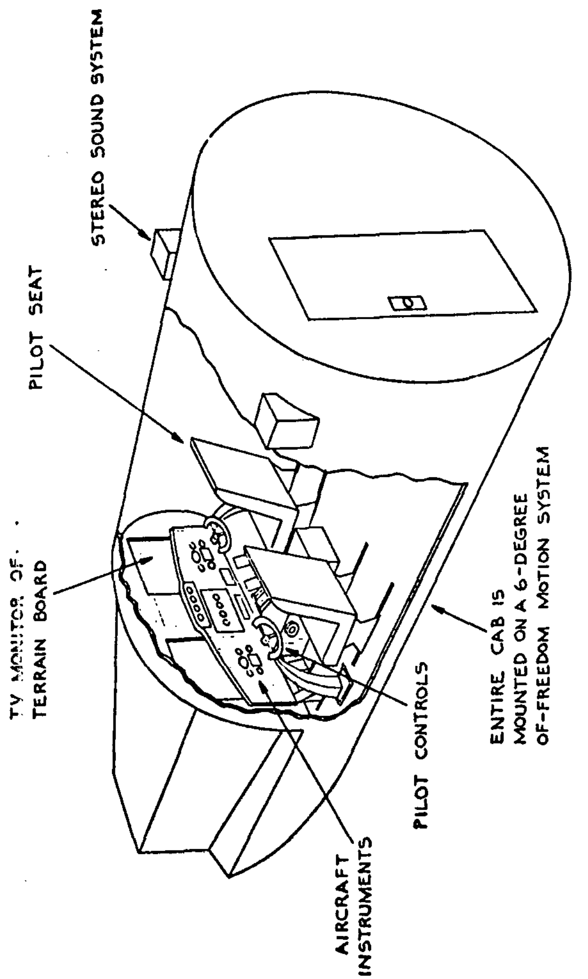

Figure 1: DIAGRAM OF SIMULATION CAB (CUTAWAY VIEW)

present in the visual display? The purpose of the experiment reported in this paper is to take a step forward toward answering these questions.

There are three practical reasons why the answers to the above questions would be useful to aircraft simulation. It is desirable to improve the reality of a simulation so that results obtained are more applicable to and representative of actual flight. Secondly, it is useful in aircraft design to have insight into how a pilot controls an aircraft, especially in terms of what information he uses to guide his control commands. Finally, one must know what capabilities are required from a simulator in order to provide realistic aircraft simulations.

The next section of this paper outlines work already in the literature which bears on these questions. A description is then given of an experiment used to check for the effects of a difference in the performance of the visual and motion servomechanisms (the experiment uses a single-axis, compensatory, roll-tracking task). The results of the experiment are then presented and analyzed.

Literature Review

Much of the early research performed on moving-base simulators was related to a roll control task, since a major contribution to the lateral maneuverability of an aircraft is provided by its roll dynamics. The primary goals of these earlier research efforts were (1) to compare pilot performance in fixed-base and moving-base simulators to actual flight data and (2) to define and evaluate parameters for aircraft handling qualities. The methods used in these studies were measurements of pilot describing functions (pilot amplitude ratio, phase and noise versus frequency) such as those described in reference 1, subjective ratings similar to the Cooper-Harper Rating Scale (described in reference 2), and various measures of system performance (such as integral squared error).

In his experiments, Newell (reference 3) reported data which showed that pilot performance for instrument-only, fixed-base simulations was similar to that for instrument-only flight conditions. Pilot describing functions

showed lower amplitude ratios for fixed-base, instrument-only simulations and instrument-only flight conditions than for in-flight visual conditions. Newell and Smith (reference 4) verified these results and also observed that visual flight conditions and fixed-base visual simulations produced similar pilot describing functions. In addition, fixed-base visual simulations showed pilot performance which was closer to that for in-flight visual conditions than that for instrument-only conditions (either flight or fixed-base simulations). In other words, the absence or presence of a visual scene in addition to the instruments had more effect on pilot performance than the absence or presence of motion cues. It should be noted that these results were obtained in the absence of turbulence.

In 1959 Creer, et. al. (reference 5) used simulator and in-flight studies to define the effects of roll damping and roll control power on the pilot by recording pilot opinion ratings for the different parametric conditions. Based upon these pilot ratings, their results showed that there was good correlation between moving-base simulator and in-flight pilot opinions. The fixed-base simulator results agreed with moving-base simulator and in-flight conditions only for small roll accelerations. For larger roll accelerations, the moving-base simulations and actual flights produced similar data, while the fixed-base simulation led to significantly different pilot opinion ratings. Because of the results of Creer and others, which indicated that a moving-base simulator would be necessary for realistic ground-based simulation of flight, further simulator research proceeded in the direction of evaluating various motion display systems.

The methodology pursued by subsequent research efforts was to change the dynamic characteristics of the motion simulator, visual display and/or aircraft plant, and measure these effects upon pilot performance. Shirley and Young (reference 6) studied the effects of visual and/or motion cues on pilot describing functions in a roll compensatory tracking task. Their conclusions were that the effect of adding simulator motion to the visual display was to increase pilot phase lead above 3 rad/sec and to increase pilot gain between 0.1 rad/sec and 10 rad/sec. They also observed that low stick gain or very slow plant dynamics tended to minimize the advantage of roll motion as a cue to the pilot.

Schmidt and Conrad (reference 7) used a six-degree-of-freedom simulation in their investigation of a formation flying task with various choices of aircraft dynamics. They showed that motion cues decreased the scatter of the lateral and vertical deviation error scores as compared to a fixed-base condition. The scatter of the fixed-base error scores increased as the simulated aircraft dynamics became less acceptable. They also observed that without motion cues, pilots were unable to damp out the dutch roll mode.

Recently, Junker and Repolgle (reference 8) have investigated the effects of motion simulation for a large amplitude, roll control task upon pilot performance as a function of increasing plant complexity. Their data showed that simulator motion had the effect of reducing task learning time and improving tracking ability as compared to fixed-base runs. The error scores increased as plant order increased, as did the pilot effort required to maintain stable control of the plant. Differences between fixed-base and moving-base simulator error scores became more pronounced as the order of the plant increased.

A previous study closely related to the research described in this report was that of Stapleford, et. al. (reference 9), who determined separate pilot describing functions for the visual and motion display systems. Their data showed that the remnant spectrum was flat throughout the bandwidth investigated (1-20 rad/sec) with a fixed-base task producing twice as much remnant as a moving-base task, and that the error score was lower when motion cues were added to the simulation. They concluded that motion cues became more important as the need for the pilot to generate lead was increased. With the motion display, the pilot describing functions showed that the crossover frequency increased by 1 rad/sec, and the time delay between input and pilot control response was reduced by 0.15 seconds. They also concluded that the visual display cues were dominant at low frequencies, and that motion display cues were dominant at the higher frequencies.

Bergeron (reference 10) performed an instrumented, moving-base tracking task study in a single-axis mode (roll) and a dual-axis mode (pitch and roll, and

pitch and yaw). With the relatively slow, third order dynamics used, Bergeron found that the addition of motion cues to the visual cues reduced error scores for the dual-axis task, but not for the single-axis task. In other words motion cues were important for the higher workload, dual-axis task, but not for the lower workload, single-axis task. Furthermore, Bergeron found no difference in error scores for dual-axis tracking (pitch and yaw) as the amplitude of the simulator motion was scaled by factors as small as one fourth.

Research related to the effect of motion system configurations on simulations was performed by Ringland, et. al. (reference 11). He ranked simulator motion conditions in the order of their adverse effect upon pilot performance (beginning with the least adverse) as (1) angular motion, (2) angular plus linear motion and (3) no motion (fixed-base).

Miller and Riley (reference 12), investigating a four degree-of-freedom tracking task and using error scores, showed that increasing the task difficulty decreased the amount of acceptable delay. With complete motion cues, the pilot could tolerate longer dead time delays in the dynamics than with a limited amount of motion.. This is reasonable, as a dead time delay can be viewed as a phase lag which increases with frequency. Thus increased time delay requires the pilot to generate more lead, which motion cues facilitate.

In summary, research to date indicates that piloted aircraft simulations can be used for training and to obtain valid data for use in the development of aircraft and aircraft systems. Additionally, under many flight conditions, motion cues are needed to produce a valid simulation. Consequently, numerous simulation facilities have the capability for producing motion cues. Because of the relatively large mass to be moved, the frequency response of most motion systems drops off in the vicinity of 6 rad/sec, in contrast to the visual cues which usually have a frequency response which is flat past 20 rad/sec. This paper reports on an experiment designed to investigate the effects of such a mismatch between the visual and motion cueing systems.

The Experiment

Figure 2 shows the compensatory roll tracking task used for the experiment. The pilots were able to perceive the roll error through a visual and a motion simulator, and were requested to maintain level flight in the presence of turbulence during each run. In other words, while sitting in the closed motion simulator with a TV picture in front of them, the pilots attempted to keep the cab and the TV picture at a zero degrees roll angle. Perfect performance was not possible because of turbulence.

The dynamics of the visual and motion simulators were not identical, producing a slight mismatch between the information presented to the pilot through these two displays of roll error. In order to measure the effects of such a mismatch (or conflict of cues) on pilot performance, the visual and motion dunamics were systematically compensated or degraded (see Figure 2) to create four display combinations (see Figure 3):

- Case A - normal visual and motion displays, consequently a conflict of cues
- Case B - visual display degraded to match the motion display, no conflict of cues
- Case C - motion display compensated to match the visual display, no conflict of cues
- Case D - visual display degraded to match uncompensated motion display, and motion display compensated to match undegraded visual display, producing a slight conflict of cues (opposite of Case A)

The dynamics shown in Figure 3 are discussed later in the paper under Description of Equipment.

Two different aircraft roll dynamics were used during the experiment, and the data analyzed separately. The dynamics, described in the next section, were typical of medium transport aircraft.

During the runs the roll error and pilot control output were sampled every .05 seconds. These data were used to calculate pilot quasi-linear describing

Figure 3

Visual/Motion Roll Display Dynamics

Visual \ Motion	Normal	Compensated
Normal	**Case A** Visual: 1 Motion: $\frac{1}{.21s+1}$ (normal)	**Case C** Visual: 1 Motion: 1 (high ω)
Degraded	**Case B** Visual: $\frac{1}{.21s+1}$ Motion: $\frac{1}{.21s+1}$ (low ω)	**Case D** Visual: $\frac{1}{.21s+1}$ Motion: 1 (reverse normal)

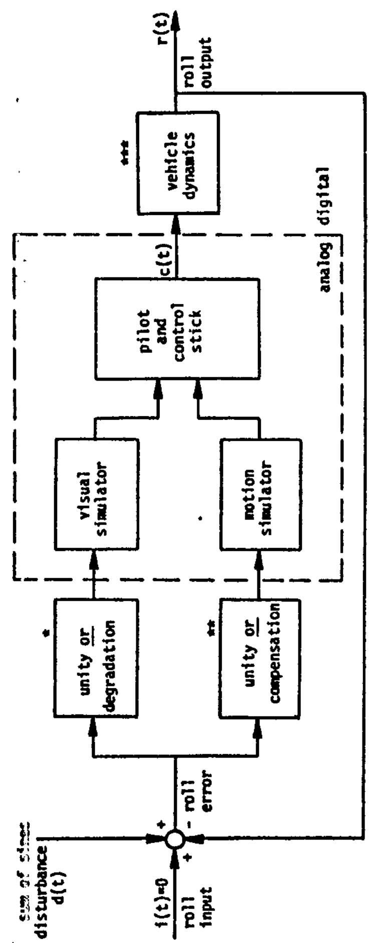

*visual degradation: $1/(.21s+1)$

**motion compensation: $(.21s+1)$

***vehicle roll dynamics:

case 1: $8.8/s(.5s+1)$

case 2: $37.25/s(.5s+1)$

Figure 2: Single-Axis Compensatory Roll Tracking Task

functions and error scores. At the end of each set of runs pilot opinion ratings were obtained.

The following sections describe the aircraft dynamics, the equipment, the experimental procedures and the analysis techniques used for the experiment. Experimental results are then presented, and conclusions are made based on these results.

The Aircraft Dynamics

The aircraft roll dynamics used in two separate experimental cases were:

1) $$\frac{\phi_a}{\delta} = \frac{17.6\ (0.5)}{s(0.5s + 1)}$$

2) $$\frac{\phi_a}{\delta} = \frac{74.5\ (0.5)}{s(0.5s + 1)}$$

where ϕ_a is the roll angle of the aircraft, δ is the control stick deflection, and s is the Laplace operator. Using the pilot opinion boundries of reference 5, dynamics 1 is in the middle of the "Satisfactory" range, while dynamics 2 is just into the "Unacceptable" range.

Description of Equipment

The experimental hardware consisted of a motion display (motion simulator), visual display (visual simulator), stick controller and digital computer system. The motion simulator was the NASA-Ames Six-Degree-of-Freedom (S.01) simulator described by Fry, Grief and Gerdes (reference 13). The simulator was configured as a single-seat, closed-cockpit enclosure with a television video monitor positioned directly in front of the pilot, and was limited to roll motion for this experiment. The simulator roll angle was limited to $\pm 45°$ of rotation, and the pilot's head was located 1.5 feet above the simulator roll axis.

Simulator transfer functions for the normal and compensated roll motion systems were determined using a least-squares computational technique operating on the phase angle versus frequency data. Retaining only the first order terms, these were:

$$\frac{\phi_m}{d} \approx \frac{1}{.21s+1} \qquad \text{(normal)}$$

$$\frac{\phi_m}{d} \approx 1 \qquad \text{(compensated)}$$

where ϕ_m is the roll angle of the motion simulator, d is the roll command and s is the Laplace operator. The measured amplitude ratios and phases of the S.01 for the normal and compensated cases are shown in Table I. The normal transfer function measured for this experiment compares favorably with the results of Fry, et. al., who approximated the transfer function as:

$$\frac{\phi_m}{d} = \frac{1}{.17s+1}$$

The visual display was transmitted via a six-degree-of-freedom, servo-controlled television camera positioned behind a model of a jet tanker over a terrain board. The tanker never rolled relative to inertial space during the experiment. Consequently any rolling of the tanker image on the TV screen was a display of the roll error of the controlled aircraft as diagrammed in Figure 2, and the task was a compensatory roll tracking task. The roll angle limits for the visual servo system were $\pm 100°$. The visual scene was limited to move only in roll.

Using least-squares computational techniques for phase data, the transfer function for normal and degraded visual display conditions were determined to be:

$$\frac{\phi_v}{d} \approx 1 \qquad \text{(normal)}$$

$$\frac{\phi_v}{d} \approx \frac{1}{.21s+1} \qquad \text{(degraded)}$$

Table I

	S.01		VFA	
Freq. rad/sec	AR* normal	AR compensated	AR normal	AR degraded
.35	.98	.98	.99	.99
.70	.98	.99	.99	.98
1.05	.97	.99	.99	.97
1.75	.96	1.01	.99	.93
2.62	.92	1.05	.99	.87
3.50	.88	1.09	.99	.80
6.28	.75	1.24	.99	.60
10.47	.58	1.41	1.00	.42
Freq. rad/sec	Phase normal (degrees)	Phase compensated (degrees)	Phase normal (degrees)	Phase degraded (degrees)
.35	-4	+1	0	-5
.70	-8	0	-1	-9
1.05	-12	0	-1	-14
1.75	-20	0	-2	-22
2.62	-28	+1	-3	-32
3.50	-38	-1	-4	-41
6.28	-60	-7	-8	-60
10.47	-89	-23	-13	-79

*AR, Amplitude Ratio

Roll Frequency Response of the S.01 Motion Simulator and the Visual Flight Attachment (VFA) Used for the Experiment.

where ϕ_v is the roll angle of the visual simulator, d is the roll command, and s is the Laplace operator. The measured amplitude ratios and phases for the normal and degraded visual displays are shown in Table I.

Roll axis commands were made by means of lateral movements of the spring-loaded pencil control stick. The maximum allowable stick movement was $\pm 30°$. The controller was mounted on a metal box and connected to analog signal lines by means of a flexible cable. The pilot had the option of choosing either his left or right hand to operate the controller.

The computers used to implement the simulation were a medium-size digital and a medium-sized analog computer. The digital computer was equipped with 64K of core memory. The analog computer was the interface between the digital computer and the analog equipment. The only analog components of the system were the visual and motion simulators, the pilot and the stick controller. All other components were implemented as part of the digital computer program.

Experimental Procedure

The experimental subjects were all commercial aircraft pilots with 2,000 to 10,000 hours of flight time. Their experience included single and multi-engine propeller aircraft, single and multi-engine jet aircraft, and helicopters. All had experience with and were currently qualified to fly one or more transport aircraft. Eight pilots participated in the experiment: five flew both dynamics 1 and 2, two flew only dynamics 1, and one flew only dynamics 2.

Once seated in the closed cockpit of the motion simulator, with the TV visual display in front of him, the pilot's task was to maintain zero degrees roll angle in the presence of the sum-of-sines disturbance. There was a ten-second transition phase at the beginning of each run to gradually introduce the disturbance and minimize transient effects on the pilot and simulation equipment. In addition, a fifteen-second warmup period followed the transition phase. The warmup period allowed longer transients to die out and the pilot to become accustomed to the task. The warmup period was then followed by 108 seconds of simulation runtime during which data were taken. The transition phase, warmup period and data-taking period constituted one run.

Each pilot was assigned a particular display case sequence, and the order of presentation for one subject was balanced by the reverse order of another subject to eliminate possible learning effects. During training each subject was presented with his first display case, and would repeat runs for that case until his error scores remained nearly constant and no more than three data points were rejected. The training then continued with the next display case. Data points were rejected if the response power at the disturbance frequency was less than four times the power of the output response at the two remnant frequencies adjacent to the disturbance frequency (see Table II).

Rest periods of at least ten minutes were provided between training sessions. Training sessions ranged from thirty minutes to an hour depending upon the pilot. Total training time for each pilot ranged from two to eight hours, with an average of slightly over four hours.

Data runs were made in groups of six at each display case. A data-taking sequence started with two warmup runs, and was immediately followed by the six data runs. A rest break was taken before another data-taking sequence was made at the next display case. Total elapsed time for the two warmup and six data runs was typically thirty minutes.

<u>Analysis Techniques</u>

The analysis portion of the experiment included calculation of pilot describing functions, pilot performance scores, average results and an analysis of variance, as well as use of two types of pilot ratings.

The method used to calculate describing functions is described by Shirley (reference 14), and is summarized by Appendix A. The disturbance function used in the experiment was a sum-of-sines whose frequencies and amplitudes are given on Table II. The sinusoids were scaled with frequency to approximate turbulence. The maximum amplitude for the sum-of-sines function was 9°, and the RMS value was 4.5°. In addition to the pilot amplitude ratio and phase calculated at the disturbance frequencies, pilot remnant was calculated at the "remnant" frequencies shown on Table II.

Table II

Parameters for Sum-Of-Sines and Remnant Frequencies

k	W_k Input Disturbance frequency (rad/sec)	K_k Individual sinusoid gain	Remnant frequency (rad/sec)
1	.35	1.	.17
2	.70	-1.	.62
3	1.05	.9	.87
4	1.75	.9	1.57
5	2.62	.8	2.09
6	3.49	-.6	3.14
7	6.28	-.4	5.23
8	10.5	.1	7.85
9	-----	----	15.7

Disturbance $= d(n\Delta t) = G \sum_{k=1}^{8} K_k \sin(W_k n\Delta t)$ where $G = 2.$ and $\Delta t = .05$ seconds.

Pilot performance scores were computed as the normalized sum of the absolute values of the performance variable over time (integral-absolute, IA), and the normalized sum of the squares of the performance variable over time (integral-squared, IS).

$$IA_x = K \sum_{n=1}^{N} |x(n)|$$

$$IS_x = K \sum_{n=1}^{N} x^2(n)$$

where x refers to the variable being measured (either roll attitude error or control stick position), and K is a constant. Data samples were taken every .05 seconds.

The pilot describing functions and pilot performance scores for each experimental run were stored on magnetic tape in a 200 word data block. The run number, data, time of day, subject code, aircraft dynamics code, display condition code, and analog scale factors were also stored within the same data block. Using this tape, averages and standard deviations of the data for a sequence of runs under the same experimental conditions and pilots were computed. The variables analyzed were the amplitude and phase of the pilot describing functions, the remnant spectrum and pilot performance scores.

A three-dimensional analysis of variance was performed on the pilot describing functions, remnant and error scores with the following dimensions: display case, pilot, and repeated runs. Each measurement of pilot amplitude ratio, phase, and remnant at separate frequencies, plus each pilot rating and performance score was considered an independent measure of pilot performance. Because the same experimental subjects were used for all of the display cases, the three-dimensional analysis used in this experiment is a special case of a two-dimensional analysis with data replication. The number of data runs was determined using an approach described by Kirk (reference 16). Based upon a set of sample runs performed by a test subject, 42 runs were required for dynamics 1, and 36 runs for dynamics 2.

Finally, a detailed investigation of the effects of the experimental display conditions upon pilot performance was conducted by decreasing the display dimension of the analysis of variance to two variables, and performing the variance analysis for different combinations of paired displays (i.e., display case A versus display case B, etc.).

The pilot opinion ratings used were the Cooper-Harper rating (reference 2) and the Hoh rating (reference 15). The Cooper-Harper rating scale has been used in many studies and is well known. The Hoh rating scale is more recent, and was designed in an attempt to obtain more consistent ratings.

Results

The average pilot describing functions for the four display cases are shown in Figures 4 and 5. Figure 4 shows the average of 42 runs for each display case for dynamics 1 (6 runs for each of 7 pilots). Figure 5 shows the average of 6 runs for each display case for dynamics 2 (6 runs for each of 6 pilots). Similarly, Table III shows the average pilot opinions ratings and error scores as a function of display case, and for each of the two aircraft dynamics.

Using data from all the subjects, two-sided F-tests applied to the analysis of variance are used to determine whether significant differences exist between the results for the four display cases. The results of the analysis are presented in Table IV, which lists only those data points for which there is a significant trend at the .02 confidence level.

Conclusions

The following conclusions are made in the context of this experiment. They consequently apply to trained pilots flying a single-axis, roll compensatory tracking task with both visual and motion cues. In the following discussion, "high frequencies" means above 3.5 rad/sec, and "low frequencies" means below 3.5 rad/sec. Conclusions are based on the results summarized in Table IV, and the direction of trends as shown by Figures 4 and 5. See Figure 3 for a summary of the four display cases A, B, C and D.

ORIGINAL PAGE IS
OF POOR QUALITY

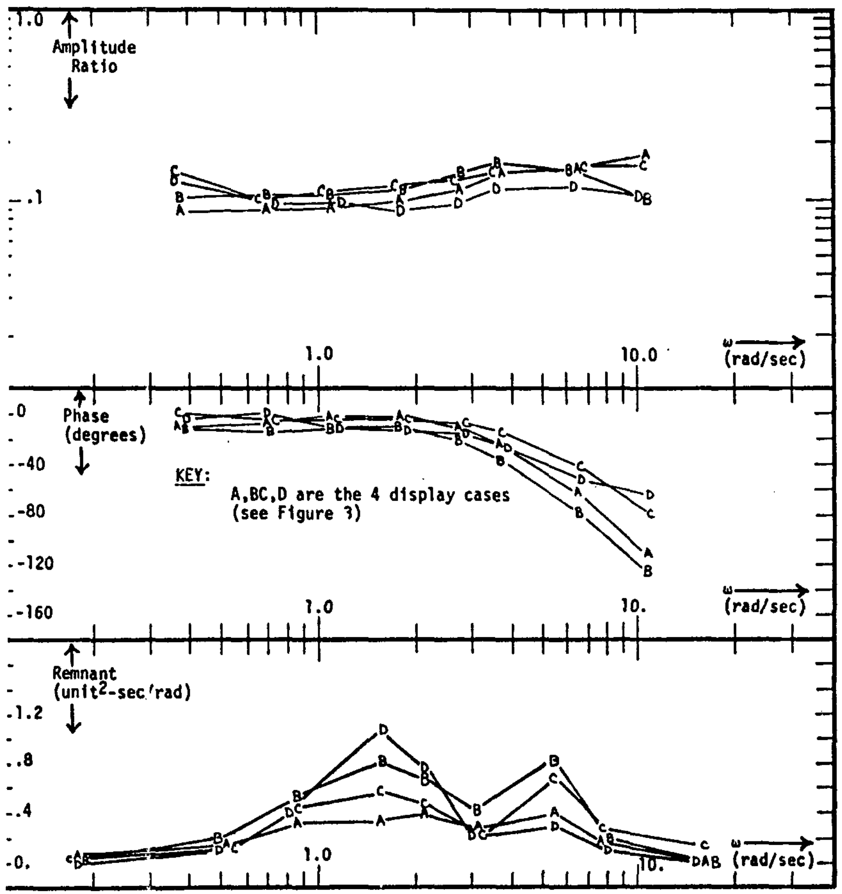

Figure 4: Average Pilot Quasi-Linear Describing Function for Dynamics 1

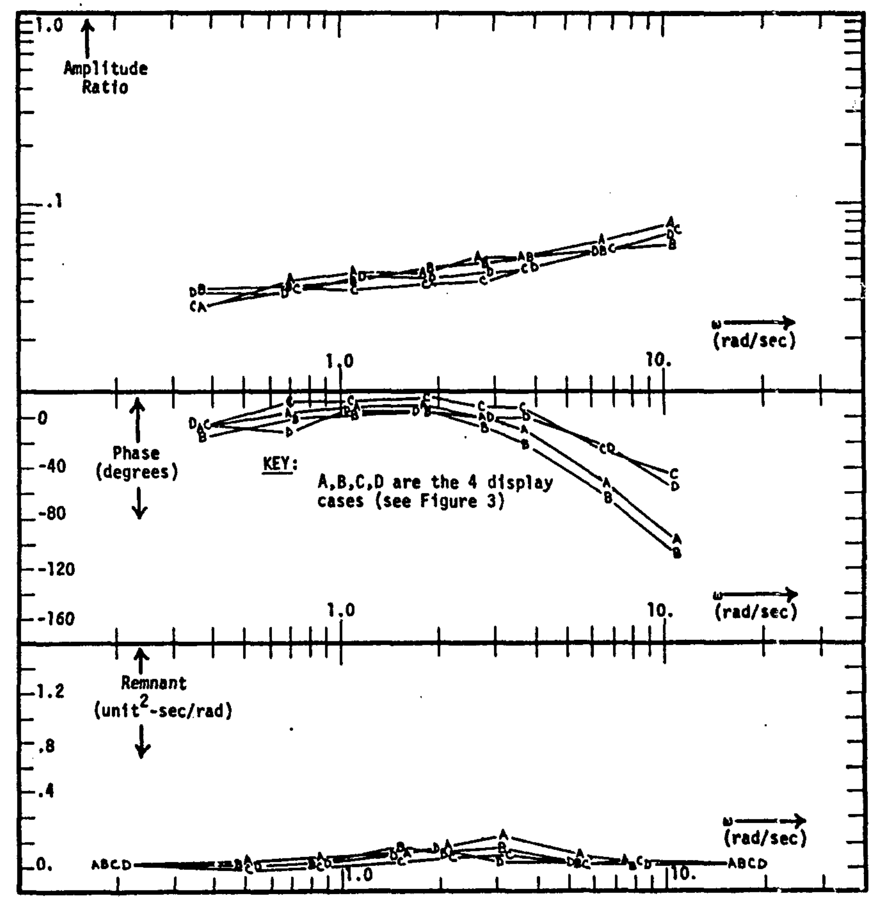

Figure 5: Average Pilot Quasi-Linear Describing Function for Dynamics 2

Table III

Summary of Average Pilot Ratings and Error Scores

	Average Cooper-Harper Pilot Ratings			
	Display Case A	Display Case B	Display Case C	Display Case D
Dynamics 1	4	5	4	5
Dynamics 2	6	5	5	5

	Average Subjective (Hoh) Pilot Ratings			
	Display Case A	Display Case B	Display Case C	Display Case D
Dynamics 1	2.65	2.85	2.55	3.02
Dynamics 2	2.75	2.56	2.72	2.85

	Average Integral Square Error Score			
	Display Case A	Display Case B	Display Case C	Display Case D
Dynamics 1	309	343	297	348
Dynamics 2	369	361	316	328

	Average Integral Absolute Error Score			
	Display Case A	Display Case B	Display Case C	Display Case D
Dynamics 1	64	68	63	68
Dynamics 2	70	68	64	66

	Between Displays **	Dynamics 1: 8.8/s(.5s+1)	Dynamics 2: 37.25/s(.5s+1)
1)	A and B	error scores lower at display A remnant lower at display A *less phase lag (freq. 4,5,6) at display A	less phase lag (freq. 7) at display A
2)	A and C	less phase lag (freq. 7,8) at display C	less phase lag (freq. 6,7) at display C
3)	A and D	less phase lag (freq. 7) at display A	no significant effects
4)	B and C	less phase lag (freq. 2,3,5,6) at display C	less phase lag (freq. 6,7) at display C
5)	B and D	no significant effects	less phase lag (freq. 5,6,7,8) at display D
6)	C and D	less phase lag (freq. 4,5,6) at display C	no significant effects

*frequencies: (rad/sec) 1) .35 2) .70 3) 1.05 4) 1.75 5) 2.62 6) 3.49 7) 6.28 8) 10.47

**Display Cases (see figure 3)

	motion normal	motion compensated
visual normal	A	C
visual degraded	B	D

Table IV: Summary of Significant Effects
(at .02 confidence level)

1) The conflict between visual and motion display characterisitics does not affect pilot performance, but the presence of high frequency information in the visual and/or motion displays does significantly affect pilot performance. Case B (no conflict of cues) is not a more effective display than either A or D, yet both display cases A and D have a conflict of cues. In other words, improving either the motion or visual display used in case B provides information the pilot uses, despite the conflict of cues. Furthermore, improving both displays (i.e. using display C) provides still further information the pilot uses, as case C allows the pilot to generate more lead than either case A or D. Thus the more information available to the pilot, the more he uses, despite the conflict of cues generated by display cases A and D.

2) The most sensitive measure of the display differences was the pilot's phases. Error scores, pilot opinion ratings, pilot amplitude ratios and remnant all showed very little, if any, significant changes. Specifically, in the experiment significant effects were found for one remnant (between cases A and B), for one error score (between cases A and B), and for twenty-two phases (see Table III). It is felt that significant differences would be found for pilot amplitude ratio and overall error scores in a more difficult or complex task, similar to the experiments of Junker and Replogle (reference 8) or Bergeron (reference 10).

3) Pilots use roll motion cues to generate lead at high frequencies. Significantly more lead was generated by pilots with the motion display compensated in case C, than with the uncompensated motion display in case A. This was true despite the fact that for both cases the visual display contained the same high frequency information present in the compensated motion display. This result agrees with references 6 and 9.

4) The usefulness of roll motion cues for generating high frequency lead increases with plant gain. In going from display case B to D for dynamics 1 (gain 8.8) there are no significant effects despite the compensation of the motion display. For dynamics 2 (gain 37.25), however, going from display case B to D significantly increases the high frequency lead generated by the pilots. The fact that motion cues are more useful at higher plant gains agrees with the results of references 6 and 9.

5) For dynamics 1 (low gain), pilots use visual cues to generate lead at low frequencies. Degrading the visual display (i.e. going from case A to B or from case C to D) leads to significantly less lead being generated by the pilots at 3.5 rad/sec and below. This is true despite the fact that in both cases C and D the motion display contains the same information as the undegraded visual display. The fact that the visual display is most useful to the pilots at frequencies below 3.5 rad/sec agrees with the results of references 6 and 9.

6) The need for visual cues to generate low frequency lead decreases as plant gain increases. Whether going from display case A to B, or from display case C to D, there are significant effects for dynamics 1 (low gain), and almost no significant effects for dynamics 2 (high gain).

In addition to these six conclusions, it is possible to make some general statements based on the visual and motion cues used in the experiment. When a flight simulation has both visual and motion cues, each cue should be made as close to actual flight conditions as is practical, despite the fact that there may be some conflict of cues between sensory modalities. In the experiment, degrading the visual or motion cues to a first order filter at 4.8 rad/sec was sufficient to change pilot performance, but degrading both visual and motion cues had an even more profound effect.

Motion cues in vehicle simulations are used because in some cases they lead to data which are more representative of actual flight data. The reasons for this are that motion cues can both enhance the overall aura of realism of a simulation, and that motion cues provide an additional feedback path by which the pilot can control the vehicle. Pilot-vehicle crossover frequencies are typically placed at 3 to 4 rad/sec (reference 1). Although it

may not be critical to overall task performance, the experiment clearly shows that pilot performance can be changed by visual and/or motion cues at frequencies as high as 10 rad/sec. Thus motion and visual simulator frequency response requirements may have to be extended to 10 rad/sec for some tasks, especially for the rotational axes.

APPENDIX A

Equations Used to Calculate Pilot Describing Functions

The pilot model used for the experiment is the quasi-linear describing function shown in Figure 6 and reference 1. It is used in the context of a single-axis, compensatory, roll tracking task as shown in Figure 2. The sum of sinusoids disturbance, d(t) used to drive the system (as indicated in Figure 2) is digitally calculated as:

$$d\,(n\Delta t) = G \sum_{k=1}^{8} K_k \sin\,(\omega_k n\Delta t) \qquad (1)$$

where Δt is .05 seconds, and K_k, G and ω_k are given in Table II. The following characteristics of the disturbance should be noted:

- an exact integer number of cycles of each frequency, ω_k, occur each 36 seconds
- all the sinusoids pass through either 0° or 108° at the start and end of each data taking period
- there is a phase-in period before the data taking period during which the disturbance is gradually introduced
- there is a warmup period after phase-in to ensure that the pilot is in a steady state condition for data taking
- each data run is 108 seconds long (3 times 36 seconds)

During the data taking period the pilot's input and output, e(t) and c(t), are recorded every Δt. A Fourier analysis is then performed at the driving frequencies (i.e. at those frequencies which comprise the disturbance) as follows:

$$A_{ek} = \sum_{n=1}^{N} e(n\Delta t) \sin\,(\omega_k n\Delta t) \qquad (2)$$

PAGE IS

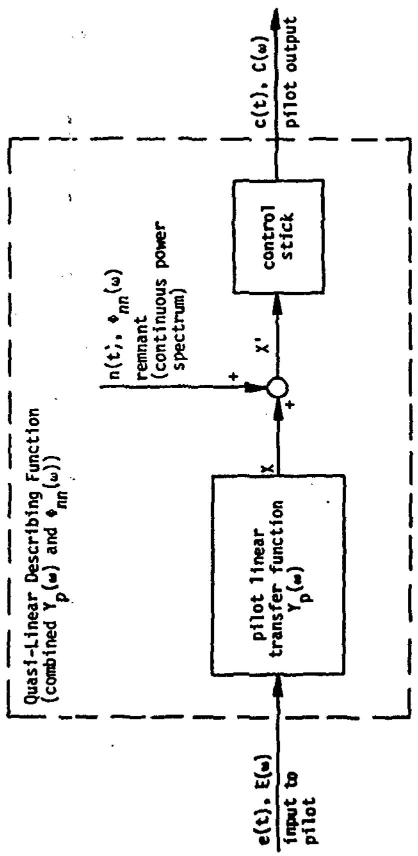

Figure 6: Pilot Quasi-Linear Describing Function

$$B_{ek} = \sum_{n=1}^{N} e(n\Delta t) \cos(\omega_k n\Delta t)$$

$$A_{ck} = \sum_{n=1}^{N} c(n\Delta t) \sin(\omega_k n\Delta t) \qquad \text{(2 Con't.)}$$

$$B_{ck} = \sum_{n=1}^{N} c(n\Delta t) \cos(\omega_k n\Delta t)$$

where Δt and ω_k are given in Table II, and

$$N = \frac{(3 \text{ Periods})\left(36 \frac{\text{seconds}}{\text{period}}\right)}{\left(.05 \frac{\text{seconds}}{\text{sample}}\right)} = 2160 \text{ samples} \qquad (3)$$

The Fourier coefficients are then processed to calculate the pilot's linear transfer function as

$$|Y_p(\omega_k)| = \frac{\left[(A_{ek} A_{ck} + B_{ek} B_{ck})^2 + (A_{ek} B_{ck} - A_{ck} B_{ek})^2\right]^{1/2}}{A_{ck}^2 + B_{ck}^2} \qquad (4)$$

$$\angle Y_k(\omega_k) = \tan^{-1}\left[\frac{A_{ek} B_{ck} - A_{ck} B_{ek}}{A_{ek} A_{ck} + B_{ek} B_{ck}}\right] \qquad (5)$$

Equations 4 and 5 represent the linear part of the quasi-linear describing function. The non-linear part is the remnant, which requires a Fourier analysis at frequencies ω_j as follows:

$$A_{cj} = \sum_{n=1}^{N} c(n\Delta t) \sin(\omega_j n\Delta t) \qquad (6)$$

$$B_{cj} = \sum_{n=1}^{N} c(n\Delta t) \cos(\omega_j n\Delta t) \qquad \text{(6 Con't.)}$$

where N is defined in equation 3, Δt is .05 seconds, and the ω_j are shown in Table II. Note that the ω_j frequencies lie between the driving frequencies, ω_k. The remnant is then calculated as

$$\Phi_{nn}(\omega_j) = K_{nn}(A_{cj}^2 + B_{cj}^2) \qquad (7)$$

where K_{nn} is a scale factor which normalizes the remnant with respect to the input disturbance power, corrects for the run time, and corrects for the bandwidth of the Fourier analysis. K_{nn} is derived as follows: with reference to Table II, the total input power TIP, is given by

$$TIP = 0.5\, G^2 \sum_{k=1}^{8} K_k^2 \quad \text{units}^2/\text{Hz} \qquad (8)$$

The bandwidth of the signals in the digital computer, BW, is determined by the Nyquist frequency as

$$BW = \frac{1}{2\Delta t} \quad \text{Hz} \qquad (9)$$

and therefore the total input power per Hz, TIPH, is given by

$$TIPH = TIP/BW \qquad (10)$$

K_{nn} must include a factor, K_1, to normalize for the input:

$$K_1 = \frac{1}{TIPH} = \frac{BW}{TIP} \qquad (11)$$

Because the A_{cj} and B_{cj} are calculated according to equations 6, a factor of $1/N\Delta t$ is needed to correct for the number of samples taken. This factor occurs in both A_{cj} and B_{cj}, and is squared in equation 7. Hence K_{nn} must contain a factor

$$K_2 = \left(\frac{1}{N\Delta t}\right)^2 \qquad (12)$$

The Fourier analysis represented by equations 6 has an effective bandwidth of $2/N\Delta t$ Hz. For the remnant to be in terms of power/Hz, K_{nn} must include the factor

$$K_3 = \frac{N\Delta t}{2} \qquad (13)$$

Combining the factors

$$K_{nn} = K_1 K_2 K_3 = \left(\frac{BW}{TIP}\right) \left(\frac{1}{N\Delta t}\right)^2 \left(\frac{N\Delta t}{2}\right) \qquad (14)$$

$$K_{nn} = \frac{BW}{TIP} \quad \frac{1}{2N\Delta t} \qquad (15)$$

substituting for BW using equation 9,

$$K_{nn} = \frac{1}{TIP\ 4N(\Delta t)^2} \qquad (16)$$

where TIP is given in equation 8.

References

1. McRuer, D., D. Graham, L. Krendel and W. Reisener, Jr. 1965. Human pilot dynamics in compensatory systems - theory, models and experiments with controlled element and forcing function variations. AFFDL TR-65-15.

2. Cooper, G.E. and R.P. Harper, Jr. 1969. The use of pilot ratings in the evaluation of aircraft handling qualities. NASA TN D-5153.

3. Newell, F.D. 1968. Human transfer characteristics in flight and ground simulation for a roll tracking task. AFFDL TR-67-30.

4. Newell, F.D. and H.J. Smith 1969. Human transfer characteristics in flight and ground simulation for a roll tracking task. NASA TN D-5007.

5. Creer, B.Y., J.D. Stewart, R.B. Merrick and F.J. Drinkwater III 1959. A pilot opinion study of lateral control requirements for fighter-type aircraft. NASA Memo 1-29-59A.

6. Shirley, R.S. and L.R. Young 1968. Motion cues in man-vehicle control. IEEE Trans Man-Machine System. MMS-9: 121-128.

7. Schmidt, S.F. and B. Conrad 1970. Motion drive signals for piloted flight simulators. NASA CR-1601.

8. Junker, A.M. and C.R. Replogle 1975. Motion effects on the human operator in a roll axis tracking task. Aviation, Space and Environment Medicine. 46: 819-822.

9. Stapleford, R.L., R.A. Peters and F.R. Alex 1969. Experiments and a model for pilot dynamics with visual and motion inputs. NASA CR-1325.

10. Bergeron, H.P. 1970. Investigation of motion requirements in compensating control tasks. IEEE Trans. Man-Machine System. MMS-11: 123-125.

11. Ringland, R.F., R.L. Stapleford and R.E. Magdaleno 1971. Motion effects on an IFR hovering task - analytical predictions and experimental results. NASA CR-1933.

12. Miller, G.K. and D.R. Riley. The effect of visual motion time delays on pilot performance in a simulated pursuit tracking task. (Submitted as NASA TN)

13. Fry, E.B., R.K. Grief and R.M. Gerdes 1969. Use of a six-degree-of freedom motion simulator for VTOL hovering tasks. NASA TN D-5383.

14. Shirley, R.S. 1969. Application of a Modified Fast Fourier Transform to calculate human operator describing function. NASA TM X-1762.

15. Hoh, R.H. 1975. A pilot rating scale for vortex hazard evaluation. NASA CR-143826.

16. Kirk, R.E. 1968. Experimental Design: Procedures for the Behavioral Sciences. Brooks/Cole Publishing Co., Belmont, CA.

N79-17512

A MODEL FOR THE PILOT'S USE OF MOTION CUES IN ROLL-AXIS TRACKING TASKS

by

William H. Levison
Bolt Beranek and Newman Inc.
Cambridge, Massachusetts

and

Andrew M. Junker
Aerospace Medical Research Laboratory
Wright-Patterson AFB, Ohio

ABSTRACT

An experimental and analytical study was undertaken jointly by the Aerospace Medical Research Laboratory and Bolt Beranek and Newman Inc. to test a model for the pilot's use of motion cues in roll-axis tracking tasks. Simulated target-following and disturbance-regulation tasks were explored with subjects using visual-only and combined visual and motion cues. The effects of motion cues on task performance and pilot response behavior were appreciably different for the two task configurations and were consistent with data reported in earlier studies for similar task configurations.

The "optimal-control" model for pilot/vehicle systems provided a task-independent framework for accounting for the pilot's use of motion cues. Specifically, the availability of motion cues was modeled by augmenting the set of perceptual variables to include position, rate, acceleration, and acceleration-rate of the motion simulator, and results were consistent with the hypothesis of attention-sharing between visual and motion variables. This straightforward informational model allowed accurate model predictions of the effects of motion cues on a variety of response measures for both the target-following and disturbance-regulation tasks.

Presented at the Thirteenth Annual Conference on Manual Control, MIT, Cambridge, Mass., June 15-17, 1977.

INTRODUCTION

This paper summarizes the work performed in the second year of a joint study by the Aerospace Medical Research Laboratory (AMRL) and Bolt Beranek and Newman Inc. (BBN) to explore the use of motion cues in roll-axis tracking tasks. Results of this study have been documented by Levison and Junker [1]; results of the preceding study are reported in [2] and [3].

This study has continued to be concerned with the use of motion-related sensory information for continuous flight control. Other potential effects of motion, such as providing alerting cues to the pilot or providing "realism" to aircraft simulations, are not considered. Analysis of the experimental results has been directed towards developing a generalized description of the manner in which the pilot uses motion cues, with the ultimate goal of providing a model that can predict the effects of motion cues on system performance in a variety of control situations.

Analysis of the experimental data obtained in the preceding study revealed that the effects of motion cues on roll-axis tracking could be modeled primarily by inclusion of sensory variables likely to be provided by motion sensors (position, rate, and acceleration of the controlled vehicle). In addition, pilot time delay was incremented by 0.05 seconds. Modeling of dynamics associated with motion sensors was not required.

The experimental results did not allow us to determine conclusively whether or not the pilot had to "share attention" between visual and motion modalities. Nevertheless, tracking performance was consistent with the notion that attention was shared optimally between visual and motion cues. Moreover, model analysis indicated that the optimal allocation of attention between modalities was different for the two control tasks explored in that study.

The results of the study reported in [2] and [3] appeared to conflict with the findings of others regarding the effects of motion cues on tracking performance. Both Shirley [4] and Stapleford et al. [5] concluded that the addition of motion cues allowed the pilot to generate greater lead at high frequencies, thereby permitting an increase in gain-crossover frequency. Furthermore, Shirley concluded that motion cues were relatively more beneficial for tracking tasks involving low-order plants than for those involving high-order dynamics. On the contrary, the results of the AMRL/BBN study showed that phase lead was increased at *low* frequencies, rather than *high* frequencies;

D37

phase lag increased somewhat at high frequencies; gain-crossover frequency remained essentially unchanged; and motion cues had a greater effect with the higher-order of the two plants explored.

These apparent contradictions do not necessarily indicate that the AMRL experimental subjects used motion cues in a manner different from the subjects who participated in the studies of Shirley and of Stapleford et al. There were some important differences between the AMRL experiments and the earlier studies. Both Shirley and Stapleford et al. applied the input disturbance in such a manner that both the visual display and the motion simulator were driven by the input. (That is, the input was applied essentially in parallel with the pilot's control.) In the AMRL study, the external input was applied as a command signal; only the pilot's input drove the controlled plant. Thus, in the latter study, motion cues provided some inner-loop information that was not directly obtained from the visual cues.

In order to explore the apparent discrepancies between the initial AMRL/BBN study and earlier investigations, a small but carefully controlled experiment was conducted to compare the use of motion cues in disturbance and command situations. The results of this study form the main topic of this paper.

EXPERIMENTAL PROCEDURES

The reader is referred to a companion paper for detailed descriptions of the tracking task and experimental procedures [6]; only a brief summary is given here.

The pilot was required either to regulate against a simulated gust disturbance (the "disturbance condition") or to follow a commanded target (the "target condition"). Plant dynamics were basically $K/s(s+5)$ to approximate roll-axis characteristics of high-performance fighter aircraft. These dynamics were modified by the high-frequency rolloff properties of the moving-base simulator and by delays of approximately 0.1 seconds introduced by recording and simulation procedures. The external forcing function was a sum of thirteen sinusoids constructed to simulate white noise shaped by a second-order filter with two identical real poles. Pole locations were 1.0 rad/sec for the target input and 2.0 rad/sec for the disturbance input.

Each input condition was tracked with and without the moving-base simulator operative, making a total of four experimental conditions. In all cases, the subject was presented with a compensatory display of roll error. Subjects (six in all) were trained to asymptote on all conditions and were instructed to minimize a "cost" defined as $C = \sigma_e^2 + 0.1\,\sigma_{\ddot{p}}^2$, where σ_e^2 is the variance of the tracking error and $\sigma_{\ddot{p}}^2$ is the variance of the plant acceleration. The cost on acceleration was imposed partly to force the subjects (non pilots) to track in a smooth manner, and partly to assure that roll rates and accelerations would be well within the physical limits of the moving-base simulator most of the time.*

EXPERIMENTAL RESULTS

Analysis Procedures

Variance scores were computed for each experimental trial for the tracking error, error rate, plant position (i.e., roll angle), plant rate, plant acceleration, control force, and control force rate. (For disturbance-regulation tasks, error and error rate were identical to plant position and plant rate.) Also computed was total "cost" as defined above. Square roots were taken of the measures to yield rms performance scores.

Performance scores were first averaged across replications of a given test subject for each experimental condition; the mean and standard deviation of the subject means pertaining to each experimental condition was then computed. In order to test for significant differences between motion and static conditions, paired differences were formed from corresponding subject means; these differences were subjected to a two-tailed t-test.

Similar statistical analysis was performed for frequency-response measures. Additional details on analysis procedures are given in Levison and Junker [1].

*Pre-experimental analysis was performed with the optimal-control pilot/vehicle model to select various experimental parameters (including the relative cost penalty on acceleration) to achieve certain experimental goals. This design procedure succeeded, very successful, and experimental results were close to those predicted a priori by the model. Use of the pilot model in the design of these experiments is described in Junker and Levison [6].

Principal Results

Variables for which rms performance scores were computed, their units, and their symbolic notation are shown in Table 1. Average rms performance scores are shown in Figure 1. For ease of comparison with other performance metrics, the square root of the "cost" is shown, and various rms scores have been scaled so that all scores may be shown on the same ordinate scale. Significant static-motion differences are indicated by the arrows, where the coding of the arrow indicates the significance level as defined in Table 2. Mean performance scores and standard deviations of subject means are given in [1].

Figure 1 shows that the availability of motion cues had little effect on rms performance measures for the target-tracking task. Plant position showed the greatest effect, decreasing by about 20% in the motion case. Smaller but statistically significant reductions were found for total cost and for control-related scores. The fact that statistical significance can be shown for these relatively small differences indicates that the influence of motion cues, however slight, was consistent across subjects.

Static-motion differences were considerably greater for the disturbance-tracking task. Although no significant change was observed in the control-related scores, total cost and error-related scores were reduced substantially; these differences were significant at the 0.01 level or lower.

The average frequency-response measures presented in Figure 2 show that motion-cue effects were qualitatively different for the two tasks. The three measures shown in the figure are, from top to bottom, amplitude ratio (i.e., pilot gain), pilot phase shift, and the ratio of remnant-related to input-correlated control power (which we shall refer to as the "remnant ratio").

The effects of motion cues on pilot response behavior for the target-tracking and disturbance-regulation tasks are summarized in Table 3. The major influence of motion cues in the target task was to induce a substantial phase lead at low frequencies. There was no change in gain-crossover frequency (about 1 rad/sec), and the remnant ratio increased somewhat. In the disturbance task, however, motion cues allowed the subjects to convert a high-frequency phase lag into a substantial phase lead, increase amplitude ratio at low and mid frequencies, and thereby increase gain-crossover frequency from about 1.5 rad/sec to around 3.5 rad/sec. There was a consistent decrease in remnant ratio, although static-motion differences were largely not statistically significant.

Table 1

Tracking Variables Analyzed

Variable	Symbol	Units
Total Performance Cost	c	---
Tracking Error	e	degrees
Tracking Error Rate	$\dot{e}$	degrees/second
Plant Position	p	degrees
Plant Rate	$\dot{p}$	degrees/second
Plant Acceleration	$\ddot{p}$	degrees/second^2
Control Force	u	pounds
Control Rate	$\dot{u}$	pounds/second

Table 2

Coding for Significance Level

Symbol	Alpha Level of Significance
$\downarrow$	0.05
$\downarrow$	0.01
$\downarrow$	0.001

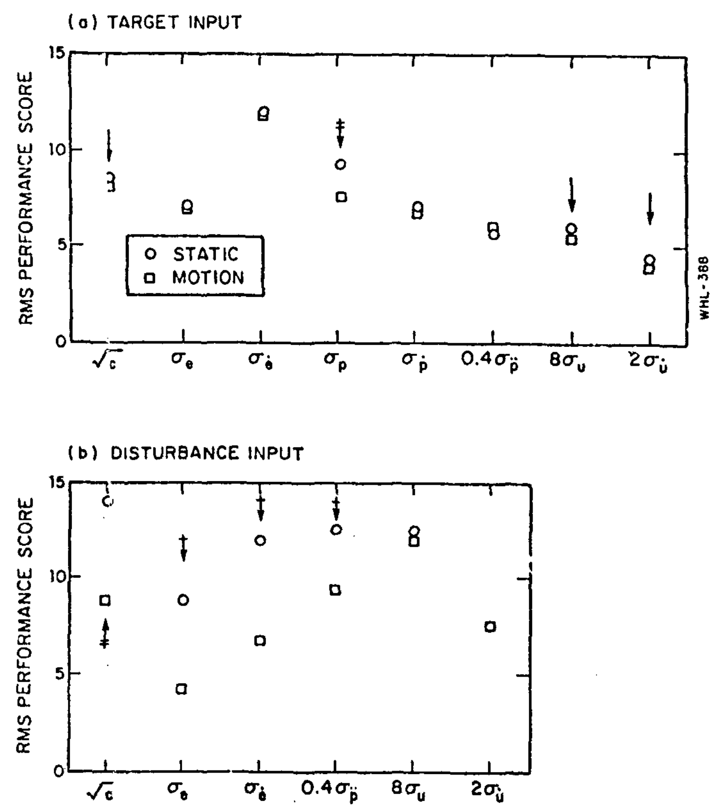

Figure 1. Effect of Motion Cues on RMS Performance Scores

Average of 6 subjects.

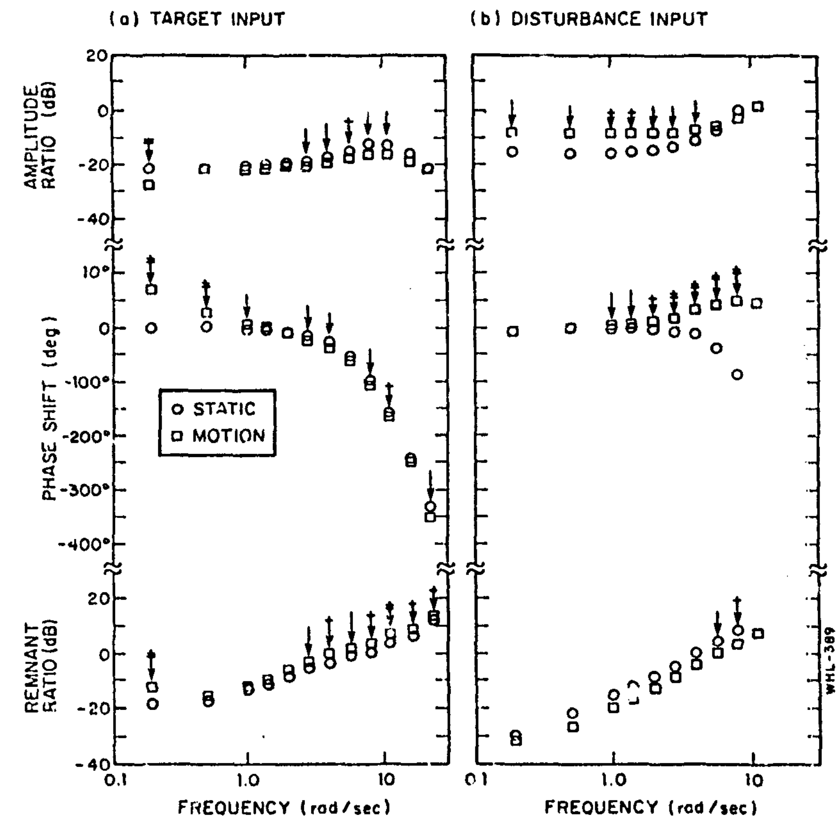

Figure 2. Effect of Motion Cues on Pilot Frequency Response

0 dB represents 1 pound con rol force per degree roll for the amplitude ratio and unity (dimensionless) for the remnant ratio.

Average of 6 subjects.

Table 3

Effects of Motion Cues on Frequency Response

Measurement	Effects of Motion Cues	
	Target Input	Disturbance Input
Low-frequency phase	Substantial increase in phase lead	No change
High-frequency phase	Small increase in phase lag	Convert phase lag to phase lead, a substantial change
Low-frequency amplitude-ratio	No change	Substantial increase
Gain-crossover frequency	No change	Increase by over factor of 2
Remnant ratio	Overall increase	Overall decrease

During the course of this analysis we addressed the question of whether or not the average pilot response characteristics shown in Figure 2 were typical of the response characteristics of individual subjects. That is, we wanted to ascertain that important response characteristics were not obscured by the averaging process. Accordingly, the procedure for eliminating atypical performance described in [1] was applied to subject means to successively eliminate all but one subject per experimental condition.

Figure 3 compares the responses of typical subjects to the average response of all six subjects for the static and motion conditions in the disturbance-regulation task. Typical and average responses very nearly coincided for the static condition. The correspondence between typical and average response was also high for the motion condition, with only small differences in overall amplitude of response. Thus, we are justified in averaging these response measures across subjects.

Discussion of Results

The results obtained in this experiment agree qualitatively with results obtained previously in similar tracking situations. The effects of motion cues in the target-tracking task are similar to those obtained in the preceding AMRL experimental study for "Task 1" (the less severe of the two tasks studied in that program). In both cases, motion cues allowed an increase in low-frequency phase shift that was unaccompanied by any substantial improvement in tracking performance.

Similarly, the effects of motion cues observed in the disturbance-regulation task agree with the effects reported by other researchers [4, 5] who found that moving-base simulation allowed the pilot to reduce high-frequency phase lag and to increase gain-crossover frequency and thereby, in many cases, lower his error score.

Motion/static performance differences were enhanced somewhat by the time delays introduced by the data-recording and computational algorithms. These delays influenced only the visual cues provided to the pilot; the motion cues were provided by the moving-base simulator. Thus, motion cues provided a double benefit to the pilot; information was obtained via motion sensors in advance of information obtained visually, and, as we infer from the model analysis described below, vehicle acceleration and possibly rate-of-change of acceleration were also sensed.

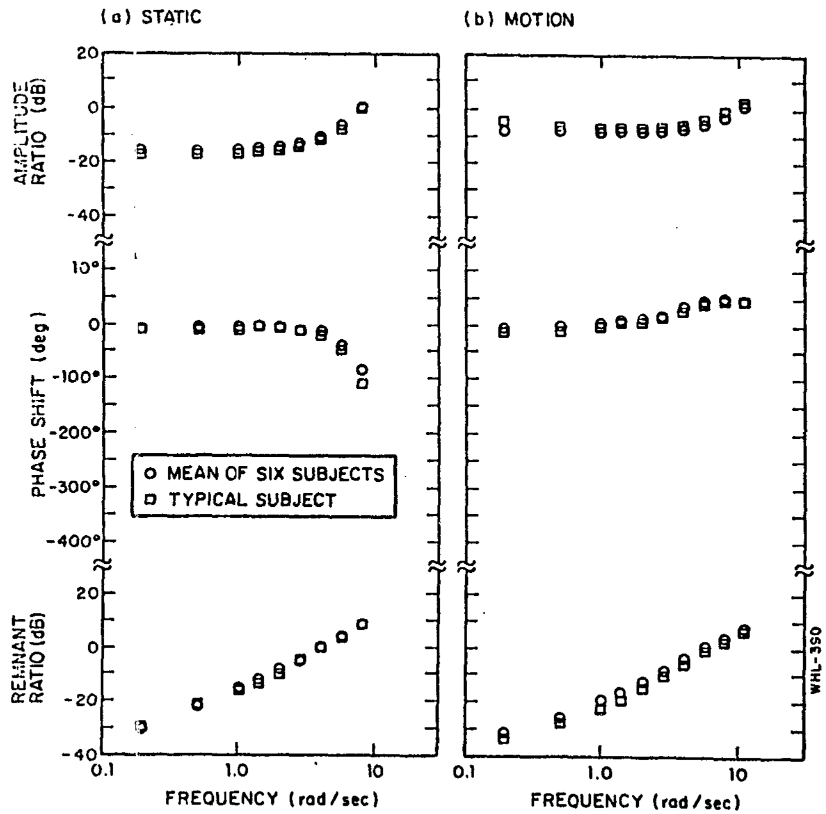

Figure 3. Comparison of Typical and Mean Responses for the Disturbance-Regulation Task

It is clear from the results of this experiment that the effects of motion cues on pilot response cannot be generalized in terms of classical response measures. We have shown that the effects of motion cues on rms performance scores, pilot describing function, and pilot remnant can all differ qualitatively from one control situation to the next.* Some form of generalization is needed, nevertheless, if we are to extrapolate the results of these and earlier experiments to other control tasks. That is, we need a model which accounts for the interaction between available motion cues and pilot response in terms that are essentially independent of the details of the control task. Such a model is discussed below.

MODEL ANALYSIS

Analysis Procedure

The revised optimal-control pilot/vehicle model developed in the preceding phase of this study was applied to the results of the experiment described above. This model is described by Levison, Baron, and Junker [2].

The treatment of motion cues was similar to that of the preceding study in that the presence or absence of motion cues was represented by an appropriate definition of the sensory variables assumed to be available to the pilot. A three-element "display vector' consisting of tracking error, error rate, and (in one instance) error acceleration was used to model static-mode tracking. To model pilot response in moving-base tasks, we simply expanded this display vector to include position, rate, acceleration, and acceleration-rate of the vehicle; no other model parameters were changed to account for motion/static differences. Model runs were also obtained which included the effects of dynamic response properties of vestibular motion sensors.

The scheme for identifying model parameters was similar to that described in [2, 3]. Parameter values were sought that would simultaneously provide a good match to performance scores, describing function, and remnant ratio. A multi-dimensional "matching error"

*Relative effects of motion cues are affected not only by the type of external input, as demonstrated here; pre-experimental model analysis indicated that input bandwidth and performance criterion would also influence motion/static differences in response behavior.

was defined, with the dimensions being (1) rms performance, (2) amplitude ratio, (3) phase shift, (4) and remnant ratio. Matching error was defined in such a way that a score of unity was obtained whenever model predictions differed on the average from experimental measurements by one standard deviation.

As in the preceding study, the primary goal of model analysis was to determine a straightforward and reliable procedure for predicting the effects of motion cues in a variety of control tasks. Therefore, we attempted to account for performance on all four tasks with the fewest variations in parameter values. we did not allow all parameters to vary in order to obtain the best match in each condition; rather, variations were made in only those parameters that could reasonably be expected to relate to the kind and quality of information provided to the pilot.

<u>Primary Results of Model Analysis</u>

Attentional parameters were the only model parameters that were varied across experimental conditions; all other parameter values were held fixed. Numerical values for pilot-related parameters, shown in Table 4, were obtained as follows:

Control-Rate Cost Coefficient. Based on previous studies of single-variable laboratory tracking tasks, the control-rate cost coefficient was adjusted to provide a "motor time constant" of 0.1 second.

Acceleration Cost Coefficient. In accordance with instructions given to the subjects, we initially attempted to match experimental results with an acceleration cost coefficient of 0.1 seconds. A somewhat better match was obtained with a coefficient of 0.05, however, and this latter value was adopted for the remainder of the analysis.

Time Delay. A time delay of 0.22 seconds provided the best match across conditions.

Motor Noise/Signal Ratios. On the basis of previous analysis, the "driving" motor noise/signal ratio was made negligibly small; a "pseudo" noise/signal ratio of -30 dB gave a reasonably good match to low-frequency phase shift (see Levison, Baron, and Junker for a discussion of the motor noise aspect of the pilot model.)

Observation Noise/Signal Ratio. On the basis of previous studies, an observation noise/signal ratio of -20 dB was adopted.

Table 4

<u>Values for Pilot-Related Model Parameters</u>

a. <u>Invariant Parameters</u>

Control-rate cost coefficient	1.0
Motor time constant	0.1 seconds
Acceleration cost coefficient	0.05
Time delay	0.22 seconds
Driving motor noise/signal ratio	(negligible)
Pseudo motor noise/signal ratio	-30 dB
Observation noise ratio for "Full Attention"	-20 dB
Perceptual thresholds, error rate, visual	3.2 deg/sec
Perceptual thresholds, all other variables	(negligible)

b. <u>Attentional Allocation</u>

Perceptual Mode	Perceptual Variable	Tracking Task: Target Static	Input Motion	Disturbance Static	Input Motion
Visual	error	1	0.95	1	0.1
	error rate	1	0.95	1	0.1
	error acceleration	---	---	0.05	0
Motion	plant	0	0.05	0	0.9
	plant rate	0	0.05	0	0.9
	plant acceleration	0	0.05	0	0.9
	plant acceleration rate	0	0.05	0	0.9

Perceptual Threshold. Because vehicle roll rates and accelerations were large compared to published detection thresholds for these variables, thresholds for motion-related variables were set to zero. A good match to the data was obtained with thresholds of 0 degrees and 3.2 deg/sec associated with visually-obtained error and error rate.

Attentional Variables. With the exception of visually-obtained error acceleration, attention was assumed to be shared between visual display variables as a group and motion variables as a group, and there was assumed to be no interference among perceptual quantities within a sensory mode. The absence of motion-related information in a tracking task was modeled as zero attention (i.e., extremely large observation noise) on motion variables and unity attention on visual variables. The attentional allocations between visual and motion cues shown in Table 4 provided the best match to the data.

Figure 4 shows that the model accurately reflected the influence of both the nature of the external input and the presence or absence of motion cues. Of the 28 performance scores predicted by the model, all but three were within 10 percent of corresponding experimental measures; and in only one of these cases did the model score fail to be within one standard deviation of the experimental mean.

As shown in Figure 5, model outputs agreed quite well with experimental frequency-response measures, and major trends in the data were predicted. Specifically, inclusion of motion-related sensory information caused the model to predict an increase in low-frequency phase shift for the target task. For the disturbance task, the model correctly predicted large increases in low-frequency gain and high-frequency phase lead. The model also predicted an overall decrease in remnant ratio for this task.

It is worthwhile to re-emphasize that the effects of motion cues have been accounted for solely by changes in model parameters related to the information availability and quality; other parameters have been kept fixed for the four experimental conditions.

Additional Model Results

Values for two of the parameters – cost-of-acceleration and time delay – were somewhat different from those initially expected. The acceleration cost coefficient that provided the best fit to the data was half that used in computing the total performance cost during the experiments. In order to estimate the subject's ability to detect differences between subjective and objective cost criteria,

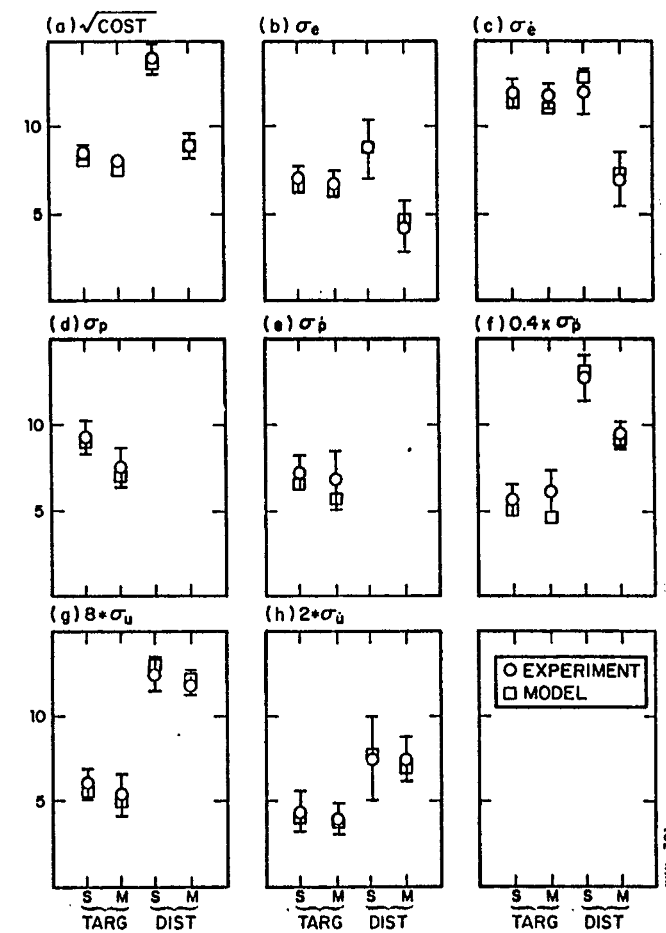

Figure 4. Comparison of Model and Experimental Performance Scores
S=static condition, M=motion condition.
Average of 6 subjects.

The inclusion of acceleration rate in the display vector had a considerable influence on the matching error for the disturbance-regulation task; the matching error on phase shift was reduced by over a factor of 4, and other component matching errors were substantially reduced as well. The improvement occurred largely at high frequencies. Inclusion of acceleration rate had no influence on the match to the data obtained in the target-following task, since high-frequency information was of less importance in performance of this task.

Although matching of the data for the disturbance-regulation task was enhanced by consideration of acceleration-rate information, predicted system performance was little effected by this factor. Model analysis indicated that both rms tracking error and rms roll acceleration would be reduced by about 10% with such information available for a high level of attention to the task, with this benefit disappearing at lower levels of attention.

The disturbance-regulation task was re-analyzed with the vestibular sensor dynamics suggested by Curry, Hoffman, and Young [8] added to the system equations of motion. The "display vector" assumed for model analysis was further augmented by the addition of the outputs of the semicircular and otolith sensors, as well as the rates of change of these outputs. In this analysis, the best match to the data was obtained with the assumption of no interference between visual and motion variables.

The match to the data was nearly identical to that shown above for the simple informational analysis. We therefore conclude that, while models of vestibular dynamics are consistent with the results obtained experimentally, model accuracy is not enhanced by the consideration of such models. For the type of tasks explored in this study, a simple informational analysis appears to be adequate.

One should be careful not to make the conclusion that sensor dynamics can be ignored in all instances. The experiments described in the paper employed steady-state tasks for which response power was concentrated largely within the passband of the vestibular motion sensors. For transient maneuvers where very low frequency characteristics are important, sensor dynamics may have to be considered. This is particularly true for situations in which the low-frequency washout characteristics of the sensors may induce illusions [9].

Reanalysis with Typical Pilot Parameters

By allowing nearly all pilot-related model parameters to vary from one study to the next, we have been able to obtain close agreement between model and experimental results for all tasks explored in this study program. Many of these parameter differences have been attributed to the relative insensitivity of overall system performance to such parameter values.

If the model is to be used as a *predictive* rather than as a *diagnostic* tool, it is important that one be able to predict the effects of task variables on system performance using a single set of typical pilot parameter values. Because there generally exists a range of pilot response behavior that gives near-optimal system performance in a typical control situation, one would not expect such a procedure to yield accurate predictions of all response metrics. Nevertheless, one would expect that important trends in system behavior would be revealed.

To test the predictive capability of the model, a comparison was obtained between measured and predicted rms tracking error for all eight tasks explored in this program, using a set of "typical" pilot parameter values. These values were chosen largely on the basis of previous laboratory studies and are not necessarily those that would provide the best overall fit to the data base. The following parameter values were used:

Cost Functional. Cost functionals were $J = \sigma_e^2 + G\,\sigma_{\dot{u}}^2$ for the tasks explored in the previous study phase [2, 3] and $J = \sigma_e^2 + 0.1\,\sigma_{\dot{e}}^2 + G\,\sigma_{\dot{u}}^2$ for the tasks described in this paper.* The coefficient G was chosen to provide a motor time constant of 0.1 seconds in all cases.

Time Delay. A pilot time delay of 0.2 seconds was assumed.

Perceptual Thresholds. Thresholds of 1.6 degrees for visual perception of tracking error and 6.4 degrees/second for visual perception of error rate were calculated as described in [1]. Because of the large vehicle motions, thresholds for motion-derived perceptions were assumed negligible.

* No penalty was associated with acceleration in the preceding study.

Motor Noise/Signal Ratios. Driving motor/noise signal ratio was negligibly small; pseudo noise/signal ratio was set at -35 dB.

Observation Noise/Signal Ratio. A value of -20 dB was used.

As shown in Figure 6, model predictions correlated well with experimental measures. ("Year 1" and "Year 2" refer to the studies described in [2,3] and in this paper, respectively.) All significant trends related to task configuration and availability of motion cues were predicted. Furthermore, individual scores were predicted, on the average, to within 15%.

CONCLUSIONS

The principal results of this study may be summarized as follows:

1. The effects of motion cues on task performance and pilot response behavior are strongly dependent on the structure of the tracking task. The major effect of motion cues in a target-following task is to allow the pilot to generate low-frequency phase lead; in a disturbance-regulation task, the main effects are more phase lead (alternatively, less phase lag) at high frequencies accompanied by an increase in gain-crossover frequency.

2. Because of the strong interaction between motion-cue effects and task structure, a pilot/vehicle model is required to extrapolate the results from one task to the next.

3. The "optimal-control" model for pilot/vehicle systems provides a task-independent framework for accounting for the pilot's use of motion cues. Specifically, the availability of motion cues is modeled by augmenting the set of assumed perceptual variables to include position, rate, acceleration, and acceleration rate of the moving vehicle.

4. Results are consistent with the hypothesis that the subject shares attention between visual variables as a group and motion variables as a group. This hypothesis has not been conclusively proven, however.

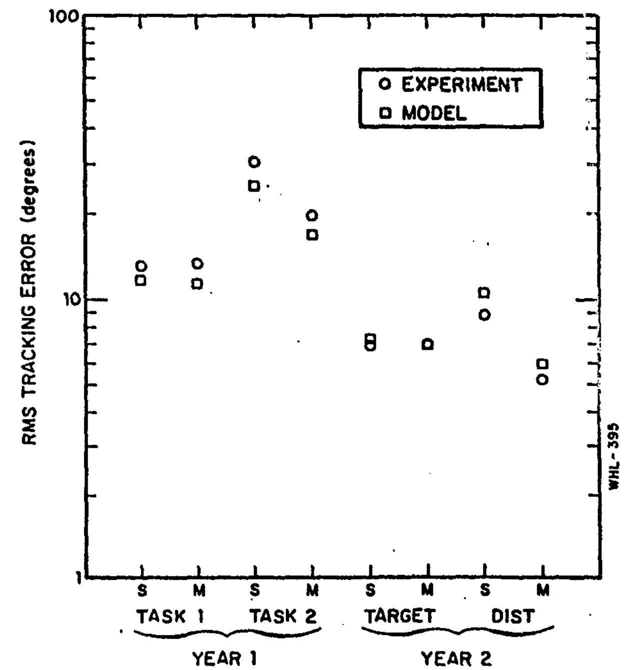

Figure 6. Comparison of Model and Experimental RMS Error Scores for Two Studies

S=static condition, M=motion condition.

5. Variations in model parameters relating to motion-cue availability and attention-sharing are sufficient to enable the model to replicate the effects of motion on all performance metrics for the tasks explored in this study.

6. Using the model for motion-cue utilization defined above, plus a single "typical" set of pilot-related model parameters, one can obtain accurate model predictions of rms tracking error scores for all task configurations explored in this study and in the preceding study.

7. There is some evidence that low-quality acceleration information can be obtained directly from the visual display in some tasks. The influence of such information processing on tracking performance appears to be minimal, however.

8. Use of acceleration-rate information appears to allow a modest reduction in rms tracking error in some tasks.

9. Results are consistent with existing models for motion perception by vestibular sensors. Such models are not needed to explain the data obtained in this study, however.

REFERENCES

1. Levison, W. H. and A. M. Junker, "A Model for the Pilot's Use of Motion Cues in Roll-Axis Tracking Tasks," Bolt Beranek and Newman Inc., Cambridge, Mass., Report No. 3528, April 1977.

2. Levison, W. H., S. Baron, and A. M. Junker, "Modeling the Effects of Environmental Factors on Human Control and Information Processing," AMRL-TR-76-74, Aerospace Medical Research Laboratory, Wright-Patterson AFB, Ohio, August 1976.

3. Levison, W. H., "Use of Motion Cues in Steady-State Tracking," Twelfth Annual Conference on Manual Control, NASA Technical Memorandum, NASA TM X-73,170, pp. 895-917, May 1976.

4. Shirley, R. S., "Motion Cues in Man-Vehicle Control," M.I.T., Cambridge, Mass., Sc.D. Thesis, January 1968.

5. Stapleford, R. L., R. A. Peters and F. Alex, "Experiments and a Model for Pilot Dynamics with Visual and Motion Inputs," NASA CR-1325, May 1969.

6. Junker, A. M. and W. H. Levison, "Use of the Optimal Control Model in the Design of Motion Cue Experiments," presented at the Thirteenth Annual Conference on Manual Control, June 15-17, 1977, Mass. Inst. Tech., Cambridge, Mass.

7. Levison, W. H., "The Effects of Display Gain and Signal Bandwidth on Human Controller Remnant," AMRL-TR-70-93, Wright-Patterson AFB, Ohio, March 1971.

8. R. E. Curry, W. C. Hoffman, and L. R. Young, "Pilot Modeling for Manned Simulation," AFFDL-TR-76-124, Volume I, Final Report April 1975 - June 1976, Air Force Flight Dynamics Laboratory, Wright-Patterson AFB, Ohio, December 1976.

9. Peters, R. A., "Dynamics of the Vestibular System and Their Relation to Motion Perception, Spatial Disorientation, and Illusions," NASA CR-1309, April 1969.

N79-17513

D38

MANUAL CONTROL OF YAW MOTION WITH COMBINED VISUAL AND VESTIBULAR CUES *

Greg L. Zacharias and Laurence R. Young

Man Vehicle Laboratory
Department of Aeronautics and Astronautics
Massachusetts Institute of Technology

ABSTRACT

Measurements are made of manual control performance in the closed-loop task of nulling perceived self-rotation velocity about an earth-vertical axis. Self-velocity estimation was modelled as a function of the simultaneous presentation of vestibular and peripheral visual field motion cues. Based on measured low-frequency operator behavior in three visual field environments, a parallel channel linear model is proposed which has separate visual and vestibular pathways summing in a complementary manner. A correction to the frequency responses is provided by a separate measurement of manual control performance in an analogous visual pursuit nulling task. The resulting dual-input describing function for motion perception dependence on combined cue presentation supports the complementary model, in which vestibular cues dominate sensation at frequencies above 0.05 Hz. The describing function model is extended by the proposal of a non-linear cue conflict model, in which cue weighting depends on the level of agreement between visual and vestibular cues.

*Research supported in part by NASA Grant NSG 2032. GLZ supported by an NIH National Research Service Award.

1.0 Introduction

Considerable attention has been directed toward the problem of understanding how our sense of self-motion is determined by the sensory cues available to us. The concentration on vestibular sensation has met with a fair degree of success in developing descriptive models which predict sensation as a function of actual motion. Efforts directed at determining how motion cues in the peripheral visual field affect sensation have emphasized the qualitative aspects of the cues which best elicit motion illusions, although some work has also been directed toward explaining the dynamics of such illusions. A natural extension of both visual and vestibular studies is understanding response to simultaneous cue presentation; the research reported here is directed toward that goal.

Neurophysiological studies (1,2,3,4,5) of combined visual-vestibular cue presentation point to a mixing of the two sensory modalities at the level of the vestibular nucleus, in a manner which is consistent with normal head motion in an inertially fixed visual field environment. That is, a unit which responds in an excitatory manner to right head motions responds similarly to left visual field motions, although the response dynamics are clearly different in the two cases. In the dark, a step in angular velocity of the head results in a rapid rise in firing rate followed by a nearly exponential decay, characteristic of semicircular canal transduction. In contrast, a step in visual field velocity results, after a delay, in a slow rise to a new steady state firing rate, a rate which is held for as long as the visual stimulus continues. The implication, of course, is that the visual motion cue provides DC velocity information to augment the AC transduction characteristics of the canals, thereby producing a wide-band motion sensation system.

Psychophysical studies (6,7,8,9) show sensation to roughly parallel unit behavior in response to separate and combined cue presentations. Specifically, a circularvection (CV) illusion can be generated in a subject when he is seated upright and presented with a peripheral visual field which rotates at a constant velocity about an earth vertical axis. Even though he is motionless, the subject eventually feels himself rotating at constant velocity and perceives the field to be fixed in space. The differential velocity transfer takes about 10 seconds (6). Since the response time is so long, when compared with visual motion detection times which must be orders of magnitude smaller, one is tempted to implicate the canal dynamics in the sensory processing. How this is to be done is not clear at present, although the framework of the "conflict model" proposed by Young (10) appears to be a logical starting point for a functional modelling effort.

2.0 Background

There have been several qualitative studies and a few quantitative attempts to measure the interaction dynamics of sensation in response to combined cue presentation. In one study (9), velocity and acceleration detection indications were made by subjects in response to earth-vertical yaw-axis rotational cues. These consisted of angular acceleration pulses in conjunction with the presentation of a visual field moving at a constant angular velocity with respect to the subject. A pulse was considered confirming when it was in the direction of the induced circularvection and conflicting when in the opposite direction. The study showed the following. First, subjective velocity was found to be biased in the direction of the induced CV, but not to the extent of a simple summation of CV and expected vestibular response. Second, detection of a confirming pulse generally led to a moderate increase in subjective velocity, whereas a conflicting pulse, if detected, resulted in a marked decrease.

A similar study conducted by Berthoz et al (11) combined linear fore-aft acceleration pulses with linear visual field motion. They found qualitatively the same subjective dependence on dual cue presentation: a slow rise in sensation when only visual cues were presented, and a subjective velocity bias due to constant field velocity. Vestibular pulse detection performance was also similar, the study showing detection to be degraded during linearvection.

It is appropriate to note that both of the above studies used a constant velocity visual field and thus were unable to provide a closer look at visual channel response dynamics. In effect, what was studied was the "vestibular" transfer function, and its dependence on visual motion cues.

The objective of the research reported here is to develop a simplified functional model of motion sensation dependence on combined visual and motion cues, thus directly extending the results of the work just described. The study is restricted to yaw-axis motion about an earth-vertical in order to take advantage of past work on this type of motion, and to avoid possible complications of otolith involvement in subjective response.

3.0 General Experimental Approach

To avoid the possible pitfalls of using subjective magnitude estimation (12) to measure motion sensation, a compensatory tracking task was devised to give a subject control over his own (sensed) velocity, with a task objective of keeping himself (apparently) fixed in space. Visual and vestibular motion cues were given to the subject, and his compensatory behavior used to infer his perception of self-motion. Such an approach avoids magnitude estimation as such, since the subject's objective is one of simply matching sensation with the sensation of sitting still.

This approach has its own drawback, however, since the tracking dynamics of the human operator are imbedded in the results. To provide an operator correction, an initial experiment determined the operator describing function, under conditions functionally similar to those used in the motion sensation experiments. This is described immediately below, following which will be discussed the results of two experiments aimed directly at developing a dual-input functional model of motion sensation.

4.0 Human Operator Dynamics

4.1 Experimental Design

Operator behavior was measured in nulling the velocity of a projected stripe pattern on the translucent front window of a small aircraft trainer. The pattern consisted of alternating black and white vertical stripes, subtending 12° each and filling approximately 60° of the subject's frontal visual field. This arrangement minimized the possibility of circularvection (6); further, the trainer remained stationary throughout the task, and the subject was informed of this prior to the experiment. No sensation of self-motion arose, as indicated by post-test questioning of the subjects.

Figure 1 is a block diagram of the nulling task, with the subject represented (within the dashed line) as a linear operator with remnant. It is presumed that the subject generates an internal estimate of visual field velocity, through an accurate estimator which is fast with respect to the motion sensation dynamics we are trying to investigate; hence the unity gain. A negative feedback structure for the subject is also presumed, with the velocity estimate subtracted from the task objective to generate an error signal for control action.

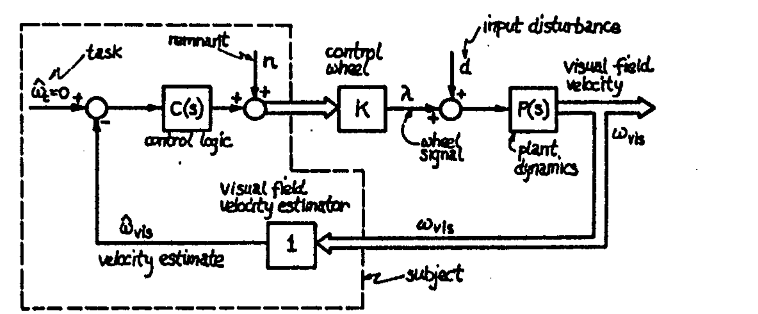

Figure 1: Visual Field Velocity Nulling Task

The subject controls field velocity via a wheel mounted horizontally in front of him; the wheel has no mechanical centering cues and is effectively featureless, providing neither visual nor tactile cues as to true center. Full deflection results in maximum field speed of $20^{o}/s$, in the direction of wheel rotation. As shown in the figure, the wheel signal is added to a loop disturbance signal, against which the subject must provide compensatory control. The disturbance is a pseudo-random zero mean signal with a period of 128 seconds, consisting of a sum of 13 sinusoids spanning the frequency range from 0.01 to 1.0 Hz. The disturbance line spectrum follows that of a double lag-lead with a roll-off at 0.15 Hz, dropping 20 dB to level off at 0.48 Hz. The combined wheel and disturbance signal are then passed through simulated plant dynamics, given by:

$$P(s) = \omega_n/[s^2 + 2\zeta_n\omega_n s + \omega_n^2] \qquad (\omega_n, \zeta_n) = (5.65, 0.7) \qquad [1]$$

The output of this filter is then used to command a servo-driven projection system responsible for generating the front window moving stripe pattern.

4.2 Results

Six subjects attempted to maintain zero field velocity for two full presentations of the disturbance signal. Fast Fourier Transforms (FFTs) were performed on the wheel deflection and field velocity histories, and gain and phase were computed according to:

$$[\lambda(s)/\omega(s)]\big|_{s=j2\pi f_i} \qquad [2]$$

where the f_i are the frequencies contained in the disturbance d. Figure 2 shows the six subject average Bode plots, with one-sigma deviations indicated by error bars. Also shown is a least-squares fit, to the gain data, of the following function

$$C(s) = \frac{K_c}{s}(\tau_c s + 1)e^{-\tau_d s} \qquad K_c = 1.80\ s^{-1},\ \tau_c = 0.45\ s,\ \tau_d = 0.41\ s \qquad [3]$$

The dead-time τ_d was calculated from a least squares fit to the phase residuals based on the gain fit. Remnant corrections to the data were calculated according to the method suggested by Shirley (13), but were not found to significantly change the parameter values of the subsequently fitted transfer function. Although the fit could certainly be improved by the choice of a higher order transfer function, the simplified operator model of [3] is adequate for the purpose of the analysis to follow.

5.0 Visual Cues and Low Frequency Sensation

Our initial objective was to verify the hypothesis of frequency separation during sensory processing of simultaneous visual and vestibular motion cues. Specifically, we wished to demonstrate how low-frequency visual cues dominate low-frequency sensations, and how they can be used to augment the AC vestibular transduction characteristics of the vestibular system.

Figure 2: Operator Describing Function for Visual Pursuit Task

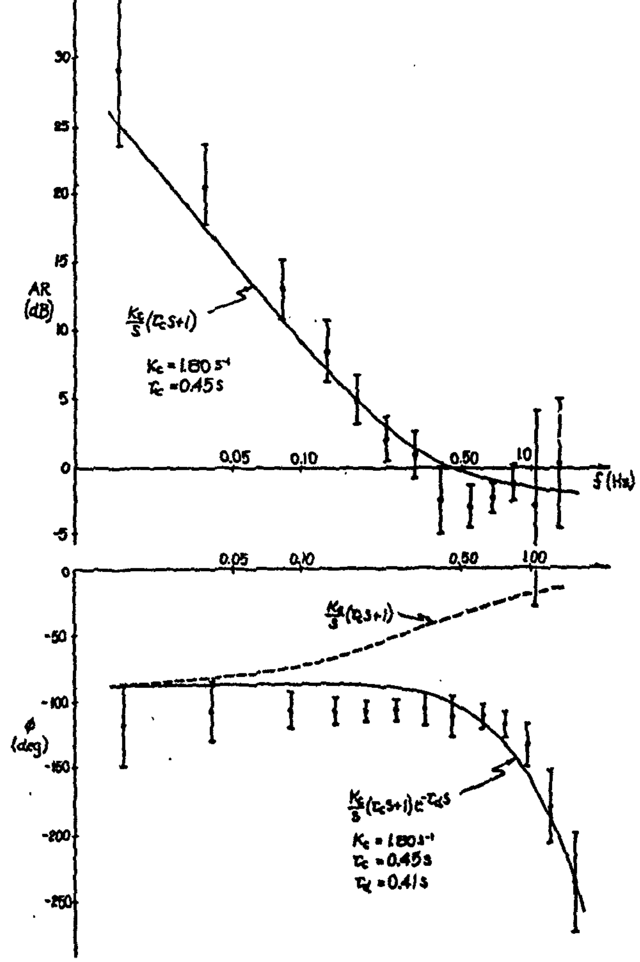

5.1 Experimental Design

Motion sensation was measured by giving the subject the task of nulling his own sense of self-motion, and effected by providing him with active control over his actual velocity, while seated in a LINK GAT-1 small aircraft trainer, modified for use as a simple velocity servo in yaw. Figure 3 is a block diagram of the experiment with the same type of schematic representation of the subject used earlier. The model proposes that the subject processes both visual and vestibular cues to arrive at an estimate of self-velocity, which, in turn, is used as a basis for providing compensatory wheel deflections. The wheel signal is combined with the same type of disturbance signal used in the previous experiment (pseudo-random, zero mean), although for this experiment a shelf spectrum is used to define the sinusoid amplitudes, with a corner frequency of 0.25 Hz and a 20 dB gain drop from high to low frequencies. This pseudo-random disturbance requires the subject to provide continuous compensation throughout a run. The combined wheel and disturbance signal then commands the trainer, used simply as a velocity servo in yaw and having the same second-order dynamics which were simulated in the previous experiment (P(s) defined by [1]).

The front window of the trainer is made opaque and the two translucent side windows are used for presenting the vertical stripe pattern to the subject's peripheral field. Field velocity can be directly controlled, since the projection system is mounted on the trainer. The optics are arranged so that as the pattern moves forward on one side window, it moves aft on the other, mimicking the rotational movement one would see inside a cylindrical drum.

The figure indicates a switch for presenting the subject with three types of visual field motion. In the CTR position, a tachometer feedback from the trainer counterrotates the visual field with respect to the trainer, providing moving-base isolation for the field. The subject sees the field as effectively fixed in space, and thus this mode mimics the everyday correspondence between visual and vestibular cues. In the FIX position, the field is fixed with respect to the trainer, depriving the subject of any visual motion cues. Finally, in the CV position, the field is driven at constant velocity with respect to the trainer, 4°/s to the right; this would normally induce a left CV sensation in a motionless subject.

5.2 Experimental Protocol

Six subjects participated in the experiment. All were in normal health with normal peripheral vision, and had no known vestibular dysfunction. Each subject was specifically told to keep the trainer as motionless as possible, by concentrating on his own sensation of motion and providing the appropriate compensatory wheel deflections. Each subject was then given a practice session of two minutes, under counterrotating field conditions. Headphones were used to mask auditory cues, and a head rest provided head stabilization with respect to the trainer. Subjects were instructed to look forward, but not to the extent of fixing their gaze on a specific point.

Figure 3: Closed-loop Velocity Nulling Task (Single Disturbance Input).

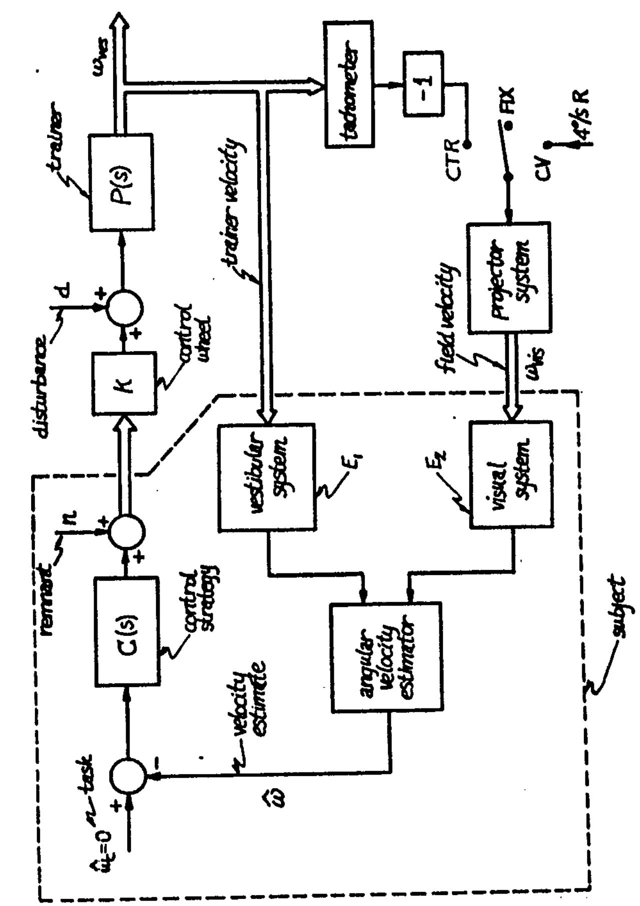

A typical run lasted for approximately 12 minutes, during which time the subject was required to provide continuous velocity-nulling compensation. During this period, each of the three visual field conditions (CTR, FIX and CV) was repeatedly presented to the subject in random order, the start of each presentation synchronized with the start of a new period of the disturbance signal ($T = 128$ s). Each field presentation lasted for 128 seconds, unless stick saturation necessitated early termination of the stimulus.

5.3 Results

Figure 4 shows one subject's strip chart recording of the disturbance signal and three trainer velocity histories, one for each visual field presentation type. Under counterrotating field conditions (CTR), the mean trainer velocity was maintained near zero by all subjects, with an RMS error, for the population of $1.34^{\circ}/s$. Under fixed field conditions (FIX), subjects drifted away from zero, either left or right, at a constant steady acceleration ($\bar{\alpha} = 0.011^{\circ}/s^2$; $\sigma_{\alpha} = 0.050^{\circ}/s^2$) (typical vestibular thresholds to yaw rotation are 0.1 to $0.2^{\circ}/s^2$). Over the population, the mean rate is not significantly different from zero, indicating a left-right balance in the population. With a constant velocity field presentation (CV), all subjects accelerated to the right, at a rate ($\bar{\alpha} = 0.29^{\circ}/s^2$, $\sigma_{\alpha} = 0.21^{\circ}/s^2$) significantly larger than that seen in the FIX presentations ($p < 0.005$). It should be noted that in all of the field presentations, the subjects felt that they were maintaining themselves at zero mean velocity, in spite of the suprathreshold accelerations they sometimes subjected themselves to.

5.4 Low Frequency Response

Some additional points regarding the field effects on motion are worth noting. With a counterrotating field, the subject successfully performs the task, as expected. This is the "normal" cue situation, in which visual and vestibular cues complement one another, and presumably provide an accurate velocity estimate. With a fixed field, one might be tempted to explain the observed drift as simply subthreshold acceleration; however, the fact that a subject's mean acceleration remains constant argues against this, since, presumably, any subthreshold acceleration profile would be just as likely. A more promising candidate to explain the observed drift is a vestibular "bias". Finally, with a constant velocity field, all subjects chase the field to the right, suggesting that the circularvection illusion is influencing the subject into thinking he is moving to the left, and leading him to provide inappropriate rightward compensation. Presumably, the left CV illusion and right vestibular acceleration cancel each other out, on the average.

Figure 4: Trainer Velocity Drift as a Function of Visual Field Type

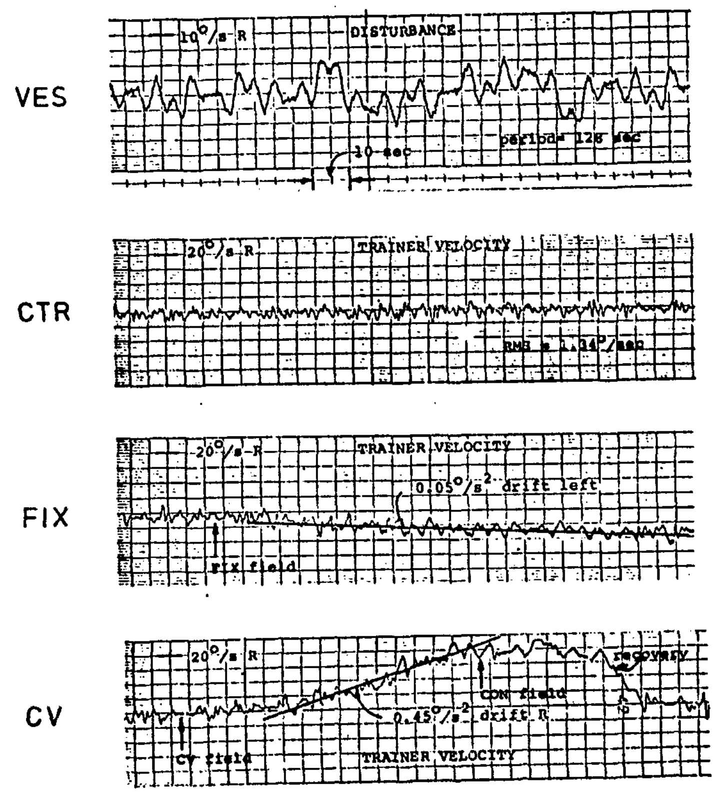

ORIGINAL PAGE IS OF POOR QUALITY

5.5 Low Frequency Response Model

A simple estimator model consistent with the experimental findings is illustrated in Figure 5. The vestibular path is based on the familiar cyclopean torsion pendulum model (14) with slow and fast time constants τ_1 and τ_2 respectively. The long vestibular adaptation time constant is ignored. Provision is made for a biased output ω_b, which is assumed constant in the analysis following. The visual path is modelled as a linear filter of unspecified dynamics, having a unity DC gain.

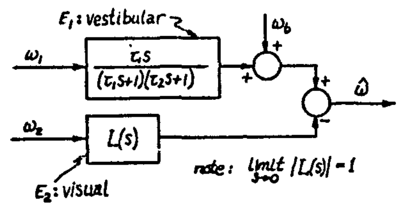

Figure 5: Dual-Input Velocity Estimator (LF)

Under fixed field conditions (FIX), the model predicts a constant average trainer acceleration in the nulling task. To illustrate this, the estimator above may be combined with the loop diagram of Figure 3. Block diagram manipulation then yields the following expression for trainer velocity as a function of bias, disturbance, and remnant:

$$\omega_1(s) = \frac{P}{1 + PCE_1}(-C\omega_b + d + n) \qquad [4]$$

assuming unity control wheel gain. Since we are interested in low-frequency behavior, we recall, from [1], that the plant P has unity DC gain; that, from [3], the control strategy C behaves as an integrator (K_c/s); and that, from Figure 5, the vestibular estimator E_1 behaves as a differentiator ($\tau_1 s$). In terms of DC signal content, the bias ω_b is modelled as a constant (ω_b/s). Further, since the disturbance d is zero mean and the remnant n is assumed to contain no DC power, neither of these loop inputs contributes to low frequency response. The model thus predicts, from [4], a ramp in trainer velocity:

$$\lim_{s\to 0} \omega_1(s) = \lim_{s\to 0} -\kappa(\omega_b/s^2) \qquad [5]$$

where we have defined the loop gain κ to be

$$\kappa \equiv K_c/(1 + K_c\tau_1) \qquad [6]$$

In other words, the model predicts a steady trainer acceleration under FIX conditions, α_{FIX}, given by

$$\alpha_{FIX} = -\kappa\omega_b \qquad [7a]$$

A similar derivation may be used to show that, under constant velocity field conditions (CV), the model again predicts a steady trainer acceleration:

$$\alpha_{CV} = \alpha_{FIX} + \kappa\omega_{VIS} \qquad [7b]$$

Finally, under counterrotating field conditions (CTR), the model predicts no steady trainer acceleration; instead, a trainer velocity bias, equal and opposite to the subject's vestibular bias, is predicted:

$$\omega_{CTR} = -\omega_b \qquad [7c]$$

Although these results qualitatively agree with the observed behavior, it is of interest to consider some quantitative aspects of the model's predictions.

Clearly the gain factor κ varies among individuals, but a rough estimate can be obtained from [7b] by using the mean drift rates observed under FIX and CV conditions (in section 5.3), and using the fact that the CV field speed was 4°/s:

$$\kappa \approx 0.073\ s^{-1} \qquad [8]$$

Assuming κ is constant across the population and using the observed FIX drift rate statistics (section 5.3), we can then use [7a] to calculate the model's vestibular bias statistics:

$$\bar{\omega}_b = 0 \qquad \sigma_{\omega_b} = 0.68°/s \qquad [9]$$

It should be recognized that a subject with a three-sigma bias still perceives himself stationary in space, during the nulling task, since his steady state self-velocity estimate is given by

$$\hat{\omega}_{ss} = (\kappa/K_c)\omega_b = (\kappa/K_c)(3\sigma_{\omega_b}) \approx 0.08°/s \qquad [10]$$

where we have used the value of K_c given in [3].

In summary, when the subject is deprived of visual motion cues, and feels himself stationary, the model ascribes the observed constant trainer acceleration to a bilateral vestibular bias, a bias not inconsistent with the notion of a left-right canal imbalance (14). Under counterrotating field conditions, this bias model also predicts, from [7c] and [9], one-sigma trainer velocity offsets of less than 1°/s, entirely consistent with the observed behavior.

The model also allows us to estimate the "slow" vestibular time constant τ_1. From the definition of κ given in [6], its computed value in [8], and the value of K_c in [3], we find

$$\tau_1 \simeq 13.1 \text{ s} \qquad [11]$$

The agreement between this computed value and the 10 to 15 second range found by other researchers (15) lends additional support to this dual-channel model.

6.0 Combined Cues and Dynamic Motion Sensation

To look more closely at what is essentially a dynamic dual-input problem, a third experiment was performed to see if the above parallel channel model could be extended to account for the subject's dynamic behavior. The approach chosen was to work with two describing functions: one relating trainer motion to wheel deflection and the other relating visual field motion to wheel deflection.

6.1 Experimental Design

The same velocity nulling task as in the second experiment was given the subject: that is, to keep himself fixed in space. Instead of having him control only trainer velocity, however, he was also given control of field velocity. This allowed him to null either vestibularly-induced or visually-induced motion sensations by using the control wheel appropriately. Disturbance signals were injected into both the trainer and projector drives, requiring constant compensation. By choosing the disturbance signals to be uncorrelated, simultaneous nulling of both cues becomes an impossible task objective. Clearly, the resulting analysis will be based on whichever portion of which cue the subject chooses to null.

Figure 6 is a functional block diagram of the experiment, with the same type of schematic model of the human operator introduced earlier. Trainer velocity is as in the previous experiment. Field velocity, however, is determined by both wheel deflection and the second disturbance input. It should be noted that the sign of the wheel signal is changed prior to being sent to the projector drive, to make the resulting visual field motion consistent with trainer motion (i.e. right wheel deflection results in right trainer motion and left field motion). To ensure that the visual field dynamics mimic trainer response, a prefilter was added to the projector drive (which has a relatively high bandwidth), so that, as shown on the figure, FG = P. Thus, without a visual field disturbance signal, the experiment would be functionally equivalent to the counterrotating series conducted earlier.

6.2 Identification Method

It is appropriate to consider how an estimator model can be derived from

Figure 6: Closed Loop Velocity Nulling Task (Dual Disturbance Input)

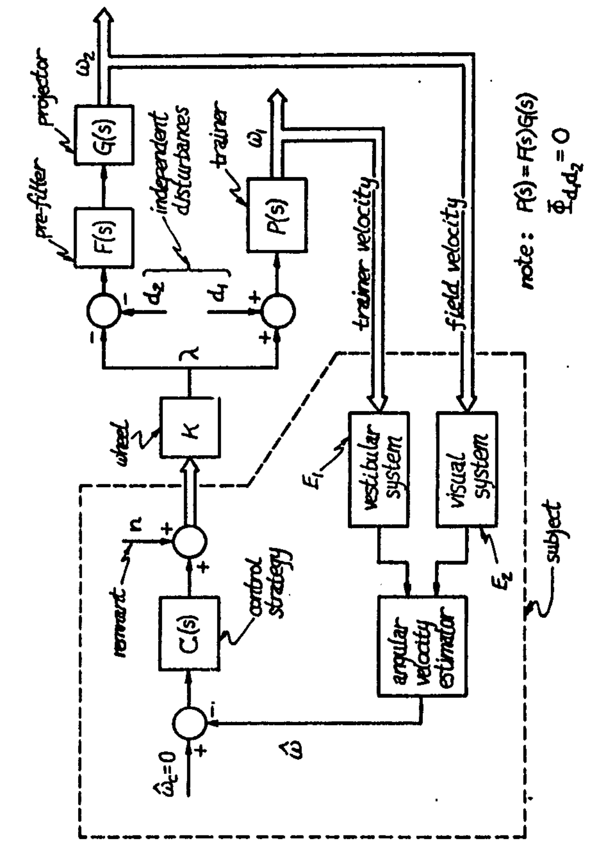

ORIGINAL PAGE IS
OF POOR QUALITY

the results of this experiment. We assume that the velocity estimate is a linear function of the two cues, but presume no particular channel dynamics:

$$\hat{\omega} = E_1(s)\omega_1 + E_2(s)\omega_2 \qquad [12]$$

where ω_1 is the trainer velocity, and ω_2 is the visual field velocity with respect to the trainer (and subject). If we define the remnant (n) to be uncorrelated with the input disturbances,

$$\Phi_{nd_1} = \Phi_{nd_2} = 0 \qquad [13]$$

and choose the disturbances to be uncorrelated:

$$\Phi_{d_1d_2} = \Phi_{d_2d_1} = 0 \qquad [14]$$

then, block diagram calculation using Figure 6 shows that:

$$\Phi_{\lambda d_1}/\Phi_{\omega_1 d_1} = -CE_1/(1 + PCE_2) \qquad [15a]$$

$$\Phi_{\lambda d_2}/\Phi_{\omega_2 d_2} = CE_2/(1 + PCE_1) \qquad [15b]$$

Since the left-hand side is computable from experimentally measured variables, we define

$$\alpha_1 \equiv \Phi_{\lambda d_1}/\Phi_{\omega_1 d_1} \qquad \alpha_2 \equiv \Phi_{\lambda d_2}/\Phi_{\omega_2 d_2} \qquad [16]$$

so that one can compute the operator transfer functions:

$$CE_1 = \alpha_1(1 + P\alpha_2)/[1 + P^2\alpha_1\alpha_2] \qquad [17a]$$

$$CE_2 = \alpha_2(1 - P\alpha_1)/[1 + P^2\alpha_1\alpha_2] \qquad [17b]$$

As expected, the control strategy C is inseparable from the estimator transfer functions, E_1 and E_2.

Rather than work with cross-power spectral densities, it was found computationally more convenient to use conventional input-output calculations based on Fourier transforms of the signals themselves. Thus, if f_{ij} is a frequency contained in the loop disturbance d_i, then the α_i are calculated according to

$$\alpha_i(f_{ij}) = \lambda(f_{ij})/\omega_i(f_{ij}) \qquad (i = 1,2)\ (\forall_j) \qquad [18]$$

The direct correspondence with [16] is made possible by the independence of d_1 and d_2, and the assumption of a small remnant contribution at the disturbance frequencies. Since [17] requires that α_1 and α_2 be defined at the same set of frequencies, linear interpolation in the frequency domain is used to generate additional values of the α_i; these are then used in [17] to calculate the CE_i.

6.3 Experimental Protocol

Six subjects participated in the experiment. After a familiarization period with the procedure and equipment, each subject performed one continuous run of velocity nulling which lasted for approximately eight minutes. The visual environment alternated between two modes: the counterrotating field mode (CTR) which provides accurate confirmation of vestibular cues, and the dual-input mode (DI) illustrated in Figure 6. Two presentations of each were given, alternating with one another:

Series A: CTR, DI, CTR, DI
Series B: DI, CTR, DI, CTR

Three subjects received series A and three received series B, to provide balance for fatigue and learning.

6.4 Results

After performing FFTs on the histories of the wheel deflection, trainer velocity and field velocity, the operator transfer functions were computed according to [17], at each disturbance frequency. The resulting six-subject gain and phase averages are given in Figure 7, along with smooth curves sketched in to indicate trends with frequency. Several points are worth noting. First, the "vestibular" gain follows what might be expected from a lag-lead, augmented by a lead at high frequencies and a washout at low frequencies. This washout characteristic is entirely consistent with our notion of negligible canal response at low frequencies, and, of course, is consistent with the functional model presented earlier.

The Bode plots defining the visual transfer function, CE_2, show quite contrasting behavior. At low frequencies, the gain is higher than in the vestibular channel, supporting the drift rate findings in which the dominance of a DC visual cue was demonstrated. Up to approximately 0.1 Hz, the visual channel behaves as a simple integrator (in gain and phase), which, as might be surmised from the manual control results, is simply a reflection of the operator's control dynamics. Although the visual gain levels off at about 0.1 Hz, it remains considerably smaller ($\approx$ 10 dB) than the vestibular gain, at frequencies above the gain crossover point ($f \approx 0.02$ Hz). The complementary filter hypothesis thus appears quite attractive.

Four of the subjects participated in both the manual control task and in the current experiment. Thus, for each individual, at each test frequency, the gain and phase data (CE_i) can be adjusted by the gain and phase data

Figure 7: Dual-Input Describing Functions (uncorrected for operator dynamics)

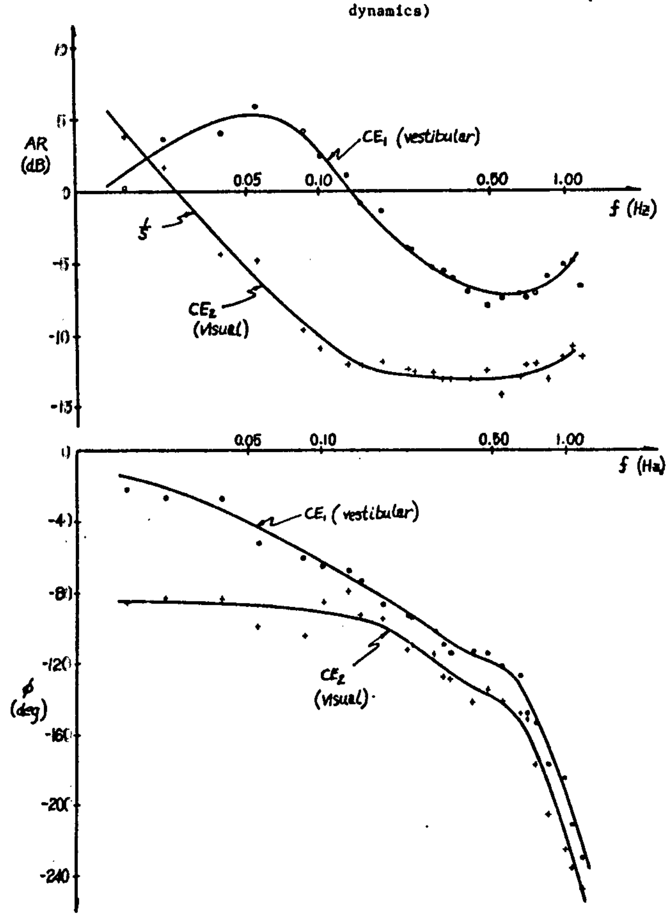

defining that subject's operator dynamics (C), obtained from the manual control experiment. Shown in figures 8a and 8b are the resulting estimator describing function data for E_1 and E_2, obtained by averaging over the four subject population. Also shown are smooth curves associated with two linear transfer functions which provide a least squares fit to the data.

The vestibular channel data (figure 8a) exhibit, at first glance, the AC characteristics we would associate with the canals: both the rapid gain drop and phase lead with decreasing frequency are qualitatively well-modelled by a washout filter. However, the break frequency is quite high: the washout time constant is 0.94 s from the fit, which is an order of magnitude smaller than the 10 s time constant we would expect from the canals (16). The discrepancy is even larger when compared with the 13.1 s value calculated from drift measurements. Finally, it is appropriate to note that we might expect unity gain at the high test frequencies; the data in contrast, is better fit with half that gain.

The visual gain (figure 8b) is a good deal lower than the vestibular gain, over much of the frequency range, with crossover occurring at the very low end ($f \approx 0.02$ Hz). In this region, the gain is approximately constant with frequency, behavior which is qualitatively consistent with the idea of DC visual cue dominance. However, we might expect the DC gain to be approximately unity; certainly not the -25 dB seen in the data. Furthermore, if the visual channel were to be truly complementary to the vestibular channel, we would expect a roll-off near 0.1 Hz. Just the opposite occurs, however.

These results suggest a reevaluation of a linear dual channel model for cue mixing.

7.0 Non-Linear Dual Channel Model

The obvious means of resolving the apparent inconsistencies just described is to propose that simultaneous cue presentation involves a mixing of the two cues at different frequencies: that is, allowing a vestibular cue at one frequency to affect a visual cue at another, and vice versa. A non-linear model is clearly called for, and a reasonable foundation on which to build has already been provided by the "conflict model" hypothesis (10), which proposes that each cue be weighted according to the perceived conflict between them. (The notion of a switching mechanism between visual and vestibular influences on vestibular unit activity was also discussed by Waespe and Henn (4)).

One implementation of this hypothesis is shown in figure 9a, in which the visual and vestibular cues are weighted in a complementary fashion according to the gain K. This gain is dependent on a measure of cue conflict, ω_{err}, which, in turn, is derived directly from the two cues. The vestibular sensory dynamics are approximated by the low frequency portion of the torsion pendulum model. No visual sensory dynamics are modelled, for two reasons: the lack of experimental data for single channel visual cue response, and the known relatively wide-band motion detection response of the visual system.

Figure 8a: Dual-Input Describing Function: Vestibular Channel

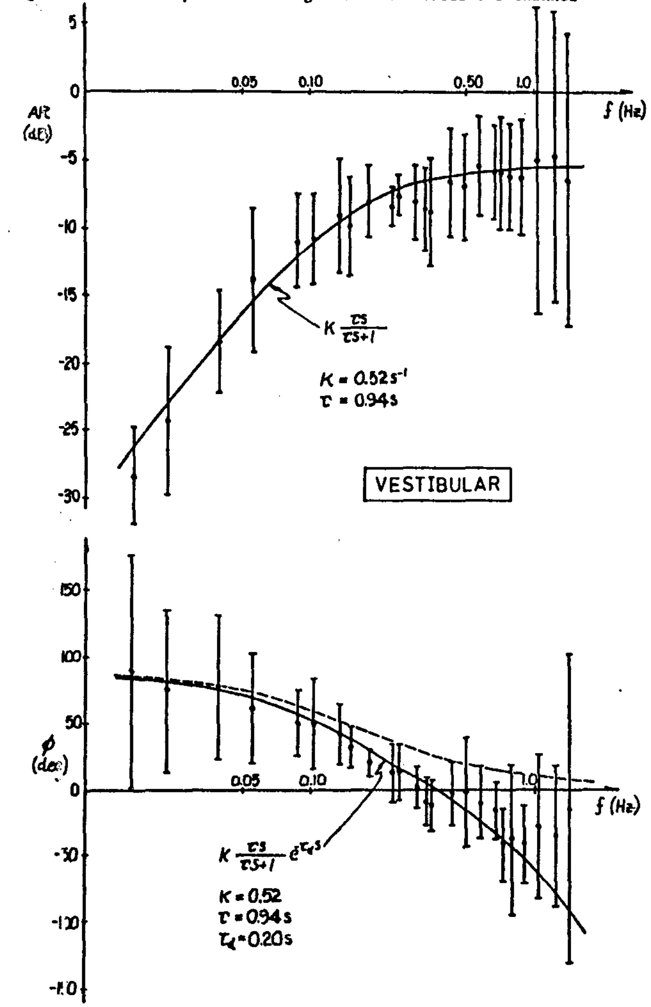

Figure 8b: Dual-Input Describing Function: Visual Channel

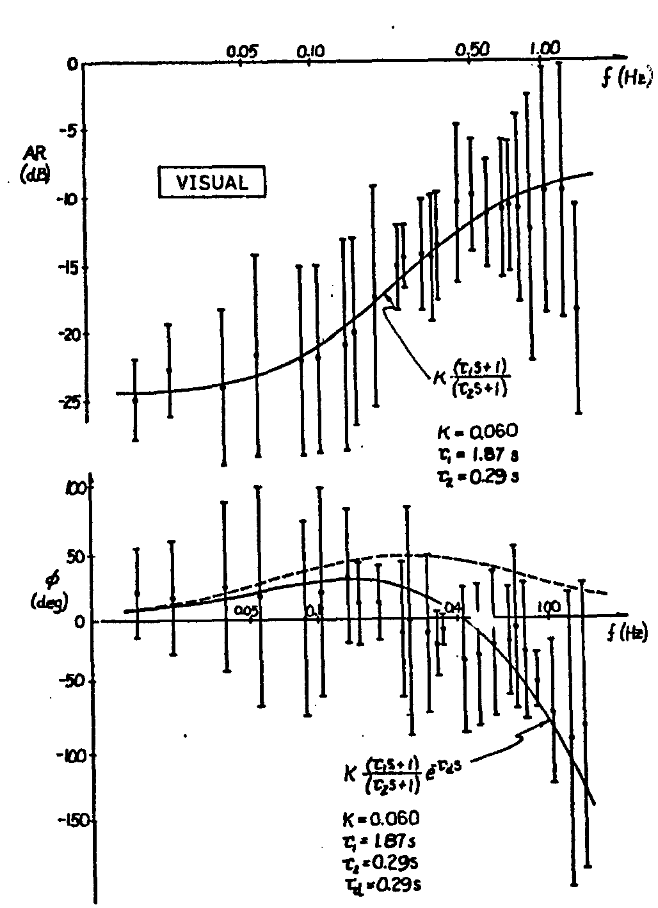

ORIGINAL PAGE IS
OF POOR QUALITY

Figure 9a: Dual input conflict model

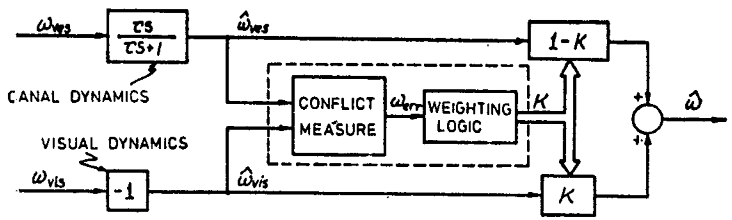

Figure 9b: Conflict measure and weighting function

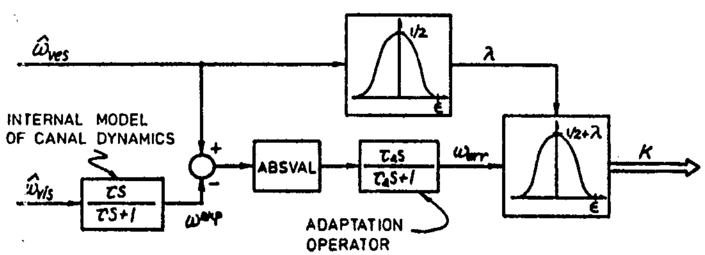

ORIGINAL PAGE IS OF POOR QUALITY

A simple conflict measure can be motivated by considering, for example, self-motion in an inertially-fixed visual field environment. Although this is clearly a zero conflict situation, a direct comparison of the two cues would lead to a discrepancy, because of the differences in the dynamic response of the two sensory channels. One is thus led to propose an internal model of canal dynamics, through which the visual information can be passed to provide a predicted vestibular response, which can then be compared with the actual vestibular signal. Effectively, then, conflict would be based on high frequency cue content.

A weighting schema can then be proposed fairly directly. Since the conflict signal is a measure of high frequency agreement, and the vestibular system provides "reliable" information at high frequency, then it would seem reasonable to heavily weight this information whenever a high conflict situation is detected. The converse might be proposed with low conflict: heavily weight the visual cue. However, this approach is only reasonable at low frequencies, when we know the vestibular channel will be providing a null signal. At high frequencies, this weighting discards confirming vestibular information which clearly could be used to improve the velocity estimate. With no apriori knowledge of each channel's noise characteristics, an estimate can be obtained by simply averaging the cues. Thus, in a low conflict situation, we propose cue averaging, unless we have a zero vestibular signal, in which case we heavily weight the visual cue.

An implementation of this type of conflict measure and weighting schema is shown in Figure 9b. The visual cue is high-passed through an internal model of the vestibular dynamics to generate an expected vestibular signal ω^{exp} which is then differenced with the actual vestibular signal and passed through a rectifier. To allow for a long term resolution of steady state conflict, an adaptation operator acts on the rectified signal to generate the actual conflict signal, ω_{err}.

The symmetric weighting function is implemented with a cosine bell. As illustrated, a large conflict signal drives the visual path gain to zero, whereas a small one drives it to a peak weighting value which varies between 1/2 and 1, depending on the amplitude of the vestibular signal (and implemented via an additional bell function). Thus, in a low conflict situation, the cues can either be averaged or the visual cue passed straight through, depending on whether or not the vestibular signal is large or small, respectively.

7.1 Dynamic Behavior of the Nonlinear Model

The non-linear model was simulated on a digital computer, to evaluate predicted response as a function of cue presentation. The results presented here are preliminary, in that no exhaustive parameter searches have been conducted to provide a best fit to the data; however, the trends predicted by the model deserve some comment as they may motivate a closer look at the details of future model implementation.

Three parameters determine model behavior. For the simulations, the vestibular time constant, τ, was assigned the 13.1 s value found from the CV drift rate of section 5.5. The *adaptation time constant* τ_a was chosen to be 10 s, which is the order of magnitude of the acceleration latencies observed when subjects were presented with a constant velocity field rotation. The presumption here is that the latency is due, in part, to the unresolved conflict between the subject's CV illusion (left) and his sensed acceleration (right), a conflict which must eventually be washed out by the adaptation operator. Finally, the velocity magnitude measure, ϵ, was chosen to equal the Meulder product (16) of $2.5^{o}/s$, the presumption being conflict detection may be characterized by the same type of threshold behavior associated with vestibular pulse detection.

7.2 Time Response

Shown in Figures 10a through d are time histories of the model's response to simple visual and vestibular cues. Figure 10a is the model's prediction of subjective response to a 5 °/s step in angular velocity, with a subject-fixed visual field. Although the response appears to be characterized by two exponentials, only the first portion *is* truly exponential, and is due to the fact that the canals provide the only information during the initial high conflict phase. As the conflict decreases with time, the null visual signal is weighted more heavily, and the response thus decays more rapidly. A similar double branch decay, following a velocity step, is seen in the velocity of slow phase nystagmus (V. Henn, personal communication). Figure 10b shows model response to a left 4°/s step in visual field velocity, in the absence of confirming vestibular cues. Again, because of the initially high conflict level, the null vestibular cue is the basis for sensation resulting in the response latency seen . As the expected vestibular signal drops to zero and matches the actual null signal from the canals, the conflict lessens and the weighting on the visual cue increases to unity (the undershoot is caused by the adaptation operator acting on the conflict signal, temporarily increasing the conflict level).

Figure 10c shows the model response to confirming visual and vestibular velocity steps (CTR presentation). Since this is a zero conflict situation, the initially large vestibular signal dictates that both cues be averaged, which results in a sensation drop-off due to the decaying canal response. As the vestibular signal grows smaller, however, the weighting emphasizes the DC visual cue, bringing the subjective response back to the true velocity level. Figure 10d shows model response to a constant field velocity of 4°/s combined with a constant body acceleration of $0.3°/s^2$, both to the right. The initial response is due to the vestibular path, but is turned around as the oppositely-directed circularvection illusion takes hold. The conflict gradually decreases, because of the adaptation operator, but the vestibular signal remains at a constant level ($\tau a = 4^{o}/s$), so that, in the steady state, both cues are averaged. The net result is approximately zero sensation, and agrees with what is observed experimentally, under CV visual field conditions (recall section 5.3).

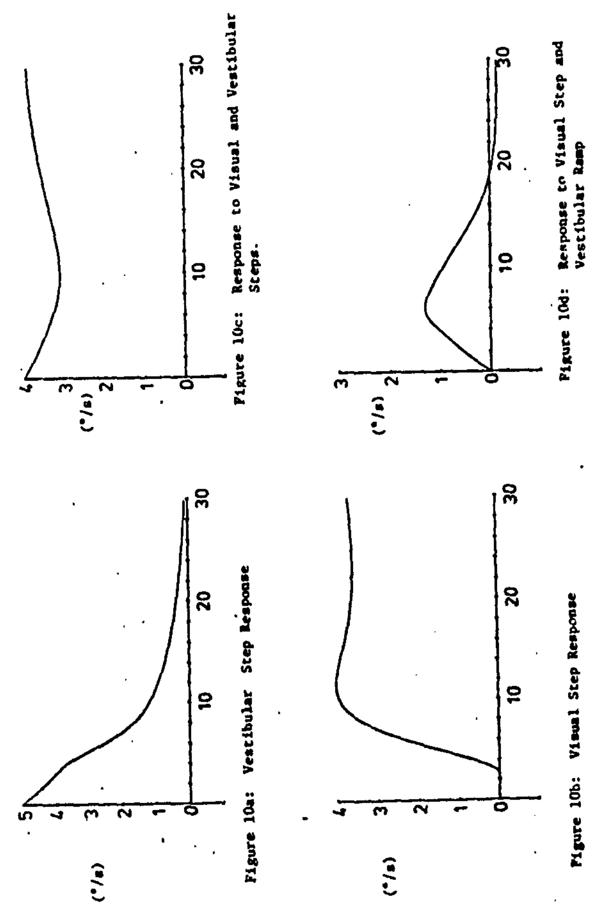

Figure 10a: Vestibular Step Response

Figure 10b: Visual Step Response

Figure 10c: Response to Visual and Vestibular Steps.

Figure 10d: Response to Visual Step and Vestibular Ramp

7.3 Frequency Response

Although the model appears to provide reasonable predictions of subjective response to simple cue presentations, of perhaps greater interest is its ability to fit the apparently inconsistent data obtained from the dual input nulling task. A digital simulation of the DI experiment was conducted using the same plant dynamics and loop disturbances as in the experiment. The subject was simulated as shown schematically in Figure 6, using the control strategy of [3] and the non-linear estimator of Figure 9. The simulation ran for one period of the disturbance signal and the simulated, trainer, visual field, and wheel histories were processed with the same software used for the experimental data analysis.

Repeated in figure 11 are the visual and vestibular gain plots obtained from the experiment; the superimposed open circles are the gains for the simulated non-linear estimators. A comparison with the earlier linear system fit makes it clear that the non-linear model does a poorer job of fitting the experimental data; however, since the linear model is untenable due to our previous considerations, this only suggests that there is room for improvement in the non-linear estimator. As it stands, however, the major data trends are reasonably well-followed by the model. In particular, the 13.1 s vestibular time constant is transformed to an effective one-second time constant by the conflicting visual cues. Similarly, conflicting vestibular cues effectively drop the unity gain of the visual channel by 25 dB, at low frequencies; at higher frequencies, the conflict lessens because of the decreased magnitudes of the loop disturbances, and the visual gain rises. The gain rise thus no longer needs to be attributed to high frequency visual lead, a dynamic characteristic inconsistent with our knowledge of circularvection response. Thus, the non-linear model provides a means of fitting the dual input results, while allowing for consistency with single stimulus experiments.

8.0 Summary

This study has confirmed the notion that we estimate self-motion by combining complementary visual and motion cues: low frequency visual cues are used to augment high frequency vestibular cues to effect a wide-band sensory system. Although a linear complementary filter provides an adequate functional description of low frequency behavior, the dual-input experiment reported on here shows that the assumption of linearity leads to model predictions which are inconsistent with the results of single cue experiments. The non-linear model proposed here circumvents these apparent inconsistencies by recognizing that cue conflict provides a means by which the two cues can be selectively weighted to arrive at a "best" estimate of self-motion.

Figure 11: DI experimental data compared with simulated conflict model response

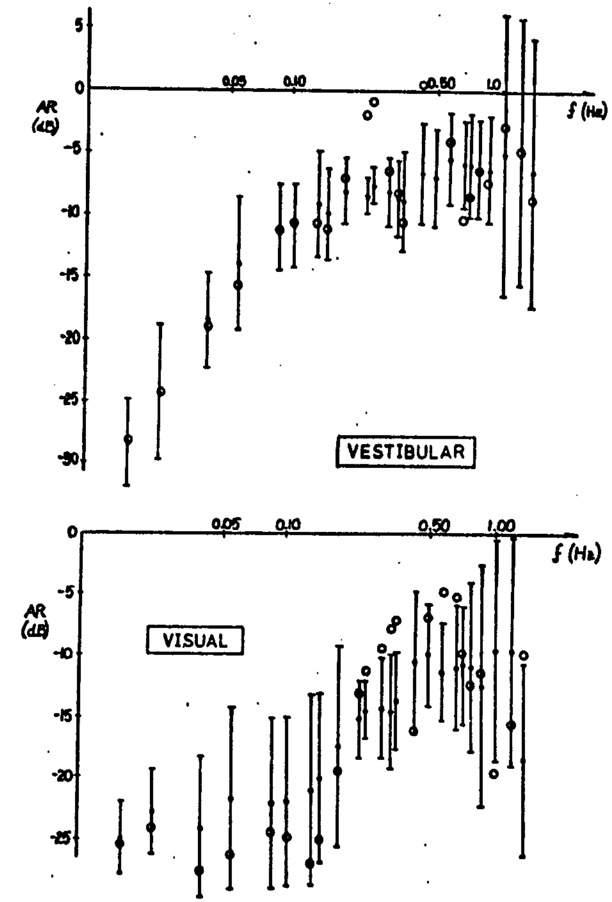

REFERENCES

1. Henn, V., Young, L.R., Finley, C. "Vestibular nuclear units in alert monkeys are also influenced by moving visual fields", Brain Research 71:144-9, 1974.

2. Dichgans, J., Schmidt, C.L., Graf, W. "Visual input improves the speedometer function of the vestibular nuclei in the goldfish", Exp Brain Research 18:319-322, 1973.

3. Allum, J.H.J., Graf, W., Dichgans, J., Schmidt, C.L. "Visual-vestibular interactions in the vestibular nuclei of the goldfish", Exp Brain Research 26:463-485, 1976.

4. Waespe, W., Henn, V. "Neuronal activity in the vestibular nuclei of the alert monkey during vestibular and optokinetic stimulation", Exp Brain Research 27:523-538, 1977.

5. Daunton, N.G. and Thomsen, D.D. "Otolith-*visual interactions in single* units of cat vestibular nuclei. Neuroscience Abstracts, Volume II, part 2, p. 1057, 1976.

6. Brandt, Th., Dichgans, J., Koenig, E. "Differential effects of central versus peripheral vision on egocentric and exocentric motion perception", Exp Brain Research 16:476-491, 1973.

7. Young, L.R., Oman, C.M. "Influence of head position and *field* position on visually induced motion effects in three axes of rotation", Proceedings of the Tenth Annual Conference on Manual Control, 1974.

8. Young, L.R., Oman, C.M., Dichgans, J. "Influence of head orientation on visually induced pitch and roll sensation", Aviation Space Environ Med 46:264-268, 1975.

9. Young, L.R., Dichgans, J., Murphy, R. and Brandt, Th. "Interaction of optokinetic and vestibular stimuli in motion perception", Acta Otol 76:24-31, 1973.

10. Young, L.R., "On visual vestibular interaction", NASA Fifth Symposium on the Role of the Vestibular Organs in Space Exploration, NASA SP-314, 1970.

11. Berthoz, A., Pavard, B., Young, L.R. "Perception of linear horizontal self motion induced by peripheral vision (linearvection)" Exp Brain Research 23:471-489, 1975.

12. Poulton, E.C. "The new psychophysics: Six models for magnitude estimation" Psychol Bull 69:1-18, 1968.

13. Shirley, R. Motion Cues in Man Vehicle Control , Sc.D. Thesis, Department of Aeronautics and Astronautics, Massachusetts Institute of Technology, Cambridge, MA, 1968.

14. Young, L.R. "Dynamic control models of the semicircular canals", extension of "The current status of vestibular system models", Automatica, 5:369-383, 1969; Presented at the Seventh Annual Conference on Manual Control, 1971.

15. Melvill Jones, G., Barry, W., Kowalsky, N. "Dynamics of the semicircular canals compared in yaw, pitch and roll", Aerospace Med 35:984-989, 1964.

16. Oosterveld, W.J., "Threshold value for stimulation of the horizontal semicircular canals", Aerospace Med 41:386-389, 1970.

N79-17514

MOTION CUE EFFECTS ON HUMAN PILOT DYNAMICS IN MANUAL CONTROL

by

Kyuichiro Washizu*, Keiji Tanaka**,
Shinsuke Endo†, and Toshiyuki Itoko††

*Department of Aeronautics, University of Tokyo, Tokyo, **National Aerospace Laboratory, Tokyo, †The Ministry of Transportation, Osaka, ††Kawasaki Heavy Industry Co., Akashi

ABSTRACT

Two experiments have been conducted to study the motion cue effects on human pilots during tracking tasks. The moving-base simulator of National Aerospace Laboratory was employed as the motion cue device, and the attitude director indicator or the projected visual field was employed as the visual cue device. The chosen controlled elements were second-order unstable systems. It was confirmed that with the aid of motion cues the pilot workload was lessened and consequently the human controllability limits were enlarged. In order to clarify the mechanism of these effects, the describing functions of the human pilots were identified by making use of the spectral and the time domain analyses. The results of these analyses suggest that the sensory system of the motion cues can yield the differential informations of the signal effectively, which coincides with the existing knowledges in the physiological area.

SYMBOLS

B	backward shift operator
$c(t)$	pilot output
$e(t)$	error
F_i	shaping filter of forcing function
$i(t)$	forcing function
K_p	pilot gain
$m(t)$	output of controlled element
s	Laplace operator
X	damping (rad/sec)
Y	static stability (rad^2/sec^2)
$Y_c(s)$	transfer function of controlled element
$Y_E(s)$	transfer function of human equlizing system
$Y_p(s)$	transfer function of human pilot
$Y_S(s)$	transfer function of human sensory system
Δ	sampling interval (sec)
$\Phi_{xy}(j\omega)$	cross power spectrum of x and y
ω	frequency (rad/sec)

INTRODUCTION

There have been several important remarks on the effect of motion cues on the control performance of the human pilot. Through many experimental comparisons between the controls with and without motion, it is well known that the presence of motion generally improves the human control characteristics: it was suggested by Shirley and Young [Ref.1] that the addition of roll-motion cues to the visual ones permitted the pilot to increase his control gain without losing system closed-loop stability; it was also reported by Stapleford et. al. [Ref.2] that the human effective time delay decreased while the lead term of his transfer function increased in the presence of motion cues. Existing human operator models based on these knowledges have been implemented by the results from the studies about the motion sensory organs, especially semicircular canals and otolith [Ref.3].

In this paper we describe two series of experimental studies, both aiming at elucidating differences between the motion and the visual sensor characteristics of the human pilot and correlating them with the physiological knowledges. Both experiments were focused on the critical tracking tasks where the motion cue effects seemed to be dominant. Three experimental conditions, i.e., motion plus visual condition, motion only condition, and visual only condition, were evaluated using the multipurpose research flight simulator of NAL (National Aerospace Laboratory).

D39

THE FIRST EXPERIMENT

Objectives

Purposes of the first experiment are

1) To evaluate the experimental controllability limits of the human pilot controlling second-order unstable systems with and without motion cues, and to confirm the motion cue effects on the controllability limits;

and

2) To investigate the variation of the describing functions of human pilots in controlling unstable systems within their limits by the difference of the kinds of control cues.

Experimental Setup (Fig.1)

In order to close the man-machine feedback loop, subjects were instructed to stabilize the angular motion about the rolling axis, while is similar to the bank angle control of an aircraft, by moving the control stick laterally. An external random forcing function was added into the loop to activate the system. All the signals in the system were recorded by an analogue data recorder to be used later for the identification of the describing functions.

Equipments in Fig.1 are now described:

Controlled element. The transfer function of the controlled element is given by

$$Y_c(s) = \frac{1}{s^2 + Xs + Y} \qquad (1)$$

where Y = 10, 20, 30, 40, 50 (rad^2/sec^2), X < 0, and X was changed with the step size of 0.1 (rad/sec). This unstable second-order controlled element was simulated on an analogue computer.

Control cues. For the input to the pilot in the compensatory tracking task, the error signal in Fig.1 was provided by the following two devices:

(a) *Visual system.* The roll angle was displayed on the attitude director indicator installed in the cockpit.

(b) *Motion system.* A single seated VTOL cockpit was installed on the moving base of the simulator, the maximum operating range of which was ±10 degrees for both sides (Fig.2). The roll axis lay between the subject's feet; his body was subject to both linear and angular accelerations.

Control stick. A single stick-type controller without restoring force was used, generating lateral movements of the control output.

Forcing function. A white noise signal was filtered by the following shaping filter to generate the random forcing function, the power spectrum of which had two gentle cutoff frequencies:

$$F_i(s) = \frac{11}{s^5+5.5s^4+17s^3+28s^2+29s+11} + \frac{1700}{s^4+27s^3+470s^2+3900s+21000} \qquad (2)$$

Two subjects participated in the first experiment; a student who had no experience of controlling aircraft (Pilot A), and a test pilot of NAL (Pilot B). The experimental data were obtained after they had become skilled in the given tracking tasks.

Measurements and Results

Three kinds of experimental situations were realized by changing the cues given to the subject:

(a) *Motion plus visual.* The motion system was drived, and also the instrument information was available.

(b) *Motion only.* Only the motion system was drived, while the room lights were turned off. The subject was requested to close his eyes, and was obliged to utilize motion cues only.

(c) *Visual only.* By fixing the base, only the instrument information was available.

Controllability limits without the forcing function were obtained for Pilot A. The limits were tentatively defined by the parameters X and Y such that the subject could marginally maintain the roll angle within ±10 degrees for one minute. The controllability limits thus obtained are shown in Fig.3. From this figure, it is evident that motion cues have enlarged the limits. This agrees with the existing knowledges concerning the controllability limits and the effectiveness of motion cues.

Next, the describing functions of human pilots were identified by the following procedures. The analogue signals i(t), e(t), c(t) in Fig.1 were converted into digital data with sampling interval Δ = 0.05(sec), with the data length being one minute. On the basis of these ditigal data, the pilot describing functions were obtained as;

$$\hat{Y}_p(j\omega) = \frac{\Phi_{ic}(j\omega)}{\Phi_{ie}(j\omega)} \qquad (3)$$

In Eq.(3) the cross spectra $\Phi_{ie}(j\omega)$, and $\Phi_{ic}(j\omega)$ were computed by Blackman-Tukey method. Correlation functions were cut off to a length of 6(sec), and Hamming window was used. At the same time, the closed-loop linear-correlation coefficient from i(t) to c(t) was calculated as follows:

$$\rho(\omega) = \frac{\Phi_{ic}(j\omega)}{\sqrt{\Phi_{ii}(\omega)\Phi_{cc}(\omega)}} \qquad (4)$$

HITAC 5020 computer was used for the calculation. An example of the obtained results is shown in Figs.4-a and 4-b, of which the values of (X,Y) of

the controlled element correspond to ⑤ in Fig.3. Distinct features easily noticed from the Fig.4-b are summarized as follows:

1) For the case of motion plus visual, gains are generally higher than other cases, and both gains and phases are least fluctuant; i.e., linear-correlation coefficients show high values over wide frequency band. Thus the pilot transfer function of this case seems to be appropriately expressed by;

$$Y_p(s) = K_p \frac{1 + T_L s + T_L s^2}{1 + T_I s} e^{-\tau s} \qquad (5)$$

where $T_L \simeq 0.05$(sec), $T_L \simeq 0.2 \sim 0.5$(sec), respectively.

2) For the case of motion only, the frequency response is similar to that of the case of motion plus visual over the frequency higher than about $1.5 \sim 3$ (rad/sec), where linear-correlation coefficients are large. For the frequency lower than about 1.5(rad/sec), on the other hand, linear-correlation coefficients are small, which implies the irregularity of the control strategy in this frequency band.
3) For the case of visual only, the result is just contrary to the case of motion only, namely, we can see high linear-correlation coefficients in lower frequency band; while in higher frequency band the response are dispersed and linear-correlation coefficients are small.
4) The increase of gains, which is obvious in higher frequency band of both motion cases, corresponds to the rather rapid control stick movements observed in Fig.4-a. This phenomenon can be seen often in tracking when a controlled element is oscillatory. In such a case, human pilot seems to obtain quickness, which is especially important for the system stability, by oscillating the stick with the frequency that is suited to him and is higher than the natural frequency of the controlled element.

The features listed above are consistently observed regardless of subjects or controlled elements. Thus, it was confirmed that motion cues improved the human control characteristics in high frequency range which was important for the system stability, and that visual cues given by the instrument were effective to the precise control in rather low frequency range; i.e., visual cues bring about such an improvement of control as cancelling the steady-state deviations.

THE SECOND EXPERIMENT

In the first experiment, the control for the case of visual only corresponds to the flight in the instrument meteorological condition (IMC) without motion cues. On the other hand, in the case of motion plus visual, subjects could use not only instrument information but also the peripheral visual information; namely the situation is equivalent to the flight in the visual meteorological condition (VMC) with motion cues. Consequently there was the difference of visual information between the above two conditions. The recent paper by Junker et. al. [Ref.4] also points out that the peripheral visual information has the same effect on the human pilot control strategy as motion cues.

The second experiment was resumed after modifying the visual system so as to equalize the visual information for the cases of visual only to motion plus visual only: the visual information was provided by the simulated visual field projected to the screen in front of the cockpit to widen the pilots' angle of vision. Moreover, to put a stress on the study of the describing functions, slightly unstable controlled elements were adopted. In addition, the time domain analysis, which has recently come into practical use, has revealed the possibility of identifying precisely both system dynamics and noise characteristics. We have employed this technique in order to investigate the human sensory characteristics.

Thus the second experiment has the following two objectives:

1) To get the differences between pilot dynamics with and without motion cues by providing the pilot with the visual cues similar to those of VMC;

and

2) To estimate the mechanism of the motion and the visual sensory organs, based on the describing functions and the remnants.

Experimental Setup

Only the modifications of the first experiment are described. The block diagram was the same as Fig.1.

Controlled element.

$$Y_c(s) = \frac{Y}{s^2 + Xs + Y} \qquad (8)$$

Static gain was set constant, and the parameters were Y = 10, 30 and X = 0, -0.3, respectively.

Cockpit and controller. Both were the same as those of the first experiment.

Control cues.

(a) *Visual system*: Simulated visual field was used, which was the scene of the scaled runway taken by a video camera, and was projected on the wall screen in front of the cockpit by Eidophor (Fig.5). The pilot visual angle was widened to 32 degrees laterally by these equipments. For the case of motion plus visual the image was fixed, while for the case of visual only it was rotated to provide pilots with the visual information of rolling, by coordinatedly rotating the video camera.
(b) *Motion system*: The same cockpit was used.

Forcing function. The random signal of limited band-width was utilized, the shaping filter of which was simplified to;

$$F_1(s) = K\left[\frac{10}{(1+s)^2} - \frac{1}{(1+0.1s)^2}\right] \qquad (7)$$

Measurement and Analysis

The subject participated in the second experiment was Pilot B of the first experiment. After having got fully accustomed to the system, he conducted about 30 runs which could be classified by the combination of the control cues provided as;

1) *Motion plus visual.* The simulated visual field was fixed, and the motion base was derived.
2) *Motion only.* The motion base was drived. The subject was requested to close his eyes, with the room lights extinguished.
3) *Visual only.* The motion base was fixed. The simulated visual field was rotated to provide visual cues as if the cockpit were rotating.

The obtained data were processed in the same manner as in the first experiment, except that the sampling interval was changed to $\Delta = 0.1$(sec). Pilot describing functions were identified according to the following two ways by making use of FACOM 230-75 computer.

1) *Cross-power spectrum method.* This is the same method as that of the first experiment, and was applied by setting the correlation length to 10 (sec) and using Hamming window.
2) *MFPE (Multiple Final Prediction Error) method.* An autoregressive model is fitted to the data by using Akaike's MFPE method [Refs.5,6]. This model can be expressed as;

$$\begin{bmatrix} c(n) \\ e(n) \end{bmatrix} = \begin{bmatrix} A_{11}(B) & A_{12}(B) \\ A_{21}(B) & A_{22}(B) \end{bmatrix} \begin{bmatrix} c(n) \\ e(n) \end{bmatrix} + \begin{bmatrix} \sigma_{11} & 0 \\ 0 & \sigma_{22} \end{bmatrix} \begin{bmatrix} \xi_1(n) \\ \xi_2(n) \end{bmatrix} \qquad (8)$$

where $c(n)$ and $e(n)$ are sampled time series obtained from $c(t)$ and $e(t)$ with the sampling interval Δ, and

$$A_{ij}(B) = a_{ij}(1)B + a_{ij}(2)B^2 + \cdots\cdots + a_{ij}(M)B^M \qquad (i,j=1,2),$$

where B is backward shift operator; i.e., $Bx(n) = x(n-1)$, and $\xi_1(n)$, $\xi_2(n)$ are mutually independent white noises. From Eq.(8), we can derive a pilot describing function as:

$$\hat{Y}_p(j\omega) = \frac{A_{12}(j\omega)}{1 - A_{11}(j\omega)} \qquad (9)$$

where $A_{11}(j\omega)$, $A_{12}(j\omega)$ are obtained from $A_{11}(B)$, $A_{12}(B)$ by substituting $e^{-j\omega\Delta}$ for B.

The describing functions obtained by both methods are in good accordance with each other. An example of the describing functions obtained by the latter method is shown in Fig.6. The controlled element of this example corresponds to ⊗ in Fig.3. The characteristics shown in Fig.6 generally coincide with those of the first experiment, i.e., when motion cues are available, high control gains are observed.

Discussions

In the following, we consider a human pilot model which consists of the sensory part, Y_S, and the equalizing and neuro-muscular part, Y_E, corresponding to the forward and the afterward part of the human describing function with respect to the injection point of the remnant source, $w(t)$ [Fig.7]. In Fig.7, $w(t)$ corresponds to $\sigma_{11}\xi_1(n)$ of Eq.(8), and assumed to be white. On the basis of this model, the estimates of the two parts, $\hat{Y}_S$ and $\hat{Y}_E$ were calculated. Refering to Appendix, we obtain the following relations;

$$\hat{Y}_S(j\omega) = A_{12}(j\omega) \quad , \qquad (10)$$

and

$$\hat{Y}_E(j\omega) = \frac{1}{1 - A_{11}(j\omega)} \quad . \qquad (11)$$

Examples of $\hat{Y}_S$ and $\hat{Y}_E$ thus obtained are shown in Figs.8 and 9. These figures show that Y_S's with motion indicate high gain and differential or second-order differential features, while Y_E's with motion remain generally the same. The estimated magnitudes of the remnant source of these cases have proved to differ depending on the provided cues by no more than 2db, which can be considered to be almost equal to one another. This suggests the validity of the above partition of the human describing function.

For further examinations of the differences in Y_S's, we should consider the remnant sources. It has been suggested that the remnant can be attributed to the following sources [Refs.7,8].

(a) *Modelling errors.* We often express the pilot dynamics as the continuous linear time-invariant system, but the human control strategy practically contains discrete, nonlinear and time-varing features, which are lumped together as the remnant when we construct a model.
(b) *The response to the signals other than the input.*
(c) *Noises that the human pilot generates by himself.* These are classified into the observation noise which is injected at the sensory system, noise during the processings in his celebrum, and the motor noise in the neuro-muscular system.

Among them, (a) and (b) are considered to be small when the subject is well trained and highly motivated, and when the task is a simple single-axis tracking. Moreover, among (c), the motor noise is usually regarded insignificant. Thus it seems proper to consider that the remnant sources of this case are injected at the sensory system or near celebrum. This leads to us to attribute the causes of the differences in Y_S's to the differences of the sensory

system. This therefore implies that the differential or the second-order differential features in Y_S's in motion cases reflect the dynamics of the motion sensor organs. We can see that motion cues could be effectively utilized with a low level remnant. On the other hand, pilot dynamics based on the visual cues proved to have smaller gain and the visual cues are more insensitive than the motion cues.

Although an assumption concerning the remnant source puts some restrictions on the previous discussion, the findings mentioned above basically agree with the physiological knowledges about the vestibular organs. It should be noted that the sensor organs investigated in this experiment are equivalent to the integrated motion sensor system including not only the vestibular organs but also the skin sensations and the deep sensations. To make the obtained results more practical, we should continue further evaluation of these findings by carefully comparing these with the knowledges about the human sensor dynamics.

CONCLUDING REMARKS

From the experiments described above, we conclude as follows:

1) Motion cues can enlarge the human pilots' controllability limits for the second-order unstable controlled elements.
2) Motion cues improve the human control characteristics in rather high frequency range, while the visual cues are effective for the precise control in rather low frequency.
3) From the discussions about human describing functions and the remnant, it was suggested that the motion sensor system can yield the *differential or* the second-order differential informations of the input.

ACKNOWLEDGEMENT

The authors are deeply indebted to Mr. Y. Terui, a test pilot of NAL, for his participation as the subject, and also to Prof. N. Goto of Kyushu University for his comments on this paper.

REFERENCES

1. Shirley, R.S.; and Young, L.R.: Motion Cues in Man-Vehicle Control. IEEE Trans., Vol.MMS-9, 1968.

2. Stapleford, R.L.; Peters, R.A.; and Allex, F.R.: Experiments and a Model for Pilot Dynamics with Visual and Motion Inputs. NASA CR-1325, 1969.

3. Curry, R.E.; Young, L.R.; Hoffman, W.C.; and Kugel, D.L.: A Pilot Model with Visual and Motion Cues. Proc. of AIAA Visual and Motion Simulation Conference, 1976, pp.50-54.

4. Junker, A.M.; and Price, D.: Comparison between a Peripheral Display and Motion Information on Human Tracking about the Roll Axis. Proc. of AIAA Visual and Motion Simulation Conference, 1976, pp.63-72.

5. Tanaka, K.; Goto, N.; and Washizu, K.: A Comparison of Techniques for Identifying Human Operator Dynamics Utilizing Time Series Analysis. 12th Ann. Conf. on Manual Control, NASA TM X-73,170, 1976, pp.673-685.

6. Akaike, H.: Autoregressive Model Fitting for Control. Ann. Inst. Statist. Math., Vol.23, 1971, pp.163-180.

7. McRuer, D.T.; and Krendel, E.S.: Mathematical Models of Human Pilot Behavior. AGARD-AG-188, 1974.

8. Levison, W.H.; and Kleinman, D.L.: A Model for Human Controller Remnant. 4th Ann. Conf. on Manual Control, NASA SP-192, 1968, pp.3-14.

APPENDIX: ON THE SHAPING FILTER OF THE HUMAN REMNANT

We generally define the remnant $r(t)$ as a portion of $c(t)$ irrelevant to $e(t)$; namely

$$r(t) = c(t) - \int_0^t y_p(t-\tau)e(\tau)d\tau \qquad \text{I}$$

where $y_p(\tau)$ is the weighting function of $Y_p(j\omega)$. From Fig.7, we can derive the following relation:

$$c(t) = \int_0^t y_p(t-\tau)e(\tau)d\tau + \int_0^t y_E(t-\tau)w(\tau)d\tau \quad , \qquad \text{II}$$

where $y_E(\tau)$ is the weighting function of $Y_E(j\omega)$. From Eq.I and II, $r(t)$ is considered to be a shaped output of Y_E activated by the white noise $w(t)$; therefore the shaping filter of $r(t)$ is Y_E. Thus we have Y_S as;

$$Y_S(j\omega) = \frac{Y_p(j\omega)}{Y_E(j\omega)} \quad . \qquad \text{III}$$

We shall begin here by introducing the way to get Y_E by making use of the spectral method. It is well known that the coherency between $i(t)$ and $c(t)$ is

$$\rho^2(\omega) = \frac{|\Phi_{ic}(j\omega)|^2}{\Phi_{ii}(\omega)\Phi_{cc}(\omega)} \quad . \qquad \text{IV}$$

If we denote the power spectrum of closed-loop contribution of the remnant as

$$\Phi_{pp}(\omega) = \left|\frac{1}{1 + Y_p(j\omega)Y_c(j\omega)}\right|^2 \Phi_{rr}(\omega) \qquad \text{V}$$

where

$$\frac{1}{1 + Y_p(j\omega)Y_c(j\omega)} = \frac{\Phi_{ie}(j\omega)}{\Phi_{ii}(\omega)} \quad ,$$

we car write

$$\Phi_{pp}(\omega) = (1 - \rho^2(\omega))\Phi_{cc}(\omega) \qquad \text{VI}$$

From Eqs.V and VI, we obtain the estimat of the power spectrum of the remnant by;

$$\Phi_{rr}(\omega) = \frac{\Phi_{ii}^2(\omega)\Phi_{cc}(\omega) - \Phi_{ii}(\omega)|\Phi_{ic}(j\omega)|^2}{|\Phi_{ie}(j\omega)|^2} \qquad \text{VII}$$

While

$$\Phi_{rr}(\omega) = |Y_E(j\omega)|^2 W \quad , \qquad \text{VIII}$$

where W denotes the intensity of $w(t)$. Thus we can estimate $|Y_E(j\omega)|$ from VII and VIII, by the spectral method.

Next, we introduce another way to obtain Y_S from the autoregressive model defined in the time domain. We shall rewrite the first equation of Eq.(8) as;

$$c(n) = A_{11}(B)c(n) + A_{12}(B)e(n) + \sigma_{11}\xi_1(n) \quad , \qquad \text{IX}$$

where

$$w(n) = \sigma_{11}\xi_1(n) \quad .$$

Arranging IX, we obtain

$$c(n) = \frac{A_{12}(B)}{1 - A_{11}(B)} + \frac{\sigma_{11}}{1 - A_{11}(B)}\xi_1(n) \quad , \qquad \text{X}$$

where the second term of the right hand side corresponds to the open-loop contribution of $w(t)$ to $c(t)$; namely

$$r(n) = \frac{\sigma_{11}}{1 - A_{11}(B)}\xi_1(n) \quad . \qquad \text{XI}$$

Therefore we obtain the shaping filter of $r(t)$ by Fourier-transforming $\{1 - A_{11}(B)\}^{-1}$ as;

$$\hat{Y}_E(j\omega) = \frac{1}{1 - A_{11}(j\omega)} \quad . \qquad \text{XII}$$

While the human describing function is,

$$\hat{Y}_p(j\omega) = \frac{A_{12}(j\omega)}{1 - A_{11}(j\omega)} \quad . \qquad \text{XIII}$$

Thus, we can easily estimate Y_S by,

$$\hat{Y}_S(j\omega) = A_{12}(j\omega) \quad . \qquad \text{XIV}$$

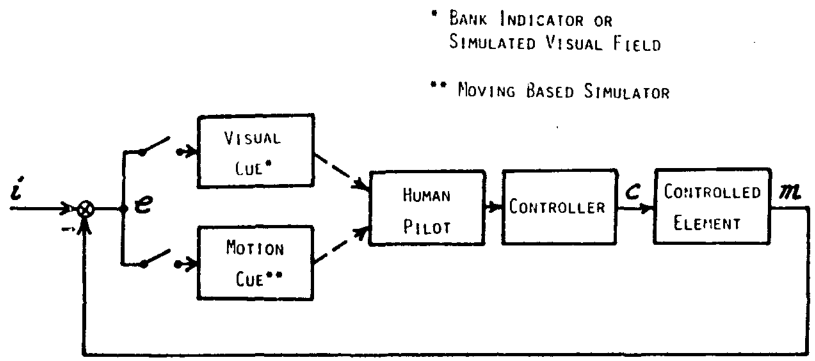

Figure 1. Block Diagram of the Experiments

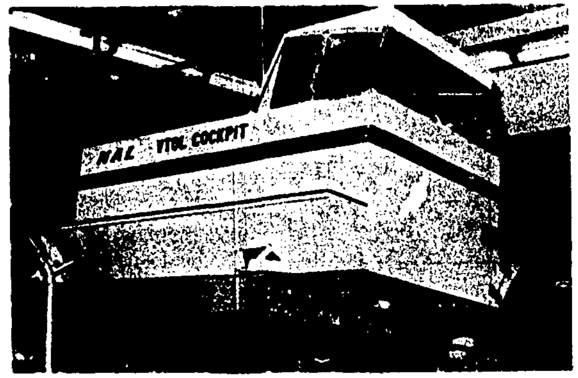

Figure 2. NAL VTOL Cockpit

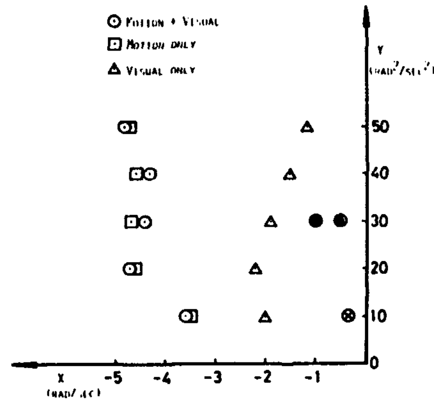

Figure 3. Controllability Limits for Unstable Second-Order Controlled Elements

ORIGINAL PAGE IS
OF POOR QUALITY

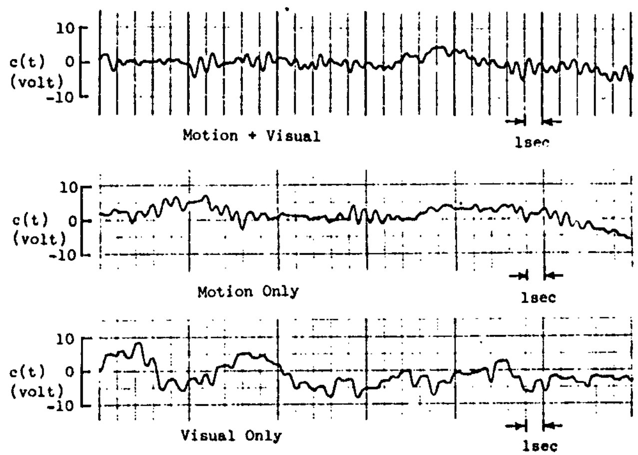

Figure 4-a. Typical Control Deflections

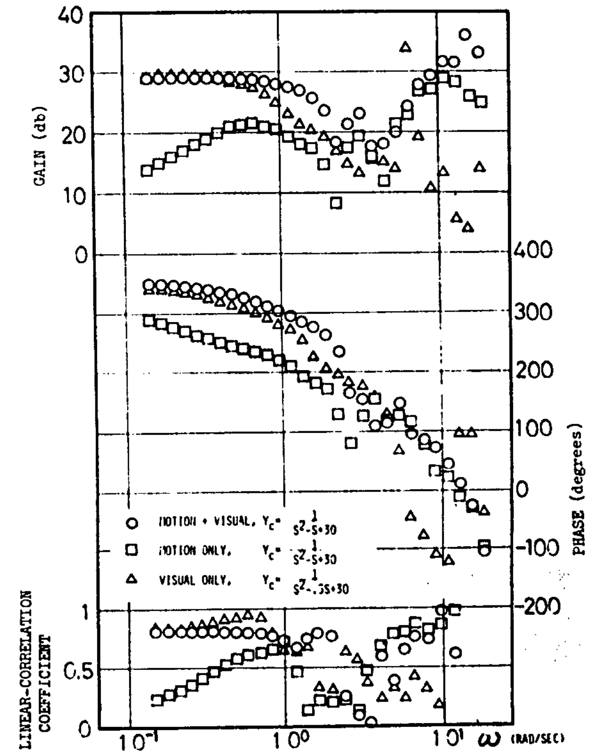

Figure 4-b. Identified Pilot Describing Functions, $\hat{Y}_p(j\omega)$'s by Spectral Method

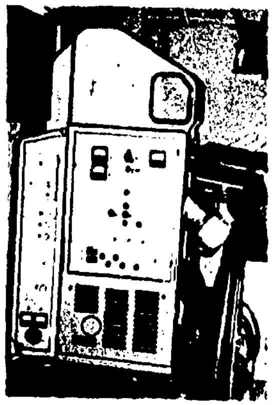

Figure 5-a. Video Projector (Eidophor)

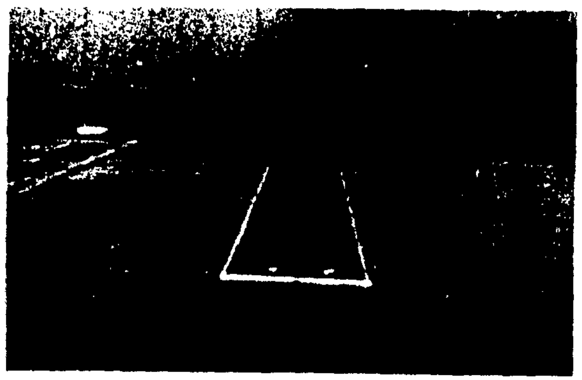

Figure 5-b. Simulated Visual Field

ORIGINAL PAGE IS
OF POOR QUALITY

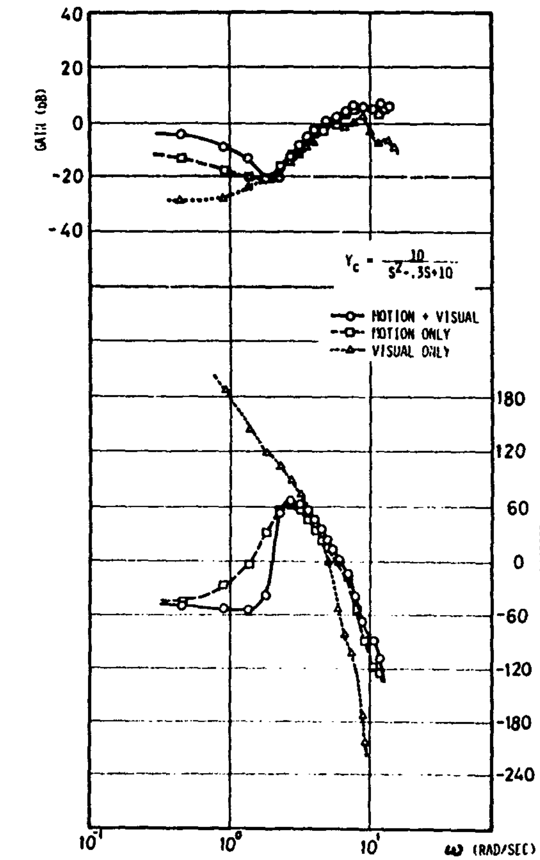

Figure 6. $\hat{Y}_p(j\omega)$ by MFPE Method

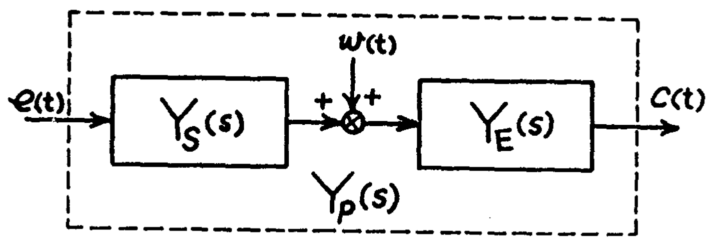

Figure 7. Partition of $Y_p(s)$

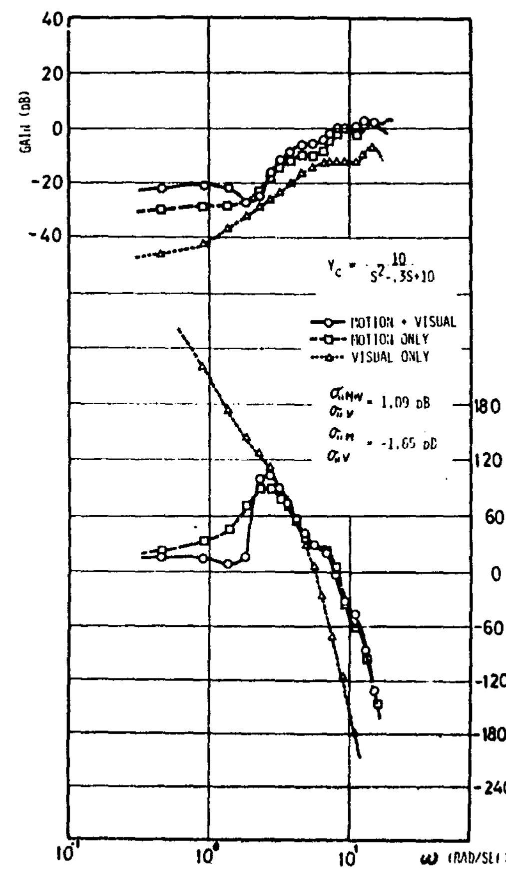

Figure 8. $\hat{Y}_S(j\omega)$

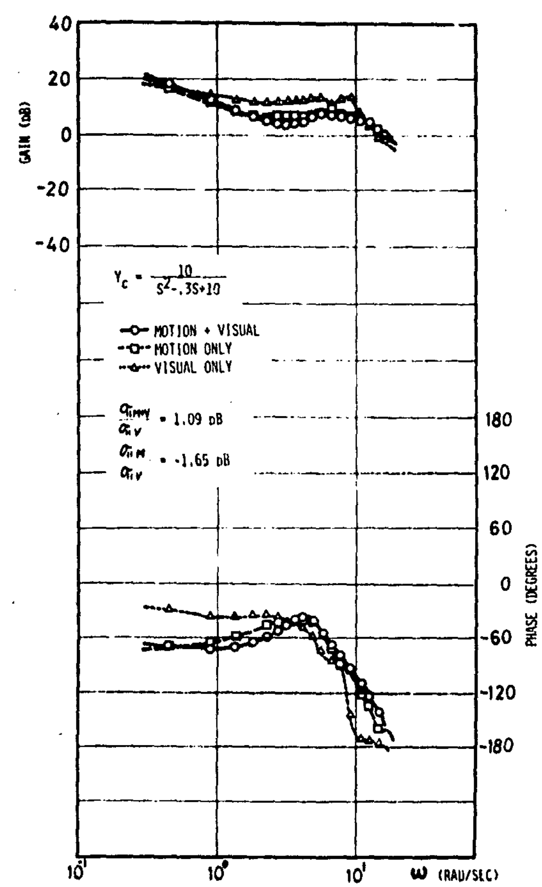

Figure 9. $\hat{Y}_E(j\omega)$

Session VIII

DISPLAYS AND CONTROLS

Chairman: R. W. Pew

N79-17515

STUDY OF THE USE OF A NONLINEAR, RATE LIMITED, FILTER ON PILOT CONTROL SIGNALS

by

James J. Adams
Langley Research Center

SUMMARY

Analysis of pilot response while performing in a closed loop control situation has shown that there is a large remnant in the pilot's control output that does not add to the goodness of the control, but does add unwanted motion to the system response. The use of a filter on the pilot's control output could improve the performance of the pilot-aircraft system. What is needed is a filter with a sharp high frequency cut-off, no resonance peak, and a minimum of lag at low frequencies. The present investigation studies the usefulness of a nonlinear, rate limited, filter in performing the needed function. The nonlinear filter is compared with a linear, first order filter, and no filter. An analytical study using pilot models and a simulation study using experienced test pilots was performed.

The results showed that the nonlinear filter does promote quick, steady maneuvering. It is shown that the nonlinear filter attenuates the high frequency remnant and adds less phase lag to the low frequency signal than does the linear filter. It is also shown that the rate limit in the nonlinear filter can be set to be too restrictive, causing an unstable pilot-aircraft system response.

INTRODUCTION

Analysis of pilot response while performing closed loop control of dynamic systems has shown that the pilot's response is composed of a signal that is linearly related to the input signal and a random noise with a band pass equal to the band pass of the linear signal. The study which led to these conclusions is presented in reference 1, where the vehicle being controlled was an acceleration response type of plant, $\frac{K}{s^2}$, and the pilot band pass was around 10 radians per second. Since the pilot remnant does not contribute to the goodness of the system response, any means of reducing its effect would be beneficial. In fly-by-wire control systems, it is possible to use a low pass filter on the pilot's control signal which, ideally, would eliminate the high frequency remnant signal while having no effect on the low frequency, linear part of the control signal. What is needed is a filter with a very sharp cut-off, but with no resonance peak, and with very little phase shift below the cut off frequency. The purpose of the present investigation is to examine the usefulness of a nonlinear, rate limited, filter in providing this needed function. The nonlinear filter was compared with a no filter condition, and with a linear, first order filter.

Reference 2 is a study that is similar to the present study in many ways. In reference 2, flight tests were conducted with an elevator control booster which contained a variable rate limit. It was found that the rate limit could be restricted to 7 degrees per second with no detrimental effects on the controllability of the system. It should be noted that in reference 2 the control rate limit is not included in any stability augmentation loop closure, and the present study does not suggest that the filter be included in any stability augmentation loop. Reference 3 shows that including a rate limit in a stability augmentation loop can destroy the effectiveness of the stability augmentation.

SYMBOLS

Values are given in SI Units. The measurements and calculations were made in U.S. Customary Units.

F_x	x axis force, N
h	altitude, m

PRECEDING PAGE BLANK NOT FILMED

D40

I_y	moment of inertia, Kg-m^2
K	general gain
K_θ	pilot model pitch loop static gain
K_h	pilot model altitude loop static gain
K_n	remnant static gain
L_α	$-\frac{1}{mV}\frac{\partial F_z}{\partial \alpha}$ per sec
M_y	y axis moment, N-m
M_α	$\frac{1}{I_y}\frac{\partial M_y}{\partial \alpha}$ per sec
M_q	$\frac{1}{I_y}\frac{\partial M_y}{\partial q}$ per sec^2
M_{δ_e}	$\frac{1}{I_y}\frac{\partial M_y}{\partial \delta}$ per sec^2
m	mass, Kg
q	pitching velocity, rad/sec
s	Laplace variable, per sec
V_{x_0}	velocity, m/sec
α	angle of attack, rad
δ_e	elevator deflection, rad
θ	pitch angle, rad
ω_{sp}	short period natural frequency, rad/sec
ξ_{sp}	short period damping ratio
λ	pilot-model, aircraft system pitch mode root, rad/sec
ω_α	pilot-model, aircraft system short period mode frequency, rad/sec
ξ_α	pilot-model, aircraft system short period mode damping ratio
ω_δ	pilot-model, aircraft system control mode frequency, rad/sec
ξ_δ	pilot-model, aircraft system control mode damping ratio
ω_h	pilot-model, aircraft system altitude mode frequency, rad/sec
ξ_h	pilot-model, aircraft system altitude mode damping ratio
γ	flight path angle, rad
ϕ	frequency response phase angle, deg

Subscript

c	command
e	error

Experimental Procedure

The three filter configurations, no filter, nonlinear filter, and linear filter, were examined with pilot models in an analytical study and with real pilots in a fixed base simulator. Three different tasks were executed in each case: (1) performing a step pitch attitude change, (2) performing a step altitude change, and (3) following a sinusoidal altitude command. These tasks were performed with three different aircraft configurations which represented a medium speed condition of approximately Mach number 0.6 at an altitude of 25,000 feet, a high speed condition of approximately Mach number 1.0, and a low speed, low altitude condition.

The pilot model used in the analytical study was

$$\frac{\delta_e}{\theta_e} = \frac{K_\theta}{(1 + .2s)^2}$$

for pitch control. No lead term has been included in the pilot model because the intention of this study is to combine the pilot model with aircraft that

are considered to have satisfactory handling qualities, and it has been shown that no lead is required to represent a pilot's response with these aircraft. The lag time constant of 0.2 second has been shown to be proper value for the pilot model when controlling a aircraft with at least tolerable handling qualities. The gain K_θ was adjusted to provide a pilot-model aircraft system response with the real root larger in magnitude than -0.4 radian per second and a damping ratio of the oscillatory mode of motion greater than 0.1. These selections for the lag time constant and gain provide typical pilot-aircraft system characteristics. The selected pilot model was used without any further adjustment with each filter configuration to provide a clear indication of the effect of the filter on the system response. It was, of course, necessary to adjust the gain, K_θ, for each aircraft configuration to provide the desired system response, but the pilot model coefficients were kept constant for each filter configuration. For altitude control the pilot model consisted of an outer loop added to the pitch control loop as shown in figure 1, with a constant gain, K_h, on the outer loop control block. For the altitude control cases the gains K_h and K_θ were adjusted to provide a system response with the lower frequency greater than about 1 radian per second and the lowest damping ratio greater than 0.1. Again, these system characteristics are assumed to be typical for altitude control by a real pilot. With the high speed aircraft configuration, a small amount of lead was added to the pitch control loop pilot model in the altitude control system. Also, for all three aircraft configurations, a limit was placed on the pitch command (the output of the K_h block) in the altitude control systems. To complete the pilot models, a random white noise signal was filtered with a second order filter $\frac{K_n}{(1 + .2s)^2}$ and added to the output of the pilot model to represent the remnant of the real pilot. The amplitude of this remnant signal was adjusted so that the variance of the remnant was between 40 to 50 percent of the total control signal. All of these items have been shown to be reasonable for the representation of pilot response.

The pilot model was combined with a simplified, two degree-of-freedom representation of the aircraft

$$\dot{\alpha} - \dot{\theta} = - L_\alpha \alpha$$

$$\ddot{\theta} = M_q q + M_\alpha \alpha + M_{\delta_e} \delta_e$$

and the relationship for altitude

$$\dot{h} = V_{x_0}(\theta - \alpha)$$

The coefficients for the three aircraft configurations are given in Table I, together with the aircraft response characteristics. Also given are the pilot model gains, K_θ and K_h, and the pilot-model aircraft system characteristics.

The nonlinear filter equations are:

$$\dot{\delta}_e = 100\,\delta_c - 100\,\delta_e \qquad |\dot{\delta}_e| < \text{limit value}$$

$$\dot{\delta}_e = \text{limit value} \qquad |\dot{\delta}_e| > \text{limit value}$$

An analog diagram for the nonlinear filter is shown in the sketch. The linear filter had a 5 radians per second break point, and was represented in a straight forward manner.

In the simulation tests, three experienced test pilots performed the tasks. The simulator cockpit used by the pilots was equipped with a televised, out-the-window display of the horizon and a target airplane. The included angle of the display was 20 degrees vertically and 35 degrees horizontally. The control stick was a force stick with an unlimited, linear

output and no hysteresis. The force stick was mounted on a rubber block base which gave it a small amount of rotational movement. There was no restriction in the rate of movement of the control stick. When the nonlinear filter was added to the system, only the input to the aircraft was rate limited.

The simulator was controlled by a full set of nonlinear aircraft equations of motion presented in Appendix A. The pilot performed the attitude control tasks with reference to the horizon, and the altitude control tasks with reference to the target airplane. While the pilots were performing these longitudinal tasks, they also had to regulate the lateral-directional response of the aircraft as an additional task. The target aircraft was driven so that it remained at a constant 183 meters in front of the test aircraft. The target flew either straight and level or with a sinusoidal variation in altitude. The simulator equations of motion were solved with a digital computer that operated with a sample rate of 32 samples per second. In order to properly represent the high frequency response of the nonlinear filter when it was operating on its linear region, it was necessary to use special computational techniques.

RESULTS

Comparison of Filters - To illustrate the differences in the operation of the nonlinear and linear filters, the frequency response of the two devices can be compared. The data for the nonlinear filter is actually describing function data, and was obtained with an analog representation. Sinusoidal input signals with a number of difference frequencies were applied to the nonlinear filter, and the time history of the output recorded. The frequency response phase angle data was obtained by measuring the time difference in the zero crossing of the input and output, and using the formula

$$\phi = \frac{\Delta t \omega 360}{2\pi}$$

The amplitude ratio was obtained from the ratio of the peak values of the input and output. These data are shown in figure 2a, where it is compared with the frequency response of the linear filter. It can be seen that the phase lag for the nonlinear filter is less than for the linear filter at frequencies below 3 radians per second. This small phase lag at low frequencies for the nonlinear filter is the result of the 100 radians per second break point used in the linear part of the nonlinear filter. It can also be seen that the reduction in amplitude ratio with increasing frequency is much steeper for the nonlinear filter than for the linear filter. The results of these two factors is that the nonlinear filter would have less effect on low frequency signals, and would attenuate high frequency signals better than would the linear filter.

Where the response of the linear filter would be invariant with the amplitude of the input, the nonlinear filter response is affected by the amplitude of the input. This is illustrated in figure 2b, where the describing function data of the nonlinear filter for three different input amplitudes is presented. The figure shows that the larger the amplitude of the input, the more phase lag is created at any given frequency. This situation indicates a potential stability problem with large inputs for a system incorporating the nonlinear filter.

To indicate the effect on stability of the nonlinear filter for a typical pilot-model, aircraft system, figure 3 is presented. The pilot model was simplified in this case by leaving out the remnant term. Figure 3a shows the response of a typical system with the nonlinear filter included, but with the rate limit set so high that it does not come into effect. The commanded pitch angle change is 5 degrees in this case. Figure 3b shows the response of the same system with the nonlinear filter rate limit set so that it does come into operation. It can be seen that while the nonlinear filter does noticeably change the control moment time history as compared to figure 3a, there is no noticeable effect on the pitch angle time history. Figure 3c shows the response of the same system used in figure 3b to a 10 degrees pitch angle change command. In this last case the initial overshoot in pitch angle is noticeably larger in proportion to the steady state value of pitch angle than in the case with the 5 degree pitch angle change.

This change in the stability of the response of the system with an increase in the size of the input command illustrates a possible disadvantage of the nonlinear filter.

In this report, control action will be presented as the normalized control moment, $M_{\delta_e}\delta_e$, instead of using control deflection. The purpose for using this particular method of data presentation is to generalize the results rather than leaving the results as the function of a particular control effectiveness value.

Pilot Model Analysis - To test the usefulness of the nonlinear filter, a study using pilot models for both attitude and altitude control was undertaken to compare the nonlinear filter with both no filter and with a linear, first order filter. The comparison was made with each of three different aircraft configurations. The nonlinear filter rate limits were established initially in these tests by noting the maximum rate required in the 5 degree attitude change maneuver, and setting the rate limit at one-half of this maximum value. Further restrictions in the rate limit were then tried.

The first aircraft configuration to be discussed represents a medium speed flight configuration of a fighter type aircraft. The aircraft speed was 214 meters per second, and the aircraft short period response characteristics were $\omega_{sp}^2 = 20$ radians² per second², $2\zeta\omega_{sp} = 5$ radians per second ($\omega_{sp} = 4.48$ radians per second, $\zeta_{sp} = .56$). The results obtained when the filters were inserted in a system containing this aircraft and the typical pilot model, and a step change in pitch angle is performed are shown on figure 4. The figure shows a reduction in the pitching motion activity that occurs in this maneuver with each of the two filters included in the system as compared to that which occurs with no filter. The nonlinear filter brings about a greater reduction in pitching activity than does the linear filter. Each of the filters reduces the effect of the pilot remnant, but the linear filter also reduces the damping of the oscillatory mode of motion of the system. This reduction in system damping is illustrated more clearly in figure 5, where the pilot remnant has been removed from the pilot model.

The same type of result was obtained when a step change in altitude was computed using the multiloop pilot model. These results are shown on figure 6 and again a decrease in system damping can be seen to occur when the linear filter is added to the pilot-model, aircraft system, and slightly less pitching motion activity occurs with the nonlinear filter as compared with the linear filter.

When the high speed aircraft configuration (V = 305 meters per second, $\omega_{sp}^2 = 100$ per second², $2\zeta\omega_{sp} = 3$ per second) was considered, the reduction in pitching activity that occurred with the nonlinear filter as compared to the no filter configuration or the linear filter was very evident. The results are shown on figure 7, where the response to a step change in altitude is shown. The same result was obtained with the step change in pitch angle computation. It should be noted that a small amount of pilot lead (a lead time constant of 0.2 second) was used in the computation of the altitude change shown in figure 7. This amount of lead is an addition that a pilot is very likely to try in his control response in an attempt to improve the system response.

With the low speed aircraft configurations (V = 122 meters per second, $\omega_{sp}^2 = 5$ per second², $2\zeta\omega_{sp} = 5$ per second), the results as regards the step pitch angle and step altitude change were the same as for the first two configurations. One test in which the filters had a pronounced effect with the low speed aircraft configuration was in following a sinusoidal altitude command. A typical computed run is shown in figure 8. The command in this case was a sine wave with a period of 30 seconds and an amplitude of 120 meters. A summary of the results obtained from these computations are presented in Table II. Presented are the root-mean-square values for altitude error for all three aircraft configurations with all three filters. These root-mean-square error values have been normalized to the no filter case so as to show at a glance the effect of the nonlinear filter and the linear filter. The results show that with the low speed aircraft configuration both the nonlinear filter and the linear filter provide considerable improvement in the sinusodial command following ability of the pilot-model, aircraft system. Less improvement was provided by the two filters with the high speed aircraft, and with the medium speed aircraft the filters reduced the accuracy of the sinusoidal altitude following.

Simulation Tests - Three experienced test pilots served as subjects in the simulation tests. Each pilot tested each filter configuration with each of the three aircraft configurations. In this investigation the rate limit in the nonlinear filter was set by combining the pilot model with the 5 degree-of-freedom, nonlinear aircraft representation, noting the maximum control moment rate that was required in a 3 degree pitch angle change maneuver, and setting the rate limit at one-half of this maximum value. While this method of setting the rate limit proved to be very useful in determining the value to use initially, preliminary tests showed that the rate limit could be restricted a little bit more. The task of following the target airplane which was moving vertically in a sine wave with a period of 30 seconds and an amplitude of 120 meters proved to be the most sensitive tests of required control moment rate, and so this task was used in this preliminary investigation. Sample tests with the high speed aircraft are shown in figure 9. With the initial $M_{\delta_e}\dot{\delta}_e$ limit value of 45 per second^3, the pilot was able to perform the maneuver with no difficulty. When the limit value was reduced to 25 per second^3, the pilot experienced some difficulty at first, as is indicated by the one cycle of a divergent oscillation that can be seen in the figure. However, the pilot made the necessary adjustment and regained control. It was concluded from this test that the limit value of 25 per second^3 was close to the greatest amount of restriction that could be used, and this is the value that was used in the remainder of the investigation with the high speed aircraft configuration. Similar tests were made with the other two aircraft configurations, and resulted in values of $M_{\delta_e}\dot{\delta}_e$ of 8 per second^3 for the medium speed configuration and 6 per second^3 for the low speed configuration being selected for use in the remainder of the investigation.

The results obtained with the pilots in the simulator closely parallel those obtained with the pilot model in the analytical study. Time history records obtained with pilot P for the step change in pitch angle are shown in figure 10. These results are typical for all the subjects. The pilots performed these tests in a systematic manner by first performing a very slow maneuver (using a low gain) which they were sure would be well damped. They increased the maneuver rate in the next try, and then made a final maneuver which was done as rapidly as they felt they would ever do the maneuver. It is this final maneuver that should compare with the pilot model results. It can be seen in figure 10 that there is a definite reduction in system damping for the rapid maneuver with the lin . filter included in the system as compared to the response with either . filter or nonlinear filter, and that the pitching activity is the least . the nonlinear filter. Figure 11 shows the step altitude change maneu and again, the pitching activity is slightly less with the nonlinear filter than with either the no filter or the linear filter configurations.

With the high speed aircraft configuration, the pitching activity is clearly the smallest with the nonlinear filter in both the attitude change and the altitude change tasks. These results are shown in figures 12 and 13, where pilot P was the subject. These figures show that not only does the nonlinear filter reduce the random noise generated by the pilot, but also it does not effect the linear portion of the pilot's response. The result is that with the nonlinear filter in the system, the final steady state condition of the maneuver is arrived at quickly and with only a small oscillation about this steady state value. This type of response character would be a great value doing maneuvers that must be done rapidly with great accuracy.

With the low speed aircraft configuration, the most pronounced effect in the simulation tests was, as it was in the pilot model analysis, in the task of following a sinusoidal altitude command. A set of typical time histories is shown in figure 14. There was a great deal of learning involved in this task. The performance measure used was the difference in the altitude of the target airplane and the controlled airplane, but the pilot had a tendency to want to only keep the gun sight pipper on the target. As they learned that a good score would result from staying at the same altitude as the target, and, at the same time, learned to use a small amount of lead to accomplish this task, the scores improved by a large amount. To show the final result, the last three scores of the one subject who performed a complete set of tests are given in Table II. It can be seen that no improvement in root-mean-square values of the altitude error was provided by either the nonlinear filter or the linear filter with the medium speed aircraft

configuration, there was some improvement with the high speed aircraft, and there was a very noticeable improvement due to the filters with the low speed aircraft. These results closely match the results obtained in the pilot model analysis.

The pilots were asked to rank the different filter configurations as best (1), in between (2), and worst (3). This rating data is given in Table III. It can be seen that there was no agreement among the pilots in their rankings. Further, any one pilot varied in his ratings when different aircraft configurations were involved. The effect of the filter, as shown in the time histories presented previously, was small, and this is probably the reason the pilots were not able to reach an agreement in rankings in the small amount of experience they had with the different filters in the course of the present experiment. Nevertheless, it is concluded that the nonlinear filter does promote quick, nonoscillatory system response, and that it deserves further consideration.

In the present investigation, the filters were not located inside any stability augmentation loops. The intention was that the filters be inside only pilot loop closures, and, therefore, the airplane was represented as having no stability augmentation. Even if the airplane did include stability augmentation, the intention is to locate the filter outside these loops.

The nonlinear filter was also tried on the aileron control system. Tests were made both with pilot models in an analytical study and with real pilots in the simulation study. In each situation it was found that a small amount of rate restriction caused a very noticeable deterioration in the stability of the system response. For this reason the use of the nonlinear filter, as defined in this study, is recommended for use only in the elevator control system.

In the present investigation, the rate limit in the nonlinear filter was set individually for each aircraft configuration, and was a different value for each aircraft. This situation would indicate that if the nonlinear filter were to be used in an airplane which had a large flight envelope the rate limit value would have to be scheduled as a function of flight conditions to achieve the best results possible. This scheduling problem was bypassed in the present investigation.

During the course of the present study there were no instances found where the nonlinear filter caused a divergent oscillation to occur in an attitude control task. However, there were cases involving altitude control in which pilot induced unstable oscillations did occur. In the pilot model analytical study, it was found that a rate restriction in the nonlinear filter which did not cause an unstable oscillation in the attitude change task would cause an unstable oscillation in the altitude change task if the pitch angle command limit was not included in the pilot model. Including the pitch angle command limit would eliminate the problem. In the simulation study it was found that using a rate limit in the nonlinear filter greater than the value reported in this study would cause pilot induced unstable oscillations to occur in altitude control tasks. Figure 9b is an example of a borderline case. It is concluded that a rate restriction that is too great must be avoided. The critical tasks where trouble might arise are tasks that require rapid and accurate altitude regulation. Formation flying, short range air-to-air combat, and landing are examples of such tasks. It is felt that large altitude changes such as are required in navigation tasks, but which do not require rapid and accurate response, would not be critical.

CONCLUDING REMARKS

Analytical studies using pilot models and simulation studies using pilot subjects has lead to the following conclusions on the usefulness of a nonlinear, rate limited, pilot pitch control filter.

1. The nonlinear filter will promote rapid competion of maneuvers while minimizing the oscillatory motion involved in the maneuver. Time history records obtained with pilot subjects show that the nonlinear filter allows better system response than does either a linear, first order filter, or the absence of any filter.

2. The differences between the nonlinear filter, the linear filter, or no filter were too small to be detected by the pilots in the short study of this investigation.

3. The pilot model analytical study confirmed the conclusion that the nonlinear filter will promote rapid completion of maneuvers, and indicated that the superiority of the nonlinear filter is due to the fact that it introduces less lag into the system than does the linear filter, and also attenuates the pilot's remnant better than does the linear filter.

4. The study showed that the rate limit in the nonlinear filter can be set to produce a rate restriction that is too great and will cause a system instability. The pilot model analysis was useful in establishing a safe rate limit.

REFERENCES

1. Adams, James J. and Bergeron, Hugh P.: A Synthesis of Human Response in Closed-Loop Tracking Tasks. NASA TN D-4842, October 1968.
2. Mathews, Charles W.; Talmage, Donald B.; and Whitten, James B.: Effects on Longitudinal Stability and Control Characteristics of a B-29 Airplane of Variations in Stick-Force and Control Rate Characteristics Obtained Through Use of a Booster in the Elevator-Control System. NACA TN 2238, January 1951.
3. Schmidt, Stanley F. and Triplett, William C.: Use of Nonlinearities to compensate for the Effects of a Rate-Limited Servo on the Response of an Automatically Controlled Aircraft. NACA TN 3387, January 1955.

APPENDIX A

Equations of Motion for the Simulation Study

The equations of motion used for the pilot simulation experiment were:

$$A_x = 0$$

$$A_y - V_{x_0} Y_\beta \beta$$

$$A_z = - V_{x_0} (L_\alpha \alpha - L_0)$$

$$\dot{p} = L'_p p + L'_\beta \beta + L'_r r + L_{\delta_\alpha} \delta_\alpha$$

$$\dot{q} = M_\alpha \alpha + M_q q + M_{\delta_e} \delta_e$$

$$\dot{r} = N'_r r + N'_\beta \beta + N'_p p + N'_{\delta_r} \delta_r$$

$$\dot{\phi} = p + q \sin\phi \tan\theta + r \cos\phi \tan\theta$$

$$\dot{\theta} = q \cos\phi - r \sin\phi$$

$$\dot{\psi} = \frac{r \cos\phi + q \sin\phi}{\cos\theta}$$

$$\xi_1 = \cos\psi \cos\theta$$

$$m_1 = \cos\psi \sin\theta \sin\phi - \sin\psi \cos\phi$$

$$n_1 = \cos\psi \sin\theta \cos\phi + \sin\psi \sin\phi$$

$$\xi_2 = \sin\psi\cos\theta$$

$$m_2 = \sin\psi\sin\theta\sin\phi + \cos\psi\cos\phi$$

$$n_2 = \sin\psi\sin\theta\cos\phi - \cos\psi\sin\phi$$

$$\xi_3 = -\sin$$

$$m_3 = \cos\theta\sin\phi$$

$$n_3 = \cos\theta\cos\phi$$

$$\dot{V}_x = \xi_1 a_x + m_1 a_y + n_1 a_z$$

$$\dot{V}_y = \xi_2 a_x + m_2 a_y + n_2 a_z$$

$$\dot{V}_z = \xi_3 a_x + m_3 a_y + n_3 a_z + g$$

$$u = \xi_1 V_x + \xi_2 V_y + \xi_3 V_z$$

$$v = m_1 V_x + m_2 V_y + m_3 V_z$$

$$w = n_1 V_x + n_2 V_y + n_3 V_z$$

$$V = (V_x^2 + V_y^2 + V_z^2)^{1/2}$$

$$\alpha = \tan^{-1}\frac{w}{u}$$

$$\beta = \sin^{-1}\frac{v}{V}$$

These additional symbols are used in these equations.

a_x, a_y, a_z	body axis components of acceleration, m/sec^2
u, v, w	body axis components of velocity, m/sec
V_x, V_y, V_z	inertial axis components of velocity, m/sec
p, r	rolling and yawing velocity, rad/sec
β	sideslip angle, rad
δ_a, δ_r	aileron and rudder deflection, rad
ψ, ϕ	yaw and roll angle, rad
M_x	rolling moment, N-m
L_0	$\frac{g}{V_{x_0}}$ per sec
L_i'	$\left(1 - \frac{I_{xz}^2}{I_x I_z}\right)^{-1} \left(L_i + \frac{I_{xz}}{I_x} N_i\right)$ $(i = \beta, p, r, \delta_a, \delta_r)$
L_p	$\frac{1}{I_x}\frac{\partial M_x}{\partial p}$ per sec
L_r	$\frac{1}{I_x}\frac{\partial M_x}{\partial p}$ per sec

L_β	$\frac{1}{I_x}\frac{\partial M_x}{\partial\beta}$ per sec^2
L_{δ_a}	$\frac{1}{I_x}\frac{\partial M_x}{\sigma\delta a}$ per sec^2
M_z	yawing moment, N-m
N_i'	$\left(1 - \frac{I_{xz}^2}{I_x I_z}\right)^{-1}\left(N_i + \frac{I_{xz}}{I_z}L_i\right)$ $(i = \beta, p, r, \delta_r, \delta_a)$
N_p	$\frac{1}{I_z}\frac{\partial M_z}{\partial_p}$ per sec
N_r	$\frac{1}{I_z}\frac{\partial M_r}{\partial_r}$ per sec
N_β	$\frac{1}{I_z}\frac{\partial M_z}{\partial\beta}$ per sec^2
N_{δ_a}	$\frac{1}{I_z}\frac{\partial M_z}{\partial\delta_a}$ per sec^2
F_y	side force, N
Y_p	$\frac{1}{mV}\frac{\partial F_y}{\partial_p}$
Y_r	$\frac{1}{mV}\frac{\partial F_y}{\partial_r}$
Y_β	$\frac{1}{mV}\frac{F_y}{\partial\beta}$ per sec
I_x, I_z	moments of inertia, kg-m^2
I_{xz}	product of inertia, Kg-m^2

$L_\beta' = -42.14$

$L_p' = -2.74$

$L_r' = 2.058$

$N_\beta = 5.54$

$N_p' = .0148$

$N_r' = -.278$

$Y_\beta = -.159$

$N_{\delta_r}' = -10.0$

$L_{\delta_r}' = -10.0$

TABLE I

AIRCRAFT STABILITY DERIVATIVES AND

OPEN AND CLOSED LOOP CHARACTERISTICS

	AIRCRAFT CONFIGURATION		
Parameter	Medium Speed Aircraft	High Speed Aircraft	Low Speed Aircraft
V_{x_0}	214.	305.	122.
L_α	1.3	1.3	0.6
L_0	.0461	.0322	.0805
M_α	- 15.2	- 97.8	- 2.36
M_q	- 3.70	- 1.70	- 4.40
M_{δ_e}	- 10.0	- 10.0	- 10.0
ω^2_{sp}	20.	100.	5.
$2\omega^2_{sp}$	5.	3.	5.
ω_{sp}	4.48	10.	2.24
ζ_{sp}	.55	.15	1.11
	PILOT-MODEL, AIRCRAFT SYSTEM ALTITUDE CONTROL CHARACTERISTICS		
K_θ	24.	60.	15.
λ	- .890	- .567	- .526
ω_c	3.92	9.30	2.75
ζ_α	.10	.11	.10
ω_δ	7.55	6.25	7.25
ζ_δ	.89	.83	.96

TABLE I - CONTINUED

	PILOT-MODEL, AIRCRAFT ALTITUDE CONTROL CHARACTERISTICS		
Parameter	Medium Speed Aircraft	High Speed Aircraft	Low Speed Aircraft
K_θ	24.	60.	15.
K_h	2.	2.	1.
ω_h	1.35	1.02	.740
ζ_h	.125	.103	.244
ω_α	3.85	9.33	2.67
ζ_α	.156	.224	.133
ω_δ	7.55	6.47	7.29
ζ_δ	.89	.82	.95

TABLE II

ROOT-MEAN-SQUARE ALTITUDE ERROR IN THE
SINUSOIDOL ALTITUDE COMMAND TASK

Pilot Model Results
Normalized Error

Aircraft Configuration	Filter Configuration		
	No Filter	Nonlinear Filter	Linear Filter
Medium Speed	100	105.5	105.5
High Speed	100	94.	93.
Low Speed	100	90.5	90.

Piloted Results, Subject G
Error in Meters
Medium Speed Aircraft

Trail	No Filter	Nonlinear Filter	Linear Filter
1	12.2	12.8	11.5
2	9.9	6.9	8.5
3	6.2	7.6	6.8

High Speed Aircraft

1	9.7	8.7	8.8
2	9.7	5.8	8.4
3	8.2	6.6	8.4

Low Speed Aircraft

1	30.0	20.8	25.0
2	24.6	20.2	21.1
3	21.7	21.0	27.7

TABLE III

PILOT RANKING OF THE THREE
FILTER CONFIGURATIONS

Medium Speed Aircraft

Pilot	Filter Configuration		
	No Filter	Nonlinear Filter	Linear Filter
P	3	1	2
K	2	3	1
E	1	2	3

High Speed Aircraft

P	2	2	1
K	1	3	2
E	3	1	2

Low Speed Aircraft

All Filters were ranked equal by all pilots

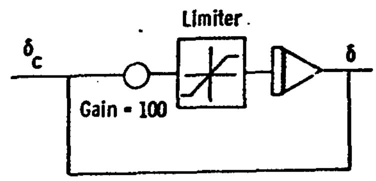

Sketch. - Nonlinear filter

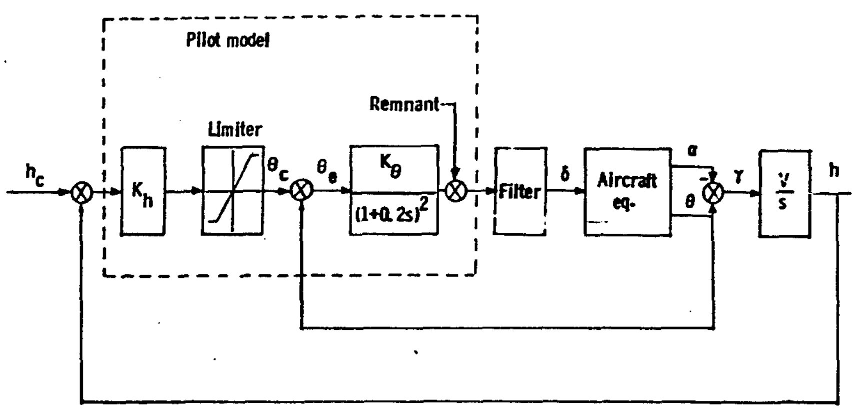

Figure 1. - Block diagram of pilot-model, Aircraft system.

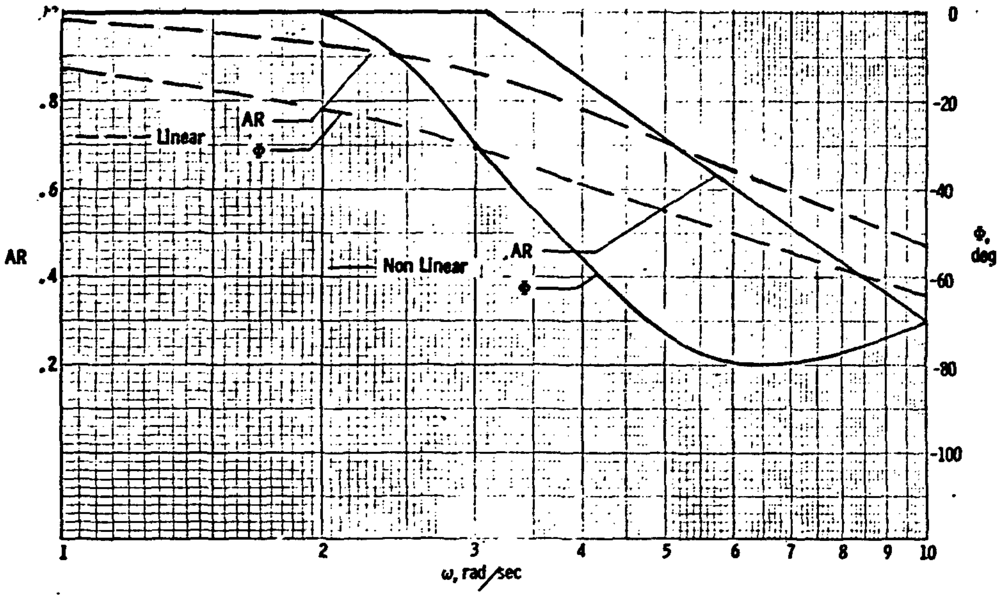

(a) Comparison of nonlinear and linear filter.

Figure 2. Filter frequency response.

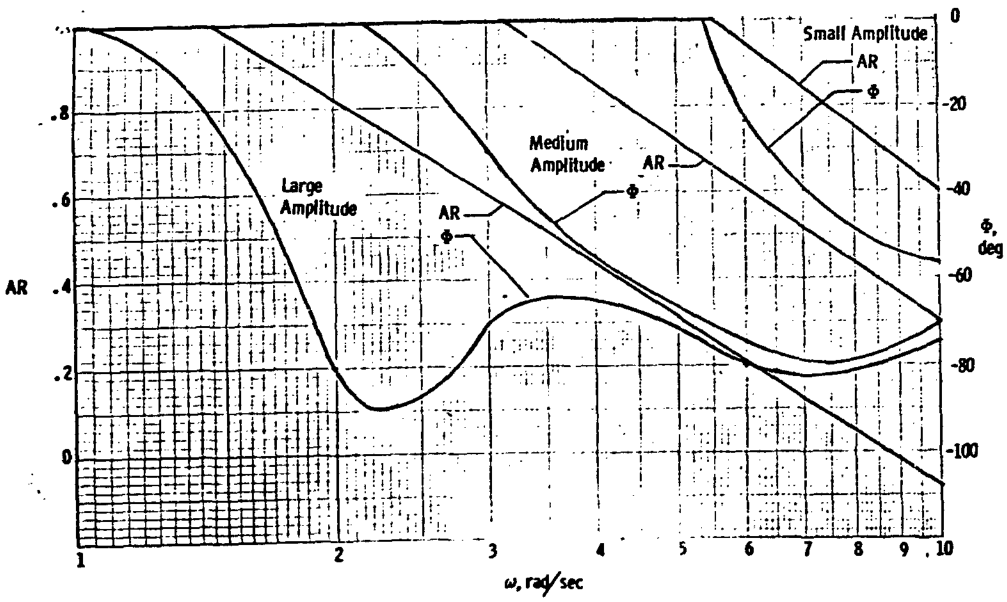

(b) Nonlinear filter with three different input amplitudes.

Figure 2. Concluded.

ORIGINAL PAGE IS
OF POOR QUALITY

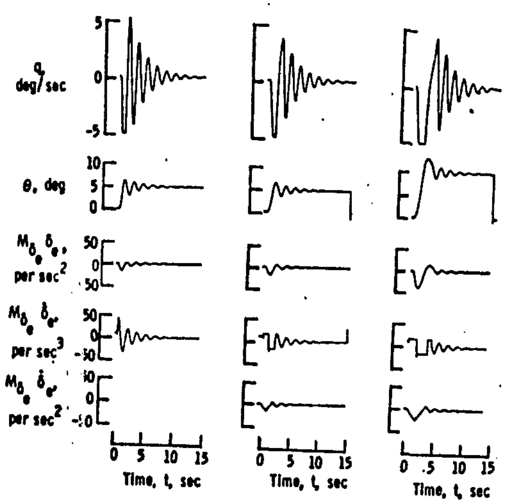

Figure 3. - Effect of nonlinear rate limit on system stability. Medium speed aircraft.

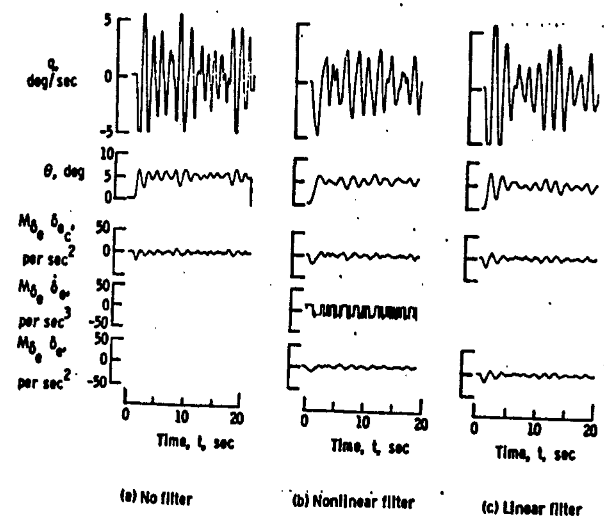

Figure 4. - Step pitch angle change, medium speed aircraft

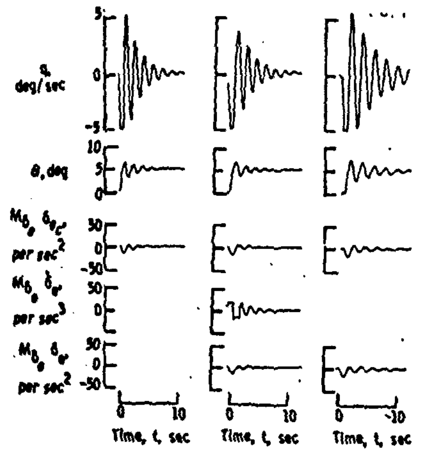

(a) No filter (b) Nonlinear filter (c) Linear filter

Figure 5. - Step pitch angle change, medium speed aircraft, remnant ommitted from pilot model.

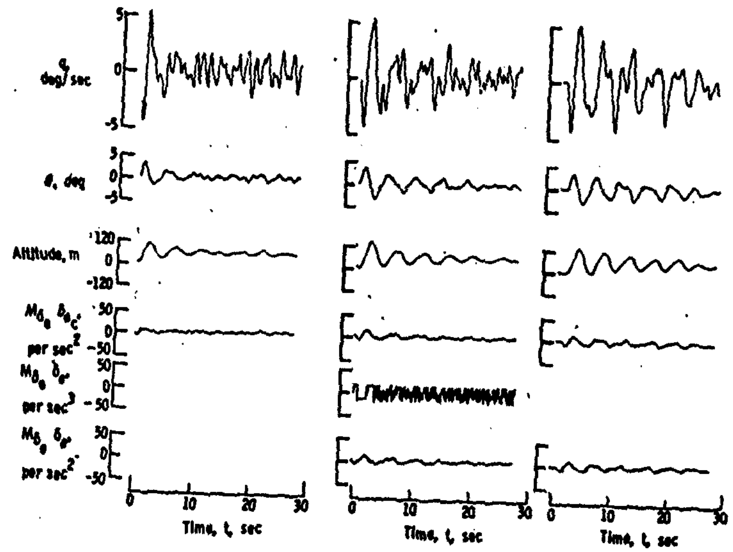

(a) No filter (b) nonlinear filter (c) Linear filter

Figure 6. - Step altitude change, medium speed aircraft.

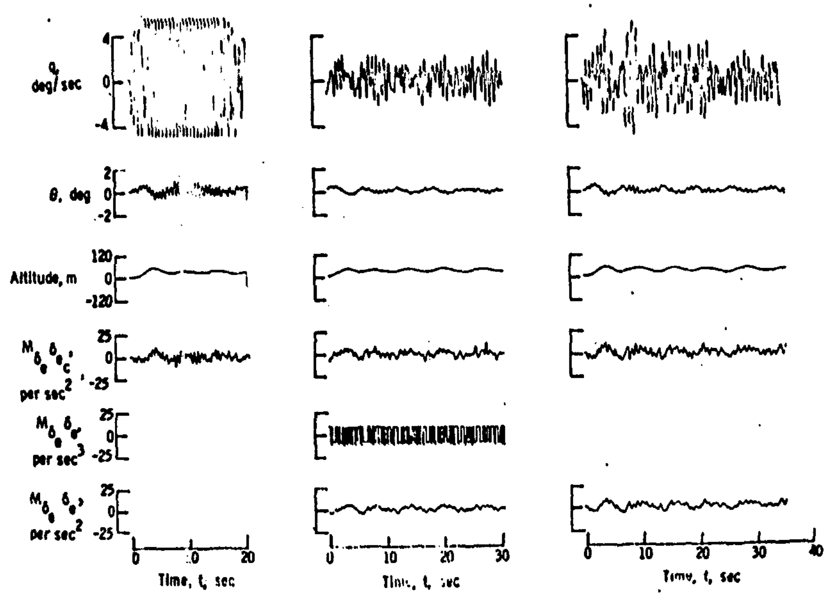

Figure 7. - Step altitude change, high speed aircraft.

ORIGINAL PAGE IS OF POOR QUALITY

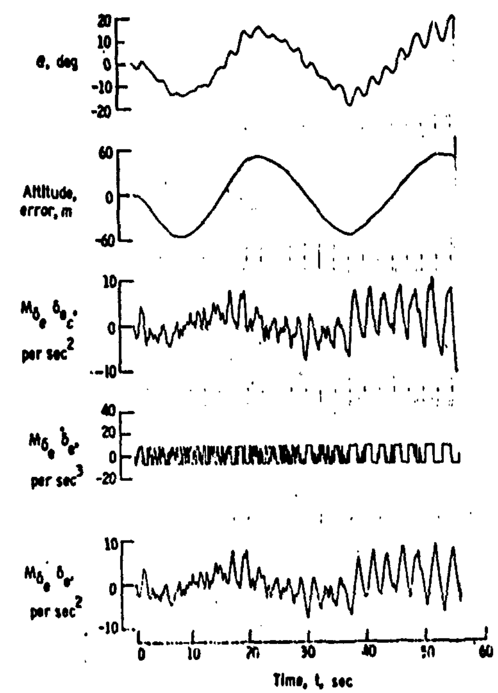

Figure 8. - Sinusoidal altitude command, low speed aircraft.
h_c = 120 cos. 21t-120

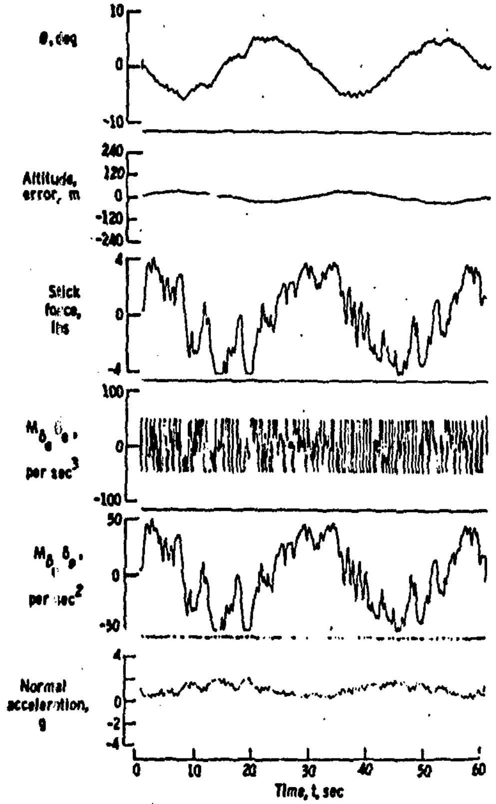

(a) Large rate limit in nonlinear filter

Figure 9. - Sinusoidal altitude command, high speed aircraft, $h_c = 120 \cos .21t - 120$

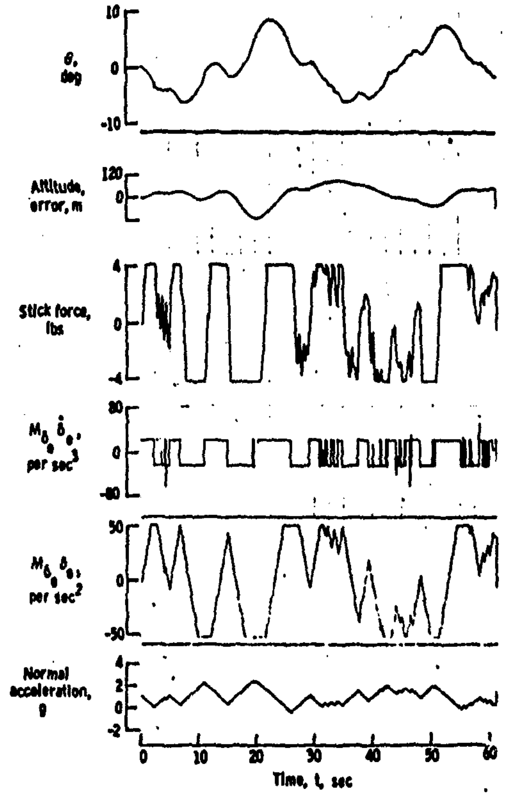

(b) Low rate limit in nonlinear filter

Figure 9. - Concluded

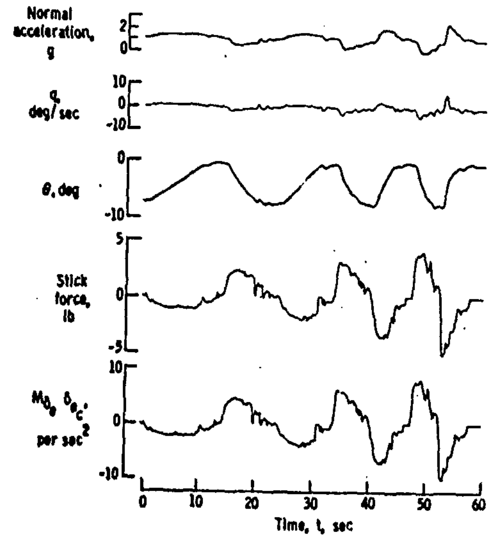

(a) No filter

Figure 10. - Step pitch angle change, pilot P, medium speed aircraft.

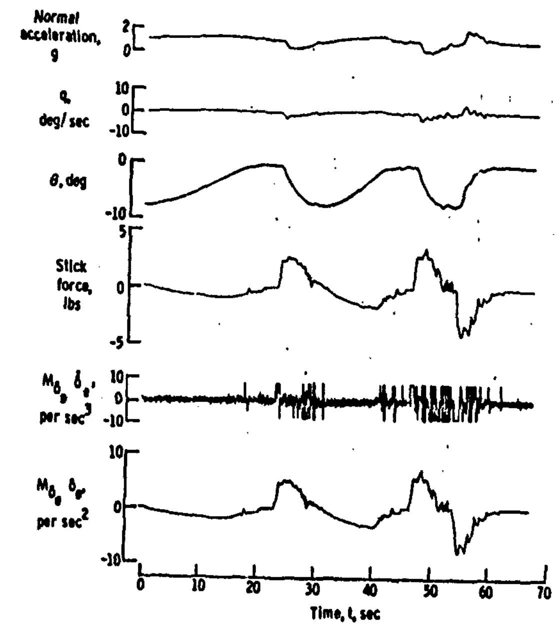

(b) Nonlinear filter

Figure 10. - Continued

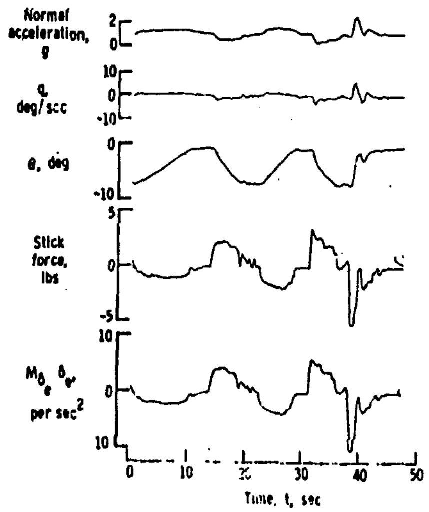

(c) Linear filter

Figure 10. - Concluded.

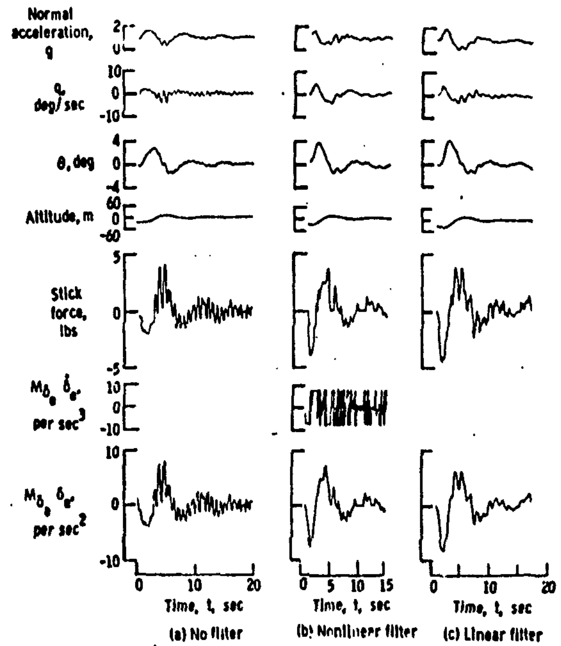

Figure 11. - Step altitude change, pilot F, medium speed aircraft.

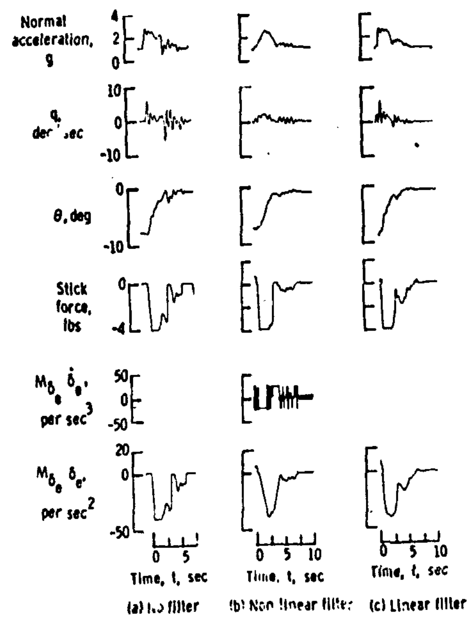

Figure 12. - Step pitch angle change, pilot P, high speed aircraft.

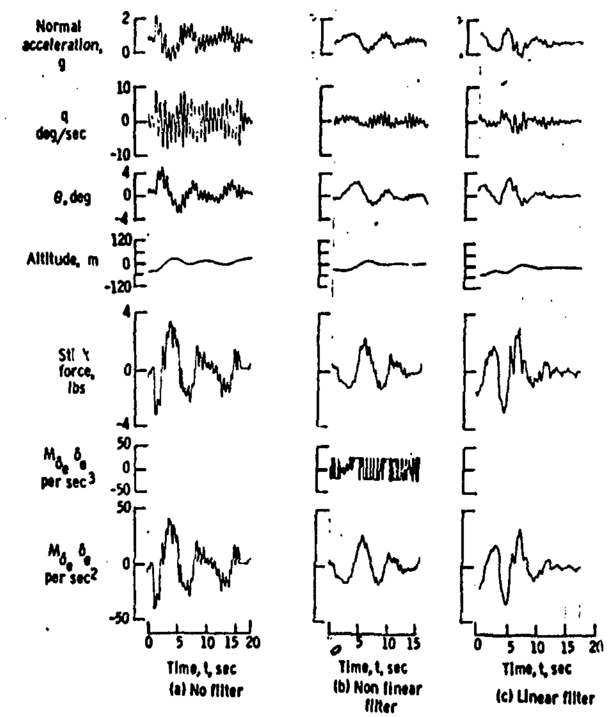

Figut Figure 13. - Step altitude change, pilot P, high speed aircraft.

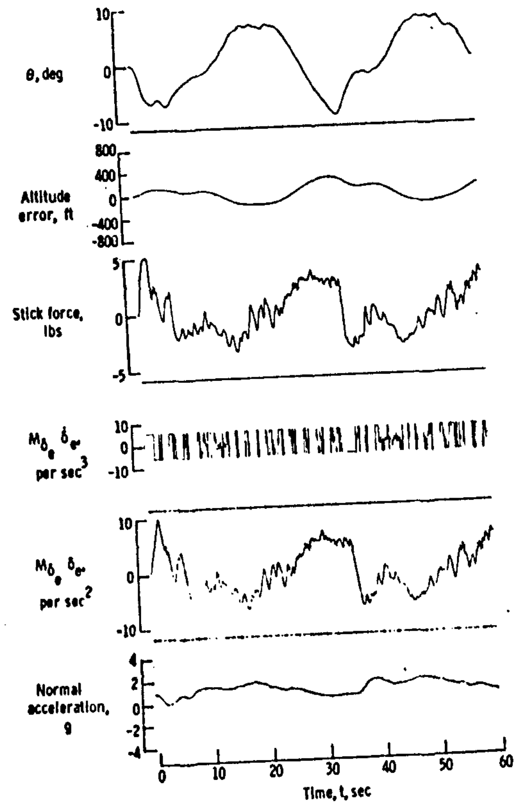

Figure 14. - Sinusoidal altitude command, low speed aircraft.

N79-17516

EVALUATION OF KINESTHETIC-TACTUAL DISPLAYS USING A CRITICAL TRACKING TASK[1]

by

Richard J. Jagacinski, Dwight P. Miller, Richard D. Gilson, and Robert T. Ault

Departments of Psychology and Aviation
Human Performance Center
The Ohio State University
Columbus, Ohio

ABSTRACT

The present study sought to investigate the feasibility of applying the critical tracking task paradigm to the evaluation of kinesthetic-tactual displays. Four subjects attempted to control a first-order unstable system with a continuously decreasing time constant by using either visual or tactual unidimensional displays. Display aiding was introduced in both modalities in the form of velocity quickening. Visual tracking performance was better than tactual tracking, and velocity aiding improved the critical tracking scores for visual and tactual tracking about equally. The present results suggest that the critical task methodology holds considerable promise for evaluating kinesthetic-tactual displays.

INTRODUCTION

In an effort to alleviate the high levels of visual and auditory work load typically involved in aircraft control, a number of different tactual displays have been explored for presenting information to the skin. For example, stick shakers have served for a number of years as an effective means of alerting a pilot to a potentially dangerous situation.

More recently, techniques for providing control feedback by impressing stimulation onto the skin have been investigated, including matrices of air jets (Seeley & Bliss, 1966), arrays of vibrotactile elements (Triggs, Levison, & Sanneman, 1973), and arrays of electrocutaneous stimulators (Schori, 1970). Although these techniques provide a wide flexibility for patterns or codes, a close, invariant proximity between the stimulators and the skin is required for good tracking performance.

An alternative method is to allow the natural manipulations by the fingers of embossed display features, as with braille letters. Accordingly, a feedback control technique developed by Fenton (1966) employed essentially a variable height "braille dot" to indicate tracking error. The display consisted of a servo-controlled slide embedded in a control handle (see Figure 1). The slide protrudes fore and aft from the handle corresponding to unwanted positive and negative errors. The operator follows the slide in the direction in which it protrudes until the error is nullified and the slide returns to the flush position in the control handle. In essence, the display provides continuous information relative to single-axis compensatory tracking.

Experimental investigations of this display have included numerous multitask simulator studies conducted by Fenton and Gilson since 1966 (Fenton, 1966; Fenton & Montano, 1968; Gilson & Fenton, 1974) as well as actual automobile and aircraft control investigations. The full scale vehicular control studies have validated the tactual display as both a practical and effective supplement to tasks with high visual loading, i.e., close headway car following (Fenton, 1966) and aircraft ground reference and landing maneuvers (Gilson & Fenton, 1974; Gilson, 1976).

Up to now, given that visual displays are traditionally the primary source of control information, little work has been carried out to assess the utility of the tactual display as the sole source of control feedback. However, in order to study and optimize features inherent in the display itself, a sensitive, reliable, and valid single-task tracking measure is required for systematic parametric investigations.

The present study was undertaken to test the feasibility and reliability of a methodology developed by Jex, McDonnell, and Phatak (1966) with this tactual display as the sole source of information in a progressively more difficult single-task compensatory tracking situation. In addition, the validity and sensitivity of the methodology was tested by (a) comparing performance on the same task with a single-dimensional visual display and by (b) examining the visual and tactual displays with and without aiding information. The inclusion of the visual display provided a comparison of performance on the present tracking system with the previous work of Jex and others. Aiding was used as the primary intra-modality variable because previous work (Fenton, 1966) has shown it to have a strong influence on tracking performance.

The critical tracking task developed by Jex, McDonnell, and Phatak (1966) requires a subject to stabilize a first-order unstable system. The time constant of the unstable system is made progressively shorter until the subject finally loses control. The value of the time constant at the point where control is lost is a measure of the subject's tracking ability with the given display and control device. The inverse of this critical

[1]This research is sponsored by the U.S. Army Air Mobility Research and Development Laboratory monitored through NASA-Ames grant NSG-2179.

D41

value is referred to as the critical root, λ_C, which has been shown to be a sensitive measure of performance (Jex & Allen, 1970). Other properties of this measure which recommend its use in display evaluations are low run-to-run variability and a strong correlation with subject's effective time delay in tracking with fixed values of λ less than λ_C.

In addition to testing the critical task with visual and tactual displays, the present experiment also tested those displays with and without aiding in the form of velocity quickening. Fenton (1966) and Hirsch (1973) have demonstrated the usefulness of providing aiding in tactual displays when they are used to supplement unaided visual displays. However, the usefulness of aiding in tactual displays used as a sole source of information remained to be investigated. The present experiment compared the relative usefulness of aiding for visual and tactual displays in an attempt to determine differences in information processing between the visual and tactual modalities and to compare the sensitivity and validity of the critical task methodology.

METHOD

Apparatus

The kinesthetic-tactual display consisted of a rectangular section of the cylindrical control handle which moved vertically through the handle to indicate the direction and magnitude of the system error (Figure 1). The rectangular section was 2.1 x 1.9 cm and the diameter of the handle was 6.2 cm. The frequency response of the display had an amplitude ratio which was down 3 dB at a frequency of 8 Hz when tested with input signals having a peak about 20% of maximum.

The visual display depicted system error as a 2 mm diameter green dot of light moving vertically on a Tektronix Type 602 CRT display. A 2 x 10 mm marker attached horizontally at the vertical center of the oscilloscope screen extending to the right of horizontal center served as the reference for zero error.

The control stick consisted of a lever arm, 40 cm long from display to pivot point. It moved through a vertical plane orthogonal to the planes of the chair seat and back, and range of angular travel was restricted to 30 degrees above horizontal with 15 degrees above horizontal representing the neutral control position. The lever was pivoted 38 cm above the floor, 8.5 cm from the left side of the chair seat and even with the chair back. Friction was maintained at a nominal level and the display handle was counterbalanced so that no force was necessary to maintain the angular position of the lever. The chair seat was 46 cm from the floor, positioned so that the operator's eyes were 24 in (61 cm) from the center of the visual display screen.

The simulation was performed on an Electronics Associates Incorporated PACE TR-48 analog computer. Logic for integrator control, comparator control, and trial event sequencing was supplied by BRS/LVE logic modules programmed through a patchboard.

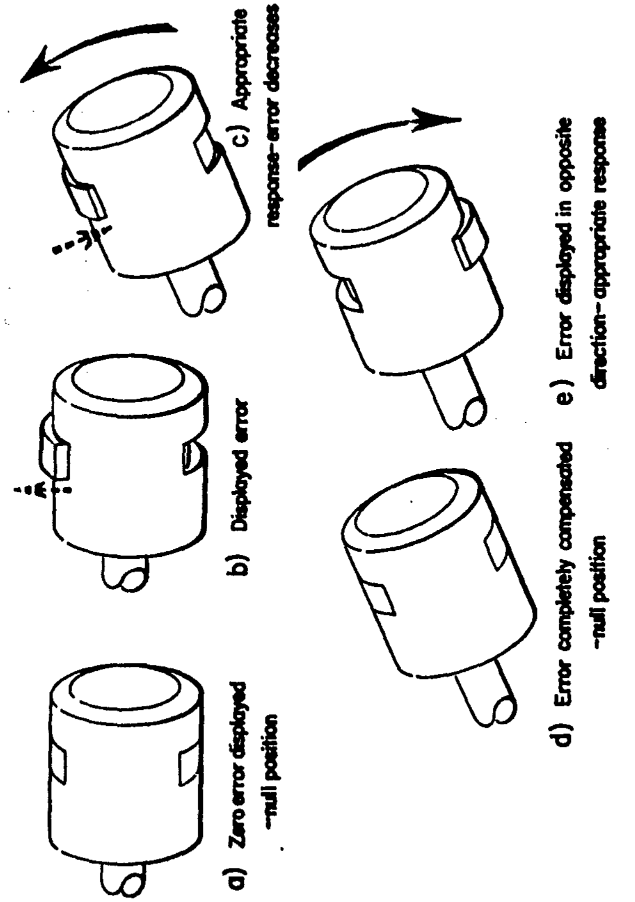

Figure 1. Control/display relationship for KT display.

A Sanborn Model 320 two channel strip chart recorder was used to monitor and record system error and control response. The subjects performed in an isolated 5 x 7 ft (2.1 x 1.5 m) room lit only by the CRT scale illuminator.

Control System Implementation

The first-order unstable system was controlled by the position of the control stick (Figure 2) which was operated in a manner similar to a helicopter collective. No forcing function was used because the operator's inherent variability or "remnant" in positioning the lever arm provided sufficient input to excite the controlled element. The system output, or error, was displayed as either a vertical displacement of a small round dot on a CRT (visual), or as a vertical displacement of a section of the control lever handle (kinesthetic-tactual). The critical task employed an autopaced instability function (Jex, McDonnell & Phatak, 1966) such that on each trial the initial instability was zero (λ_{IC}), but linearly increased rapidly over time as long as good control was maintained (λ_H). When sufficient difficulty was encountered, the rate was reduced to .25 λ_H for the remainder of the trial (λ_L). The error criterion for switching lambda rates, e_C, was specified as 10% of the maximum allowable error (e_{max}), filtered through a 1-second time constant. The two lambda rates (λ_H and λ_L), which were used both in the visual and tactual display modes, were chosen so that a typical trial lasted between 30 and 75 seconds, just long enough to provide a reliable measure of critical instability. Loss of control was defined as the displayed system output going off scale (e_{max}) and the resulting dependent measure was the level of lambda attained at the trial's conclusion (λ_C). In the velocity aided conditions the aiding ratio of error velocity ($\dot{e}$) to error position (e) was 1:1. In order to make the total display ranges of aided and unaided displays comparable, the aided signal was scaled down by 50% so that the effective signal was $\frac{1}{2}(e + \dot{e})$. (See Table 1 for a detailed summary of system parameters.)

<u>Subjects</u>

Subjects were four students (two male and two female) at The Ohio State University who were randomly selected from the eight highest scoring subjects of 16 on a visual critical tracking pretest. The 16 subjects were paid \$2.50 for the pretest. The four selected subjects were paid \$2.50 per session for the first four subsequent sessions; the subject with the highest average score also received a \$5.00 bonus. On the last four sessions, subjects were paid a base rate of \$1.00 plus 1.67¢ x λ_C for each trial.

<u>Procedure</u>

<u>Pretest</u>: Sixteen subjects received 25 trials on a visual critical tracking task. Subjects heard 72 dBA white noise through a set of monaural headphones except when spoken to by the experimenter over an intercom. Before the first trial subjects centered the control stick with verbal feedback from the experimenter and were instructed to center it before each subsequent trial. There was no feedback after the beginning of the first trial. Each trial was preceeded by a ½ second 400 Hz warning tone, a 3-second interval, and a ½-second start tone. At the start tone, a green

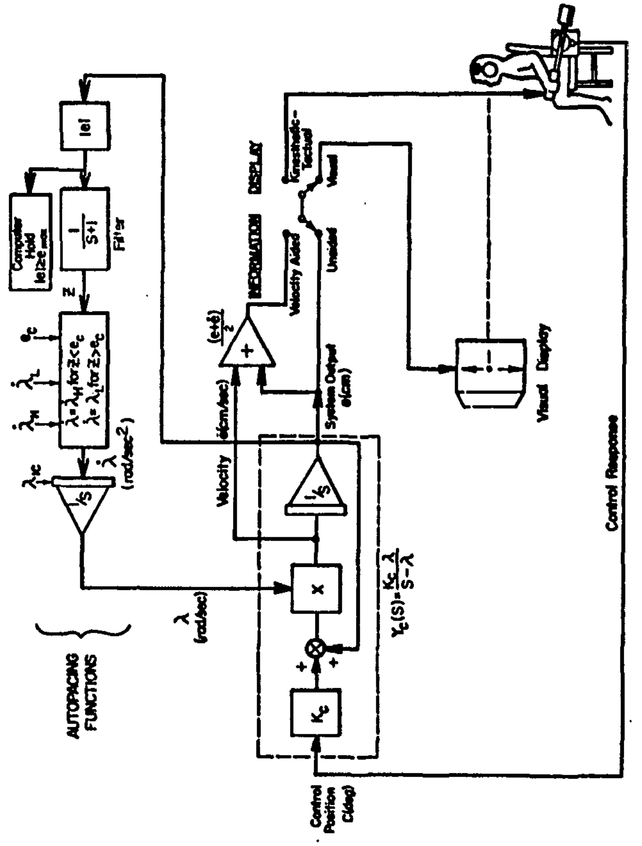

Figure 2. Control system implementation for visual and tactual critical tracking task.

Control System and Display Parameters	Units	Pretest	T	TA	V	VA
K_c - control-display sensitivity	cm/deg	.4	04	.04	.2	2
e_{max} - maximum allowable error	cm	±4 0	±.4	±.4	±2.0	±2 0
corresponding total degrees visual angle	degrees	7 5	NA	NA	3.75	3.75

Autopacing Parameters	Units	Pretest	T	TA	V	VA
λ_{IC} - initial value of unstable root	rad/sec	0	0	0	0	0
$\dot{\lambda}_H$ - initial (high) λ rate	rad/sec^2	2	.15	.15	15	15
$\dot{\lambda}_L$ - final (low) λ rate	rad/sec^2	05	0375	0375	0375	.0375
e_c - error criterion for switching $\dot{\lambda}$	cm	4	04	04	.2	2
T_f - error criterion time constant	sec	10	1.0	1 0	1 0	1 0

Control Stick Parameters	Units	All Conditions
maximum deflection	degrees	±15 0
nominal required force	N	20

Table 1. Control systems parameters.

dot appeared at the center of the CRT display, moving vertically. Subjects were instructed to move the control stick opposite to the direction of the displayed error in order to keep the dot centered. When the displayed error reached ± 4.0 cm there was a 2-second tone which indicated the end of the trial and the dot disappeared from the screen. There was a 10-second interval between trials. The median value of λ_c for the last seven trials was used to select the top eight subjects.

Test: Four subjects were randomly selected from the top eight subjects and were each tested in the following display conditions on each day of the experiment:

1. visual unaided (V) - error displacement on CRT;
2. visual aided (VA) - error displacement + error velocity on CRT;
3. kinesthetic-tactual unaided (T) - error displacement in control handle;
4. kinesthetic-tactual aided (TA) - error displacement + error velocity in control handle.

Subjects received a block of 15 trials in each condition on each day with a 2-minute rest between blocks (60 trials per day). The four conditions were presented to the four subjects in a Latin square design with a different Latin square selected each day of the 8 days.

Subjects were instructed to move the control stick in the same direction as the displayed error (Figure 1) in the two tactual conditions. The direction of the displayed error was selected to be compatible with the direction of appropriate control response. The visual display was inoperative during all tactual display conditions. Subjects centered the control stick with verbal feedback and were told which condition they would be receiving before each block of trials. The beginning and end of each trial was signalled with the same tone sequence used in the pretest. Subjects were given no further feedback for the first 4 days. During the last 4 days, subjects were verbally informed of the value of λ_c they had just achieved during the intertrial interval.

RESULTS

Medians of 15-trial blocks were averaged across subjects and plotted over days for each of the four conditions in Figure 3. At no point during the 8 days did the ordinal relationship of display conditions change. The best tracking performance was attained in the VA condition, followed in order by conditions V, TA and T.

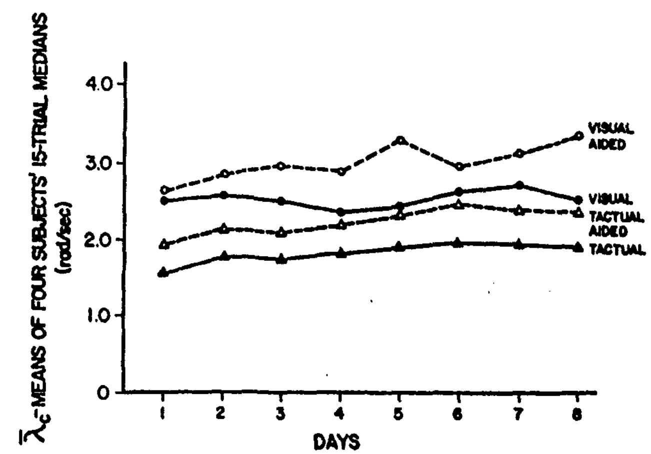

Figure 3. Average performance of four subjects over eight days of tracking.

A four-way (modality x aiding x subjects x days) analysis of variance for the last four days' performance yielded highly significant main effects for both modality, $F(1,3)=39.2$, $p<.01$ and velocity aiding, $F(1,3)=44.9$, $p<.01$. The visual modality was found to be superior to the tactual modality, and velocity aiding improved performance in both modalities. No interaction was found between modality and aiding, nor for any other factor combinations ($p>.65$). The additive nature of modality and aiding effects is displayed in Figure 4 which shows the mean and standard deviation for each condition averaged across subjects and days. The main effect of days was found to be non-significant ($p>.97$), indicating stable performance over the four days analyzed. Four two-way analyses of variance (subjects x days) were performed to recover variance estimates for each of the four conditions. The VA condition had a higher standard deviation ($SD=.696$ rad/sec) than the other conditions which ranged from .202 to .291 rad/sec.

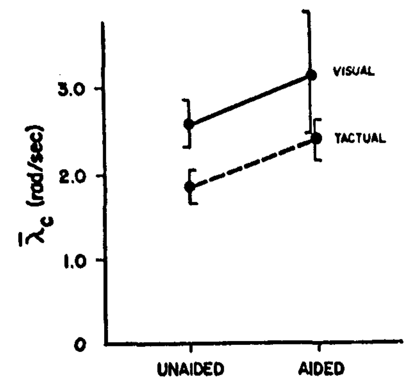

Figure 4. Means and standard deviations of λ_c in four conditions.

Sample time traces of two subjects' tracking behavior have been included to demonstrate qualitative aspects of their control responses (Figures 5 and 6). Each of the samples displays system output, e, (top) and control response, c, (bottom) as a function of time. The range of payments to subjects on Days 5 - 8 was from \$3.07 to \$3.78 per day.

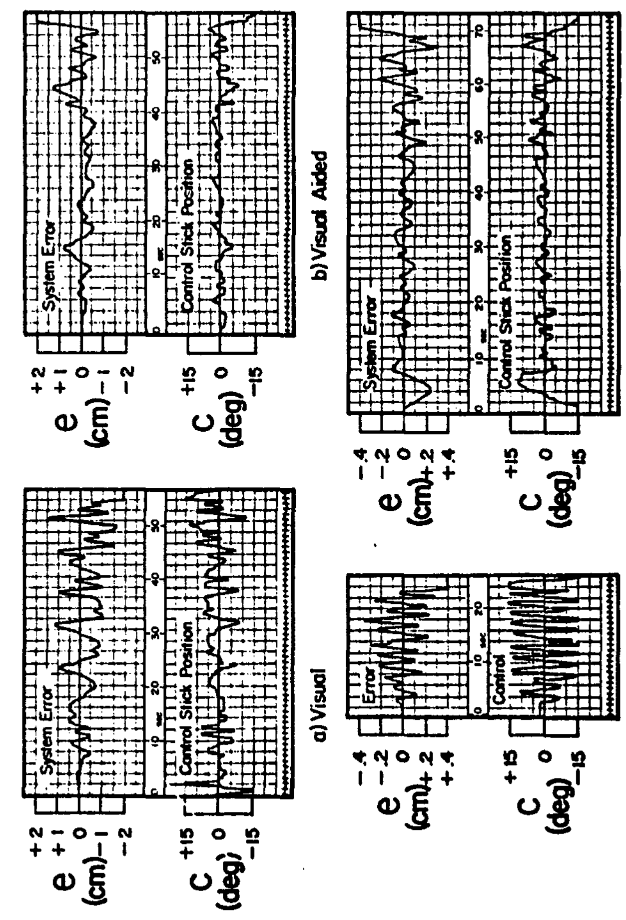

Figure 5. Time history of sample trials in each of four conditions: Subject 1, Day 8.

In questionnaires and interviews after the final sessions, two subjects indicated that using a loose grip was important in tactual tracking, while the others stressed anticipation of display movement. Three subjects thought the tactual S-R compatibility was optimal, while one would have liked the reverse relationship.

DISCUSSION

The results indicate that the critical task is both a feasible and reliable methodology for assessing tactual tracking with the above described tactual display. The feasibility is apparent in the fact that subjects performed this task with no particular difficulties despite the fact that the tactual display was novel and no pretraining trials were employed. Reliability of the methodology for tactual tracking is evident in: the smoothness of the plot of performance as a function of days in the experiment (Figure 3); the consistent ordinal relationship between testing conditions; and the relatively small standard deviation associated with the mean performance scores with the tactual display as compared to the visual display (Figure 4). Additionally, the lack of any significant effects of days in the analysis of variance carried out on the performance scores for Days 5 - 8 indicates that subjects had achieved asymptotic performance levels in all four display conditions tested.

That the critical tracking methodology is both as sensitive and valid a measure of tactual tracking as visual tracking is indicated by the approximately equal effects of aiding for the tactual and visual displays. This can be seen in Figure 4 and is indicated by the lack of a modality x aiding interaction in the analysis of variance. Given the considerable data base that has established the critical task as a useful measure for evaluating visual displays, the present results suggest that the same methodology is not only feasible, but a technique that holds considerable promise for evaluating tactual displays.

Although performance for the visual and tactual display conditions is surprisingly close, a direct comparison should be avoided for a number of reasons. First, neither the visual nor tactual displays used in the present study were intentionally optimized for display features. Second, although the subjects appear to have reached asymptotic levels of performance under the conditions of this experiment, a between-subjects design might yield different performance levels.[2] Finally, a direct comparison between tactual and visual values of λ_C should be avoided because of qualitative differences in control behaviors with the two displays.

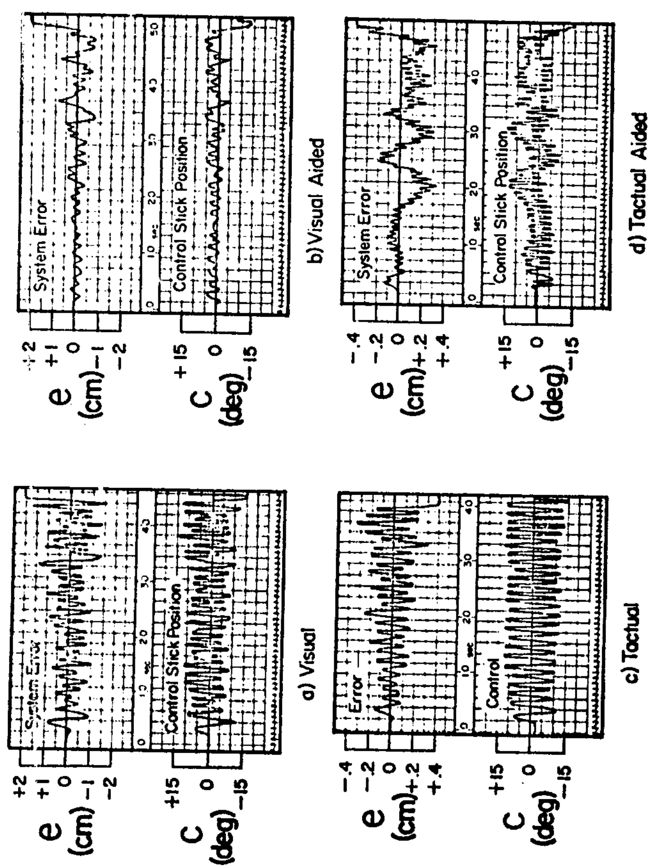

Figure 6. Time history of sample trials in each of four conditions: Subject 4, Day 8.

---

[2] A pilot experiment was carried out in addition to the main experiment wherein two additional subjects were run and achieved much higher asymptotes (λ_C= 4.4) under the tactual-aided display condition only. Thus, the lower asymptotes for the subjects in the present experiment may have been the result of interference between conditions. However, these results must be treated as pilot data for the present.

For an interpretation of the experimental effects of display quickening with visual and tactual displays, it is necessary to discuss the theoretical significance of the critical value of lambda. As determined by Jex and Allen (1970), for first, second, and third order critical tracking tasks, the inverse of the human operator's effective time delay is linearly related to the critical value of lambda. The regression equation they obtained for four practiced pilots was $\tau_e^{-1} = 1.1 + 1.2\ \lambda_C$. For the first order critical task, subjects' behavior approximated simply a gain plus time delay. For the second order tasks, subjects additionally adopted lead equalization to cancel out the lag introduced by the integration. Accordingly, with an aided visual display and a first order critical task, one would expect the human operator to introduce lag equalization to cancel out the introduction of lead.

Moreover, compensatory tracking with K and K/s plants, respectively, parallel the equalization postulated for the aided and unaided visual displays with the first-order critical task. Given that McRuer, Graham, Krendel, and Reisener (1968) observed a time delay that was .03 sec shorter for the K plant, one would similarly expect the aided display also to exhibit a shorter time delay in the first-order critical tracking experiment. In fact, if one uses the Jex and Allen regression equation to translate the critical roots obtained in the present experiment into effective time delays, the values obtained for the aided and unaided visual displays are .203 sec and .238 sec, respectively. The aided display does exhibit a time delay that is shorter by .035 sec. The closeness of this value to the .03-sec difference observed by McRuer et al. (1968) for K and K/s tracking may be fortuitous considering various differences in control devices and subject populations; however, the direction of the difference is consistent with the postulated equalization. This analysis of course assumes proportional control strategies which were in fact exhibited in the visual display conditions as exemplified in Figures 5 and 6.

Although aiding increased the critical value of lambda about equally for the visual and tactual tracking conditions, there was a strong qualitative difference in the style of tracking performance. Namely, for the unaided tactual condition, subjects' behavior more closely resembled bang-bang rather than proportional control (Figure 5). Subject 4 (Figure 6) also followed this pattern, but differed from the other three subjects in that he additionally superimposed a small amplitude, rapid oscillation or "dither" over a smoother, slower control pattern evident in the tactual aided condition. This behavior may represent an attempt to overcome deadband or other nonlinear effects associated with the tactual display. It is noted, however, that the degree of control amplitude modulation in the visual condition was relatively minimal for this subject.

Subjects typically go to non-linear behavior when they have difficulty producing the equalization necessary for stable linear control (e.g., see Hall, 1963). In the present task, this generalization suggests that subjects were unable to adopt the necessary gain plus time delay configuration for proportional control with the tactual unaided display, although they were apparently able to adopt lag equalization for the aided tactual display for which proportional control was generally exhibited.

These results suggest that in using the tactual display, subjects may always exhibit a lag if they are using proportional control. A lag would be appropriate for proportional control of the aided, but not the unaided display. If there is an unwanted lag in the tactual unaided tracking, it is important to demonstrate that the lag is not associated with the electro-mechanical construction of the tactual display. By implication the lag can then be attributed to the human subject's use of the information from the display. A Fourier analysis of the tactual tracking is presently underway to test this hypothesis.

A second point of interest with regard to the tactual tracking data is that theoretically, a linear relationship can exist between λ_C and a parameter analogous to effective time delay when the subjects exhibit a bang-bang control pattern. If the subject's control can be approximated as a regular alternation between two control values with the time between switches equal to T_e, then a phase-plane analysis reveals that the critical value of lambda will be proportional to T_e^{-1}. The proportionality constant will depend on the control value (movement amplitude x system gain) and the error criterion used to terminate the critical task trials. Jex, McDonnell, and Phatak (1966) derived a similar prediction assuming a linear control strategy in which the subject approximated a gain and time delay, τ_e. For the linear control strategy the proportionality constant between λ_C and τ_e^{-1} was unity, rather than a function of control amplitude and the error criterion.

In summary, the present results suggest that the critical task methodology will be an effective tool for evaluating tactual displays. Furthermore, the qualitative differences found between tactual and visual tracking may lead to a better understanding of the information-processing differences between these modalities.

REFERENCES

1. Seeley, H. F., & Bliss, J. C. Compensatory tracking with visual and tactile displays. IEEE Transactions on Human Factors in Electronics, 1966, 7, 84-90.

2. Triggs, T. J., Levison, W. H., & Sanneman, R. Some experience with flight-related electrocutaneous and vibrotactile displays. In F. A. Geldard (Ed.), Cutaneous Communication Systems and Devices. Austin, Texas: The Psychonomic Society, 1973.

3. Schori, T. R. Tracking performance as a function of precision of electrocutaneous feedback information. Human Factors, 1970, 12, 447-452.

4. Fenton, R. E. An improved man-machine interface for the driver-vehicle system. IEEE Transactions on Human Factors in Electronics, 1966, 7, 150-157.

5. Fenton, R. E., & Montano, W. B. An intervehicular spacing display for improved car-following performance. IEEE Transactions on Man-Machine Systems, 1968, 9, 29-35.

6. Gilson, R. D., & Fenton, R. E. Kinesthetic-tactual information presentations - inflight studies. IEEE Transactions on Systems, Man and Cybernetics, 1974, 4, 531-535.

7. Gilson, R. D. A tactual display aid for primary flight training. National Aeronautics and Space Administration, Annual Report No. NAS 2-8954, July, 1976.

8. Jex, H. R., McDonnell, J. D., & Phatak, A. V. A "critical" tracking task for manual control research. IEEE Transactions on Human Factors in Electronics, 1966, 7, 138-145.

9. Jex, H. R., & Allen, R. W. Research on a new human dynamic response test battery. Part I: Test development and validation; Part II: Psychophysiological correlates. 6th Annual NASA-Univ. Conference on Manual Control, AFIT, Wright-Patterson AFB, Ohio, 7-9 April, 1970, pp. 743-777.

10. Hirsch, J. Rate control in man-machine systems. In F. A. Geldard (Ed.), Cutaneous Communications Systems and Devices. Austin, Texas: The Psychonomic Society, 1973.

11. Hall, I. A. M. Study of the human pilot as a servo element. Journal of the Royal Aeronautical Society, 1963, 67, 351-360.

12. McRuer, D., Graham, D., Krendel, E., & Reisener, W., Jr. Human pilot dynamics in compensatory systems. Air Force Flight Dynamics Laboratory, Wright-Patterson AFB, Ohio, Tech. Rept. 65-15, January, 1965.

N79-17517

Influences of joystick spring resistance on the execution of simple and complex positioning movements 1)

Günter Rothbauer

Forschungsinstitut für Anthropotechnik (FAT)
5309 Meckenheim/Bonn, W.-Germany

Abstract

To provide good proprioceptive feedback in a manual control device for a designation task, spring resistance of a joystick was optimized by adjustment of centering force and deflection nonlinearly with each other by using the psychophysical method of cross modality matching. Designation with zero and first order systems showed that the coarse adjustment was insensitive to stick and certain task parameters, although it was influenced by some biomechanical parameters and the anticipated demands of the final control positioning. Only the more difficult fine adjustment is sensitive to parameter alterations and therefore suitable for optimization attempts. The strong centering of the stick by a nonlinear degressive spring resistance facilitates fine adjustment. Through this, total adjustment time with the first order system is reduced by more than thirty percent, compared to a linear resistance. Tracking experiments affirm the usefulness and preference of nonlinear spring resistance.

To reduce the one-sided load through visual information transmission channels in modern, complex man-machine-systems, there are basically two possibilities :

1. Reducing the complexity of visual information by selecting and integrating only the necessary information (BERNOTAT, 1970).
2. Increasing the use of nonvisual information channels.

One possible nonvisual human information channel is the proprioceptive feedback. It is especially interesting, as it is implicit in every motor action of the human operator and therefore is present anyway in every control movement. The increasing use of servo-systems in manual control, for example in airplanes or even in motor cars, makes possible the introduction of any deflection-resistance characteristic into the control. This possibility may be advantageous to system performance, if the movement resistance of the control is designed according to the psychophysiological characteristics and anthropometrical limits of the human controller.

In order to investigate the proprioceptive feedback in control movements exclusively, visual feedback must be suppressed in the experimental mock-up. So that the relation between stimuli, such as visually presented deflections of light, and proprioceptively controlled motor responses may be measured :

$$R = f(S)$$

This relationship can be understood as a simple psychophysical function and according to STEVENS (1957) it is written as a power function

$$R = S^m$$

The method of "cross modality matching" provides the means to establish a relationship between two separate response modalities R_a and R_b via one independent simulus S :

$$R_a = S^m$$

$$R_b = S^n$$

The resulting relationship between R_a and R_b :

$$R_b = R_a^{\frac{n}{m}}$$

In several experiments, the working group around STEVENS could prove empirically the adequacy of this theoretical relationship (see e.g. STEVENS, 1969).

If an event can be fed back to the operator in several sense modalities, it is appropriate, to match the intensities of stimuli to each other, according to the psychophysiological nature of the human. In cross modality experiments, this is implied through measurement of the subjects' behavior and one should expect good informational equivalency and redundancy in the matched sensory modalities.

Trying to determine the spring resistance of a control in respect to good proprioceptive feedback, one has to match perception of applied force with limb position according to the above mentioned procedure.

1) This article is based on a more extensive report by the author (see references).

D42

In psychophysical experiments with eleven subjects, matching of the motor response to the deflection of a light point on a TV-screen was investigated. One motor response was the deflection of the free-moving, the other, the applied force on the isometric joystick. A freely moving control offers no *resistance to movement*, an isometric stick offers no movement to applying force on it.

Position of the stick and applied force are matched nonlinearly to the independent signal, namely the visual perceivable jump of the light point. The subjects had no visual control of the motor activity and they were left solely to their proprioceptive feed-back.

The matching power function $R = S^n$ has an exponent n equal .7 for the free-moving stick. Remarkable is the pronounced nonlinearity with the isometric stick. The fitting power function has an exponent of .33. For comparison with data from the literature, one has to take the reciprocal value, which is 1.43, respectively 3.03.

Determining the spring resistance for the stick according to the method of cross modality matching, the resulting fraction is about .5. Taking values from the literature for the same sense modalities you come to an exponent of about .6.

If the spring resistance of a stick is determined according to the above defined rule for the dependancy of perceived force and position, it can be expected, that spring resistance is optimal in respect to proprioceptive feedback of the motor activity during activation of the stick.

To test the effect of different, and especially of nonlinear stick spring resistances on performance in a *target acquisition* task, several experiments were run with visual feedback on the display. The number of subjects ranged between four and eleven.

The acquisition task can be seperated into two parts; a coarse, fast part and one which is fine, and slow. One may expect, that manipulation of proprioceptive feedback should especially influence that part, which is too fast for effective visual control; this means, especially the coarse adjustment movement should be influenced by the spring characteristic of the stick.

The whole *adjustment movement* was divided into coarse and fine adjustment at the acceleration minimum (AMI) i.e. deceleration maximum, which is at least correlated with the beginning of fine control (see figure 1).

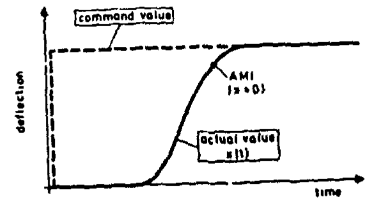

Figure 1 : Step response with a zero order system
(AMI : acceleration minimum = deceleration maximum)

First experiments were done with a zero order system. Analysis of variance of the measured 880 movements in several directions with several amplitudes showed, that neither coarse, nor total adjustment time were significantly influenced by varying the spring resistance of the stick, which means the variation of the proprioceptive feedback provided to the operator (figure 2). Only in fine control

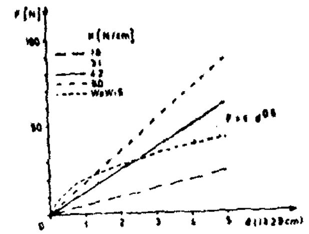

Figure 2 . Spring resistance of the control (zero order system)
d : stick deflection
F : centering force

are there small, but insignificant differences due to various spring characteristics.

C-6

A tendency for an influence of mechanical parameters of the moving arm-control system on such movement parameters as maximum acceleration and speed was seen and can be explained in terms of movement time optimality.

In the next experiment, a first order system was used. With a single integration control system, the complexity of the control movement is increased and especially the fine control into the target area is more difficult, compared to a position control system. A small position error of the stick will be integrated and can by detected visually only with some time lag. This can result in an oscillation of the system output.

The experiment was run with four amplitudes and three directions of the command step, two different sizes of the target circle and several spring characteristics of the control : two linear and two nonlinear characteristics which are shown in figure 3. Ohne control was isometric. The experiment consisted of about 1500 trials.

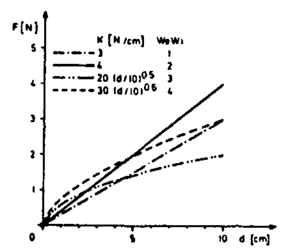

Figure 3 : Spring resistance of the control (first order system)
d : stick deflection
F : centering force

Analysis of variance results indicate, that the coarse adjustment time is almost perfectly invariant over all conditions and only fine adjustment time is sensitive to parameter alterations, and then only with the small target circle. This means, that with high demands on the precision of adjustment the difference between the various stick characteristics are quite pronounced. The following rank order

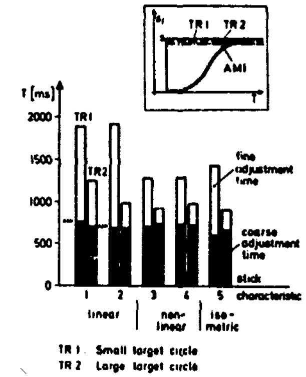

Figure 4 : Target acquisition time, separated into coarse and *fine adjustment by the point of maximum deceleration*

resulted : the shortest adjustment times are achieved with the nonlinear spring characteristics ; the longest times result with the linear ones. The isometric performance times are in between these two. The differences are highly significant and are as high as thirty percent. The results show, that contrary to what might be expected, variation of the proprioceptive feedback, produced by variation of the spring resistance, has no effect on the coarse adjustment time, but rather a lot on the final, precise adjustment. From this result and an additional experiment to determine the effect of spring characteristic on the precision of movement repetition without visual feedback, one can draw the conclusion, that the variation of proprioceptive feedback has only negligible effects on the fast part of the acquisition task. It is supposed, that this part is executed according to the idea of preprogramming as SCHMIDT, R.A. and others advocate.

With these results, the influence of proprioceptive feedback on the execution of movements is not disproved, but only shifted to final adjustment movements, which are usually unterstood to be mainly controlled visually. There is no problem, to understand fine adjustment control as a process, where command values are given by the visual sense, which are then executed in detail by the proprioceptive sense.

The experimental results show, that just fine control is significantly influenced by proprioceptive feedback.

The importance of final control time to total adjustment time is demonstrated in figure 5. It shows an almost negligible correlation between coarse and total

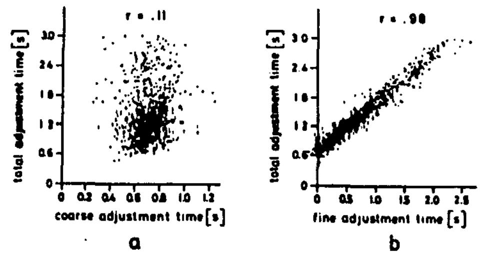

Figure 5 : Relationship (a) between total and coarse adjustment times and (b) between total and fine times (fine adjustment time is less than zero, if maximum deceleration point occurs in the target circle)

adjustment time, but a strong connection between fine and total adjustment time. With a correlation coefficient of .98, fine adjustment time accounts for about 96 percent of the variation of total adjustment time, whereas coarse adjustment time accounts for only about one to two percent. Conclusions of acquisition task experiments :

In target acquisition tasks, main concern should be directed towards facilitating fine control. Obviously, during coarse adjustment, parameter alterations are compensated by the operator in order to achieve a rather constant time and movement pattern, a finding, which is supported by some other authors (e.g. DIJKSTRA et.al. 1973). Strong centering of the stick by a nonlinear spring characteristic proved to facilitate final approach to the target without increasing the necessary force for wide deflections during the fast movement.

Continuous pursuit tracking runs with a two-dimensional forcing function with a .33 Hz cut-off frequency showed again the superiority of nonlinear spring characteristic. When subjects are able to adjust the spring characteristic by themselves, they all selected nearly the same nonlinear characteristic with an exponent of about .6 to the deflection term of the spring characteristic equation (see figure 6).

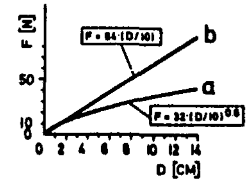

Figure 6 : Self adjusted nonlinear spring characteristic (a) For comparison a linear spring with similar force gradient near the neutral region (b)

Final conclusions :

1. Spring resistance of the control in higher order systems, as are most real systems, ought to be nonlinearly degressive to facilitate fine control adjustments without impeding coarse control movement.

2. For practical use, it is sufficient to take the self-adjusted values of a few well trained operators to determine the spring resistance of a control.

References :

BERNOTAT, R. : Operation Functions in Vehicle Control. Anthropotechnik in der Fahrzeugführung (In German with an english summary) Ergonomics, 1970, vol. 13(3), 353-377

DIJKSTRA, Sj. & DENIER VAN DER GON, J.J. : An analog computer study of fast, isolated movements. Kybernetik 12, 1973, 102-110

ROTHBAUER, G. : Zum Einfluß der Weg-Widerstandscharakteristik des Bedienelements auf den Vollzug einfacher und komplexer Stellbewegungen des Armes. Forschungsbericht des Forschungsinstituts für Anthropotechnik, Meckenheim/Bonn, 1977 (in press)

SCHMIDT, R.A. : The Index of Preprogramming (IP) : A statistical method of evaluating the role of feedback in simple movements.
Psychon. Sci. 1972, 27 (2), 83 - 85

STEVENS, S.S. : On the psychophysical law.
Psychol. Rev. 64 (3), 1957, 153 - 181

STEVENS, S.S. : On predicting exponents for cross-modality matches.
Percept. & Psychophysics, 6 (4), 1969, 251 - 256

AN ITERATIVE TECHNIQUE FOR FLIGHT DIRECTOR DESIGN

by

David L. Kleinman
University of Connecticut

ABSTRACT

A flight director design technique is developed by applying the optimal control model of human response to synthesize director signals that presumably simplify manual control compensation requirements. It is assumed that the additional flight director display information modifies human control objectives, thus giving rise to an iterative design approach. The technique is applied to a CH-47 helicopter hover task. The results are evaluated with respect to input-director transfer functions, shifts in attentional allocation, and improved hovering performance.

N79-17518

ACQUISITION OF CONTROL INFORMATION IN A WIND SHEAR

by J. M. Naish

Introduction

When an aircraft encounters a change of air mass it may experience a change in horizontal wind sufficient to cause appreciable change in airspeed and, therefore, in lift. It may also suffer a change in vertical wind and, therefore, in vertical speed. The adverse combination of these effects may result in a significant excursion below the correct vertical profile and this may be especially serious if it happens during the latter part of an approach. Appropriate action should then be taken very quickly to avoid a situation from which the aircraft can scarcely recover, implying that suitable information needs to be readily accessible to the pilot. The purpose of this paper is to explore circumstances in which it is difficult to meet this requirement in conventionally equipped aircraft, because of time factors affecting the flow of information.

Temporal Aspects of Acquisition of Control Information

The manner of acquiring information affecting control of an aircraft as it encounters wind shear may vary according to the flight mode and may influence the delay in gaining that information. If an instrument approach is in progress, so that the onset of shear is learned from the instruments, the delay may be small compared with the time remaining until touchdown because of the pilot's habitual division of attention between the panel instruments. The longest dwell (or reading) time for an instrument is about two seconds, which is the value for the attitude-director indicator (reference 1). Allowing for an instrument lag of about one second, the delay in noticing the onset of shear would be about three seconds, assuming the first signs of shear to be shown by other instruments, such as the altimeter, the vertical speed indicator, or the airspeed indicator. A delay of this magnitude would perhaps be sufficiently small in relation to the time until touchdown, unless the shear occurred at very low altitude. For example, some thirty seconds of flight would remain after meeting shear at 400 feet during a 3° approach at 135 knots (though this time could be reduced by path steepening due to the shear).

In the case of a purely visual approach, information relating to control in the vertical plane would be gained from the information mechanisms which support visual flight. If the relevant mechanism were the apparent expansion of the ground scene in relation to the end point of the flight path (reference 2), the time taken to determine that point would depend on the time for which the expansion had been apparent. Supposing the flight path to be directed towards a point lying between two ground objects, such as runway approach lights, which are distance S apart and subtend an angle $S\gamma^2/H$ at the pilot's eye, to the first order, where γ is the inclination of the flight path and H is the height of eye, as in Figure 1. Then for an approach at constant γ the objects appear to expand with angular velocity $S\gamma^2 V_z/H^2$, where V_z is the vertical speed. So expansion of the ground scene is less apparent for points close to the projected flight path than for points more remotely situated, and the limit of perceptible movement, at a particular time, occurs at that value of S for which the rate of expansion exceeds the threshold for detecting angular velocity. Conversely, for ground points at a given separation, the expansion becomes apparent when H is reduced sufficiently, assuming the vertical speed to remain constant. Taking the velocity threshold to be 10 minutes of arc per second of time for objects moving in a field having no reference framework (reference 3), the value of S is given with sufficient accuracy by

$$S = H^2/350\,\gamma^2 V_z$$

in which S and H are in feet, V_z is in feet per second, and γ is in radians.

Variation of S with height is shown in Figure 2 for two cases of interest. In one case, the approach is for a conventional path angle of 3° and a vertical speed of 12.5 feet per second. In the other, the path is assumed to have been steepened by wind shear to give a path angle of 5° and the vertical speed is taken to be 25 feet per second. If the conventional approach is directed to a point 1000 feet beyond threshold, the 3° curve shows that an apparent expansion with respect to the aim point will first become perceptible at a height of just over 110 feet, indicating that the flight path will terminate beyond threshold. On the other hand, if the 5° path finishes at a point short of threshold by, say, 2000 feet, expansion of threshold with respect to this point is first perceptible at a height of just over 360 feet, when the path may be seen to be dangerous.

Combining these results, if shear of the kind assumed is encountered at 400 feet during a 3° approach, the (safe) end point of the flight path will not have been detected visually at this time, and the steepened (unsafe) path will not become discernible until about 1.6 seconds later, when the height of 360 feet is reached at the increased vertical speed. Since the remaining flight time will be about 14.5 seconds, it should be possible to save the situation if visibility is adequate and if the new end point is perceived as rapidly as is theoretically possible. But this is only so if the relevant ground points are continuously identifiable, otherwise the end point may be misjudged through observing the apparent expansion of another part of the external scene.

Another temporal effect to be considered is the time needed for the transition between instrument and visual flight modes. This process requires muscular action to alter the line of regard and to refocus the eyes. It also requires a change in the method of interpreting visual patterns because information is already abstracted and quantified in the instrument flight mode but it has to be abstracted from a perspective scene and, as far as possible, quantified in the visual flight mode. The transition thus takes time and since the components of the process would appear susceptible, on general grounds, to effects of age, training, stress, and physical condition, the total transition time may be expected to vary between quite wide limits. For present purposes, the transition time will be taken as not less than 3 seconds, which is the time for one complete cycle between instrument and visual fields when only muscular actions are involved (reference 4), and possibly as great as 8 seconds. On this basis, the transition may act to constrain the flow of information when there is only limited time available, as in the latter stages of an approach. A simple illustration of this effect is shown in Figure 3, where acquisitions from the field of flight instrument information and from the external visual field are shown cumulatively, and where each acquisition is for simplicity assumed to be discrete and to occupy an equal interval of time. The horizontal bar represents the transition, during which no information is acquired from either field.

<u>Information Flow During Approach to Kennedy Airport in Low-Altitude Wind Shear</u>

By considering these temporal aspects of the acquisition of control information, it is possible to construct a model for the approach by Eastern Airlines Flight 66 to Kennedy International Airport on June 24, 1965, when the shear effect was similar to that which has been assumed and the pilots were, or were about to be, in visual flight during the period following the encounter. Thus, Table 1 shows mean sea-level height, vertical speed, and indicated airspeed as extracted from Appendix F of the National Transportation Safety Board's report on the ensuing accident (reference 5). It is seen that vertical speed increases significantly at a height of 425 feet and this is followed by a decrease in indicated airspeed beginning at 350 feet. So the aircraft started to encounter adverse shear at about 400 feet and this resulted in a vertical speed of 21 feet per second, increasing later to 30 feet per second, or about 25 feet per second overall. The flight path angle, as shown by the height trace of the appendix, was approximately 5°.

Table 1 also lists pilots' comments which can be used to infer sources of control information. Thus, the pilot made a visual acquisition of the approach lights at a height of 450 feet, when he said "I have approach lights." From then on, he probably continued to search the forward view until observing the runway lights at 200 feet ("Runway in sight"). This can be inferred with some confidence because it would be his primary concern to see the runway as soon as possible, because a complete transition cycle would occupy a large part of the interval up to the time of the second acquisition (13.6 seconds), and because there seems to have been no recognition of the effect of shear on the flight instruments. In this interval, it would have been possible to observe the change in path direction, from the apparent expansion of the approach lights, at a height of 360 feet, according to the model which has been proposed and assuming adequate visibility. But no change seems to have been observed, in spite of having advance warning of the possibility of shear (a report by another flight, Eastern 902, was acknowledged). It has therefore to be assumed that, if the model is correct, visibility was insufficient to support the visual mechanism on which it is based. This assumption is consistent with reports of poor visibility by ground observers and the recorded sound of heavy rain.

The copilot made an instrument approach, with an eventual transition to visual flight at a time which cannot be determined precisely. In response to the pilot's instructions to "stay on the gauges" at 525 feet and at 440 feet, the copilot was evidently in the instrument flight mode until at least 425 feet ("I'm with it"). From this point on, his source of information is uncertain until the pilot acquired the runway at 200 feet and, almost immediately (0.9 second), the copilot indicated his own acquisition of the runway by saying "I got it" (it could scarcely mean he was continuing an instrument approach at that height). The inference can thus be drawn that the copilot had already completed his transition by that time, and this is consistent with the prohibition on instrument flight below 200 feet at Kennedy Airport. If this were so, the copilot could have started his transition at, say, 300 feet which, at the prevailing rate of descent, would allow barely 5 seconds for the change of flight mode. It seems reasonable to suppose that the transition was actually started earlier at, say, 350 feet. In that event, the copilot would have been observing flight instruments for only 3 or 4 seconds from the time of the first instrument indication of windshear, at 425 feet, when vertical speed increased. And it is quite

possible that the vertical speed indicator was not included in the copilot's scan during this short interval, because of the small dwell fraction and link value associated with this instrument (Reference 1), in which case the wind shear would not be noticed. On establishing contact with the external visual world, the copilot would be in the same situation as the pilot, in that the steepened flight path would have been discernible below 360 feet, according to the model and given adequate visibility. Since the copilot was also unable to make this visual observation, at that time, the apparent expansion of the ground scene was either not used or not usable, through impaired visibility.

From the height of 200 feet onwards, both pilots were probably in visual flight, without recourse to instruments, because it would hardly have been possible to make a complete transition in the remaining 5.2 seconds of flight. Yet the direction of the flight path remained unknown, even though the threshold of perception had been exceeded by a factor of 2 at 180 feet. The moment of first recognizing the true state of affairs cannot be identified with certainty. It could perhaps have been as early as 120 feet, when the pilot said "Got It?" or it could have been as late as 90 feet, when 'Takeoff thrust' was commanded. In any event, the direction of the flight path was perceived at a time when the apparent expansion of any visible ground objects would seem to have reached gross proportions, and in a situation where flight instrument information was inaccessible through the constraint imposed by transition time.

Discussion

It has been taken as axiomatic that an excursion below the correct approach path due to low-altitude wind shear must be corrected as rapidly as possible, with the implication that the requisite information needs to be immediately accessible. This appears to be possible for the instrument flight mode when shear is encountered at about 400 feet and conventional instruments are used but it can be seen that instrument lag begins to be significant in this context, contributing a sizable fraction of the delay expected in recognizing the situation. It may therefore be desirable to use flight instruments having a rapid response in such cases, and this suggests consideration of an electronic flight instrument system, with which negligible delays can be achieved.

In the visual flight mode, an indefinite delay is possible when flying a 3° path, until the end point becomes discernible quite late in the approach. The situation could be improved by superimposing a ground-stabilized reference on the visual scene, with the effect of reducing the threshold of perceptible angular velocity (reference 3) and thus increasing the discernibility of apparent expansion of the ground scene. When the approach path is steepened by wind shear, the end point should be discerned in time, without any such aid, if visibility is adequate and perception continuous. In the approach to Kennedy Airport by Eastern Flight 66, however, both pilots seem to have been in a position to make such a determination, and since the end point was

TABLE I INFORMATION ANALYSIS FOR ACCIDENT AT KENNEDY AIRPORT ON JUNE 24, 1975

Time H.m.s.	Height* MSL ft	Vertical Speed* ft/min	Indicated Airspeed* Kts	Pilot's Source of Information	Copilot's Source of Information	Pilot's Comment	Copilot's Comment
1604:40.5	525	725	147		Instruments	Stay on the gauges	
1604:41.5	500	725	145				Oh yes, I'm right with it
1604:52.6	450	0	139	External World		I have approach lights	
1604:53.2	450	0	139				Okay
1604:54.7	440	725	140			Stay on gauges	
1604:55.8	425	1250	140		Instruments		I'm with it
1605:00.0	350	1250	138				
1605:02.5	265	1250	123				
1605:06.2	200	1250	125	External World		Runway in sight	
1605:07.1	160	1250	128		External World		I got it
1605:09.3	120	1800	129			Got it?	
1605:10.2	90	1800	128				Takeoff thrust
1605:11.4	50	1800	127			- - - -	- - - -

* Approximate values from Appendix F of NTSB Report

only seen to be dangerous at a time when the phenomenon of apparent ground expansion had reached gross proportions, this mechanism of visual information could evidently not be used in the prevailing circumstances of visibility. In such cases, a superimposed display might help stabilize the flow of otherwise interrupted information by filling in gaps caused, for example, by intermittent cloud, as well as by improving the detection of angular velocity.

The transitional phase between instrument and visual flight modes is highly significant to the flow of information when wind shear is met at low altitude because it may occupy a time large in relation to the remaining time of flight, especially when the path is steepened by the shear. In the Kennedy approach, the transition may have prevented the copilot observing important instrument indications shortly after meeting adverse wind shear. This kind of situation could, of course, be avoided by using a flight instrument system which effectively eliminates the transition, and allows observations in the flight instrument and external visual fields to be made in rapid succession, as indicated in Figure 4. It would then be possible to continue to acquire significant instrument information while observing the forward view, or while starting to do so.

The temporal constraint imposed by the transition appears also to have prevented both pilots acquiring vital instrument information during the final, visual, phase of the approach. Had vertical speed and airspeed information been immediately accessible at that time, steepening of the flight path could have been detected earlier, but this was not possible with the conventional display equipment used in the aircraft. Again, this type of situation could be avoided by eliminating the transition with a suitable display system.

By stressing the importance of temporal factors, the analysis thus leads to the simple conclusion that safety could be improved in a low-altitude wind shear situation by changes in the method of presenting information. The display system could be given the rapid response of an electronic medium to improve reaction time for the man-machine system. Presentation could be made in the head-up mode to provide a stabilized visual reference and thus improve detection of angular velocity. And the same type of presentation could be used to eliminate the transition, as is well known, and thus allow immediate access to critical information. In short, much could be done to improve the capacity for arousal to timely action.

The analysis also goes beyond the accident report (Reference 5) which concluded that the delay in recognizing the large descent rate was probably due to reliance on visual rather than flight instrument cues, while acknowledging that the copilot needed to make a transition to visual flight in order to complete the approach. The dilemma implicit in this finding may perhaps be resolved by the present proposal to change quite radically the flight instrument system.

The question of what should be shown in a head-up display is beyond the scope of the present paper. It should be noted, however, that not all information is equally useful or reliable in a wind shear. For example, a velocity vector symbol driven by a signal computed from an angle of attack sensor can be dangerously misleading in the presence of a strong vertical wind. On the other hand, an entirely suitable and reliable guidance signal can be derived from inertial sources, according to the method of J. R. Lowe.

References

1. Weir, D. H. and Klein, R. H., "Measurement and Analysis of Pilot Scanning Behavior During Simulated Instrument Approaches", 6th Annual Conference on Manual Control Proceedings, Wright Patterson Air Force Base, Ohio, April 1970, 83-108

2. Naish, J. M., "Control Information in Visual Flight", 7th Annual Conference on Manual Control Proceedings, U.S.C., Los Angeles, California, June 1971, 167-176

3. Graham, Bartlett, Brown, Hsia, Mueller, and Riggs, Vision and Visual Perception, Wiley, 1965, 575.

4. Naish, J. M., "Combination of Information in Superimposed Visual Fields", Nature, Volume 202, May 16, 1964, 641-646, Experiment 2

5. Todd, McAdams, Thayer, Burgess, and Haley, "Eastern Air Lines, Inc., Boeing 727-225, John F. Kennedy International Airport, Jamaica, New York, June 24, 1975", Aircraft Accident Report, National Transportation Safety Board, Washington, D.C., AAR-76-8, March 1976

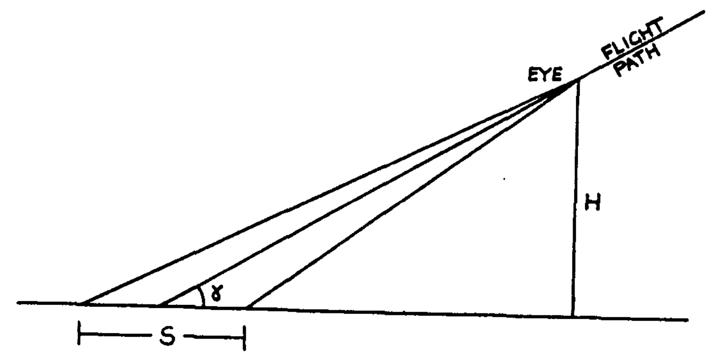

FIGURE 1 APPARENT EXPANSION OF GROUND OBJECTS

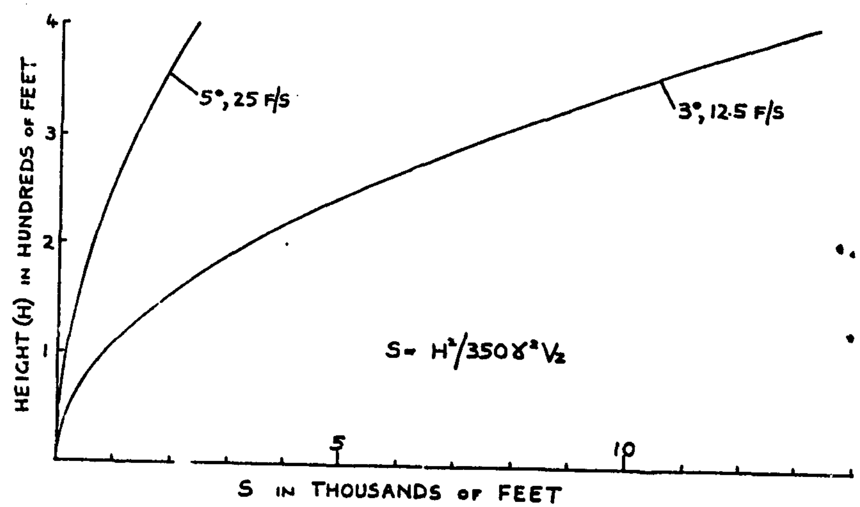

FIGURE 2 DISCERNIBLE SEPARATION OF EXPANDING OBJECTS

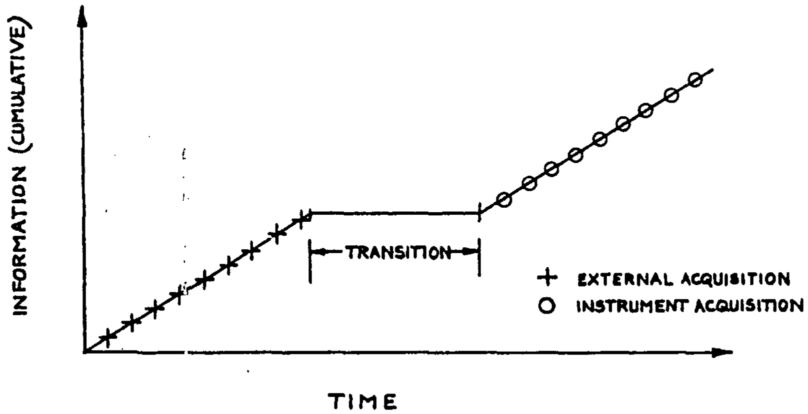

FIGURE 3 EFFECT OF TRANSITION ON INFORMATION ACQUIRED FROM SEPARATED FIELDS

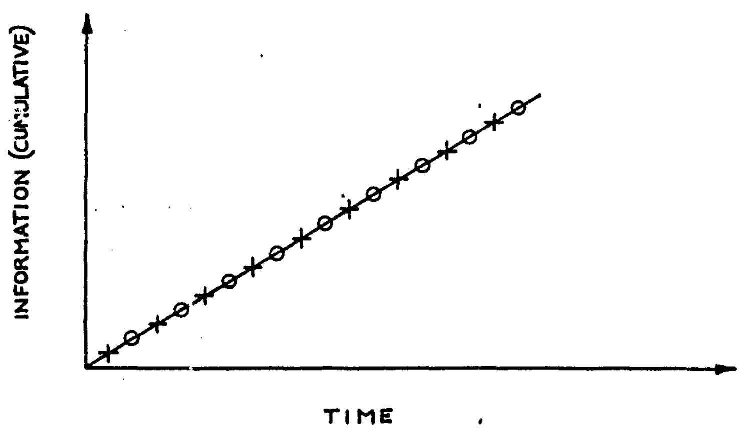

FIGURE 4 INFORMATION ACQUIRED WITH TRANSITION ELIMINATED

R. P. Bateman
WPAFB, Ohio

ABSTRACT

EULER ANGLE CONTROL AND DISPLAY FOR CCVs

The basis for all-weather operation of today's aircraft is attitude instrument flying in which aircraft performance is achieved by controlling the aircraft attitude and power. Control Configured Vehicle technology is using additional control surfaces and computer managed equations which essentially reduce coupling between attitude and flight path to gain increased performance. While the end result is an increased ability to control the aircraft, this capability creates additional problems.

The major problem is the standardization of controls used to attain the additional performance. Although the test bed aircraft may use discrete discontinuous selectable modes of operation to assign functions to various controls, a pilot needs to be able to transition from one mode of operation to another smoothly, without discontinuous inputs. It is inappropriate to have the same control device doing different things in different discrete modes.

A second problem deals with the display of aircraft flight path and attitude during instrument flight. This paper discusses a proposed Euler Angle Controller and Euler angle display which permits smooth control of a CCV during maneuvering and instrument flight.

omit

D44

N79-17519

SPEECH AS A PILOT INPUT MEDIUM

R.P. Plummer
University of Utah *
Salt Lake City, Utah 84112

C.R. Coler
NASA-Ames Research Center
Moffet Field, CA 94035

ABSTRACT

An automatic speech recognition system is currently being employed to investigate the use of speech as an input medium from pilots to computers on board aircraft. Such a system would allow pilots to provide inputs without the eye-hand coordinations required with keyboards, switches, etc. One stimulus for this work is literature, briefly reviewed in this paper, demonstrating the effectiveness of speech as compared with other means of communication.

The speech recognition system under development is a trainable pattern classifier based on a maximum-likelihood technique. An adjustable uncertainty threshold allows the rejection of borderline cases for which the probability of misclassification is high. The syntax of the "command language" spoken may be used as an aid to recognition, and the system adapts to changes in pronunciation if feedback from the user is available. Words must be separated by .25 second gaps.

The system runs in real time on a mini-computer (PDP 11/10) and has been tested on 120,000 speech samples from 10- and 100-word vocabularies. The results of these tests were 99.9% correct recognition for a vocabulary consisting of the ten digits, and 99.6% correct recognition for a 100-word vocabulary of flight commands (using command language syntax), with a 5% rejection rate in each case. With no rejection, the recognition accuracies for the same vocabularies were 99.5% and 98.6% respectively.

Plans for the system include fixed-base flight simulations, a motion simulator study, and in-flight tests.

INTRODUCTION

The increasing use of computers on board aircraft requires that increasing attention be paid to the design of the pilot-computer interface. The airborne use of computers usually takes place concurrently with other tasks, with time constraints on the interaction, and with a need for high accuracy of inputs and intelligibility of outputs.

The research reported here is concerned with the selection of an input medium for airborne computers, and, specifically, with the use of an automatic speech recognition system that allows inputs to be given verbally. The attractiveness of spoken inputs in the cockpit environment stems mainly from the fact that a large percentage of the workload is visual and manual. It is felt that the use of another communication channel (speech) for providing computer inputs will be less disruptive of (and less disrupted by) other tasks than the use of a manual input system.

BACKGROUND

Although considerable literature exists on the development of speech recognition systems [7, 9], less work has been done on the effectiveness of using such a system as a communications medium. This section reviews briefly work relating at least indirectly to the use of speech in cockpits.

Braunstein and Anderson [1] performed an early study comparing the speed and accuracy of speaking and keypunching digits. Their subjects, who had no prior keypunching experience, were able to read digits aloud twice as fast as they could keypunch, even with several hours practice. Accuracy of speaking was determined by human judges and found to be slightly better than that of keypunching.

A recent study by Williams [10] measured the keystroking ability of commercial and airline pilots. On a five-minute typing test, the subjects averaged 95.35% correct keystrokes. This provides a useful figure for comparison with the accuracy of speech recognition systems.

A general discussion of the use of speech for man-computer interaction has been given by Turn [8]. He cites the following attractive features of speech:

(1) the independence of speech from the visual channel and manual activities,
(2) the omnidirectional nature of speech,
(3) the ability of a speaker to communicate simultaneously with computers and humans, and
(4) the simplicity of converting speech to electronic form.

Turn also discusses the difficulties in implementing speech recognition systems. These lie mainly in the area of continuous speech recognition; he points out that isolated word recognition is already a reality. (The system discussed below uses isolated words.)

Also relevant to the question of speech as a communications medium is the work of Chapanis, et al, on interactive cummunication [2, 3, 4, 5]. Most important from the standpoint of

* Presently on leave to NASA-Ames Research Center.
This work was supported under NASA Grant NGR 45-003-108.

man-computer interaction are the following results [3]:

(1) Problems are solved significantly faster in communication modes that have a voice channel than in those that do not.
(2) Oral communication is highly redundant and most communication can be carried on effectively with a small, carefully selected set of words.

In summary, the work cited suggests that a speech recognition system would provide a natural, accurate, and rapid means of communicating with computers, especially in environments where the visual and manual workload of concurrent tasks is high.

AN ISOLATED WORD RECOGNITION SYSTEM

As a tool for experimentation in the cockpit, an automatic speech recognition system has been constructed. The system recognizes isolated words, that is, words separated by pauses of at least .25 seconds. The resulting "staccato" style of speech is not felt to be a problem for the anticipated command-oriented applications.

An utterance is digitally encoded by the use of 16 bandpass filters, sampled at 60 Hz. A time-warping algorithm divides the utterance into 8 subintervals (of possibly unequal duration), such that the amount of spectral change is the same within each subinterval. The data within each subinterval is then reduced to a 15-bit representation, producing a 120-bit encoding of the uttrerance.

Recognition is achieved by applying a maximum-likelihood pattern classification technique [6] to these 120-bit patterns. The system is trained to a particular speaker's voice by providing it with a set of samples of each word in the vocabulary to be spoken (the number of "training" samples of each word is generally between 5 and 25). These samples are used to estimate the probabilities of the occurrence of a 0 or 1 at each of the 120 bit positions for each vocabulary word. Given an unknown utterance to be classified, the probabilities are used to compute a similarity score for each vocabulary word, and the unknown is classified as being an example of the word with the highest score.

Three additional features augment this basic recognition scheme. In many applications it is preferable to reject (fail to classify) an utterance rather than misclassify it. The system rejects those utterances whose classification is "uncertain", where uncertainty is measured by computing the ratio of the second highest score to the highest score. A word is rejected if its uncertainty exceeds a preselected threshold (if no rejection is desired, the threshold is made >1).

A second feature of the system concerns the fact that even trained speakers vary their pronunciation of words slightly over time. Thus, the characterizations of the vocabulary words obtained from the training samples become less accurate as the speaker subsequently uses the system for recognition. In applications where feedback from the user is available, the system uses the words spoken to continually update its probabilities, thus compensationg for pronunciation shifts. Feedback may simply inform the system whether its classification was correct, in which case updating is done after each correctly classified utterance. If the system is also told the correct classification for each missed utterance, then updating can always be done.

Finally, in applications where the user is speaking a "command language" of known structure, the syntax of the language may be used to determine the subset of vocabulary words that are possible at each point in a command. For example, after "landing gear", the only meaningful words might be "up", "down", and "status". Recognition could be done only against this small subset rather than the entire vocabulary of, say, 100 words. This technique provides a considerable hedge against any degradation of performance with increasing vocabulary size.

The system is implemented on a PDP 11/10 minicomputer. About 13K 16-bit words of data storage are required for a 100-word vocabulary, and recognition time is slightly less than .5 seconds.

RECOGNITION RESULTS

The system has been tested extensively, on both 10- and 100-word vocabularies. Speech samples for the vocabulary consisting of the ten digits were obtained from 20 subjects, with each subject providing 25 training samples and 100 recognition samples of each word. As shown in Table I, recognition with this vocabulary is near perfect, especially when rejection is allowed. Syntax was not involved in this experiment, but feedback for updating was provided.

TEN DIGIT VOCABULARY

% Correct	% Rejected
99.5	0.0
99.9	5.0

Table I

A 100-word vocabulary of flight commands was tested with a group of 10 subjects, with each subject providing 25 training samples and 100 reconition samples of each word. A command language using this vocabulary was constructed; its syntax grouped the commands into 15 subsets ranging in size from 3 to 10 words (average size = 8.7 words). Table II shows the recognition results with and without rejection and with and without the use of syntax. Feedback for updating was again provided.

100 FLIGHT COMMAND VOCABULARY

	% Correct	% Rejected
without syntax	93.2 95.7	0.0 5.0
with syntax	98.6 99.6	0.0 5.0

Table II

FUTURE PLANS

The results to date demonstrate that an effective speech recognition system has been constructed. A set of experiments will begin shortly that will compare the system with a keyboard input device from the standpoint of accuracy and speed in laboratory conditions, and in conditions of noise and turbulence similar to those encountered in aircraft. The speech recognition system will then be used for providing inputs to a 4-D area navigation system in a full mission flight simulation, and, ultimately, in actual flight tests. These experiments should provide conclusive evidence on the viability of automatic speech recognition in the cockpit environment.

REFERENCES

1. Braunstein, M. and Anderson, N.S. A Comparison of the Speed and Accuracy of Reading Aloud and Keypunching Digits. IRE Transactions on Human Factors in Electronics, HFE-2, 1, 56-57, 1961.
2. Chapanis, A. Interactive Human Communication. Scientific American, 232(3), 36-42, 1975.
3. Chapanis, A. Interactive Human Communication: Some Lessons Learned from Laboratory Experiments. Paper presented at the NATO Advanced Study Institute on Man-Computer Interaction, Mati, Greece, Sept., 1976.
4. Chapanis, A., Ochsman, R.B., Parrish, R.N., and Weeks, G.D. Studies in Interactive Communication: I. The Effects of Four Communication Modes on the Behavior of Teams During Cooperative Problem -Solving. Perceptual and Motor Skills, 38, 343-374, 1974.
5. Kelley, M.J. Studies in Interactive Communication: Limited Vocabulary Natural Language Dialogue. Doctoral Dissertation, The Johns Hopkins University, 1975.
6. Nilsson, N.J. Learning Machines. New York: McGraw-Hill, 1965.
7. Reddy, D.R. Speech Recognition by Machine: A Review. Proceedings of the IEEE, 64, 501-531, 1976.
8. Turn, R. The Use of Speech for Man-Computer Communication. Rand Corporation Report R-1366-ARPA, 1974.
9. White, G.W. Speech Recognition: A Tutorial Overview. Computer, May, 1976.
10. Williams, D.H. The Keystroking Ability of Commercial Pilots. NASA Technical Memorandum TMX-73,160, 1976.

N79

17520

UNCLAS

N79-17520

MEASUREMENT OF HUMAN ANKLE JOINT COMPLIANCE USING RANDOM TORQUE INPUTS

Gyan C. Agarwal
Gerald L. Gottlieb

College of Engineering
University of Illinois at Chicago Circle
Chicago, Illinois 60680

and

Department of Physiology
Rush-Presbyterian-St. Luke's Medical Center
Chicago, Illinois 60612

ABSTRACT

The compliance of the human ankle joint is measured by applying 0 to 50 Hz band-limited gaussian random torques to the foot of a seated human subject. These torques rotate the foot in a plantar-dorsal direction about a horizontal axis at a medial maleolus of the ankle. The applied torques and the resulting angular rotation of the foot are measured, digitized and recorded for off-line processing. The data are analyzed by computing the auto-power and cross-power spectra of the angle and the torque using 4.096 second data records with 2.048 seconds of overlap between successive records. For 30 seconds of data, approximately 15 sets of spectra are computed and averaged. From these averages, the transfer function of compliance (ratio of angle to torque) is computed as is the coherence function. High values of coherence in the frequency range of 2 to 30 Hz and well-behaved compliance and phase curves suggest that the system may be reasonably approximated by a second-order, linear-differential equation. Using such a best-fit, second-order model, the effective moment of inertia of the ankle joint, the angular viscosity and the stiffness are calculated.

The ankle joint stiffness is shown to be a linear function of the level of tonic muscle contraction, increasing at a rate of 20 to 40 Nm/rad/Kg.m. of active torque. In terms of the muscle physiology, the more muscle fibers that are active, the greater the muscle stiffness. Joint viscosity also increases with activation. Joint stiffness is also a linear function of the joint angle, increasing at a rate of about 0.7 to 1.1 Nm/rad/deg from plantar flexion to dorsiflexion rotation.

INTRODUCTION

The design and development of devices for rehabilitation of paralyzed and paretic patients would be facilitated by more accurate knowledge about the dynamic response of the joint under control (1). For example, simple devices have been proposed for correcting foot drop by functional electrical stimulation (2).

The measurement of mechanical impedance in biomechanical systems has diverse applications. Many workers have used such measurements to study the vibration response of the whole body (3,4,5), the head (6), the knee (7) and the hand-arm system (8,9). The impedance concept has been used to assess the type and degree of ligamentous injury to the knee (7), to determine the moment of inertia of a limb segment (10) and to measure muscle tone (11).

Mechanical impedance is measured by applying a disturbance and measuring the appropriate force and displacement variables. In the absence of conscious intervention on the part of the subject, a limb will resist an externally applied torque. This resistance will have three components: 1) passive inertia about the joint; 2) visco-elastic stiffness of the joint and the muscles which act about it; and 3) the reflex contraction of stretched muscles.

The first of these may be presumed constant although it is somewhat a function of joint angle. The second is a function of the level of muscle activation (12). The third is time-varying and is sensitive to influences from a host of central nervous processes. Reflex effects, which directly influence the level of muscle activation will consequently alter the visco-elastic properties of the muscle. Even if we exclude voluntary changes in innervation, we are still dealing with mechanisms which are adaptive with relation to external disturbances.

D45

The rotation caused by external torques may be characterized as the joint compliance. Several techniques have been used for its measurement. One approach is to apply impulses of torque and measure the mechanical and electrical responses (13, 14). A disadvantage of this technique is that such stimuli may be "unphysiological" and the results difficult to extrapolate to other less stressful inputs. A second approach is to apply sinusoidal disturbances over a range of frequencies (8, 9, 15, 16). Predictions of the responses to other classes of input signals can then be made if the system is sufficiently linear to allow the principal of superposition to be applied. A third approach is to apply a relatively wideband, gaussian torque input covering the frequency spectrum of significant system dynamics.

Although linearity of the motor system has not been established, linear analysis has proven to be a versatile tool in describing components of the motor system such as muscle (17, 18), the muscle spindle (19, 20) and the integrated system (13, 14, 21, 22).

In this paper we will consider the measurement of ankle joint compliance using a band-limited gaussian torque disturbance and compare the responses with our earlier work using impulse torque inputs (tendon-jerk response) and sinusoidal torque inputs (13, 16). Muscle properties are known to be dependent on the level of active contraction (12) and on the length of the muscle (23). Consequently, we have examined joint compliance as a function of the muscle contraction and the mean angular operating point.

METHODS

These experiments have been done on over twelve normal, adult, male human subjects. A subject sat in a chair with the right foot strapped to a footplate which could rotate about a horizontal, dorsal-plantar axis through the medial maleolus. A schematic of the equipment used is shown in Figure 1.

The plate could be rotated by a D.C. torque motor (Inertial Motors Corp. No. 06-024) via a gearbelt and pulley system for torque amplification. Constant tension springs are also used to counter-balance the planter gravitational torque. With the subject completely relaxed, the resulting joint position (approximately 90° between the foot and the tibia) defines a reference ankle position. A dual beam oscilloscope provides the subject with visual feedback of foot angle on one channel and the reference position on the other.

A band-limited gaussian (0-50 Hz) signal was prerecorded from a noise generator. In the first experiment, these time-varying signals were superimposed on a mean motor torque level. The applied torque was controlled via a torque servo-mechanism. The subject was instructed to try to maintain a constant mean force against the bias torque of the motor so that foot movement was nearly symmetrical with respect to the reference angle. This was accomplished with little difficulty by all subjects. The input was applied for 30 sec or more and the data continuously recorded on a digital tape.

In the second experiment, with the subject completely relaxed, a biasing torque was added to displace the resting position of the foot in the dorsal or plantar direction and another 30 second measurement was made. This procedure was repeated for various angles over a range of about 12° in each direction about a neutral position. Bias torques were then added to the guassian signal and the subject was instructed to counteract them by keeping the motion of his foot centered about the visual reference.

The torque was measured by a strain gauge bridge on the side arms of the foot-plate. Angular rotation was measured by a continuous potentiometer. Electromyograms (EMGS) were recorded from disc surface electrodes placed over the bellies of the gastrocnemius-soleus (GS) and the anterior tibial (AT) muscles. These were amplified, full-wave rectified and filtered (10 msec averaging time) before recording. A digital computer (General Automation SPC - 16/65) generated the motor drive voltage at a conversion rate of 250/sec and digitized data on four channels. The angle and the torque signals were sampled at a rate of 250/sec and the filtered EMG at a rate of 500/sec.

The data was analyzed by computing the autopower and crosspower spectra of the angle and torque records using 4.096 second data records (1024 points) and a cosine taper (24) with 2.048 seconds of overlap between successive records. For 30 seconds of data, approximately 15 sets of spectra were computed and averaged.

Transfer functions were computed by the following method. Let $S_\tau(j\omega)$ and $S_\theta(j\omega)$ denote the Fourier transform (FFT) of torque and angle. The average auto and crosspower spectra are given by:

$$G_{\tau\tau}(\omega) = \overline{S_\tau(j\omega)\ S_\tau(-j\omega)}$$

$$G_{\theta\theta}(\omega) = \overline{S_\theta(j\omega)\ S_\theta(-j\omega)}$$

$$G_{\theta\tau}(\omega) = \overline{S_\theta(j\omega)\ S_\tau(-j\omega)}$$

These were computed as ensemble averages using the transformed data $S_\theta(j\omega)$ and $S_\tau(j\omega)$.

The transfer function of compliance (ratio of angle to torque) is given by

$$\text{Joint Compliance} = \frac{G_{\theta\tau}(\omega)}{G_{\tau\tau}(\omega)}$$

and the coherence function is defined as

$$\gamma^2 = \frac{G_{\theta\tau}(j\omega)G_{\theta\tau}(-j\omega)}{G_{\tau\tau}(\omega)\cdot G_{\theta\theta}(\omega)}$$

The coherence function lies between zero and one. For a linear noise free system it is equal to one.

RESULTS

The application of bandlimited gaussian torque (0 to 50 Hz) produces a response such as illustrated in Figure 2. The angular rotation shows that the torque input has been significantly lowpass filtered by the mechanical and neuromuscular properties of the limb. Considerable electromygraphic activity can be seen in both muscles. In this record, the gastrocnemius-soleus muscles were undergoing voluntary, tonic contraction opposing a motor bias torque of 0.26 Kg.m. The RMS value of the gaussian torque was 0.20 Kg.m.

The effective compliance of the ankle joint as a function of frequency is shown in Figure 3. This shows the results for the relaxed limb and at bias torque levels of 0.13 and 0.26 Kg.m. Figure 4 shows the corresponding phase relationship (foot angle always lags the applied torque). Figure 5 shows the measured coherence functions for this experiment.

The high values of coherence in the frequency range of 2 to 30 Hz. and well-behaved compliance and phase curves suggest that the system may be reasonably approximated by a second-order, linear differential equation with constant coefficients. The solid lines drawn in Figure 3 are from a best-fit, second order model:

$$\text{Joint Compliance} = \frac{\theta}{\tau} = \frac{1}{JS^2 + BS + k}$$

where:

- J = moment of inertia of the foot and the plate with respect to the axis of rotation through the medial maleolus (in $N.m.sec^2/rad$)
- B = angular viscosity coefficient (in N.m.sec/rad)
- K = angular stiffness (in N.m./rad)
- S = Laplace transform complex frequency

The criterion used for the model fit was:

$$\text{Error} = \sum_f \left[\log\left(\frac{\text{Model Compliance}}{\text{Measured Compliance}}\right)\right]^2$$

Table 1 shows the values of J, B, and K as well as the damping factors (ζ) and natural frequencies (ω_n) for three subjects as the bias torque is varied. The RMS value of the gaussian torque was kept at 0.2 Kg.m. throughout these runs. The bottom lines in this table show the mechanical parameters of the foot plate system.

As one would expect, the moment of inertia is independent of the bias torque. The mean values for these three subjects are 0.0157, 0.0180, and 0.0186 $N.m.sec^2/rad$. Of this inertia, 0.0097 $N.m.sec^2/rad$ is from the apparatus leaving 0.0060, 0.0083 and 0.0089 $N.m.sec^2/rad$ for the foot. These values are comparable to the values of 0.0107 $N.m.sec^2/rad$ for an average male subject calculated by Hogins (25) by considering serial sections of the foot from anatomical data and of 0.024 $N.m.sec^2/rad$ calculated by Trnkocsy et.al. (1) by considering foot as a prism. (Hogins' estimates of moment of inertia after correcting for the body weight and foot length for the first two subjects are 0.0074 and 0.0102 $N.m.sec^2/rad$, respectively).

The viscous coefficient and the stiffness are clearly functions of the bias torque. These variables are plotted in Figure 6.

The solid lines are the first order, least square regression lines. The equations of these regression lines for the three subjects are:

K: $23.3\tau_\beta + 22.5$ (0.992)

$40.5\tau_\beta + 15.3$ (0.996)

$38.9\tau_\beta + 14.9$ (0.999)

B: $0.161\tau_\beta + 0.383$ (0.891)

$0.332\tau_\beta + 0.237$ (0.915)

$0.143\tau_\beta + 0.412$ (0.686)

where τ_β is the bias torque. The correlation coefficients are given in the parentheses in each case.

Figures 7, 8 and 9 show the ankle joint compliance, phase angle and the coherence function respectively for a case of zero bias torque at three different mean joint angles. The solid lines plotted in Figures 7 and 8 are for the best second-order fit.

Joint stiffness as a function of the mean joint angle is shown in Figure 10 for one subject at three different levels of bias torques. The solid lines are the first order, least squares regression lines. The equations of these lines are:

τ_b = 0 Nm, K = $20.3 + 0.695\bar{\theta}$ (0.931)

τ_b = 1.1 Nm(D), K = $41.1 + 0.788\bar{\theta}$ (0.823)

τ_b = 2 Nm(P), K = $40.4 + 1.12\bar{\theta}$ (0.903)

Where τ_b is the bias torque and $\bar{\theta}$ is the mean joint angle in degrees. The correlation coefficients are given in parentheses in each case.

The viscous coefficient for this experiment is given by the following regression lines for the three cases:

τ_b = 0 Nm, B = $0.504 + 0.014\bar{\theta}$ (0.960)

τ_b = 1.1 Nm(D), B = $0.595 - 0.001\bar{\theta}$ (-0.215)

τ_b = 2 Nm(P), B = $0.675 + 0.013\bar{\theta}$ (0.793)

All other subjects tested for this experiment (four in all), showed similar behavior in the relationship of K vs. θ. That is, in the relaxed limb there was a monotonic change in K over the range of about $\pm 12°$ from neutral and voluntary contractions shifted the curve vertically. Angles greater than 12° were not systematically examined but as the angle increased beyond about 12° in either dorsiflexion or planter-flexion, the stiffness of the ankle increased due to passive mechanical properties of the joint.

DISCUSSION

At frequencies above 10 Hz, the foot and footplate offer an inertial load to the applied torque. At the low end of the spectrum, the limb acts like a spring. The spring constant is a linear function (Fig.6) of the level of tonic contraction, stiffness increasing at a rate of 20 to 40 N.m./rad/Kg.m. of active torque. This is a well known finding (see Wilkie (12) for human arm muscle and Joyce and Rack (26) for cat soleus).

The basis for the elastic coefficient being a function of activation lies in the physiology of muscle. The length-tension relationship of the muscle sarcomere indicates that at presumed physiological muscle lengths, an active muscle fiber will increase its contractile tension in a

"spring-like" manner when stretched. An inactive muscle fiber will produce negligible tension. As a consequence, the more muscle fibers that are active, the greater the muscle stiffness.

The values of B and K for the ankle joint obtained in these experiments compare reasonably well with the data obtained in other studies. Trnkoczy, et al. (1) report B = 1 N.m.sec/rad and k = 7.5 N.m/rad for the human ankle joint. Stark et al. (27) in their experiments on the human arm pronator and supinators found B and K increasing with voluntary tension, the values obtained were B = 0.0001 to 0.0003 N.m.sec/rad and K = 0.02 to 0.60 N.m/rad. The same experiment was repeated by Agarwal et al. (13) and their values were B = 0.009 to 0.056 N.m.sec/rad and K = 1.05 to 6.66 N.m./rad. Ishida and Umetani (28) found B = 1.5 N.m.sec/rad and K = 21 N.m/rad for the human upper arm.

Fig. 10 indicates that over a range of $\pm 12^\circ$ on either side of the neutral position, the joint stiffness is linearly dependent on the angular position increasing at a rate of about 0.7 to 1.1 Nm/rad/degree of mean angular rotation. Most of this dependence can be accounted for by the passive properties of the joint. The same functional angular dependence exists at all levels of muscle contraction and is small compared to the effects of contraction itself.

The use of random torque excitation for measuring joint compliance provides a description of the ankle joint which differs in at least two very distinct ways from the description obtained with sinusoidal torque excitation (15, 16, 29).

Within the 5-8 Hz region of the spectrum, sinusoidal torques produce a strong and narrow resonance with a frequency which is dependant on the level of tonic muscle contraction. The resonance is not evident with random torque. Within the 8-12 Hz region, foot rotation often becomes highly non-sinusoidal. Up to 80% of the angular signal power may be at frequencies other than the excitation frequency, particularly at ½ the excitation frequency. Such nonlinearities are also not evident here.

In both of these phenomena, the stretch reflex is very likely playing an important role when the excitation is sinusoidal. The contribution of the stretch reflex when the excitation is gaussian is not clear. A number of studies of human muscle (1, 18, 30, 31, 32) using widely differing methods have shown that the bandwidth of large muscles functioning as isometric torque generators is only 2 to 3 Hz. Given this sluggish response together with the 50 msec neural transport delay around the reflex arc could indicate that reflexes play a small role when random torques are used.

However, reflex activation of muscle not only produces torque by excitation-contraction processes, it also alters muscle compliance and the dynamics of these compliance changes are not known. It is probable that reflex activation of the muscle by spectral components of the random torque above 5 Hz would increase the stiffness of the muscle to spectral components below 5 Hz. Such an interaction would be quite complex and could account for some of the differences between random and sinusoidal measurements.

There is no question that the neuromuscular systems about the ankle joint are both non-linear and adaptive. The data in this report show that under the present experimental conditions, the system resembles a simple, linear one. Such a description, if taken literally can lead to many false impressions about the functioning of the motor system and extrapolation of these results to other classes of inputs or experimental conditions must be done with utmost caution. Although linear models exist for essentially all the subsystems of the reflex arc, they cannot be "wired" together to produce a more complete and general model. In biological systems, the whole is considerably more than the sum of its parts and we cannot yet identify, let alone understand or even describe, the many complex and subtle differences that exist.

ACKNOWLEDGMENT

This work was supported in part by the National Science Foundation Grant ENG - 7608754 and by NINCDS grant NS - 00196.

REFERENCES

1. Trnkoczy, A., Bajd, T., and Malezic, M., "A Dynamic Model of the Ankle Joint under Functional Electrical Stimulation in Free Movement and Isometric Conditions", J. Biomechanics, Vol. 9, pp. 509-519, 1976.

2. - Functional Neuromuscular Stimulation (report of a workshop), U.S. National Academy of Sciences, Washington, D.C., 1972.

3. Coermann, R. R., "The Mechanical Impedance of the Human Body in Sitting and Standing Position at Low Frequencies", Human Factors, Vol. 4, pp. 227-253, 1962.

4. Goldman, D. E., and von Gierke, H. E., "The Effects of Shock and Vibration on Man", Report No: 60-3, Naval Medical Research Institute, Bethesda, 1960.

5. Garg, D. P. and Ross, M. A., "Vertical Mode Human Body Vibration Transmissibility", IEEE Transactions Systems, Man & Cybernetics, Vol. SMC-6, pp. 102-112, 1976.

6. Smith, J. B., and Suggs, C. W., "Dynamic Properties of the Human Head", Journal of Sound and Vibration, Vol. 48, pp. 35-43, 1976.

7. Crowninshield, R., Pope, M. H., Johnson, R., and Miller, R., "The Impedance of the Human Knee", J. Biomechanics, Vol. 9, pp. 529-535, 1976.

8. Reynolds, D. D., and Soedel, W., "Dynamic Response of the Hand-Arm System to Sinusoidal Input", in The Vibration Syndrome, W. Taylor (Editor), pp. 149-168, Academic Press, New York, 1974.

9. Suggs, C. W., "Modelling of the Dynamic Characteristic of the Hand-Arm System", in The Vibration Syndrome, W. Taylor (Editor), pp. 169-186, Academic Press, New York, 1974.

10. Allum, J. H. J., and Young, L. R., "The Relaxed Oscillation Technique for the Determination of the Moment of Inertia of Limb Segments", J. Biomechanics, Vol. 9, pp. 21-25, 1976.

11. Duggan, T. C., and McLellan, D. L., "Measurement of Muscle Tone: A Method Suitable for Clinical Use", Electroencephalography and Clinical Neurophysiology, Vol. 35, pp 654-658, 1973.

12. Wilke, D. R., "The Relation Between Force and Velocity in Human Muscle", J. Physiology, Vol. 110, pp. 249-280, 1950.

13. Agarwal, G. C., Berman, B. M., and Stark, L., "Studies in Postural Control Systems. Part I: Torque Disturbance Input", IEEE Transactions Systems Science and Cybernetics, Vol. SSC-6 pp. 116-121, 1970.

14. Wieneke, G. H., and Denier van der Gon, J. J., "Variations in the Output Impedance of the Human Motor System", Kybernetik, Vol. 15, pp. 159-178, 1974.

15. Joyce, G. C., Rack, P. M. H., and Ross, H. F., "The Forces Generated at the Human Elbow Joint in Response to Imposed Sinusoidal Movements of the Forearm", J. Physiology, Vol. 240, pp. 351-374, 1974.

16. Agarwal, G. C., and Gottlieb, G. L., "Oscillation of the Human Ankle Joint in Response to Applied Sinusoidal Torque on the Foot", J. Physiology, Vol. 268, pp. 151-176, 1977.

17. Mannard, A., and Stein, R. B., "Determination of the Frequency Response of Isometric Soleus Muscle in the Cat Using Random Nerve Stimulation", J. Physiology, Vol. 229, pp. 275-296, 1973.

18. Bawa, P., and Stein, R. B., "Frequency Response of Human Soleus Muscle", J. Neurophysiology, Vol. 39, pp. 788-793, 1976.

19. Poppele, R. E., and Bowman, R. J., "Quantitative Description of Linear Behavior of Mammalian Muscle Spindles", J. Neurophysiology, Vol. 33, pp 59-72, 1970.

20. Hasan, Z., and Houk, J. C., "Analysis of the Response Properties of De-efferented Mammalian Spindle Receptors Based on Frequency Response", J. Neurophysiology, Vol. 38, pp. 663-672, 1975.

21. Poppele, R. E., and Terzuolo, C., "Myotatic Reflex: Its Input-Output Relation", Science, Vol. 159, 743-745, 1968.

22. McRuer, D. T., Magdaleno, R. E., and Moore, G. P., "A Neuromuscular Actuation System Model", IFAC Symposium on Technical and Biological Problems in Cybernetics, Yerevan, USSR, 1968.

23. Gordon, A.M., Huxley, A. F. and Julian, F. J., "The Variation in Isometric Tension with Sarcomere Length in Vertebrate Muscle Fibers", J. Physiology, Vol. 184, pp. 170-192, 1966.

24. Bendat, J. S., and Piersol, A. G., Random Data: Analysis and Measurement Procedures, Wiley, New York, 1971.

25. Hogins, M. T., "Identification of the Human Ankle Control System", Ph.D. Thesis, University of Illinois at Urbana, 1969.

26. Joyce, G. C., and Rack, P. M. H., "Isotonic Lengthening and Shortening Movements of Cat Soleus Muscle", J. Physiology, Vol. 204, pp. 475-491, 1969.

27. Stark, L., Neurological Control Systems: Studies in Bioengineering, Plenum Press, New York, 1968.

28. Ishida, A., and Umetani, Y., "A Model of the Stretch Reflex Arc for the Upper Arm with Respect to Tremor", in 1973 Biomechanics Symposium, edited by Y. C. Fund and J. A. Brighton, pp. 51-52, ASME, New York, 1973.

29. Gottlieb, G. L. and Agarwal, G. C., "Two Methods of Measuring the Dynamic Behavior of the Stretch Reflex in Man", Proc. San Diego Biomedical Symposium, Feb. 2-4, 1977.

30. Coggshall, J. D. and Bekey, G. C., "EMG - Force Dynamics in Human Skeletal Muscles, Medical & Biological Engineering, Vol. 8, pp. 265-270, 1970.

31. Crochetiere, W. J., Vodovnik, L., and Reswick, J. B., "Electrical Stimulation of Skeletal Muscle - A Study of Muscle as an Actuator", Medical & Biological Engineering, Vol. 5, pp. 111-125, 1967.

32. Gottlieb, G. L., and Agarwal, G. C., "Dynamic Relationship Between Isometric Muscle Tension and the Electromyogram in Man", J. Applied Physiology, Vol. 30, pp. 345-351, 1971.

TABLE I

SUBJECT	Bias (Kg.m.)	J (N.m.sec^2/rad)	B (N.m.sec/rad)	K (N.m/rad)	ζ	ω_n (rad/sec)
GCA	0.0	0.0164	0.362	22.1	0.301	36.7
	0.1	0.0152	0.433	26.3	0.343	41.6
	0.2	0.0155	0.461	26.8	0.357	41.6
	0.4	0.0164	0.388	32.6	0.265	44.6
	0.6	0.0158	0.447	36.2	0.296	47.8
	0.8	0.0156	0.509	39.1	0.326	50.1
	1.0	0.0147	0.561	45.0	0.345	55.3
	1.2	0.0146	0.588	52.6	0.336	60.0
GLG	0.0	0.0191	0.234	14.8	0.220	27.8
	0.25	0.0172	0.364	25.3	0.274	38.6
	0.5	0.0174	0.384	37.7	0.237	46.5
	0.75	0.0182	0.401	43.8	0.225	49.1
	1.0	0.0179	0.631	56.2	0.315	56.0
BWF	0.0	0.0178	0.333	14.9	0.323	29.0
	0.25	0.0146	0.574	24.1	0.483	40.7
	0.5	0.0174	0.488	34.6	0.315	44.6
	0.75	0.0190	0.470	44.6	0.255	48.5
	1.0	0.0218	0.539	54.9	0.246	50.2
	1.25	0.0210	0.609	62.5	0.266	54.5
Foot Plate	-	0.0098	0.158	1.27	0.712	11.4
	-	0.0096	0.131	1.14	0.627	10.9

Mechanical Parameters of the Ankle Joint at different levels of voluntary contraction of the leg muscles acting about the ankle against a constant bias torque.

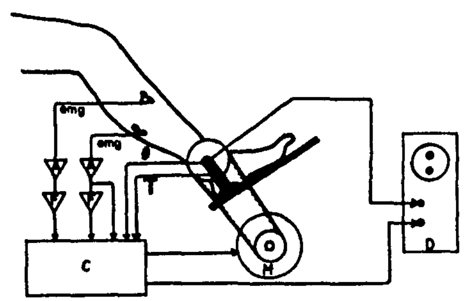

Figure 1
A schematic of the apparatus used for the measurement of the ankle joint compliance. The components are: D.C. torque motor (M) driven by a Bulova power amplifier. Electromyograms are measured using disc surface electrodes placed over the bellies of the soleus and anterior tibial muscles, EMG amplifier (A) are differential amplifiers (bandwidth 60-600 Hz), filters (F) are third order averaging (10 msec averaging time), display oscilloscope (D) and digital computer (C).

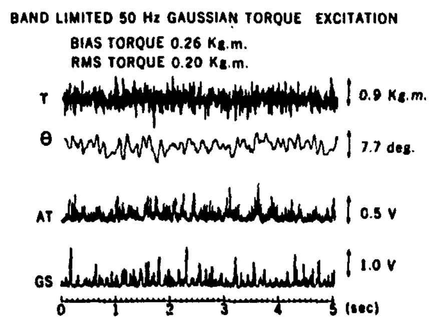

Figure 2
Response of the ankle joint and muscles in response to a band-limited 50 Hz gaussian torque input. The four traces are the motor torque (τ), foot angle (θ), anterior tibial muscle EMG (AT) and soleus muscle EMG (GS). The EMG scales are in volts after amplification, rectification and filtering of the surface EMG.

ORIGINAL PAGE IS
OF POOR QUALITY

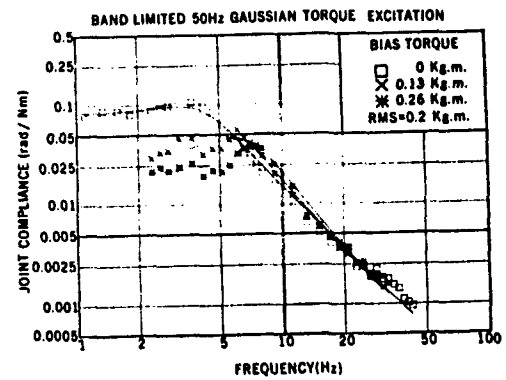

Figure 3
Effective compliance of the ankle joint measured in rad/N.m. as a function of the drive frequency at three bias torque levels. The solid lines are for a best-fit, second order model.

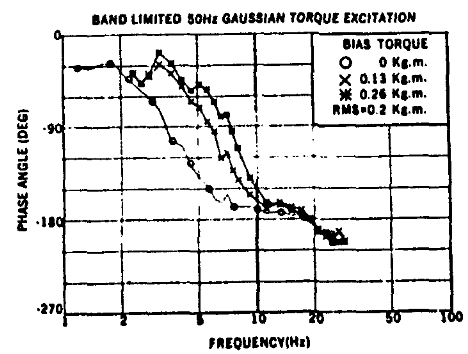

Figure 4
The phase relationship corresponding to the compliance data in Figure 3.

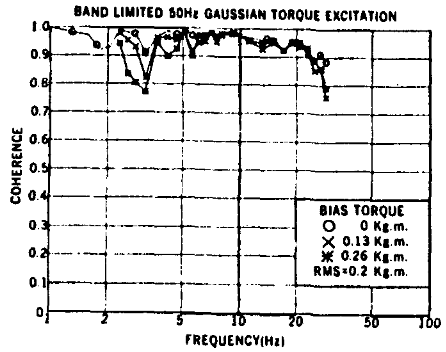

Figure 5
The coherence functions for the experiment in Figure 3. For the relaxed limb, the coherence was close to unity down to 1 Hz. With nonzero bias torque, the coherence values fell sharply below 2 Hz. Between 2 and 25 Hz, the coherence values are close to one indicating that the system appears fairly linear and noise free.

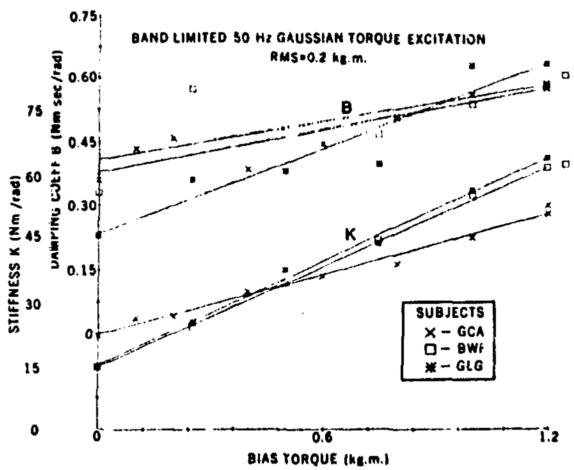

Figure 6
The joint viscous coefficient (B) in N.m.sec/rad and the stiffness (K) in N.m./rad as a function of the bias torque (average muscle activation) in Kg.m. with first order regression lines. The equations of these lines and the correlation coefficients are given in the text.

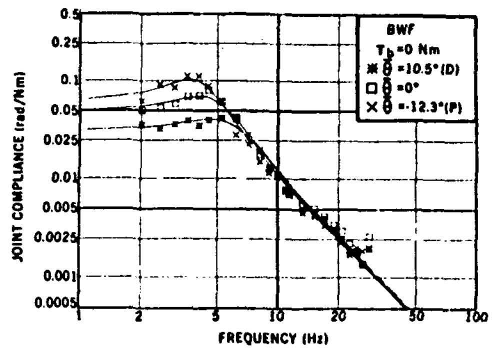

Figure 7
Effective compliance of the ankle joint measured in rad/Nm as a function of the drive frequency with zero bias torque and three values of mean joint angle (D = Dorsal, P = Plantar). The solid lines are for a best-fit, second order model.

ORIGINAL PAGE IS
OF POOR QUALITY

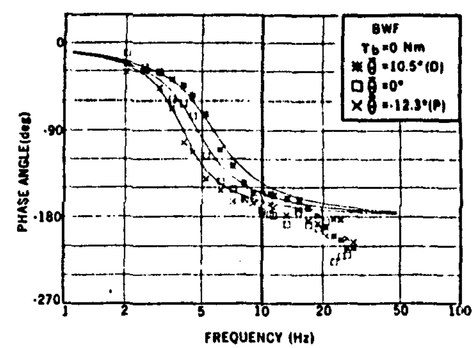

Figure 8
The phase relationship corresponding to the compliance data in Figure 7. The change in the phase angle near 18 Hz indicates a higher order system dynamics.

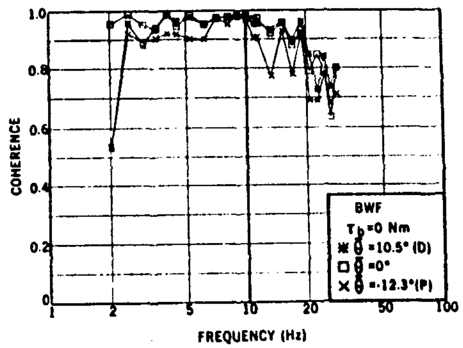

Figure 9
The coherence functions for the experiment in Figure 7.

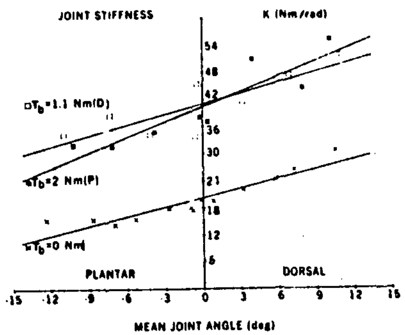

Figure 10
The joint stiffness in Nm/rad as a function of the mean joint angle with three different bias torques. The equations of the first order regression lines and the correlation coefficients are given in the text.